Dissertation zur Erlangung des Doktorgrades
der Fakultät für Chemie und Pharmazie
der Ludwigs-Maximilians-Universität München

Der Einfluss Parkinson-assoziierter Gene auf mitochondriale Morphologie, Dynamik und Funktion.

Anne Kathrin Sabine Barbara Lutz
aus
Augsburg

2012

Erklärung

Diese Dissertation wurde im Sinne von § 7 Abs. 1, 2 bzw. 4 bis 7 der Promotionsordnung vom 28.November 2011 von Frau PD Dr. Konstanze Winklhofer betreut.

Eidesstattliche Versicherung

Diese Dissertation wurde eigenständig und ohne unerlaubte Hilfe erarbeitet.

München, 23.01.2012

(Anne Kathrin Lutz)

Dissertation eingereicht am 23.01.2012

1. Gutachter PD Dr. Konstanze Winklhofer
2. Gutachter Prof. Dr. Ulrich Hartl

Mündliche Prüfung am 29.02.2012

„Der Zweifel ist der Beginn der Wissenschaft. Wer nichts anzweifelt, prüft nichts.

Wer nichts prüft, entdeckt nichts. Wer nichts entdeckt, ist blind und bleibt blind."

Teilhard de Chardin (1881-1955)

Meiner Familie, besonders meiner Oma

Inhaltsverzeichnis

Zusammenfassung

Ziel dieser Dissertationsarbeit war es, den Einfluss verschiedener Parkinson-assoziierter Gene auf die mitochondriale Morphologie, Dynamik und Funktion zu untersuchen. Unter Einsatz verschiedener zellulärer Modellsysteme wurde gezeigt, dass ein Funktionsverlust der autosomal-rezessiv vererbten Parkinson-assoziierten Gene Parkin, PINK-1 und DJ-1 in einer Fragmentierung des mitochondrialen Netzwerkes resultiert. Dieser Phänotyp wurde durch einen Anstieg an mitochondrialer Fission ausgelöst. Darüber hinaus manifestierte sich eine Verminderung der mitochondrialen Energieproduktion bei Funktionsverlust dieser Gene.

Die Überexpression des autosomal-dominant vererbten Parkinson-assoziierten Genes α-Synuclein induzierte ebenso eine Verkürzung der Mitochondrien, die in diesem Falle durch eine Reduktion der mitochondrialen Fusionsrate bedingt war. Dieser Phänotyp konnte durch die Expression von Parkin, PINK1, DJ-1 sowie des mitochondrialen Chaperones TRAP1 revertiert werden.

Ein weiterer Punkt, der im Rahmen dieser Arbeit genauer untersucht wurde, ist der Mechanismus, der dem Stress-protektiven Potential von Parkin zugrunde liegt. Pathogene Mutationen im Parkin-Gen führen zu einem Verlust der E3-Ligase-Aktivität von Parkin sowie dessen neuroprotektiver Funktion. Aus einem Teilprojekt dieser Arbeit ging hervor, dass die Missfaltung von Parkin einen zentralen Mechanismus dessen Inaktivierung darstellt.

Weiterhin konnten wir nachweisen, dass Parkin nicht nur vor Stress-induziertem Zelltod schützt, sondern auch unter verschiedenen zellulären Stressbedingungen transkriptionell hochreguliert wird. Unsere Untersuchungen zum Mechanismus der Stress-protektiven Aktivität von Parkin ergaben, dass das protektive Potential unabhängig ist von Komponenten der Mitophagie, eines Prozesses, bei dem nach Entkoppelung des mitochondrialen Membranpotentials defekte Mitochondrien durch Autophagie abgebaut werden. Als essentielle Komponente der Stress-protektiven Wirkung von Parkin konnten wir NEMO identifizieren. NEMO ist ein regulatorisches Protein des NF-κB Signalweges, das im Rahmen der NF-κB-Aktivierung durch verschiedene Ubiquitin-Ketten modifiziert und aktiviert wird. Wir konnten demonstrieren, dass Parkin die lineare Ubiquitinierung von NEMO erhöht und dass diese Form der Ubiquitinierung für die anti-apoptotische Wirkung von Parkin notwendig ist.

Einleitung

Die Parkinson-Erkrankung

Die Parkinson-Erkrankung stellt nach der Alzheimer-Erkrankung die zweithäufigste neurodegenerative Erkrankung dar. Charakteristisch ist hierbei der fortschreitende Verlust dopaminerger Neuronen der *Substantia nigra pars compacta*, was schließlich zu einem Mangel an Dopamin führt. Sichtbar wird dies als pathologisches Kennzeichen der Krankheit bei *post mortem* Analysen des Gehirns: der Verlust der dopaminergen Neuronen führt ebenso zu einem Verlust des Pigments Neuromelanin, was die Depigmentierung der *Substantia nigra* zur Folge hat (Marsden, 1983).

Bradykinese, Hypokinese, Rigor und Ruhetremor sind die Kardinalsymptome der Parkinson-Erkrankung, die in fortgeschritteneren Stadien von posturaler Instabilität begleitet werden. Das Auftreten nicht-motorischer Begleitsymptome ist durch die Degeneration weiterer Hirnregionen erklärbar. Betroffen sind hierbei das cholinerge (*Nucleus basalis Meynert*), noradrenerge (*Locus coeruleus*) und serotonerge (Raphe-Kerne) System (Dauer & Przedborski, 2003; Forno, 1996). Die sogenannten Lewy-Körperchen stellen ein weiteres pathologisches Merkmal der Erkrankung dar. Es handelt sich hierbei um zytosolische Proteinaggregate, die vorwiegend α-Synuclein, Ubiquitin und Hitzeschockproteine enthalten (Forno, 1996; Spillantini et al, 1997).

Die Hauptzahl der Krankheitsfälle, etwa 80-90% stellen die idiopathische oder sporadische Form der Parkinson-Erkrankung dar. Die Ursachen für diese Form der Erkrankung sind weitgehend unbekannt. Ein komplexes Zusammenspiel aus Umweltfaktoren und genetischen Risikofaktoren ist denkbar. Etwa 10% der Fälle sind bedingt durch autosomal-dominante oder autosomal-rezessive Vererbung und werden als familiäre Parkinson-Erkrankung bezeichnet. Die Identifizierung dieser monogenetischen Varianten stellte einen Meilenstein der Parkinson-Forschung dar. Bis heute sind sechs Gene eindeutig mit der Erkrankung verknüpft. Mutationen in den Genen, die für LRRK2 (*Leucine rich repeat kinase 2*) und α-Synuclein kodieren, sind mit der autosomal-dominanten Form der Erkrankung assoziiert. Die autosomal-rezessiven Fälle sind bedingt durch Mutation in den Genen, die für Parkin, PINK1 (*PTEN-induced kinase*), DJ-1 oder ATP13A2 kodieren (Pilsl & Winklhofer, 2011).

Mutationen im LRRK2-Gen sind die häufigste Ursache der familiären Parkinson-Erkrankung (Gilks et al, 2005; Paisan-Ruiz et al, 2004). LRRK2 ist ein zytosolisches Multidomänenprotein, das eine Kinase- und GTPase-Aktivität aufweist.

α-Synuclein ist ein präsynaptisches Protein mit hoher konfomationeller Flexibilität: in wäßriger Lösung liegt es unstruktiert vor, bildet jedoch α-helikale Strukturen nach Bindung an Lipide aus (Kamp & Beyer, 2006). Bislang sind drei pathogene Punktmutationen, A53T, A30P, E64K, sowie genomische Duplikationen und Triplikationen beschrieben (Chartier-Harlin et al, 2004; Kruger et al, 1998; Polymeropoulos et al, 1997; Singleton et al, 2003; Zarranz et al, 2004). Zur physiologischen Funktion von α-Synuclein ist wenig bekannt. Die Assoziation mit synaptischen Vesikeln legt eine Funktion bei der Regulation der Neurotransmitterfreisetzung nahe (Vekrellis et al, 2011).

Mutationen im PINK1-Gen sind die zweithäufigste Ursache für das Auftreten der autosomal-rezessiven Erkrankung (Valente et al, 2004a; Valente et al, 2004b). PINK1 besitzt eine N-terminale mitochondriale Signalsequenz, eine putative Transmembran-Domäne sowie eine Serin/Threonin-Kinase-Domäne (Beilina et al, 2005; Silvestri et al, 2005). DJ-1 ist ein redox-sensitives Protein, das vor oxidativem Stress schützen kann (Canet-Aviles et al, 2004; Mitsumoto et al, 2001). ATP13A2 kodiert für eine lysosomale P-Typ ATPase, deren Funktion weitgehend unbekannt ist (Lees & Singleton, 2007; Ramirez et al, 2006).

Mutationen im Parkin-Gen sind die häufigste Ursache für die autosomal-rezessive Parkinson-Erkrankung. Mehr als 100 pathogene Parkin-Mutationen sind mittlerweile identifiziert, die einen Funktionsverlust von Parkin zur Folge haben. Eine Inaktivierung von Parkin durch Missfaltung, beispielweise bedingt durch oxidativen oder nitrosativen Stress oder pathogene Mutationen, führt zu dessen Funktionsverlust und könnte auch an der Entstehung der sporadischen Erkrankung beteiligt sein (Cookson et al, 2003; LaVoie et al, 2007; LaVoie et al, 2005). Bestärkt wird diese These durch das Auffinden missgefalteter Parkin-Spezies in Gehirnen von Patienten, die unter der sporadischen Form der Erkrankung litten (LaVoie et al, 2005).

Parkin ist eine E3-Ubiquitin-Ligase, mit einer N-terminalen UBL (*ubiquitin like*)-Domäne und einer C-terminalen RBR (*ring-between-ring*)-Domäne. Die RBR-Domäne besteht aus zwei RING (*really interesting new gene*)-Fingern, die eine IBR (*in-between-RING*)-Domäne umschließen und die Bindung von Zink-Ionen koordinieren.

Zwischen der UBL- und der RBR-Domäne wurde eine weitere RING (RING0)-Domäne identifiziert, die ebenfalls Zink-Ionen binden kann. Parkin ist in der Lage, unterschiedliche Arten der Ubiquitinierung zu vermitteln (Joazeiro & Weissman, 2000). Die Präsenz von insgesamt sieben Lysin-Resten innerhalb eines Ubiquitin-Moleküls ermöglicht die Bildung von Ubiquitin-Ketten unterschiedlicher Topologie. Die Verknüpfung über Lysin-48 des Ubiquitin-Moleküls in Poly-Ubiquitin-Ketten führt klassischerweise zu einer proteasomalen Degradierung des ubiquitinierten Substrates. Mono-Ubiquitinierung oder eine Verknüpfung der Poly-Ubiquitin-Ketten über Lysin-63 spielt eine Rolle bei der Regulation verschiedener zellulärer Prozesse wie etwa Signaltransduktion, Endozytose, DNA-Reparatur und Autophagie.

Eine breite neuroprotektive Aktivität von Parkin konnte bereits von mehreren Arbeitsgruppen beobachtet werden. Es wurde in verschiedenen Modellsystemen gezeigt, dass eine erhöhte Parkin-Expression vor Stress-induziertem Zelltod schützen kann. Eine Beteiligung unterschiedlicher Signalwege wurde mit der Stress-protektiven Aktivität von Parkin in Verbindung gebracht: der NF-κB Signalweg, JNK- und PI3K-*Signalling*. Kürzlich wurde von der Arbeitsgruppe um Ted Dawson beschrieben, dass Parkin die Degradierung von PARIS (*parkin interacting substrate*) über das Ubiquitin-Proteasom-System induziert und dadurch die Expression von PGC-1α reguliert. PARIS agiert als Repressor von PGC-1α durch Bindung an dessen Promotor. PGC-1α wiederum ist ein transkriptioneller Ko-Aktivator, der die mitochondriale Biogenese reguliert. Durch die Degradierung von PARIS durch Parkin wird die Expression von PGC-1α erhöht und mitochondriale Biogenese stimuliert (Shin et al, 2011).

Mitochondriale Dynamik

Mitochondrien sind dynamische Organellen, die sich stetig teilen und wieder fusionieren. Mitochondrien kommunizieren miteinander, um sich an veränderte Energiebedingungen anzupassen und um Lipide, Metabolite und mitochondriale DNA auszutauschen (Legros et al, 2002).

Darüber hinaus kommunizieren Mitochondrien mit anderen Zellorganellen, wie z.B. dem endoplasmatischen Retikulum (ER), um die zelluläre Calcium-Homöostase aufrecht zu erhalten. Die mitochondriale Fission erleichtert den Transport von Mitochondrien, um an Stellen hohen Energiebedarfs zu gelangen. Die Fusion ermöglicht die Kommunikation der Mitochondrien untereinander und kann zur funktionellen Komplementierung

defekter Mitochondrien beitragen. Eine intakte Regulation der mitochondrialen Dynamik ist insbesondere in Neuronen von großer Bedeutung, da diese Zellen zum einen postmitotisch sind und zum anderen aufgrund ihrer Dimensionen und Polarität Besonderheiten aufweisen (Knott et al, 2008).

Unter Basalbedingungen sind Fusion und Teilung im Gleichgewicht. Liegt eine Störung dieses Gleichgewichts vor, und die Teilung überwiegt, so erscheinen die Mitochondrien verkürzt. Ist das Gleichgewicht zugunsten der Fusion verschoben, zeichnen sich die Mitochondrien durch eine starke Verlängerung und hohe Interkonnektivität aus.

Die Dynamik dieser Prozesse wird in humanen Zellen von verschiedenen GTPasen reguliert. Die Fusion der äußeren mitochondrialen Membran wird von den Mitofusinen (Mfn) 1 und 2 vermittelt, die in der äußeren Mitochondrienmembran lokalisiert sind (Eura et al, 2003; Santel et al, 2003; Santel & Fuller, 2001). Die N-terminale Region enthält die GTPase Domäne, in der C-terminalen Region ist eine *coiled-coil* Domäne zu finden. Mitofusin 1 und 2 bilden homo- und heterooligomere Komplexe und ziehen durch Interaktion ihrer *coiled-coil* Domänen die äußeren Membranen zweier benachbarter Mitochondrien zueinander (Koshiba et al, 2004).

Die mitochondriale GTPase OPA1 (*optic atrophy1*) vermittelt die Fusion der inneren mitochondrialen Membran und ist im mitochondrialen Intermembranraum lokalisiert (Olichon et al, 2002). Durch alternatives Spleißen und proteolytische Prozessierung entstehen verschiedene distinkte OPA1-Isoformen, die für die fusionsfördernde Funktion von OPA1 essentiell sind. Eine vermehrte Prozessierung von OPA1, induziert durch mitochondrialen Stress oder energetische Defizite, führt zu einer Verminderung dieser Aktivität (Ishihara et al, 2006; Olichon et al, 2007).

Die Teilung der Mitochondrien wird durch die zytosolische GTPase Drp1 vermittelt. Die Translokation von Drp1 an die äußere Mitochondrienmembran markiert künftige Teilungspunkte am Mitochondrium. Durch eine vermehrte Anlagerung von Drp1 an diese Punkte, kommt es zur Bildung von Spiralen um das Mitochondrium, bis es schließlich zur Abschnürung und damit Teilung kommt (Smirnova et al, 2001; Smirnova et al, 1998). Mitochondriale Fragmentierung ist ein früher Schritt des intrinsischen apoptotischen Weges, der kurz vor der Permeabilisierung der äußeren Mitochondrienmembran eintritt (Frank et al, 2001). Die genaue Bedeutung der mitochondrialen Fragmentierung während der Apoptose ist nicht bekannt. Die Tatsache, dass Drp1 mit dem pro-apoptotischen Protein Bax interagieren kann, deutet auf eine

wichtige Funktion der Mitochondrien während der Apoptose hin, bedarf allerdings noch genauerer Untersuchungen (Detmer & Chan, 2007; Knott et al, 2008; Westermann, 2010).

Die Bedeutung der Regulation mitochondrialer Dynamik für Neuronen wird untermauert durch die Beobachtung, dass Mutationen im Mfn2-Gen oder OPA1-Gen mit neurologischen Erkrankungen assoziiert sind (Alexander et al, 2000; Delettre et al, 2000; Schon & Przedborski, 2011; Zuchner et al, 2004).

Apoptotischer Zelltod

Neurodegenerative Erkrankungen gehen mit neuronalem Zelltod einher. Bei der Parkinson-Erkrankung gibt es verschiedene Hinweise dafür, dass insbesondere apoptotischer Zelltod für den Verlust dopaminerger Neuronen in der Substantia nigra verantwortlich ist (Anglade et al, 1997; Dauer & Przedborski, 2003; Mochizuki et al, 1996). Apoptose oder programmierter Zelltod kann über zwei Wege aktiviert werden: den intrinsischen und den extrinsischen Weg, welche beide in der Aktivierung der Effektor-Caspasen 3 und 7 konvergieren.

Die Aktivierung des extrinsischen Weges durch Bindung spezifischer Liganden, z.B. FASL (*FAS ligand*) oder TNF (*tumor necrosis factor*) an Todesrezeptoren führt zur Trimerisierung der Todesrezeptoren an der Plasmamembran, was wiederum die Rekrutierung von Adaptormolekülen, wie z.B. FADD (*FAS-associated death domain protein*), zur Folge hat. Diese binden im Zytoplasma an den Rezeptor, dimerisieren und aktivieren wiederum die Initiator-Caspase 8. Effektor-Caspasen werden daraufhin von aktiven Initiator-Caspasen durch proteolytische Abspaltung einer Prodomäne aktiviert.

Der intrinsische Weg wird von der Familie der Bcl-2 (*B cell lymphoma* 2) Proteine reguliert, die sich aus anti-apoptotischen Proteinen, wie Bcl-2, Bcl-XL (*Bcl-2-related gene, long isoform*) und Mcl-1 (*myeloid cell leukemia 1*), und pro-apoptotischen Proteinen, wie Bax (*Bcl-2-associated X protein*) und Bak (*Bcl-2 antagonist or killer*), zusammensetzt. Die anti-apoptotischen Bcl-2 Proteine besitzen vier Bcl-2-Homologie Domänen (BH 1-4) und sind hauptsächlich in der äußeren Mitochondrienmembran lokalisiert, können sich aber auch im Zytosol oder an der Membran des endoplasmatischen Retikulums befinden. Bcl-2, Bcl-XL und Mcl-1 inhibieren die pro-apoptotischen Proteine durch direkte Interaktion.

Eine Quervernetzung des intrinsischen und des extrinsischen Weges bildet die Initiator-Caspase 8. Diese kann das *BH3-only* Protein BID spalten, wodurch die aktive Form tBID

entsteht, die wiederum direkt Bax aktivieren kann und dadurch die Permeabilisierung der äußeren Mitochondrienmembran induziert (Chipuk et al, 2010; Tait & Green, 2010).

Der NF-κB Signalweg

NF-κB (*nuclear factor kappa-light-chain-enhancer of activated B-cells*) besteht aus einer Gruppe von fünf Proteinen, die Homo- oder Heterodimere bilden: NF-κB1 (p50 und seine Vorstufe p105), NF-κB2 (p52 und seine Vorstufe p100), p65/RelA, c-Rel und Rel-B. Unter basalen Bedingungen ist NF-κB durch Bindung an inhibitorische Proteine, die sogenannten IκBs (*inhibitor of* NF-κB: IκBα , IκBβ, IκBε, Bcl-3, p100 und p105) inaktiviert und im Zytosol sequestriert. Eine Aktivierung des Signalweges führt zur Phosphorylierung der IκBs (hauptsächlich IκBα) durch den IKK (IκB kinase) Komplex, was deren Ubiquitinierung und damit proteasomale Degradierung zur Folge hat. Dadurch werden die NF-κB Untereinheiten aus der inhibierenden Bindung befreit. Sie können in den Kern translozieren und dort die Transkription ihrer Zielgene aktivieren. Der IKK-Komplex besteht aus zwei katalytischen Untereinheiten mit Kinase-Aktivität, IKKα und IKKβ, sowie einer regulatorischen Untereinheit, NEMO (*NF-κB essential modifier*), auch IKKγ genannt (Gautheron & Courtois, 2010; Gloire et al, 2006).

Lineare Ubiquitinierung und NF-κB-Aktivierung

Lineare Ubiquitin-Ketten werden durch LUBAC (*linear ubiquitin assembly complex*) generiert. Hierbei wird das C-terminale Glycin von einem Ubiquitin-Molekül mit dem N-terminalen Methionin eines anderen Ubiquitin-Moleküls verknüpft. LUBAC besteht aus zwei RING-IBR-RING Proteinen, HOIL-1L und HOIP, die zur Familie der RING-E3-Ubiquitin-Ligasen gehören (Kirisako et al, 2006). Es konnte kürzlich gezeigt werden, dass die lineare Ubiquitinierung von NEMO essentiell ist für die Aktivierung des kanonischen NF-κB-Signalweges (Iwai & Tokunaga, 2009; Tokunaga et al, 2009). NEMO wird nicht nur durch lineare Ubiquitin Ketten modifiziert, es kann mittels seiner UBAN (*ubiquitin binding in ABIN and NEMO*)-Domäne auch selbst an lineare Ubiquitin-Ketten binden (Hadian et al, 2011). Man geht davon aus, dass die Bindung von NEMO an linear-ubiquitiniertes NEMO dessen Dimerisierung induziert und damit den IKK-Komplex aktiviert. Es ist jedoch noch wenig bekannt zur genauen Funktion und Abfolge der Ubiquitinierung von NEMO (Gautheron & Courtois, 2010; Iwai & Tokunaga, 2009).

Zusammenfassung der Ergebnisse

Der Funktionsverlust der autosomal-rezessiven Parkinson-assoziierten Gene Parkin, PINK1 und DJ-1 induziert mitochondriale Alterationen

Um einen möglichen Einfluss von Parkin auf die mitochondriale Morphologie in humanen Neuroblastom-Zellen (SH-SY5Y-Zellen) zu analysieren, wurde ein transienter RNAi-mediierter *Knockdown* von Parkin etabliert. Unter Basalbedingungen zeigten etwa 30% der Zellen eine Verkürzung der Mitochondrien. Nach Herunterregulation der Parkin-Expression wiesen etwa 70% der Zellen fragmentierte Mitochondrien auf. Dieser Phänotyp konnte durch Ko-Transfektion eines siRNA-resistenten Wildtyp-Parkin-Konstruktes verhindert werden, nicht jedoch durch die Expression pathogener Parkin-Mutanten.

Der Funktionsverlust von PINK1 induzierte einen vergleichbaren mitochondrialen Phänotyp: PINK1-defiziente Zellen zeigten ebenfalls in etwa 70% der Zellen eine deutliche Verkürzung der Mitochondrien. Wir konnten ferner zeigen, dass eine verminderte Expression von Parkin oder PINK1 eine Reduktion der zellulären ATP-Produktion um etwa 40% zur Folge hatte. Interessanterweise konnte der Funktionsverlust von PINK1 durch eine erhöhte Parkin-Expression kompensiert werden, allerdings nicht umgekehrt.

Als Ursache für den signifikanten Anstieg an fragmentierten Mitochondrien wurde eine Störung der mitochondrialen Dynamik vermutet. Daher wurden Proteine der mitochondrialen Fusions- oder Teilungsmaschinerie auf ihre Wirkung in Parkin- oder PINK1-defizienten Zellen hin untersucht. Die vermehrte Expression der Fusions-fördernden Proteine Mitofusin2 oder OPA1 führte zu einer kompletten Wiederherstellung des mitochondrialen Netzwerks sowie der ATP-Produktion in Parkin- oder PINK1-defizienten Zellen. Ebenso führte die Ko-Transfektion einer dominant negativen Mutante des Fissionsproteins Drp1 zu einer Revertierung des Phänotyps.

Um herauszufinden, ob die vermehrte mitochondriale Fragmentierung in Parkin- oder PINK1-defizienten Zellen auf eine verminderte Fusion oder vermehrte Fission von Mitochondrien zurückzuführen ist, testeten wir die Abhängigkeit dieses Phänotyps von Drp1. Es zeigte sich, dass die durch Parkin- oder PINK1-Funktionsverlust verursachte mitochondriale Fragmentierung in

Drp1-defizienten Zellen nicht auftrat. Dies spricht dafür, dass die Expression von Drp1 und damit die mitochondriale Fission essentiell ist, um die durch den Funktionsverlust von Parkin oder PINK1 induzierte mitochondriale Verkürzung zu vermitteln. Schlussfolgernd lässt sich feststellen, dass der mitochondriale Phänotyp in Parkin- oder PINK1-defizienten Zellen durch einen Anstieg an mitochondrialer Teilung entsteht (Lutz et al, 2009).

Mitochondriale Veränderungen konnten auch beobachtet werden, wenn die Expression eines weiteren autosomal-rezessiven Parkinson-assoziierten Genes vermindert wird. DJ-1-defiziente Zellen zeigten ähnlich wie Parkin- oder PINK1-defiziente Zellen einen Anstieg an verkürzten Mitochondrien. Interessanterweise konnte der Verlust von DJ-1 durch Überexpression von Parkin oder PINK1 kompensiert werden, wie wir in einer Kollaboration mit Isabella Irrcher und David S. Park (University of Ottawa) zeigen konnten (Irrcher et al, 2010).

Das autosomal-dominante Parkinson-assoziierte Gen α-Synuclein hemmt mitochondriale Fusion

Interessanterweise sind Einflüsse auf die mitochondriale Morphologie nicht nur auf die autosomal-rezessiven Parkinson-Gene beschränkt.

Da eine Bindung von α-Synuclein an Mitochondrien bereits beschrieben wurde, untersuchten wir in einer Kollaboration mit Frits Kamp, Nicole Exner und Christian Haass den Einfluss des Proteins auf mitochondriale Morphologie und Funktion (Nakamura et al, 2008; Shavali et al, 2008). Vordaten aus der Arbeitsgruppe von Herrn Prof. Haass zeigten, dass rekombinantes α-Synuclein die Fusion von kleinen unilammellaren Vesikeln *in vitro* hemmen kann (Kamp & Beyer, 2006; Kamp et al, 2010). Im Rahmen dieser Kollaboration zeigte sich, dass die vermehrte Expression sowohl von Wildtyp-α-Synuclein als auch der beiden Mutanten A30P und A53T in humanen SH-SY5Y-Zellen zu einer Verkürzung der Mitochondrien führte. Es stellte sich die Frage, ob dieser Phänotyp durch einen Anstieg an mitochondrialer Teilung oder durch einen Abfall der mitochondrialen Fusionsrate vermittelt wird. Mittels eines zellulären PEG (Polyethylenglykol)-Fusionsassays konnten wir zeigen, dass die mitochondriale Fragmentierung induziert durch α-Synuclein durch eine verminderte mitochondriale Fusionsrate bedingt ist. Die Funktion der Mitochondrien wurde durch die Überexpression von α-Synuclein im beobachteten Zeitraum von mehreren Tagen

nach Überexpression nicht beeinträchtigt: sowohl das mitochondriale Membranpotential als auch die zelluläre ATP-Produktion war im Vergleich zu Kontrollzellen nicht verändert.

Bemerkenswerterweise konnte die mitochondriale Fragmentierung bedingt durch Überexpression von α-Synuclein durch die Ko-Transfektion von Parkin, PINK1 und DJ-1 revertiert werden (Kamp et al, 2010).

Die durch α-Synuclein induzierte mitochondriale Fragmentierung konnte ferner durch das mitochondriale Chaperon TRAP1 (*tumor necrosis factor receptor associated protein-1*) verhindert werden, wie wir kürzlich im Rahmen einer Kollaboration mit Erin Butler, Aaron Voigt und Jörg Schulz (Universität Aachen) zeigen konnten. In dieser Studie wurde das Hsp90-ähnliche Chaperon TRAP1 als Modulator der α-Synuclein-induzierten Neurotoxizität in *Drosophila melanogaster* identifiziert. Ein Funktionsverlust von TRAP1 verstärkte in α-Synuclein A53T-überexprimierenden Fliegen die Sensitivität gegenüber oxidativem Stress und den Verlust dopaminerger Neuronen. In Analogie zu den Daten aus dem Fliegen-Modell konnten wir in humanen SH-SY5Y-Zellen zeigen, dass ein RNAi-mediierter *Knockdown* von TRAP1 zu einer Fragmentierung der Mitochondrien führte, was durch Ko-Expression von α-Synuclein deutlich verstärkt wurde (Butler et al., 2011).

Die Missfaltung von Parkin ist ein zentraler Mechanismus dessen pathogener Inaktivierung

Pathogene Parkin-Mutationen führen zu einem Funktionsverlust von Parkin und sind für die Mehrheit der autosomal-rezessiven Parkinson-Erkrankungen verantwortlich. Unsere Arbeitsgruppe konnte zeigen, dass die Missfaltung von Parkin einen bedeutenden Mechanismus dessen Inaktivierung darstellt (Henn et al, 2005; Winklhofer et al, 2003).

Eine Fehlfaltung von Parkin kann durch starken oxidativen Stress oder durch pathogene Mutationen induziert werden. Im Rahmen unserer Untersuchungen zeigte sich, dass die Fehlfaltung von Parkin zwei Konsequenzen haben kann: zum einen die Bildung zytosolischer Parkin-Aggregate und zum anderen die Destabilisierung von Parkin. C-terminale Deletionsmutanten und einige Punktmutanten (insbesondere Cystein-Mutanten innerhalb der RBR-Domäne) aggregierten im Zytosol, wohingegen N-terminale Punkt-Mutationen innerhalb der UBL-Domäne verhinderten, dass Parkin

eine stabile Konformation erlangte und folglich zu einem raschen proteasomalen Abbau von Parkin führten (Schlehe et al, 2008).

Parkin ist eine Stress-induzierbare und Stress-protektive E3-Ubiquitin-Ligase

Da in einer früheren Studie unserer Arbeitsgruppe beobachtet wurde, dass die Expression von Parkin durch mitochondrialen Stress und Exzitotoxizität induziert werden kann (Henn et al, 2007), sollte die Regulation der Parkin-Genexpression und der zugrunde liegende Mechanismus genauer untersucht werden.

Eine Behandlung unterschiedlicher Zelllinien mit dem mitochondrialen Entkoppler CCCP (Carbonylcyanid-3-chlorophenylhydrazon) oder den ER-Stressoren Thapsigargin und Tunicamycin führte zu einer Hochregulation von Parkin um den Faktor 5 bis 8, sowohl auf Ebene der Parkin-Transkripte als auch auf Proteinebene. Eine bioinformatische Analyse des Parkin-Promotors gab uns Hinweise darauf, dass der Transkriptionsfaktor ATF4 bei der Stress-induzierten Hochregulation von Parkin eine Rolle spielen könnte. ATF4 ist ein Transkriptionsfaktor der *Unfolded Protein Response*, die durch ER-Stress induziert wird. Wie Lena Bouman im Rahmen ihrer Dissertationsarbeit mittels Chromatin-Immunpräzipitation zeigen konnte, kann ATF4 an den Parkin-Promoter binden. In ATF4-defizienten Modellen war die Stress-induzierte Hochregulation von Parkin deutlich beeinträchtigt.

Wir konnten ferner zeigen, dass die durch mitochondrialen Stress induzierte Hochregulation von Parkin über die *Unfolded Protein Response* und ATF4 vermittelt wird. Im Verlauf dieses Projekts konnten wir beobachten, dass sich mitochondrialer Stress auch auf das ER auswirken kann; andererseits hat ER-Stress Effekte auf mitochondriale Morphologie und Funktion (Bouman et al, 2011).

Was könnte die physiologische Relevanz der Stress-induzierten Hochregulation von Parkin sein? Die Überexpression schon geringer Mengen von Parkin, vergleichbar mit der physiologischen Menge wie wir sie nach zellulärem Stress beobachten konnten, schützte verschiedene Zelllinien (humane SH-SY5Y Zellen und *mouse embryonic fibroblasts* (MEF)) vor Zelltod in verschiedenen Stress-Paradigmen, wie z.B. mitochondrialem Stress, ER-Stress und Exzitotoxizität. Diese Stress-protektive Aktivität von Parkin korreliert mit dem Phänotyp Parkin-defizienter Modellsysteme, die eine erhöhte Anfälligkeit gegenüber Stress-induziertem Zelltod zeigen. Wir konnten diesen Phänotyp sowohl in primären Neuronen von Parkin-defizienten

Mäusen als auch in Fibroblasten von Patienten mit pathogenen Parkin-Mutationen beobachten.

Kürzlich berichtete die Arbeitsgruppe von Richard Youle, dass die Überexpression von Parkin die Beseitigung entkoppelter Mitochondrien mittels Mitophagie induzieren kann. Die Behandlung humaner HeLa-Zellen mit dem mitochondrialen Entkoppler CCCP führte zu einem Abfall des mitochondrialen Membranpotentials, was die Translokation von Parkin vom Zytosol ans Mitochondrium binnen einer Stunde induzierte. Nach weiteren 24 Stunden waren in CCCP-behandelten Parkin-exprimierenden Zellen keine Mitochondrien mehr vorhanden (Narendra et al, 2008). Die Arbeitsgruppe von Herrn Professor Youle konnte ferner zeigen, dass die Mitophagie-induzierende Aktivität von Parkin abhängig ist von verschiedenen Faktoren: einer intakten Autophagie-Maschinerie, nämlich der Expression von Atg5 und p62, sowie der Expression der mitochondrialen Kinase PINK1 (Narendra et al, 2010a; Narendra et al, 2008; Narendra et al, 2010b). Aufgrund dieser Beobachtungen stellte sich uns die Frage, ob die Mitophagie-induzierende Wirkung von Parkin dessen Stress-protektive Funktion hinlänglich erklären kann. Um diese Frage experimentell zu adressieren, untersuchten wir das Stress-protektive Potential von Parkin in Zellen, die kein Atg5, p62 oder PINK1 exprimieren. Interessanterweise war die Stress-protektive Aktivität von Parkin in Fibroblasten weder von Autophagie-defizienten Mäusen (Atg5- oder p62-*Knockout*-Mäuse) noch von PINK1-defizienten Mäusen eingeschränkt (siehe Abbildung 1).

Diese Ergebnisse sprechen dafür, dass es sich bei der Stress-protektiven Aktivität und der Parkin-induzierten Mitophagie um zwei voneinander unabhängige Aktivitäten handelt. Dieses Resultat konnte dadurch untermauert werden, dass die Deletionsmutante ΔUBL-Parkin, der die N-terminale UBL-Domäne fehlt, keine Stress-protektive Aktivität zeigte, allerdings weiterhin die Eliminierung depolarisierter Mitochondrien vermitteln konnte (siehe Abbildung 2).

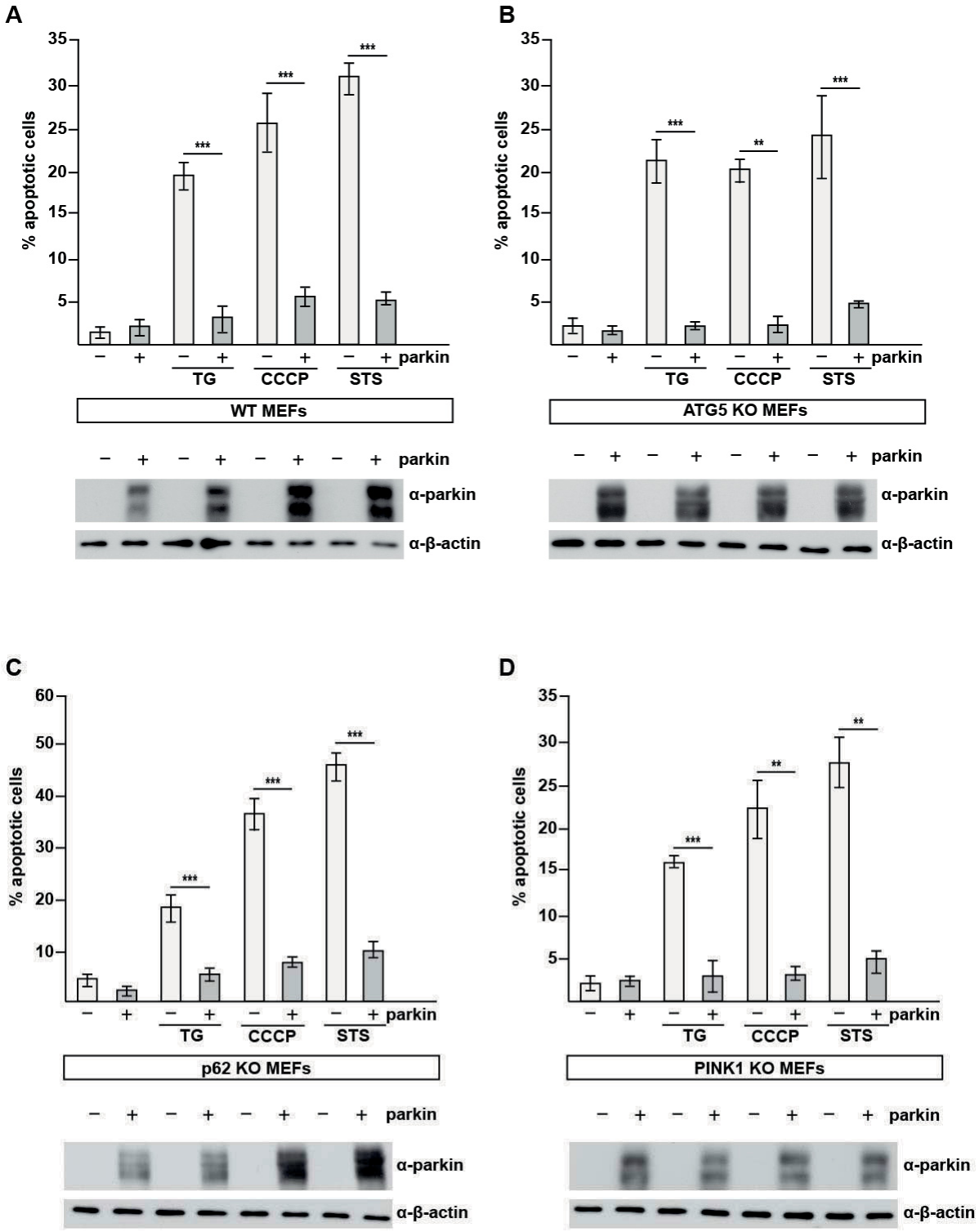

Abbildung 1: Parkin schützt *mouse embryonic fibroblasts* (MEFs) vor Stress-induziertem Zelltod unabhängig von Komponenten der Mitophagie. Wildtyp (A, WT) und entsprechende *Knockout* (KO) MEFs (B, Atg5-KO-MEFs; C, p62-KO-MEFs; D, PINK1-KO-MEFs) wurden mit dem ER-Stressor Thapsigargin (TG, 10 µM, 8 h), dem mitochondrialen Entkoppler CCCP (10 µM, 8 h) oder dem pro-apoptotischen Kinase-Inhibitor Staurosporin (STS, 1 µM, 5 h) behandelt. Apoptotischer Zelltod wurde durch indirekte Immunfluoreszenz mittels eines Antikörpers gegen aktive Caspase-3 visualisiert. Die Quantifizierung basiert auf Triplikaten von mindestens drei unterschiedlichen Experimenten. Pro Bedingung wurden mindestens 2500 transfizierte Zellen gezählt. Die Expression von Parkin wurde mittels Western Blotting überprüft, Aktin diente als Ladekontrolle.

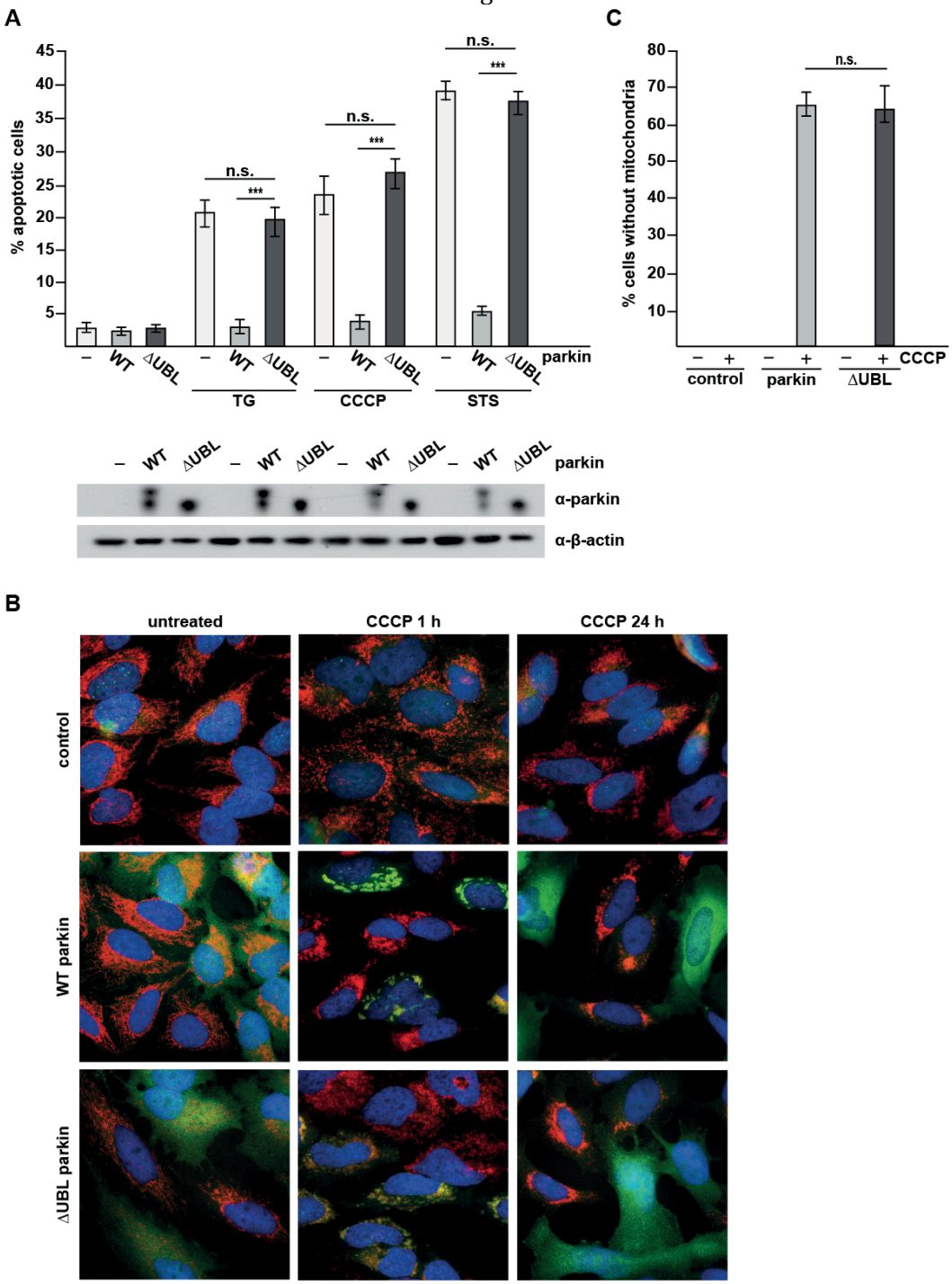

Abbildung 2: ΔUBL-Parkin besitzt keine Stress-protektive Aktivität, induziert aber Mitophagie.
A, ΔUBL-Parkin schützt SH-SY5Y-Zellen nicht vor Stress-induziertem Zelltod. SH-SY5Y-Zellen wurden mit Wildtyp-Parkin (WT), ΔUBL-Parkin (ΔUBL) oder Kontrollvektor (-) transient transfiziert und mit den Stressoren TG, CCCP und STS behandelt. Apoptotischer Zelltod wurde durch indirekte Immunfluoreszenz mittels eines Antikörpers gegen aktive Caspase-3 visualisiert. Die Quantifizierung basiert auf Triplikaten von mindestens drei unterschiedlichen Experimenten. Pro Bedingung wurden mindestens 2500 transfizierte Zellen gezählt. Die Expression von Parkin wurde mittels Western Blotting überprüft, Aktin diente als Ladekontrolle. B, C, ΔUBL-Parkin induziert Mitophagie. B, Viral transduzierte HeLa-Zellen, die Wildtyp-Parkin (WT-Parkin) oder ΔUBL-Parkin stabil exprimieren, wurden mit CCCP behandelt; die Rekrutierung von Parkin an Mitochondrien (nach 1 Stunde CCCP-Behandlung) und die Eliminierung der Mitochondrien (nach 24 Stunden CCCP-Behandlung) wurde mittels indirekter Immunfluoreszenz analysiert. Grün: Parkin (anti-Parkin-Antikörper PRK8), rot: Mitochondrien (anti-Tom20-Antikörper), blau: Nuklei (4′,6-Diamidin-2-phenylindol (DAPI)-Färbung). C, Quantifizierung der Parkin-induzierten Mitophagie nach 24-stündiger Behandlung der Zellen mit CCCP. Pro Bedingung wurden mindestens 1500 Zellen ausgezählt. Die in B und C gezeigten Experimente wurden von Anna Pilsl durchgeführt.

In einer früheren Studie unserer Arbeitsgruppe konnte beobachtet werden, dass Parkin einen permissiven Effekt auf den NF-κB-Signalweg hat: Es senkte die Schwelle, bei der unter zellulärem Stress NF-κB aktiviert wird (Henn et al, 2007). Um den Mechanismus der Stress-protektiven Aktivität von Parkin aufzudecken, untersuchten wir zunächst, ob der NF-κB-Signalweg essentiell ist für die anti-apoptotische Eigenschaft von Parkin. Dazu setzten wir Fibroblasten NEMO-defizienter Mäuse ein, in denen der kanonische NF-κB-Signalweg nicht aktiviert werden kann (Makris et al, 2000; Schmidt-Supprian et al, 2000). Interessanterweise war die Stress-protektive Aktivität von Parkin in NEMO-defizienten Fibroblasten unter allen getesteten Stressbedingungen aufgehoben. Diesen Effekt konnten wir durch Ko-Transfektion von NEMO revertieren, was für die Spezifität des beobachteten Effektes spricht (Abbildung 3).

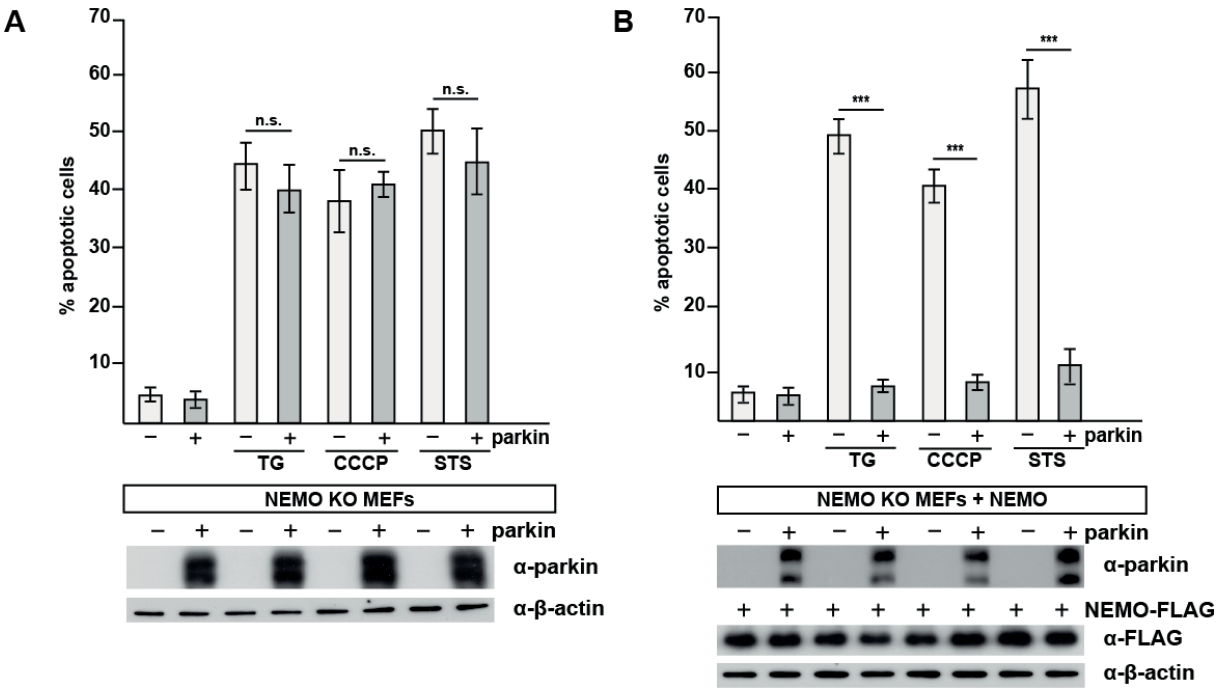

Abbildung 3: NEMO ist essentiell, um die Stress-protektive Aktivität von Parkin zu vermitteln. NEMO-*Knockout*-MEFs (A) und mit Wildtyp-NEMO rekonstituierte NEMO-*Knockout*-MEFs (B) wurden mit unterschiedlichen Stressoren behandelt: mit dem ER-Stressor Thapsigargin (TG, 10 µM, 8 h), dem mitochondrialen Entkoppler CCCP (10 µM, 8 h) oder dem pro-apoptotischen Kinase-Inhibitor Staurosporin (STS, 1 µM, 5 h). Apoptotischer Zelltod wurde durch indirekte Immunfluoreszenz mittels eines Antikörpers gegen aktive Caspase-3 visualisiert. Die Quantifizierung basiert auf Triplikaten von mindestens drei unterschiedlichen Experimenten. Pro Bedingung wurden mindestens 2500 transfizierte Zellen gezählt. Die Expression von Parkin und NEMO wurde mittels Western Blotting überprüft, Aktin diente als Ladekontrolle.

Kürzlich wurde beobachtet, dass eine Modifikation von NEMO durch lineare Ubiquitin-Ketten essentiell ist für die Aktivierung des kanonischen NF-κB-Signalweges (Rahighi et al, 2009; Tokunaga et al, 2009). Diese relativ neu beschriebene Form der Ubiquitinierung wird vermittelt durch LUBAC (*linear ubiquitin assembly complex*), der aus zwei RBR-Proteinen und möglicherweise noch aus anderen Komponenten, wie z.B. dem Adaptorprotein SHARPIN, besteht (Gerlach et al, 2011; Ikeda et al, 2011; Tokunaga et al, 2011). Eine Komponente von LUBAC, nämlich HOIL-1L, weist eine ähnliche modulare Struktur wie Parkin auf, was uns veranlasste, die Aktivität von Parkin hinsichtlich linearer Ubiquitinierung zu untersuchen. Interessanterweise wird NEMO nicht nur linear ubiquitiniert, sondern bindet über seine UBAN-Domäne lineare Ubiquitin-Ketten (Hadian et al, 2011; Rahighi et al, 2009). Daher kann die UBAN-Domäne von NEMO als Sensor für lineare Ubiquitin-Ketten eingesetzt werden. Um einen Einfluss von Parkin auf lineare Ubiquitinierung zu untersuchen, exprimierten wir in HEK293T-Zellen LUBAC mit oder ohne Parkin und versetzten die zellulären Lysate mit der rekombinanten UBAN-Domäne, die N-terminal ein Strep-TagII für eine Affinitätsreinigung aufwies. Nach Behandlung der Lysate mit Strep-Tactin-*Beads* wurden adhärente Proteine einer Affinitätsreinigung unterzogen und mittels Immunoblotting analysiert. Wir konnten beobachten, dass Parkin die Aktivität von LUBAC deutlich steigern kann (Abbildung 4).

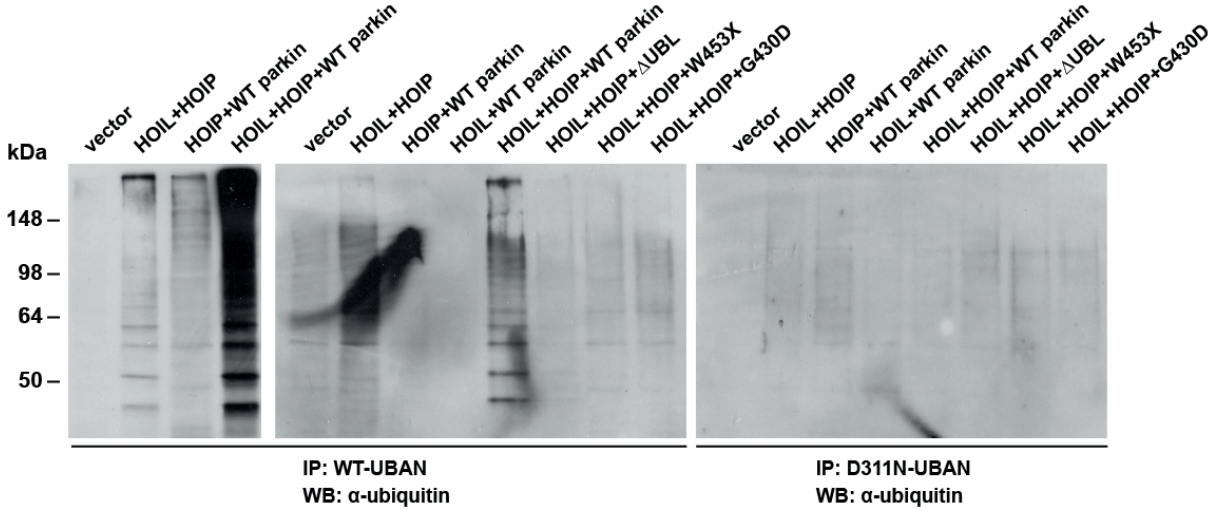

Abbildung 4: Parkin verstärkt die Aktivität von LUBAC. HEK293T-Zellen wurden mit den angegebenen Konstrukten transfiziert, denaturierend lysiert und mit der rekombinanten UBAN-Domäne von NEMO versetzt. Durch Zugabe von Strep-Tactin-*Beads* wurden gebundene Proteine einer Affinitätsreinigung unterzogen. Die Analyse mittels Immunoblotting erfolgte über einen Antikörper gegen Ubiquitin. Die Expression von Wildtyp-Parkin verstärkt die Aktivität des LUBAC deutlich (linkes und mittleres Bild). Wurden die Lysate mit der D311N-UBAN-Mutante versetzt, die nicht in der Lage ist lineare Ketten zu binden, konnte kein Ubiquitin-Signal mittels des Antikörpers detektiert werden (rechtes Bild).

Eine quantitative massenspektrometrische Untersuchung, die in Kollaboration mit der Arbeitsgruppe von Gunnar Dittmar (Max-Delbrück-Zentrum, Berlin) durchgeführt wurde, zeigte, dass Parkin die lineare Ubiquitinierung um den Faktor 3 steigern kann (Abbildung 5). In weiterführenden Experimenten wird nun untersucht, welchen Einfluss Parkin auf LUBAC ausübt, welche Proteine linear modifiziert werden und welche NF-κB-Zielmoleküle die protektive Wirkung von Parkin mediieren.

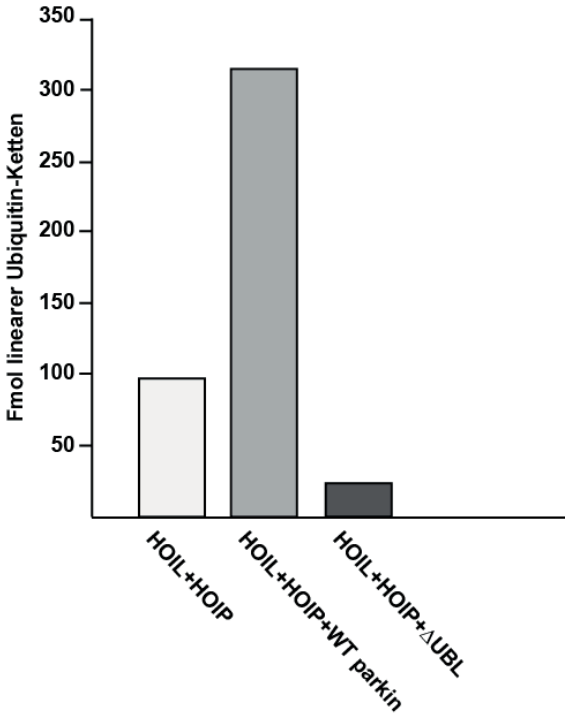

Abbildung 5: Parkin kann das Ausmass der linearen Ubiquitinierung um den Faktor 3 erhöhen. HEK293T-Zellen wurden mit den LUBAC-Komponenten und Wildtyp- bzw. ΔUBL-Parkin transfiziert, denaturierend lysiert und mit der rekombinanten UBAN-Domäne versetzt. Durch Zugabe von Strep-Tactin-*Beads* wurden gebundene Proteine einer Affinitätsreinigung unterzogen. Lineare Ubiquitin-Ketten wurden mittels SRM-basierter Massenspektrometrie analysiert. Die absolute Anzahl linearer Ubiquitin-Ketten wurde durch Isotopen-markierte Peptide (AQUA) bestimmt und auf ein NEMO-Peptid normalisiert, das als Kontrolle für die Pull-down-Effizienz fungierte. Die massenspektrometrische Analyse wurde von Patrick Beaudette und Gunnar Dittmar durchgeführt.

Publikationen

Publikation 1:

Lutz A.K.*, Exner N.*, Fett M.E.*, Schlehe J.S., Kloos K., Lämmermann K., Brunner B., Kurz-Drexler A., Vogel F., Reichert A.S., Bouman L., Vogt-Weisenhorn D., Wurst W., Tatzelt J., Haass C., Winklhofer K.F.

Loss of Parkin or PINK1 function increases Drp1-dependent mitochondrial fragmentation

Journal of Biological Chemistry 2009 Aug 21; 284 (34): 22938-51. Epub 2009 Jun 22.

*gleichberechtigte Erstautoren

Beitrag im Einzelnen:

Etablierung von Bedingungen eines optimalen Parkin- und PINK1-*Knockdowns* in SH-SY5Y–Zellen, Auswertung der mitochondrialen Morphologie mittels Fluoreszenzmikroskopie, Verifizierung der Expressionslevels mittels Immunoblotting, Rescue-Experimente: Ko-Transfektion und Auswertung des Parkin- bzw. PINK1-*Knockdowns* und Parkin-, PINK1-, Mfn2-, OPA1-, Drp1-Konstrukten, Messung des ATP-Gehaltes, Analyse der proteolytischen Prozessierung von OPA1 mittels Immunoblotting, Etablierung eines Drp1-*Knockdowns* in SH-SY5Y Zellen, Durchführung und Auswertung des Apoptoseassays durch indirekte Immunfluoreszenz mittels eines Antikörpers gegen aktive Caspase 3;

Abb. 1, Abb. 2, Abb. 3, Abb. 4, Abb. 6 F;

Publikation 2:

Irrcher I., Aleyasin H., Seifert E.L., Hewitt S.J., Chhabra S., Phillips M., **Lutz A.K.**, Rousseaux M.W., Bevilacqua L., Jahani-Asl A., Callaghan S., Maclaurin J.G., Winklhofer K.F., Rizzu P., Rippstein P., Kim R.H., Chen C.X., Fon E.A., Slack R.S., Harper M.E., McBride H.M., Mak T.W., Park D.S.

Loss of the Parkinson's Disease-linked gene DJ-1 perturbs mitochondrial dynamics. Hum Mol Genet. 2010 Oct 1; 19 (19): 3734-46, Epub 2010 Jul 16.

Beitrag im Einzelnen:
Zellkulturexperimente zum Funktionsverlust von DJ-1 und mitochondrialer Morphologie: Etablierung eines DJ-1 *Knockdowns* in SH-SY5Y-Zellen, Auswertung der mitochondrialen Morphologie, *Rescue*-Experimente mit DJ-1, Parkin und PINK1
Abb. 7 E und F

Publikation 3:

Kamp F.*, Exner N.*, **Lutz A.K.***, Wender N., Hegermann J., Brunner B., Nuscher B., Bartels T., Giese A., Beyer K., Eimer S., Winklhofer K.F., Haass C.
Inhibition of mitochondrial fusion by α-synuclein is rescued by PINK1, Parkin and DJ-1
The EMBO Journal (2010) 29, 3571-3589, Epub 2010 Sep14
* gleichberechtigte Erstautoren

Beitrag im Einzelnen:
Etablierung eines zellulären PEG-Fusionsassays in humanen SH-SY5Y Zellen, Auswertung desselben mittels konfokaler Mikroskopie, Transfektion und Messung des ATP-Gehaltes α-Synuclein-überexprimierender Zellen, Etablierung und fluoreszenzmikroskopische Auswertung eines Doppel-*Knockdowns* von Drp1 und α-Synuclein
Abb. 3, Abb. 4 C, D, Abb. 9 C

Publikation 4:

Butler E.K.*, Voigt A.*, **Lutz A.K.**, Toegel J.P., Gerhardt E., Karsten P., Falkenburger B., Reinartz A., Winklhofer K.F., Schulz J.B.
The Mitochondrial Chaperone Protein TRAP1 mitigates α-Synuclein Toxicity
Plos Genetics, zur Publikation angenommen
*gleichberechtigte Erstautoren

Beitrag im Einzelnen:
Zellkulturexperimente zur α-Synuclein-induzierten Veränderung der mitochondrialen Morphologie: *Rescue* der α-Synuclein-induzierten Veränderung durch TRAP1-Überexpression, Auswertung der mitochondrialen Morphologie, Etablierung

eines TRAP1 *Knockdowns* in SH-SY5Y-Zellen, Auswertung der mitochondrialen Morphologie in TRAP1-defizienen Zellen, die α-Synuclein überexprimieren
Abb. 6 und 7

Publikation 5:

Schlehe J.S., **Lutz A.K.**, Pilsl A., Lämmermann K., Grgur K., Henn I.H., Tatzelt J., Winklhofer K.F.
Aberrant folding of pathogenic parkin mutants: aggregation versus degradation
J. Biol. Chem. 2008 May 16;283(20):13771-9. Epub 2008 Mar 24.

Beitrag im Einzelnen:
Klonierung eines Fusionskonstruktes, Analyse der Detergens-Löslichkeit von Wildtp-, W453X-Parkin und der Parkin-HHARI-Fusionskonstrukte durch Immunoblotting, Auswertung der Apoptoseassays, Ubiquitinierungs-*Assay*
Abb. 1 B, F, Abb. 5 A, C

Publikation 6:

Bouman L., Schlierf A., **Lutz A.K.**, Shan J., Deinlein A., Kast J., Galehdar Z., Palmisano V., Patenge N., Berg D., Gasser T., Augustin R., Trümbach D., Irrcher I., Park D.S., Wurst W., Kilberg M.S., Tatzelt J., Winklhofer K.F.
Parkin is transcriptionally regulated by ATF4: evidence for an interconnection between mitochondrial stress and ER stress
Cell Death Differentiation 2011 May;18 (5): 769-82. Epub 2010 Nov 26.

Beitrag im Einzelnen:
Transfektion und Auswertung des Zelltodes induziert durch ER-Stress oder proteasomale Inhibitoren in humanen SH-SY5Y-Zellen mittels indirekter Immunfluoreszenz, Durchführung der Apoptoseassays in humanen Fibroblasten, Etablierung optimaler Stressbedingungen für ER-Stress-induzierte mitochondriale Fragmentierung, Auswertung mittels Fluoreszenzmikroskopie, Messung des ATP-Gehaltes nach ER-Stress
Abb. 6 A, B, D, Abb. 7 E, Abb. 8

Danksagung

An erster Stelle möchte ich mich ganz herzlich bei PD Dr. Konstanze Winklhofer für die hervorragende wissenschaftliche Betreuung, das Vertrauen in meine experimentellen Fähigkeiten vom ersten Praktikumstag an und die andauernde sowie ansteckende Begeisterung für sämtliche Projekte bedanken.
Danke für immer offene Türen und Ohren auch über den Laboralltag hinaus, die ständige Unterstützung und so manchen Spaß!

Mein Dank gilt Prof. Dr. Jörg Tatzelt für kritische Diskussionsbeiträge, experimentellen Rat und nicht zuletzt für humorvolle Unterhaltungen und stetige Versorgung mit Cola-Brause.

Herrn Prof. Dr. Ulrich Hartl danke ich sehr für die Übernahme des Zweitgutachtens. Herrn Prof. Dr. Martin Biel danke ich für die Übernahme des Vorsitzes meiner Prüfungskommission. Ich bedanke mich bei den Mitgliedern meiner Prüfungskommission PD Dr. Manfred Ogris und Prof. Dr. Wolfgang Frieß.

Allen Kolleginnen und Kollegen des Lehrstuhles für Stoffwechselbiochemie danke ich für die angenehme Arbeitsatmosphäre. Die Coffee-Connection, Daniel Fleck und Matthias Voss, ist an dieser Stelle besonders zu erwähnen.
Explizit bedanken möchte ich mich bei Sabine Odoy für exzellentes Labormanagement und sämtliche Bestellungen, vor allem aber für die extrem kurzfristigen und dringenden!

Ich danke all meinen Kollaborationspartnern, insbesondere Dr. Nicole Exner und Prof. Dr. Christian Haass, für die hervorragende und produktive Zusammenarbeit.

Allen ehemaligen und derzeitigen Mitgliedern der Arbeitsgruppen Winklhofer und Tatzelt danke ich für die tolle Stimmung, Hilfsbereitschaft und stimulierende Diskussionen.
Im Besonderen möchte ich mich bedanken bei:
Julia Schlehe für die kompetente Einarbeitung in den Laboralltag, wovon ich heute noch profitiere; Mareike Fett für die „Fliegenarbeit“; Alexandra Deinlein für gefühlte 100000

gemeinsame Transfektionen und Ubi-Assays, die ich alleine niemals bewältigt hätte; Anna Pilsl für die Herstellung unzähliger Viren und Transduktion verschiedenster Zelllinien; Maria Patra für zuverlässige Hilfe und vor allem Geduld bei sämtlichen „TW" Problemen; Elisa Motori, vi ringrazio per il vostro entusiasmo per i mitocondri e che ci hai portato un po di stile italiano; Carolin Schweimer für das Korrekturlesen dieser Arbeit und grenzenlose Hilfsbereitschaft; Daniela Dirndorfer für unendliche Geduld wenn es darum ging, mir das Klonieren beizubringen; Maria Funke für die Präparation von Neuronen und „Mäusemanagement" sowie das Korrekturlesen; Eva Bentmann für die Einweisung ins konfokale Mikroskopieren, Tipps und Tricks für CLC, Photoshop und Illustrator sowie das Korrekturlesen.
Maria und Eva, vielen Dank für unsere gemeinsamen Unternehmungen, die ich sehr genieße!

Einen besonderen Dank bin ich meinem Biologielehrer Josef Engel schuldig, der meine Begeisterung für die Naturwissenschaften geweckt hat.

Mein größter Dank geht an meine Familie, meine Freunde und meinen Mann Magnus – Ihr seid mein größtes Glück!

Mama, danke für Dein stetiges Interesse und Mitfiebern.

Papa, danke für Deine beruhigende und sachliche Art, die Dinge zu sehen.

Julia, danke für eine wunderbare Freundschaft!

Magnus, danke für Dein Verständnis, Deine Unterstützung und dafür, dass Du immer an meiner Seite bist und so manche Verrücktheit mit mir teilst.

Literaturverzeichnis

Alexander C, Votruba M, Pesch UE, Thiselton DL, Mayer S, Moore A, Rodriguez M, Kellner U, Leo-Kottler B, Auburger G, Bhattacharya SS, Wissinger B (2000) OPA1, encoding a dynamin-related GTPase, is mutated in autosomal dominant optic atrophy linked to chromosome 3q28. *Nature genetics* **26:** 211-215

Anglade P, Vyas S, Javoy-Agid F, Herrero MT, Michel PP, Marquez J, Mouatt-Prigent A, Ruberg M, Hirsch EC, Agid Y (1997) Apoptosis and autophagy in nigral neurons of patients with Parkinson's disease. *Histology and histopathology* **12:** 25-31

Beilina A, Van Der Brug M, Ahmad R, Kesavapany S, Miller DW, Petsko GA, Cookson MR (2005) Mutations in PTEN-induced putative kinase 1 associated with recessive parkinsonism have differential effects on protein stability. *Proceedings of the National Academy of Sciences of the United States of America* **102:** 5703-5708

Bouman L, Schlierf A, Lutz AK, Shan J, Deinlein A, Kast J, Galehdar Z, Palmisano V, Patenge N, Berg D, Gasser T, Augustin R, Trumbach D, Irrcher I, Park DS, Wurst W, Kilberg MS, Tatzelt J, Winklhofer KF (2011) Parkin is transcriptionally regulated by ATF4: evidence for an interconnection between mitochondrial stress and ER stress. *Cell death and differentiation* **18:** 769-782

Canet-Aviles RM, Wilson MA, Miller DW, Ahmad R, McLendon C, Bandyopadhyay S, Baptista MJ, Ringe D, Petsko GA, Cookson MR (2004) The Parkinson's disease protein DJ-1 is neuroprotective due to cysteine-sulfinic acid-driven mitochondrial localization. *Proceedings of the National Academy of Sciences of the United States of America* **101:** 9103-9108

Chartier-Harlin MC, Kachergus J, Roumier C, Mouroux V, Douay X, Lincoln S, Levecque C, Larvor L, Andrieux J, Hulihan M, Waucquier N, Defebvre L, Amouyel P, Farrer M, Destee A (2004) Alpha-synuclein locus duplication as a cause of familial Parkinson's disease. *Lancet* **364:** 1167-1169

Chipuk JE, Moldoveanu T, Llambi F, Parsons MJ, Green DR (2010) The BCL-2 family reunion. *Molecular cell* **37:** 299-310

Cookson MR, Lockhart PJ, McLendon C, O'Farrell C, Schlossmacher M, Farrer MJ (2003) RING finger 1 mutations in Parkin produce altered localization of the protein. *Human molecular genetics* **12:** 2957-2965

Dauer W, Przedborski S (2003) Parkinson's disease: mechanisms and models. *Neuron* **39:** 889-909

Delettre C, Lenaers G, Griffoin JM, Gigarel N, Lorenzo C, Belenguer P, Pelloquin L, Grosgeorge J, Turc-Carel C, Perret E, Astarie-Dequeker C, Lasquellec L, Arnaud B, Ducommun B, Kaplan J, Hamel CP (2000) Nuclear gene OPA1, encoding a mitochondrial dynamin-related protein, is mutated in dominant optic atrophy. *Nature genetics* **26:** 207-210

Detmer SA, Chan DC (2007) Functions and dysfunctions of mitochondrial dynamics. *Nature reviews Molecular cell biology* **8:** 870-879

Eura Y, Ishihara N, Yokota S, Mihara K (2003) Two mitofusin proteins, mammalian homologues of FZO, with distinct functions are both required for mitochondrial fusion. *Journal of biochemistry* **134:** 333-344

Forno LS (1996) Neuropathology of Parkinson's disease. *Journal of neuropathology and experimental neurology* **55:** 259-272

Frank S, Gaume B, Bergmann-Leitner ES, Leitner WW, Robert EG, Catez F, Smith CL, Youle RJ (2001) The role of dynamin-related protein 1, a mediator of mitochondrial fission, in apoptosis. *Developmental cell* **1:** 515-525

Gautheron J, Courtois G (2010) "Without Ub I am nothing": NEMO as a multifunctional player in ubiquitin-mediated control of NF-kappaB activation. *Cellular and molecular life sciences : CMLS* **67:** 3101-3113

Gerlach B, Cordier SM, Schmukle AC, Emmerich CH, Rieser E, Haas TL, Webb AI, Rickard JA, Anderton H, Wong WW, Nachbur U, Gangoda L, Warnken U, Purcell AW, Silke J, Walczak H (2011) Linear ubiquitination prevents inflammation and regulates immune signalling. *Nature* **471:** 591-596

Gilks WP, Abou-Sleiman PM, Gandhi S, Jain S, Singleton A, Lees AJ, Shaw K, Bhatia KP, Bonifati V, Quinn NP, Lynch J, Healy DG, Holton JL, Revesz T, Wood NW (2005) A common LRRK2 mutation in idiopathic Parkinson's disease. *Lancet* **365:** 415-416

Gloire G, Dejardin E, Piette J (2006) Extending the nuclear roles of IkappaB kinase subunits. *Biochemical pharmacology* **72:** 1081-1089

Hadian K, Griesbach RA, Dornauer S, Wanger TM, Nagel D, Metlitzky M, Beisker W, Schmidt-Supprian M, Krappmann D (2011) NF-kappaB essential modulator (NEMO) interaction with linear and lys-63 ubiquitin chains contributes to NF-kappaB activation. *The Journal of biological chemistry* **286:** 26107-26117

Henn IH, Bouman L, Schlehe JS, Schlierf A, Schramm JE, Wegener E, Nakaso K, Culmsee C, Berninger B, Krappmann D, Tatzelt J, Winklhofer KF (2007) Parkin mediates neuroprotection through activation of IkappaB kinase/nuclear factor-kappaB signaling. *The Journal of neuroscience : the official journal of the Society for Neuroscience* **27:** 1868-1878

Henn IH, Gostner JM, Lackner P, Tatzelt J, Winklhofer KF (2005) Pathogenic mutations inactivate parkin by distinct mechanisms. *Journal of neurochemistry* **92:** 114-122

Ikeda F, Deribe YL, Skanland SS, Stieglitz B, Grabbe C, Franz-Wachtel M, van Wijk SJ, Goswami P, Nagy V, Terzic J, Tokunaga F, Androulidaki A, Nakagawa T, Pasparakis M, Iwai K, Sundberg JP, Schaefer L, Rittinger K, Macek B, Dikic I (2011) SHARPIN forms a linear ubiquitin ligase complex regulating NF-kappaB activity and apoptosis. *Nature* **471:** 637-641

Irrcher I, Aleyasin H, Seifert EL, Hewitt SJ, Chhabra S, Phillips M, Lutz AK, Rousseaux MW, Bevilacqua L, Jahani-Asl A, Callaghan S, MacLaurin JG, Winklhofer KF, Rizzu P, Rippstein P, Kim RH, Chen CX, Fon EA, Slack RS, Harper ME, McBride HM, Mak TW, Park DS (2010) Loss of the Parkinson's disease-linked gene DJ-1 perturbs mitochondrial dynamics. *Human molecular genetics* **19:** 3734-3746

Ishihara N, Fujita Y, Oka T, Mihara K (2006) Regulation of mitochondrial morphology through proteolytic cleavage of OPA1. *The EMBO journal* **25:** 2966-2977

Iwai K, Tokunaga F (2009) Linear polyubiquitination: a new regulator of NF-kappaB activation. *EMBO reports* **10:** 706-713

Joazeiro CA, Weissman AM (2000) RING finger proteins: mediators of ubiquitin ligase activity. *Cell* **102:** 549-552

Kamp F, Beyer K (2006) Binding of alpha-synuclein affects the lipid packing in bilayers of small vesicles. *The Journal of biological chemistry* **281:** 9251-9259

Kamp F, Exner N, Lutz AK, Wender N, Hegermann J, Brunner B, Nuscher B, Bartels T, Giese A, Beyer K, Eimer S, Winklhofer KF, Haass C (2010) Inhibition of mitochondrial fusion by alpha-synuclein is rescued by PINK1, Parkin and DJ-1. *The EMBO journal* **29:** 3571-3589

Kirisako T, Kamei K, Murata S, Kato M, Fukumoto H, Kanie M, Sano S, Tokunaga F, Tanaka K, Iwai K (2006) A ubiquitin ligase complex assembles linear polyubiquitin chains. *The EMBO journal* **25:** 4877-4887

Knott AB, Perkins G, Schwarzenbacher R, Bossy-Wetzel E (2008) Mitochondrial fragmentation in neurodegeneration. *Nature reviews Neuroscience* **9:** 505-518

Koshiba T, Detmer SA, Kaiser JT, Chen H, McCaffery JM, Chan DC (2004) Structural basis of mitochondrial tethering by mitofusin complexes. *Science* **305:** 858-862

Kruger R, Kuhn W, Muller T, Woitalla D, Graeber M, Kosel S, Przuntek H, Epplen JT, Schols L, Riess O (1998) Ala30Pro mutation in the gene encoding alpha-synuclein in Parkinson's disease. *Nature genetics* **18:** 106-108

LaVoie MJ, Cortese GP, Ostaszewski BL, Schlossmacher MG (2007) The effects of oxidative stress on parkin and other E3 ligases. *Journal of neurochemistry* **103:** 2354-2368

LaVoie MJ, Ostaszewski BL, Weihofen A, Schlossmacher MG, Selkoe DJ (2005) Dopamine covalently modifies and functionally inactivates parkin. *Nature medicine* **11:** 1214-1221

Lees AJ, Singleton AB (2007) Clinical heterogeneity of ATP13A2 linked disease (Kufor-Rakeb) justifies a PARK designation. *Neurology* **68:** 1553-1554

Legros F, Lombes A, Frachon P, Rojo M (2002) Mitochondrial fusion in human cells is efficient, requires the inner membrane potential, and is mediated by mitofusins. *Molecular biology of the cell* **13:** 4343-4354

Lutz AK, Exner N, Fett ME, Schlehe JS, Kloos K, Lammermann K, Brunner B, Kurz-Drexler A, Vogel F, Reichert AS, Bouman L, Vogt-Weisenhorn D, Wurst W, Tatzelt J, Haass C, Winklhofer KF (2009) Loss of parkin or PINK1 function increases Drp1-dependent mitochondrial fragmentation. *The Journal of biological chemistry* **284:** 22938-22951

Makris C, Godfrey VL, Krahn-Senftleben G, Takahashi T, Roberts JL, Schwarz T, Feng L, Johnson RS, Karin M (2000) Female mice heterozygous for IKK gamma/NEMO deficiencies develop a dermatopathy similar to the human X-linked disorder incontinentia pigmenti. *Molecular cell* **5:** 969-979

Marsden CD (1983) Neuromelanin and Parkinson's disease. *Journal of neural transmission Supplementum* **19:** 121-141

Mitsumoto A, Nakagawa Y, Takeuchi A, Okawa K, Iwamatsu A, Takanezawa Y (2001) Oxidized forms of peroxiredoxins and DJ-1 on two-dimensional gels increased in response to sublethal levels of paraquat. *Free radical research* **35:** 301-310

Mochizuki H, Goto K, Mori H, Mizuno Y (1996) Histochemical detection of apoptosis in Parkinson's disease. *Journal of the neurological sciences* **137:** 120-123

Nakamura K, Nemani VM, Wallender EK, Kaehlcke K, Ott M, Edwards RH (2008) Optical reporters for the conformation of alpha-synuclein reveal a specific interaction with mitochondria. *The Journal of neuroscience : the official journal of the Society for Neuroscience* **28:** 12305-12317

Narendra D, Kane LA, Hauser DN, Fearnley IM, Youle RJ (2010a) p62/SQSTM1 is required for Parkin-induced mitochondrial clustering but not mitophagy; VDAC1 is dispensable for both. *Autophagy* **6:** 1090-1106

Narendra D, Tanaka A, Suen DF, Youle RJ (2008) Parkin is recruited selectively to impaired mitochondria and promotes their autophagy. *The Journal of cell biology* **183:** 795-803

Narendra DP, Jin SM, Tanaka A, Suen DF, Gautier CA, Shen J, Cookson MR, Youle RJ (2010b) PINK1 is selectively stabilized on impaired mitochondria to activate Parkin. *PLoS biology* **8:** e1000298

Olichon A, Elachouri G, Baricault L, Delettre C, Belenguer P, Lenaers G (2007) OPA1 alternate splicing uncouples an evolutionary conserved function in mitochondrial fusion from a vertebrate restricted function in apoptosis. *Cell death and differentiation* **14:** 682-692

Olichon A, Emorine LJ, Descoins E, Pelloquin L, Brichese L, Gas N, Guillou E, Delettre C, Valette A, Hamel CP, Ducommun B, Lenaers G, Belenguer P (2002) The human dynamin-related protein OPA1 is anchored to the mitochondrial inner membrane facing the inter-membrane space. *FEBS letters* **523:** 171-176

Paisan-Ruiz C, Jain S, Evans EW, Gilks WP, Simon J, van der Brug M, Lopez de Munain A, Aparicio S, Gil AM, Khan N, Johnson J, Martinez JR, Nicholl D, Carrera IM, Pena AS, de

Silva R, Lees A, Marti-Masso JF, Perez-Tur J, Wood NW, Singleton AB (2004) Cloning of the gene containing mutations that cause PARK8-linked Parkinson's disease. *Neuron* **44:** 595-600

Pilsl A, Winklhofer KF (2011) Parkin, PINK1 and mitochondrial integrity: emerging concepts of mitochondrial dysfunction in Parkinson's disease. *Acta neuropathologica*

Polymeropoulos MH, Lavedan C, Leroy E, Ide SE, Dehejia A, Dutra A, Pike B, Root H, Rubenstein J, Boyer R, Stenroos ES, Chandrasekharappa S, Athanassiadou A, Papapetropoulos T, Johnson WG, Lazzarini AM, Duvoisin RC, Di Iorio G, Golbe LI, Nussbaum RL (1997) Mutation in the alpha-synuclein gene identified in families with Parkinson's disease. *Science* **276:** 2045-2047

Rahighi S, Ikeda F, Kawasaki M, Akutsu M, Suzuki N, Kato R, Kensche T, Uejima T, Bloor S, Komander D, Randow F, Wakatsuki S, Dikic I (2009) Specific recognition of linear ubiquitin chains by NEMO is important for NF-kappaB activation. *Cell* **136:** 1098-1109

Ramirez A, Heimbach A, Grundemann J, Stiller B, Hampshire D, Cid LP, Goebel I, Mubaidin AF, Wriekat AL, Roeper J, Al-Din A, Hillmer AM, Karsak M, Liss B, Woods CG, Behrens MI, Kubisch C (2006) Hereditary parkinsonism with dementia is caused by mutations in ATP13A2, encoding a lysosomal type 5 P-type ATPase. *Nature genetics* **38:** 1184-1191

Santel A, Frank S, Gaume B, Herrler M, Youle RJ, Fuller MT (2003) Mitofusin-1 protein is a generally expressed mediator of mitochondrial fusion in mammalian cells. *Journal of cell science* **116:** 2763-2774

Santel A, Fuller MT (2001) Control of mitochondrial morphology by a human mitofusin. *Journal of cell science* **114:** 867-874

Schlehe JS, Lutz AK, Pilsl A, Lammermann K, Grgur K, Henn IH, Tatzelt J, Winklhofer KF (2008) Aberrant folding of pathogenic Parkin mutants: aggregation versus degradation. *The Journal of biological chemistry* **283:** 13771-13779

Schmidt-Supprian M, Bloch W, Courtois G, Addicks K, Israel A, Rajewsky K, Pasparakis M (2000) NEMO/IKK gamma-deficient mice model incontinentia pigmenti. *Molecular cell* **5:** 981-992

Schon EA, Przedborski S (2011) Mitochondria: the next (neurode)generation. *Neuron* **70:** 1033-1053

Shavali S, Brown-Borg HM, Ebadi M, Porter J (2008) Mitochondrial localization of alpha-synuclein protein in alpha-synuclein overexpressing cells. *Neuroscience letters* **439:** 125-128

Shin JH, Ko HS, Kang H, Lee Y, Lee YI, Pletinkova O, Troconso JC, Dawson VL, Dawson TM (2011) PARIS (ZNF746) repression of PGC-1alpha contributes to neurodegeneration in Parkinson's disease. *Cell* **144:** 689-702

Silvestri L, Caputo V, Bellacchio E, Atorino L, Dallapiccola B, Valente EM, Casari G (2005) Mitochondrial import and enzymatic activity of PINK1 mutants associated to recessive parkinsonism. *Human molecular genetics* **14:** 3477-3492

Singleton AB, Farrer M, Johnson J, Singleton A, Hague S, Kachergus J, Hulihan M, Peuralinna T, Dutra A, Nussbaum R, Lincoln S, Crawley A, Hanson M, Maraganore D, Adler C, Cookson MR, Muenter M, Baptista M, Miller D, Blancato J, Hardy J, Gwinn-Hardy K (2003) alpha-Synuclein locus triplication causes Parkinson's disease. *Science* **302:** 841

Smirnova E, Griparic L, Shurland DL, van der Bliek AM (2001) Dynamin-related protein Drp1 is required for mitochondrial division in mammalian cells. *Molecular biology of the cell* **12:** 2245-2256

Smirnova E, Shurland DL, Ryazantsev SN, van der Bliek AM (1998) A human dynamin-related protein controls the distribution of mitochondria. *The Journal of cell biology* **143:** 351-358

Spillantini MG, Schmidt ML, Lee VM, Trojanowski JQ, Jakes R, Goedert M (1997) Alpha-synuclein in Lewy bodies. *Nature* **388:** 839-840

Tait SW, Green DR (2010) Mitochondria and cell death: outer membrane permeabilization and beyond. *Nature reviews Molecular cell biology* **11:** 621-632

Tokunaga F, Nakagawa T, Nakahara M, Saeki Y, Taniguchi M, Sakata S, Tanaka K, Nakano H, Iwai K (2011) SHARPIN is a component of the NF-kappaB-activating linear ubiquitin chain assembly complex. *Nature* **471:** 633-636

Tokunaga F, Sakata S, Saeki Y, Satomi Y, Kirisako T, Kamei K, Nakagawa T, Kato M, Murata S, Yamaoka S, Yamamoto M, Akira S, Takao T, Tanaka K, Iwai K (2009) Involvement of linear polyubiquitylation of NEMO in NF-kappaB activation. *Nature cell biology* **11:** 123-132

Valente EM, Abou-Sleiman PM, Caputo V, Muqit MM, Harvey K, Gispert S, Ali Z, Del Turco D, Bentivoglio AR, Healy DG, Albanese A, Nussbaum R, Gonzalez-Maldonado R, Deller T, Salvi S, Cortelli P, Gilks WP, Latchman DS, Harvey RJ, Dallapiccola B, Auburger G, Wood NW (2004a) Hereditary early-onset Parkinson's disease caused by mutations in PINK1. *Science* **304:** 1158-1160

Valente EM, Salvi S, Ialongo T, Marongiu R, Elia AE, Caputo V, Romito L, Albanese A, Dallapiccola B, Bentivoglio AR (2004b) PINK1 mutations are associated with sporadic early-onset parkinsonism. *Annals of neurology* **56:** 336-341

Vekrellis K, Xilouri M, Emmanouilidou E, Rideout HJ, Stefanis L (2011) Pathological roles of alpha-synuclein in neurological disorders. *Lancet neurology* **10:** 1015-1025

Westermann B (2010) Mitochondrial fusion and fission in cell life and death. *Nature reviews Molecular cell biology* **11:** 872-884

Winklhofer KF, Henn IH, Kay-Jackson PC, Heller U, Tatzelt J (2003) Inactivation of parkin by oxidative stress and C-terminal truncations: a protective role of molecular chaperones. *The Journal of biological chemistry* **278:** 47199-47208

Zarranz JJ, Alegre J, Gomez-Esteban JC, Lezcano E, Ros R, Ampuero I, Vidal L, Hoenicka J, Rodriguez O, Atares B, Llorens V, Gomez Tortosa E, del Ser T, Munoz DG, de Yebenes JG (2004) The new mutation, E46K, of alpha-synuclein causes Parkinson and Lewy body dementia. *Annals of neurology* **55:** 164-173

Zuchner S, Mersiyanova IV, Muglia M, Bissar-Tadmouri N, Rochelle J, Dadali EL, Zappia M, Nelis E, Patitucci A, Senderek J, Parman Y, Evgrafov O, Jonghe PD, Takahashi Y, Tsuji S, Pericak-Vance MA, Quattrone A, Battaloglu E, Polyakov AV, Timmerman V, Schroder JM, Vance JM (2004) Mutations in the mitochondrial GTPase mitofusin 2 cause Charcot-Marie-Tooth neuropathy type 2A. *Nature genetics* **36:** 449-451

THE JOURNAL OF BIOLOGICAL CHEMISTRY VOL. 284, NO. 34, pp. 22938–22951, August 21, 2009

Loss of Parkin or PINK1 Function Increases Drp1-dependent Mitochondrial Fragmentation*[S]

Received for publication, June 19, 2009 Published, JBC Papers in Press, June 22, 2009, DOI 10.1074/jbc.M109.035774

A. Kathrin Lutz[‡1], Nicole Exner[§1], Mareike E. Fett[‡1], Julia S. Schlehe[‡], Karina Kloos[¶], Kerstin Lämmermann[‡], Bettina Brunner[§], Annerose Kurz-Drexler[¶], Frank Vogel[‖], Andreas S. Reichert[**], Lena Bouman[‡], Daniela Vogt-Weisenhorn[¶], Wolfgang Wurst[¶], Jörg Tatzelt[‡], Christian Haass[§], and Konstanze F. Winklhofer[‡2]

*From [‡]Neurobiochemistry and [§]Biochemistry, Deutsches Zentrum für Neurodegenerative Erkrankungen and Adolf Butenandt Institute, Ludwig Maximilians University, 80336 Munich, [¶]Helmholtz Center Munich, Institute of Developmental Genetics, Technical University Munich and Deutsches Zentrum für Neurodegenerative Erkrankungen and [‖]Max-Delbrück-Center for Molecular Medicine, 13092 Berlin, and **CEF Macromolecular Complexes, Mitochondrial Biology, Goethe University, 60590 Frankfurt am Main, Germany*

Loss-of-function mutations in the parkin gene (PARK2) and PINK1 gene (PARK6) are associated with autosomal recessive parkinsonism. PINK1 deficiency was recently linked to mitochondrial pathology in human cells and *Drosophila melanogaster*, which can be rescued by parkin, suggesting that both genes play a role in maintaining mitochondrial integrity. Here we demonstrate that an acute down-regulation of parkin in human SH-SY5Y cells severely affects mitochondrial morphology and function, a phenotype comparable with that induced by PINK1 deficiency. Alterations in both mitochondrial morphology and ATP production caused by either parkin or PINK1 loss of function could be rescued by the mitochondrial fusion proteins Mfn2 and OPA1 or by a dominant negative mutant of the fission protein Drp1. Both parkin and PINK1 were able to suppress mitochondrial fragmentation induced by Drp1. Moreover, in Drp1-deficient cells the parkin/PINK1 knockdown phenotype did not occur, indicating that mitochondrial alterations observed in parkin- or PINK1-deficient cells are associated with an increase in mitochondrial fission. Notably, mitochondrial fragmentation is an early phenomenon upon PINK1/parkin silencing that also occurs in primary mouse neurons and *Drosophila* S2 cells. We propose that the discrepant findings in adult flies can be explained by the time of phenotype analysis and suggest that in mammals different strategies may have evolved to cope with dysfunctional mitochondria.

Many lines of evidence suggest that mitochondrial dysfunction plays a central role in the pathogenesis of Parkinson disease, starting from the early observation that the complex I inhibitor 1-methyl-4-phenyl-1,2,3,6-tetrahydropyridine induced acute and irreversible parkinsonism in young drug addicts (for review, see Refs. 1–3). In support of a crucial role of mitochondria in Parkinson disease, several Parkinson disease-associated gene products directly or indirectly impinge on mitochondrial integrity (for review, see Refs. 4–6). A clear link between Parkinson disease genes and mitochondria has recently emerged from studies on PINK1 (PTEN-induced putative kinase 1), a mitochondrial serine/threonine kinase, and parkin, a cytosolic E3 ubiquitin ligase. *Drosophila* parkin null mutants displayed reduced life span, male sterility, and locomotor defects due to apoptotic flight muscle degeneration (7). The earliest manifestation of muscle degeneration and defective spermatogenesis was mitochondrial pathology, exemplified by swollen mitochondria and disintegrated cristae. Remarkably, *Drosophila* PINK1 null mutants shared marked phenotypic similarities with parkin mutants, and parkin could compensate for the PINK1 loss-of-function phenotype but not vice versa, leading to the conclusion that PINK1 and parkin function in a common genetic pathway with parkin acting downstream of PINK1 (8–10). We recently demonstrated that PINK1 deficiency in cultured human cells causes alterations in mitochondrial morphology, which can be rescued by wild type parkin but not by pathogenic parkin mutants (11). We now present evidence that parkin plays an essential role in maintaining mitochondrial integrity. RNAi[3]-mediated knockdown of parkin increases mitochondrial fragmentation and decreases cellular ATP production. Notably, mitochondrial fragmentation induced by PINK1/parkin deficiency is observed not only in human neuroblastoma cells but also in primary mouse neurons and insect S2 cells. Alterations in mitochondrial morphology are early manifestations of parkin/PINK1 silencing that are not caused by an increase in apoptosis. The mitochondrial phenotype observed in parkin- or PINK1-deficient cells can morphologically and functionally be rescued by the increased expression of a dominant negative mutant of the fission-promoting protein Drp1. Moreover, manifestation of the PINK1/parkin knockdown phenotype is dependent on Drp1 expression, indi-

* This work was supported by the Deutsche Forschungsgemeinschaft (SFB 596 and CEF Macromolecular Complexes), German Ministry for Education and Research (Nationales Genomforschungsnetz plus "Functional Genomics of Parkinson's Disease"), the Helmholtz Alliance Alliance "Mental Health in an Ageing Society," the Virtual Institute of "Neurodegeneration and Ageing," the Center for Integrated Protein Science Munich, and the Hans and Ilse Breuer Foundation.
[S] The on-line version of this article (available at http://www.jbc.org) contains supplemental Figs. 1–3.
[1] These authors contributed equally to this work.
[2] To whom correspondence should be addressed: Schillerstr. 44, D-80336 Munich, Germany. Tel.: 49-89-2180-75483; Fax: 49-89-2180-75415; E-mail: Konstanze.Winklhofer@med.uni-muenchen.de.

[3] The abbreviations used are: RNAi, RNA interference; pAb, polyclonal antibody; mAb, monoclonal antibody; $DiOC_6(3)$, 3,3′-dihexyloxacarbocyanine iodide; siRNA, small interfering RNA; EYFP, enhanced yellow fluorescent protein; DAPI, 4′,6-diamidino-2-phenylindole; TUNEL, TdT-mediated dUTP nick end labeling; shRNA, short hairpin RNA; dsRNA, double-stranded RNA.

cating that an acute loss of parkin or PINK1 function increases mitochondrial fission.

EXPERIMENTAL PROCEDURES

Antibodies and Reagents—The following antibodies were used: anti-parkin rabbit polyclonal antibody (pAb) hP1 (12), anti-parkin mouse monoclonal antibody (mAb) PRK8 (Millipore, Schwalbach, Germany), anti-parkin polyclonal antibody 2132 (Cell Signaling, Danvers, MA), anti-FLAG M2 mAb (Sigma), anti-FLAG M2 horseradish peroxidase mAb (Sigma), anti-β-actin mAb (Sigma), anti-Drp1 mAb (BD Transduction Laboratories), anti-Mfn2 pAb (Sigma), anti-OPA1 pAb (13), anti-PINK1 pAB (Novus Biologicals, Hamburg, Germany), penta-His horseradish peroxidase conjugate mouse IgG (Qiagen, Hilden, Germany), horseradish peroxidase-conjugated anti-mouse and anti-rabbit IgG antibody (Promega, Mannheim, Germany), anti-active caspase-3 pAb (Promega), anti-V5 mAb (Invitrogen), cyanine 3 (Cy3)-conjugated anti-rabbit IgG antibody (Dianova, Hamburg, Germany), anti-neuron specific β III Tubulin rabbit-pAb (Abcam, Cambridge, UK), and Cy™ 3-conjugated Affinity Pure Donkey anti-rabbit IgG (heavy and light chain) (Jackson ImmunoResearch, Newmarket, Suffolk, UK). Staurosporine, rotenone, cycloheximide, and carbonyl cyanide 3-chlorophenylhydrazone were purchased from Sigma, complete protease inhibitor mixture was from Roche Applied Science, and 3,3′-dihexyloxacarbocyanine iodide ($DiOC_6(3)$), and MitoTracker Red CMXRos was from Invitrogen.

DNA Constructs—The following constructs were described previously: wild type human parkin, W453X, R42P, G430D, Δ1–79 parkin mutant (12, 14, 15), PINK1-V5 and PINK1-G309D-V5 (11), Mfn2-His_6, OPA1-MycHis, Drp1-EYFP, Drp1(K38E)-ECFP (16, 17), and Bcl-2-FLAG (18). Mfn2 containing a C-terminal FLAG tag was subcloned into pcDNA3.1/Zeo (+) (Invitrogen). Drp1 was subcloned into the pCMV-Tag 2B (Stratagene, Amsterdam, Netherlands) vector adding an N-terminal FLAG tag. mCherry (19) was subcloned into the pCS2+ vector. For the generation of small interfering RNA (siRNA)-resistant wild type parkin, four silent mutations were introduced into the siRNA target sequence by PCR. The plasmid encoding enhanced yellow fluorescent protein (EYFP) was purchased from Clontech (Mountainview, CA).

Lentiviruses—The sequence of the PINK1 shRNA 5′-GCG GTA ATT GAC TAC AGC AAA-3′, which corresponds to nucleotides 1353–1373 of the PINK1 gene, was cloned into the pLL3.7 vector via the HpaI and XhoI cloning sites. The shRNA is driven by a U6 promotor. The green fluorescent protein portion of the pLL3.7 vector was exchanged by cloning a cytomegalovirus-driven mito-EYFP (pEYFP-mito, Clontech) into the NheI and EcoRI site. As a control virus we used the same virus without the PINK1 shRNA sequence. Lentiviruses were produced in HEK293T cells as described by Consiglio *et al.* (20). The titer of the viruses ranged from 4×10^8 to 1×10^9 colony-forming units/ml. The infection efficiency of primary neurons was not affected by different titers. shRNAs were designed using the pSico-Oligomaker 1.5 (developed by A. Ventura). Conditional knockdowns were generated by cloning shRNAs into pSico as described previously (21).

Cell Culture, Transfection, and RNA Interference—SH-SY5Y (DSMZ number ACC 209) cells were transfected with Lipofectamine Plus (Invitrogen) according to the manufacturer's instructions. *Drosophila* S2 cells were cultivated in Schneider's *Drosophila* medium (Invitrogen) supplemented with 10% heat-inactivated fetal calf serum (Sigma) and maintained at 26 °C. Transfection of S2 cells was performed in 12-well plates in serum-free medium with 5 μg of dsRNA. Serum-containing medium was added 45 min after transfection. For RNA interference, SH-SY5Y cells were reverse-transfected with Stealth siRNA (Invitrogen) using Lipofectamine RNAiMAX (Invitrogen). For each target gene at least two different effective siRNAs were used. For RNAi treatment of *Drosophila* S2 cells, the following clones from the *Drosophila* Genomics Resource Center (Bloomington, IN) were used: parkin (SD01679) and PINK1 (GH20931). They served as templates for T7-tagged primers, which were designed by a program for the *de novo* design of long dsRNAs (E-RNAi Webservice, German Cancer Research Center): T7-parkin forward primer, 5′-taa tac gac tca cta tag ggC TGT TGA CAC GCG AGG AGT A-3′, and T7-parkin reverse primer, 5′-taa tac gac tca cta tag ggA TTT TGG ACA GGG CTT TGT G-3′; T7-PINK1 forward primer, 5′- taa tac gac tca cta tag ggG CCA TGT ACA AGG AGA CGG T-3′, and PINK1 reverse primer, 5′-taa tac gac tca cta tag ggA TTG AGT ACG GCA AAC GGA C-3′. After synthesis of T7-cDNA templates by PCR, the Ambion Megascript RNA synthesis kit (Austin, TX) was used to generate dsRNA.

Preparation, Transduction, and Analysis of Primary Mouse Hippocampal Neurons—Hippocampi of C57/BL6 mice from two different litters were prepared at embryonic stage E15.5 and transferred to dissection medium (48.8 ml of Hanks' balanced salt solution (Invitrogen), 500 μl of HEPES (1 M, Invitrogen), 600 μl of $MgSO_4$ (1 M), and 500 μl of penicillin/streptomycin (100×, Invitrogen)). Tissue was washed with prewarmed trypsin 0.05% with EDTA (Invitrogen) 2 times, trypsinated for 15 min at 37 °C, and thereafter washed 3 times in culture medium (48 ml of Neurobasal (Invitrogen), 1 ml of B-27 (Invitrogen), 500 μl of L-glutamine (Invitrogen), and 500 μl of penicillin/streptomycin (100×)). Cells were dispersed with a fire-polished tip of a Pasteur pipette. 40×10^3 cells were cultivated on poly-D-lysine-coated coverslips in 24-well plates. On day 4 cells were infected with lentiviruses. Three days after infection cells were fixed in 4% paraformaldehyde for 10 min. Neurons were detected by immunocytochemistry using anti-neuron-specific β III tubulin rabbit pAB (Abcam) as primary antibody and Cy™ 3-conjugated affinity pure donkey anti-rabbit IgG (H+L) as secondary antibody (Jackson ImmunoResearch). Pictures were acquired using confocal microscopy (LSM 510, Carl Zeiss, Göttingen, Germany) to analyze the length of mitochondria in soma and processes. For quantification of mitochondrial lengths, a specified analysis software (Axiovision 4.7, Carl Zeiss) was used. Classification of mitochondria was done as follows: fragmented mitochondria (<0.5 μm), intermediate mitochondria (0.5–5 μm), and tubular mitochondria (>5 μm).

Quantitative RT-PCR—For the analysis of parkin or PINK 1 knockdown efficiencies, quantitative real-time PCR was performed. Total cellular RNA from human SH-SY5Y and *Dro-*

sophila S2 cells was isolated at the time indicated and treated with DNase I (RNeasy mini kit; Qiagen). cDNA was synthesized from 1 mg of total RNA using a High-Capacity cDNA reverse transcription kit (Applied Biosystems, Foster City, CA). For human SH-SY5Y cells, RT-PCR was performed with 2× TaqMan Universal PCR Master Mix and TaqMan Gene expression assay (parkin: Hs00247755_m1, PINK1: Hs02330592_s1; Applied Biosystems). For *Drosophila* S2 cells RT-PCR was performed with 2× Power SYBR Green PCR Master Mix (Applied Biosystems) and 1 μM concentrations of each primer pair (S2 parkin forward primer, 5′-AGC CTC CAA GCC TCT AAA TG-3′; S2 parkin reverse primer, 5′-CAC GGA CTC TTT CTT CAT CG-3′; S2 PINK1 forward primer, 5′-GCT TTC CCC TAC CCT CCA C-3′; S2 PINK1 reverse primer, 5′-GCA CTA-CAT TGA CCA CCG ATT-3′; S2 Rp49 forward primer, 5′-CCA AGC ACT TCA TCC GCC ACC-3′; S2 Rp49 reverse primer, 5′-GCG GGT GCG CTT GTT CGA TCC-3′) (22). Quantification was performed with 7500 Fast Real Time PCR System (Applied Biosystems). Triplicates were performed with each primer set for each RNA sample. RNA expression was normalized with respect to an endogenous reference gene; β-actin for SH-SY5Y cells and Rp49 for S2 cells, respectively. Relative expression was calculated for each gene using the delta delta cycle threshold method. For quantification of the knockdown efficiency in primary neuronal cultures, cells were prepared and cultivated as described above and lysed directly on the plate according to the manual of the RNeasy mini kit (Qiagen). cDNA was transcribed using cDNA reverse transcription kit (Applied Biosystems). Quantitative PCR was performed with the TaqMan expression assay (PINK1 mouse: 4m00550827_m1) with β-actin as an internal control.

Western Blotting—SDS-PAGE and Western blotting was described previously (14). Antigens were detected with the enhanced chemiluminescence (ECL) detection system (Amersham Biosciences) or the Immobilon Western chemiluminescent horseradish peroxidase substrate (Millipore).

Fluorescent Staining of Mitochondria—SH-SY5Y cells were grown on 15-mm glass coverslips, and S2 cells were grown on coverslips coated with concanavalin A (Sigma). Cells were fluorescently labeled with either 0.1 μM DiOC6(3) or 0.05 μM MitoTracker Red CMXRos in cell culture medium for 15 min. After washing coverslips with medium, living cells were analyzed for mitochondrial morphology by fluorescence microscopy as described previously (11, 13) using a Leica DMRB microscope (Leica, Wetzlar, Germany). Cells were categorized in either two or three classes according to their mitochondrial morphology: tubular, fragmented, or highly connected. Cells displaying an intact network of tubular mitochondria were classified as tubular. When this network was disrupted and mitochondria appeared predominantly spherical or rod-like, they were classified as fragmented. Cells with considerably elongated mitochondria that were more interconnected were classified as highly connected. The mitochondrial morphology of at least 300 cells per plate was determined in a blinded manner, *i.e.* the researcher was blind to transfection status. Quantifications were based on triplicates of at least three (SH-SY5Y cells) or two (S2 cells) independent experiments.

Measurement of Cellular ATP Levels—Cellular steady state ATP levels were measured using the ATP Bioluminescence assay kit HS II (Roche Applied Science) according to the manufacturer's instructions. SH-SY5Y cells were reversely transfected with the indicated siRNAs and/or DNA constructs. 24 h before harvesting cells, the culture medium was replaced by medium containing 3 mM glucose. Cells were washed twice with phosphate-buffered saline, scraped off the plate, and lysed according to the provided protocol. Bioluminescence of the samples was determined using an LB96V luminometer (Berthold Technologies), analyzed with WinGlow Software (Berthold Technologies), and normalized to total protein levels. Each transfection was performed at least in triplicate, and all experiments were repeated at least three times.

Apoptosis Assays—For detection of apoptotic cells the ApopTag Fluorescein Direct *in Situ* Apoptosis detection kit (Chemicon, Temecula, CA) was used according to the manufacturer's protocol. Briefly, SH-SY5Y/S2 cells were grown on glass coverslips. At days 1, 2, 3, and 4 after siRNA/dsRNA transfection the positive controls were incubated with staurosporine (1 μM, SH-SY5Y cells) or cycloheximide (10 μM, S2 cells) for 4 and 6 h, respectively. The cells were fixed with 1% paraformaldehyde for 10 min at room temperature, permeabilized with a 2:1 mixture of ethanol and acetic acid for 5 min at −20 °C, and equilibrated with the supplied buffer. Fixed cells were incubated with Working Strength TdT enzyme in a humidified chamber for 1 h at 37 °C in the dark. After washing with Working Strength Stop/Wash buffer (Chemicon, Temecula, CA) for 10 min at room temperature cells were mounted onto glass coverslides using FluorSave Reagent (Calbiochem/Merck KGaA). Nuclei were stained using 4′,6-diamidino-2-phenylindole (DAPI). To detect cells undergoing apoptosis, the number of TdT-mediated dUTP nick end labeling (TUNEL)-positive cells of at least 300 DAPI-stained cells was determined using a Zeiss Axioscope 2 plus microscope (Carl Zeiss). Quantifications were based on at least three independent experiments. Activation of caspase-3 was determined as described previously (18, 23). Briefly, SH-SY5Y cells were grown on glass coverslips. 3 days after transfection cells were incubated with rotenone (10 μM, 3 h) as a positive control. The cells were then fixed, and activated caspase-3 was detected by indirect immunofluorescence. Nuclei were stained with DAPI, and caspase-3-positive cells were quantified as outlined above.

Statistical Analyses—For cell culture experiments, data are expressed as the means ± S.E. Experiments were performed in triplicate and repeated at least three times. Statistical analysis was carried out using analysis of variance; *, $p \leq 0.05$; **, $p \leq 0.01$; ***, $p \leq 0.001$. For primary mouse hippocampal neurons, data are expressed as the means ± S.E. Statistical analysis of the mitochondrial lengths were carried out using analysis of variance. The statistical analysis of the fragmented and intermediate mitochondria were analyzed via analysis of variance, whereas the *p* values of tubular mitochondria were calculated via Fisher's Exact Test. *, $p \leq 0.05$; **, $p \leq 0.01$; ***, $p \leq 0.001$.

RESULTS

Down-regulation of Parkin Induces Fragmentation of the Mitochondrial Network—We recently reported that RNAi-mediated down-regulation of PINK1 in cultured human cells

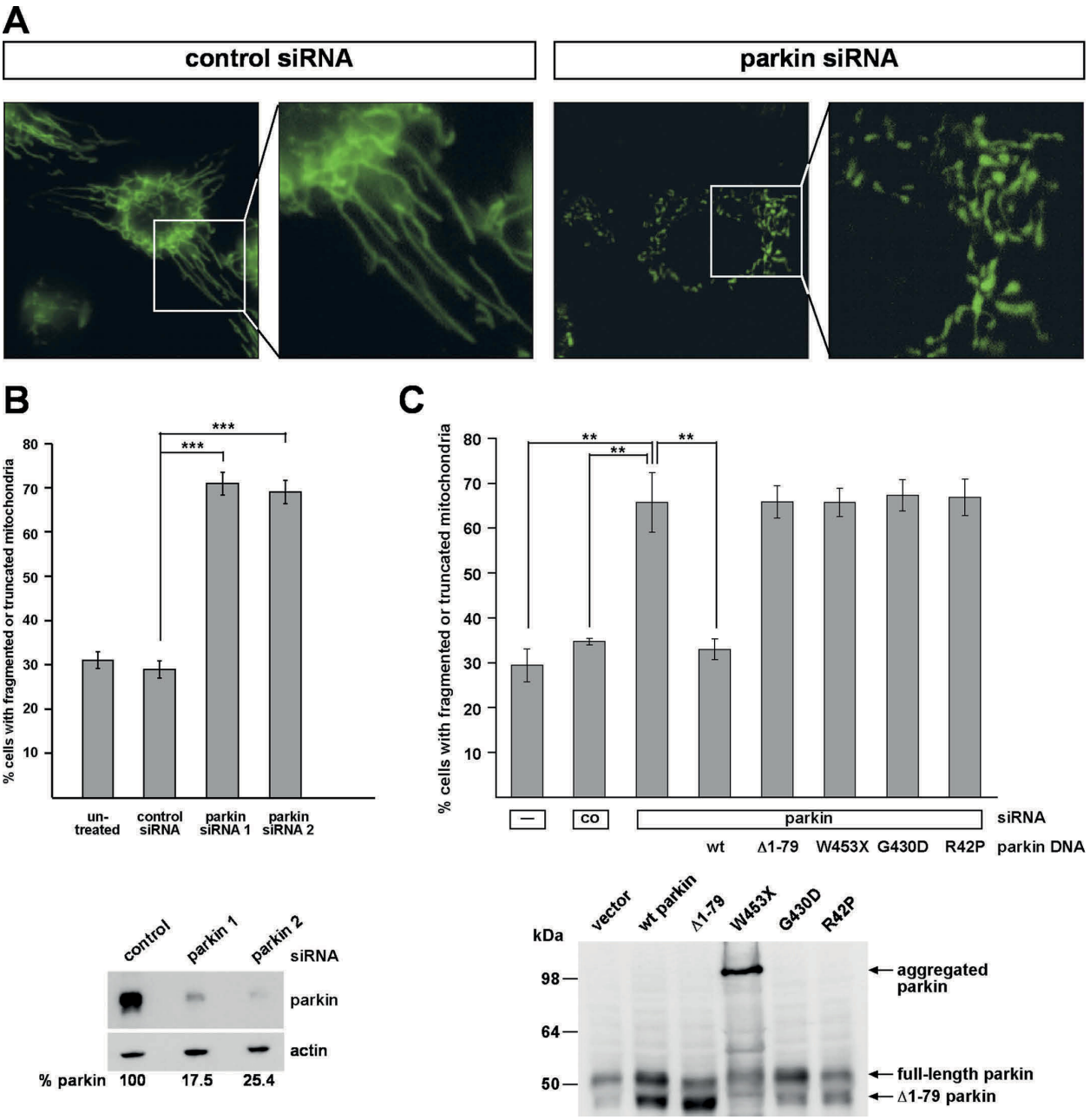

FIGURE 1. **Down-regulation of parkin by RNAi leads to alterations in mitochondrial morphology.** *A* and *B*, SH-SY5Y cells transfected with control siRNA or siRNA targeting parkin were stained with the fluorescent dye $DiOC_6(3)$ to visualize mitochondria and analyzed by fluorescence microscopy. The analysis was performed 3 days after transfection. Cells displaying an intact network of tubular mitochondria were classified as tubular. When this network was disrupted and mitochondria appeared predominantly spherical or rod-like, they were classified as fragmented. *B*, for quantification, the mitochondrial morphology of at least 300 cells per plate was determined in a blinded manner. Quantifications were based on triplicates of at least three independent experiments. Shown is the percentage of cells with fragmented or truncated mitochondria. *Lower panel*, the efficiency of parkin knockdown is shown by Western blotting using the monoclonal anti-parkin antibody PRK8. β-Actin was used as a loading control. *C*, SH-SY5Y cells were transfected with parkin-specific siRNA and either siRNA-resistant wild type (*wt*) parkin, Δ1–79, W453X, G430D, or R42P mutant parkin. The cells were analyzed by fluorescence microscopy as described under *A*. *Lower panel*, expression of parkin or parkin mutants was analyzed by Western blotting using the monoclonal anti-parkin antibody PRK8. Please note that the overexpression of parkin gives rise to two parkin species, full-length parkin of 52 kDa and a smaller parkin species of about 42 kDa, due to the usage of the second translation initiation site (15).

results in abnormal mitochondrial morphology, which can be rescued by the enhanced expression of parkin (11). To address a possible role of parkin in mitochondrial integrity, we performed life cell imaging by fluorescence microscopy in human SH-SY5Y cells after siRNA-mediated down-regulation of parkin. Under physiological conditions, the majority of the cells (about 70%) showed a network of tubular mitochondria, which is in line with previous reports (24–26). Upon knockdown of

parkin, the percentage of cells with truncated or fragmented mitochondria significantly increased from about 30% in control siRNA-treated cells up to 70% (Fig. 1, *A* and *B*). This alteration in mitochondrial morphology also occurred when a second parkin-specific siRNA was used (Fig. 1*B*) and could be prevented by the co-transfection of siRNA-resistant wild type parkin (Fig. 1*C*), demonstrating the specificity of the effects observed. The pathogenic parkin mutants W453X, G430D, and R42P did not

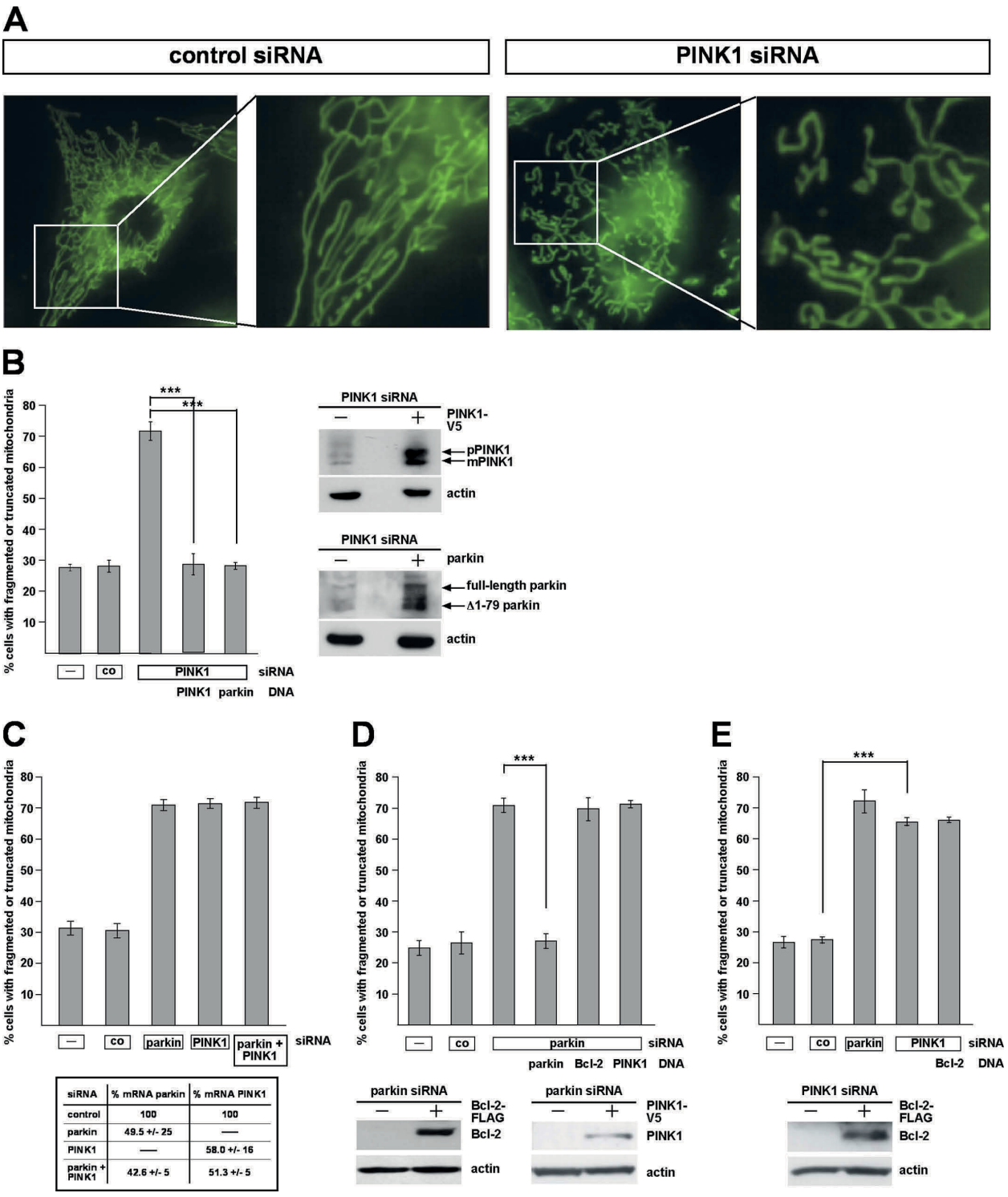

show rescue activity (Fig. 1*C*). Notably, the Δ1–79 parkin mutant, which lacks the N-terminal ubiquitin-like domain and is generated *in vivo* due to the presence of an internal translation initiation site at codon 80 (15), could not compensate for the mitochondrial phenotype observed in parkin-deficient cells. The Δ1–79 mutant has been reported previously to be impaired in its neuroprotective capacity and ubiquitylation activity (14, 27). These results indicate that an acute loss of parkin function significantly affects mitochondrial morphology.

Alterations in Mitochondrial Morphology and Cellular ATP Production Caused by Parkin or PINK1 Deficiency Can Be Rescued by Mfn2, OPA1, or Dominant Negative Drp1—In our previous study we used HeLa cells to assess the effects of PINK1 on mitochondrial morphology. HeLa cells do not express parkin due to the localization of the parkin gene within FRA6E (6q26), a common fragile site of the human genome that is frequently mutated in ovarian tumors (28). To compare the effects of parkin and PINK1 on mitochondria, we treated SH-SY5Y cells with PINK1-specific siRNA. The effects on mitochondrial morphology induced by PINK1 deficiency were comparable with those observed in HeLa cells. Moreover, PINK1-deficient SH-SY5Y displayed qualitative and quantitative alterations similar to parkin-deficient SH-SY5Y cells, *i.e.* a significant increase in the percentage of cells with truncated or fragmented mitochondria (Fig. 2, *A* and *B*). Consistent with the data from *Drosophila melanogaster*, we observed that parkin rescues the mitochondrial pathology in PINK1-deficient cells (Fig. 2*B*), whereas enhanced PINK1 expression cannot compensate for the parkin knockdown phenotype (Fig. 2*D*). Also in line with the fly model, a simultaneous down-regulation of parkin and PINK1 did not enhance alterations in mitochondrial morphology observed in a single parkin or PINK1 knockdown (Fig. 2*C*). As no anti-PINK1 antibody is available to detect endogenous PINK1 in SH-SY5Y cells (29, 30), we verified the PINK1 knockdown efficiencies by real-time PCR (Fig. 2*C*, *lower panel*). Based on the observation that Bcl-2 suppressed the mitochondrial phenotype in PINK1 null *Drosophila* mutants (9), we tested a possible effect of Bcl-2 in our model. However, overexpression of Bcl-2 had no effect on the mitochondrial morphology in parkin- or PINK1-deficient human cells (Fig. 2, *D* and *E*), suggesting that the increase in mitochondrial fragmentation was not a consequence of apoptosis (see also Fig. 6).

The increased percentage of cells with fragmented mitochondria observed in parkin- or PINK1-deficient cells prompted us to address the question of whether mitochondrial dynamics might be perturbed by a loss of parkin or PINK1 function. Overexpression of Mfn2, which mediates mitochondrial outer membrane fusion, or OPA1, implicated in inner membrane fusion, prevented the changes in mitochondrial morphology induced by parkin or PINK1 knockdown (Fig. 3, *A* and *B*, and supplemental Fig. 1). In line with these observations, overexpression of a dominant negative mutant of the fission-promoting GTPase Drp1 (Drp1 K38E) fully reverted the morphological mitochondrial alterations in parkin- or PINK1-deficient cells (Fig. 3, *C* and *D*, and supplemental Fig. 1). To test whether manipulating mitochondrial dynamics might have an impact on mitochondrial function in parkin- or PINK1-deficient cells, we determined steady state cellular ATP levels. ATP levels were significantly decreased in parkin-deficient cells (to 66.3 ± 4.7%) and PINK-deficient cells (to 70.9 ± 6.9%; Fig. 3*E*). Co-transfection of siRNA-resistant parkin or PINK1 prevented ATP depletion in parkin- or PINK1-deficient cells, confirming specificity of the observed effects (Fig. 3*E*). Consistent with the effect on mitochondrial morphology, parkin could compensate for the impaired ATP production caused by PINK1 silencing (Fig. 3*E*). Remarkably, increased expression of Drp1 K38E, Mfn2, or OPA1 also prevented the drop in ATP production caused by parkin or PINK1 depletion (Fig. 3, *F* and *G*). Collectively, these results indicate that the morphological alterations in parkin- and PINK1-deficient cells are functionally relevant.

Manifestation of the Parkin/PINK1 Knockdown Phenotype Is Dependent on Drp1 Expression—Our observations suggested that a loss of parkin or PINK1 function is associated with an imbalance in the fusion-to-fission rate. However, it remained unclear whether the mitochondrial phenotype was a consequence of reduced fusion or increased fission activity. To address this question experimentally, we first analyzed whether processing of OPA1 is altered under parkin or PINK1 knockdown conditions. The dynamin family GTPase OPA1 is a key player in promoting mitochondrial inner membrane fusion and regulating cristae morphology. Because of extensive alternative splicing and posttranslational proteolytic processing of OPA1, several isoforms are generated in mammalian cells. Recent studies revealed that OPA1 processing is implicated in the regulation of OPA1 function (13, 31, 32). It has been proposed that increased proteolytic processing of OPA1 large to small isoforms in energetically compromised mitochondria reduces the fusion-promoting activity of OPA1 (13). The pattern of endogenous OPA1 isoforms in parkin or PINK1 knockdown cells was analyzed by Western blotting. The mitochondrial uncoupler carbonyl cyanide *m*-chlorophenylhydrazone induced a decrease in longer isoforms and an increase in shorter OPA1 isoforms; however, no alterations in OPA1 processing were

FIGURE 2. **PINK1-deficient SH-SY5Y cells show alterations in mitochondrial morphology similar to parkin-deficient cells.** *A*, SH-SY5Y cells transfected with control siRNA or siRNA targeting PINK1 were stained with the fluorescent dye $DiOC_6(3)$ to visualize mitochondria and analyzed by fluorescence microscopy as described in Fig. 1. *B*, down-regulation of PINK1 by RNAi leads to an increase in mitochondrial fragmentation, which can be rescued by parkin. SH-SY5Y cells were transfected with PINK1-specific siRNA and either siRNA-resistant PINK1 or wild type parkin. The cells were analyzed by fluorescence microscopy as described in Fig. 1. *Right panel*, expression of PINK1 and parkin was analyzed by Western blotting using a monoclonal anti-V5 antibody or the anti-parkin anti-serum hP1. *pPINK1*, precursor form; *mPINK1*, mature form. *C*, simultaneous down-regulation of parkin and PINK1 does not increase mitochondrial fragmentation over the single parkin or PINK1 knockdown. SH-SY5Y cells were transfected with parkin-specific siRNA and/or PINK1-specific siRNA, and the cells were analyzed by fluorescence microscopy as described above. *Lower panel*, efficiency of PINK1 and/or parkin down-regulation was determined by quantitative RT-PCR as described under "Experimental Procedures." *D* and *E*, anti-apoptotic Bcl-2 has no effect on the mitochondrial morphology in parkin or PINK1 knockdown cells. PINK1 cannot rescue the parkin knockdown phenotype (*D*). SH-SY5Y cells were transfected with parkin-specific siRNA (*D*) or PINK1-specific siRNA (*E*) and a Bcl-2 or PINK1 expression plasmid. The cells were analyzed as described in Fig. 1. *Lower panels*, expression of Bcl-2 and PINK1 was analyzed by Western blotting. ***, $p \leq 0.001$.

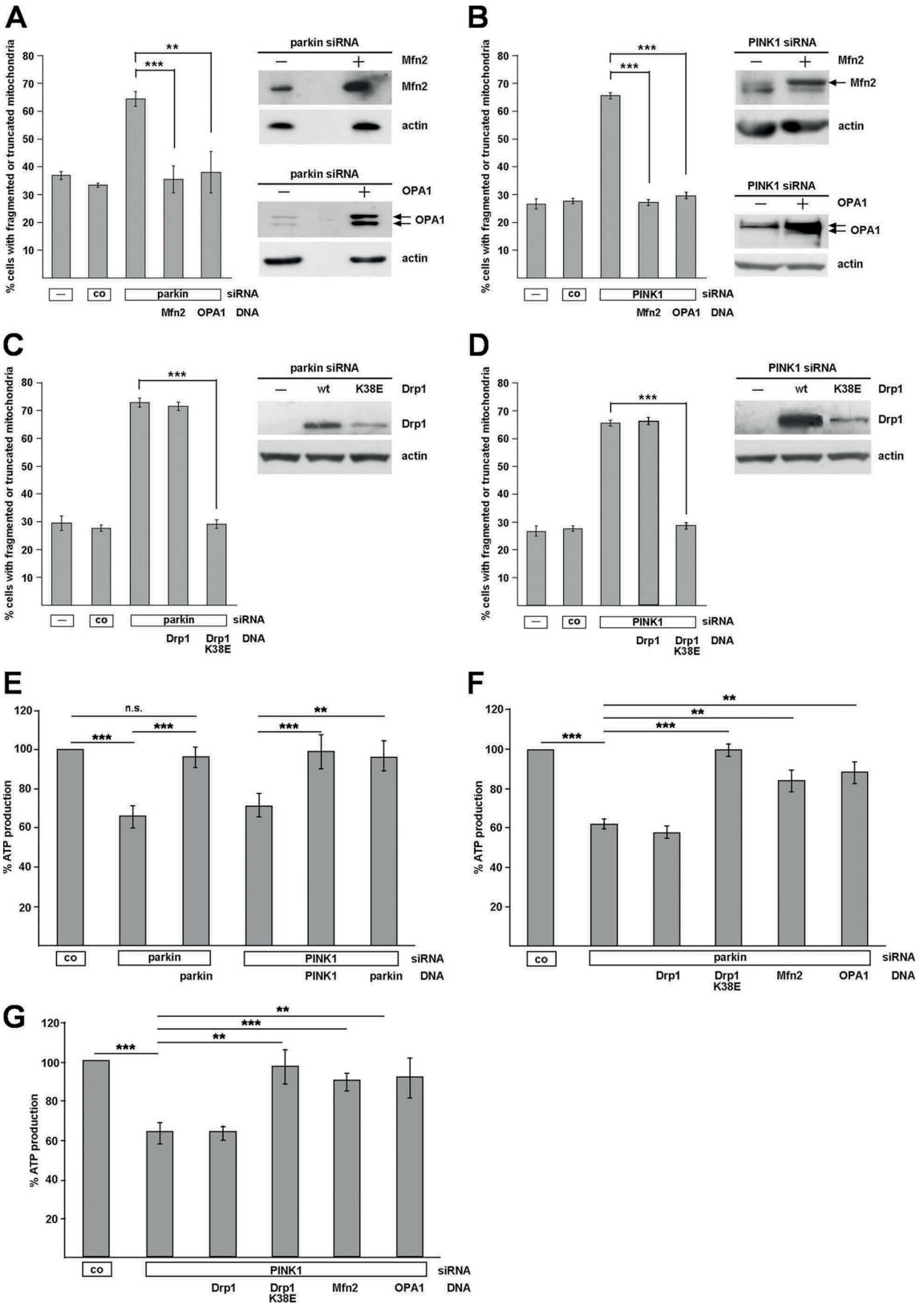

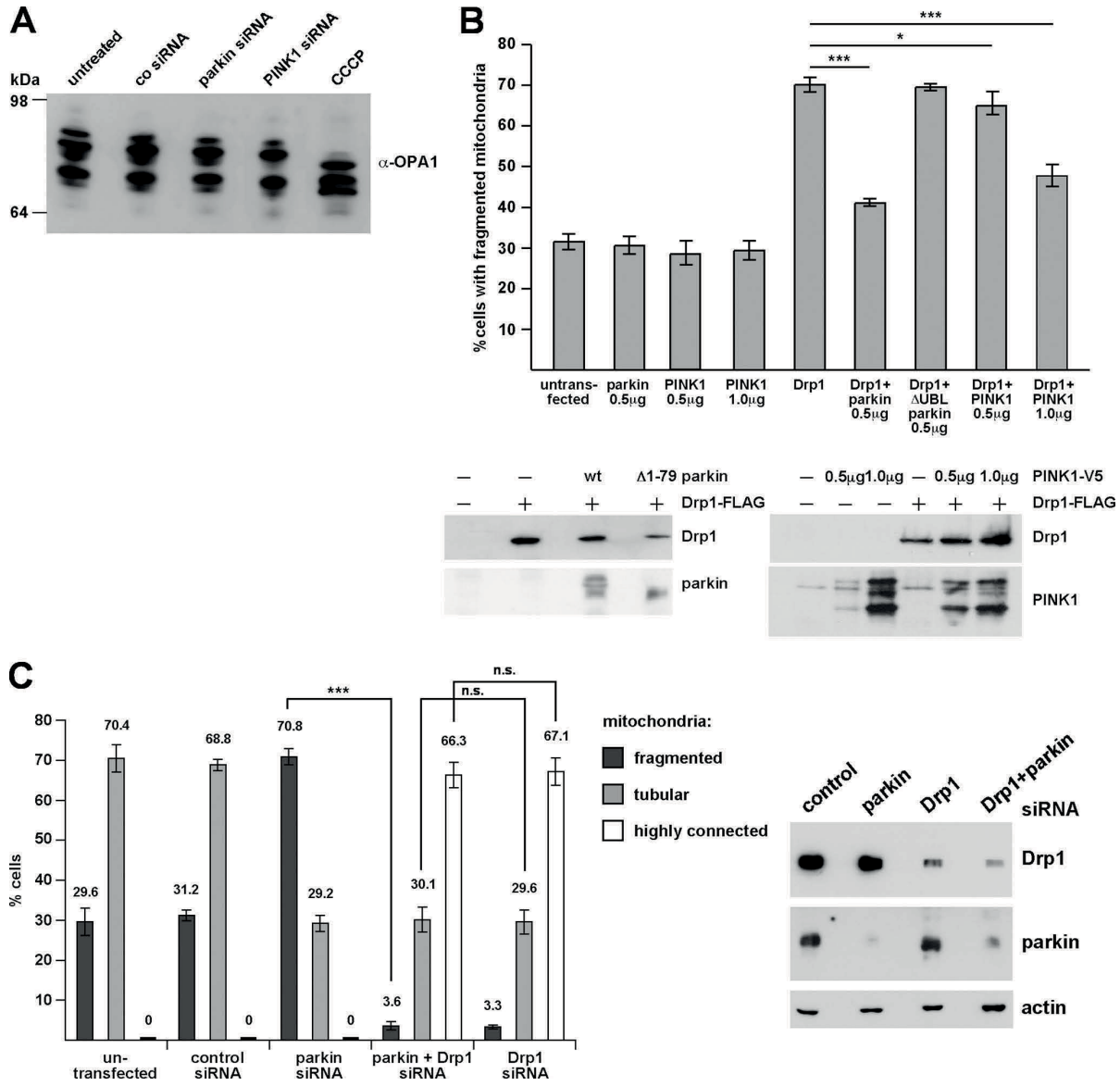

FIGURE 4. *A*, RNAi-mediated knockdown of parkin or PINK1 does not alter proteolytic processing of OPA1. SH-SY5Y cells transfected with control siRNA or siRNA targeting parkin or PINK1 were analyzed by Western blotting using a polyclonal antibody against OPA1. As a positive control to induce OPA1 processing, cells were treated with carbonyl cyanide 3-chlorophenylhydrazone (*CCCP*; 20 μM, 30 min). *B*, parkin and PINK1 (at higher expression levels) can reduce mitochondrial fission induced by Drp1. SH-SY5Y cells were transfected with the constructs indicated. 24 h after transfection mitochondrial morphology of transfected cells (identified by the coexpression of mCherry) was assessed as described in Fig. 1. *Lower panel*, expression levels of Drp1-FLAG, parkin, and PINK1-V5 in SH-SY5Y cells. 10 μg of protein were loaded per lane. See supplemental Fig. 2 for mitochondrial images. *wt*, wild type. *C*, in Drp1-deficient cells the mitochondrial phenotype induced by parkin knockdown does not occur. SH-SY5Y cells were transfected with the siRNAs indicated, and mitochondrial morphology was determined as described in Fig. 1. *Right panel*, the efficiency of Drp1 and parkin down-regulation by RNAi was shown by Western blotting using a monoclonal anti-Drp1 antibody and the anti-parkin antibody PRK8. β-Actin was used as a loading control. ***, $p \leq 0.001$.

observed upon transient down-regulation of parkin or PINK1 (Fig. 4*A*). The same results were obtained using stable PINK1 knockdown cells (data not shown). Thus, the effects of parkin or PINK1 down-regulation on mitochondrial morphology are not caused by a decrease in fusion mediated by proteolytically processed OPA1.

FIGURE 3. **Abnormal mitochondrial morphology and function caused by parkin or PINK1 loss of function can be rescued by increasing mitochondrial fusion or decreasing fission.** SH-SY5Y cells were cotransfected with siRNA targeting either parkin or PINK1 and the constructs indicated. The cells were analyzed as described under Fig. 1. *A–D*, Mfn2, OPA1, and dominant negative Drp1 (Drp1 K38E) rescued the mitochondrial phenotype observed in parkin or PINK1 knockdown cells. Shown is the percentage of cells with fragmented or truncated mitochondria. **, $p \leq 0.01$; ***, $p \leq 0.001$. *wt*, wild type. *Right panel of each set*, expression of Mfn2, OPA1, or Drp1 was analyzed by Western blotting. See supplemental Fig. 1 for mitochondrial images. *E–G*, steady state cellular ATP levels were measured in SH-SY5Y cells transfected with either parkin siRNA or PINK1 siRNA, and the expression plasmids are indicated. The analysis was performed 3 days after transfection.

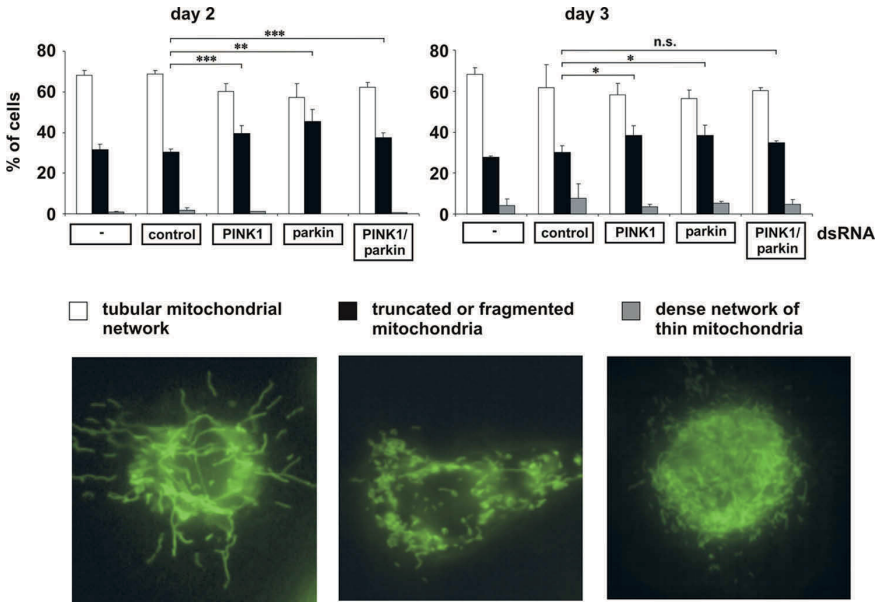

FIGURE 5. **In *Drosophila* S2 cells, mitochondrial fragmentation is an early phenotype of parkin and/or PINK1 loss of function.** S2 cells grown on glass coverslips were treated with control dsRNA and parkin- and/or PINK1-specific dsRNA. 48 h (day 2), 60 h (day 3), and 72 h (day 4, data not shown) after dsRNA treatment, S2 cells were stained with the fluorescent dye $DiOC_6(3)$ to visualize mitochondria and analyzed by fluorescence microscopy. Cells were categorized in three classes according to their mitochondrial morphology. For quantification, the mitochondrial morphology of at least 300 cells per plate was determined in a blinded manner. Quantifications were based on triplicates of at least two independent experiments. Shown is the percentage of cells with a tubular mitochondrial network (*white columns*), fragmented or truncated mitochondria (*black columns*), or a dense network of thin mitochondria (*gray columns*). *Lower panel*, fluorescence microscopy images to illustrate the different categories of mitochondrial morphologies. Efficiencies of parkin and PINK1 down-regulation is shown in Fig. 6*B*. **, $p \leq 0.01$; ***, $p \leq 0.001$.

An increase in shorter and less tubular mitochondria could also be a consequence of increased mitochondrial fission. To test whether this scenario applies to the effect of parkin and PINK1 on mitochondrial dynamics, we addressed the question of whether Drp1 might be implicated in mediating the parkin or PINK1 knockdown phenotype. First, we analyzed whether parkin or PINK1 might have an impact on mitochondrial fission induced by Drp1. This experiment revealed that the overexpression of neither parkin nor PINK1 induced significant changes in the mitochondrial morphology of transfected SH-SY5Y cells (Fig. 4*B* and supplemental Fig. 2). However, overexpression of Drp1 increased the percentage of transfected SH-SY5Y cells with fragmented mitochondria from 31.8% under control conditions to 71.0%. Remarkably, coexpression of parkin prevented mitochondrial fragmentation induced by Drp1, whereas Δ1–79 parkin had no effect (Fig. 4*B* and supplemental Fig. 2). PINK1 was also able to suppress Drp1-induced mitochondrial fragmentation but only at higher expression levels (Fig. 4*B* and supplemental Fig. 2). Second, we analyzed the consequences of parkin down-regulation in cells deficient in Mfn2 or Drp1. Mitochondrial fragmentation observed in Mfn2 knockdown cells was not influenced by parkin nor by increased parkin expression or by parkin deficiency (supplemental Fig. 3, *A* and *B*). In cells treated with Drp1-specific siRNA, the typical increase in cells with fragmented mitochondria upon down-regulation of parkin did not occur (Fig. 4*C*). Thus, Drp1 expression is necessary to mediate the effects of parkin down-regulation on mitochondrial morphology. Of note, the extent of tubular and highly connected mitochondria, which typically occurs in Drp1-deficient cells, was similar in cells lacking either Drp1 or Drp1 and parkin (Fig. 4*C*), indicating that mitochondrial fusion is not impaired in parkin-deficient cells. The same results were obtained when we used PINK1 siRNA instead of parkin siRNA (data not shown). These results corroborate that the mitochondrial phenotype induced by parkin or PINK1 deficiency is mediated by increased fission.

Mitochondrial Fission Is an Early Phenotype of Parkin or PINK1 Deficiency That Also Occurs in Drosophila S2 Cells and Primary Mouse Neurons—It has recently been demonstrated that parkin or PINK1 mutant phenotypes in flies can be rescued by increasing mitochondrial fission or decreasing fusion (33–36). To explain the discrepant results obtained in our model, we performed a comparative analysis of human SH-SY5Y cells and *Drosophila* S2 cells. For the down-regulation of parkin and PINK1 in S2 cells, we tested 2 and 3 different dsRNAs, respectively, which were all effective as determined by quantitative RT-PCR and showed the same effects on mitochondrial morphology. For the experiments shown in Figs. 5 and 6, we used the most effective dsRNAs, resulting in a 60–70% reduction in parkin- or PINK1-specific mRNA in comparison to control dsRNA-treated S2 cells (Fig. 6*B*). To monitor alterations in mitochondrial morphology, we performed time course experiments and analyzed the mitochondrial morphology of parkin- or PINK1-deficient S2 cells by fluorescence microscopy 48, 60, and 72 h after dsRNA treatment. We observed the most obvious increase in fragmented mitochondria in parkin- and/or PINK1-deficient S2 cells on day 2 after dsRNA treatment (Fig. 5), explaining why two previous studies analyzing only day 3 or 4 failed to observe mitochondrial fission induced by parkin or PINK1 loss of function (33, 34). Indeed, on day 3 after dsRNA treatment, we observed only minor differences (parkin- or PINK1 knockdown S2 cells) or no significant differences (parkin/PINK1 double knockdown S2 cells) to control cells. We never saw an increase in mitochondrial fusion in parkin- or PINK1 dsRNA-treated S2 cells. However, we noticed a dense network of fine thread-like mitochondria on days 3 and 4 after dsRNA treatment, but these mitochondria also occurred in control dsRNA-treated cells. In comparison to human SH-SY5Y cells, the extent of mitochondrial fragmentation was lower (about 70% of SH-SY5Y cells *versus* 40–50% of S2 cells), and in contrast to S2 cells, the fragmented state in SH-SY5Y cells persisted for days. As mitochon-

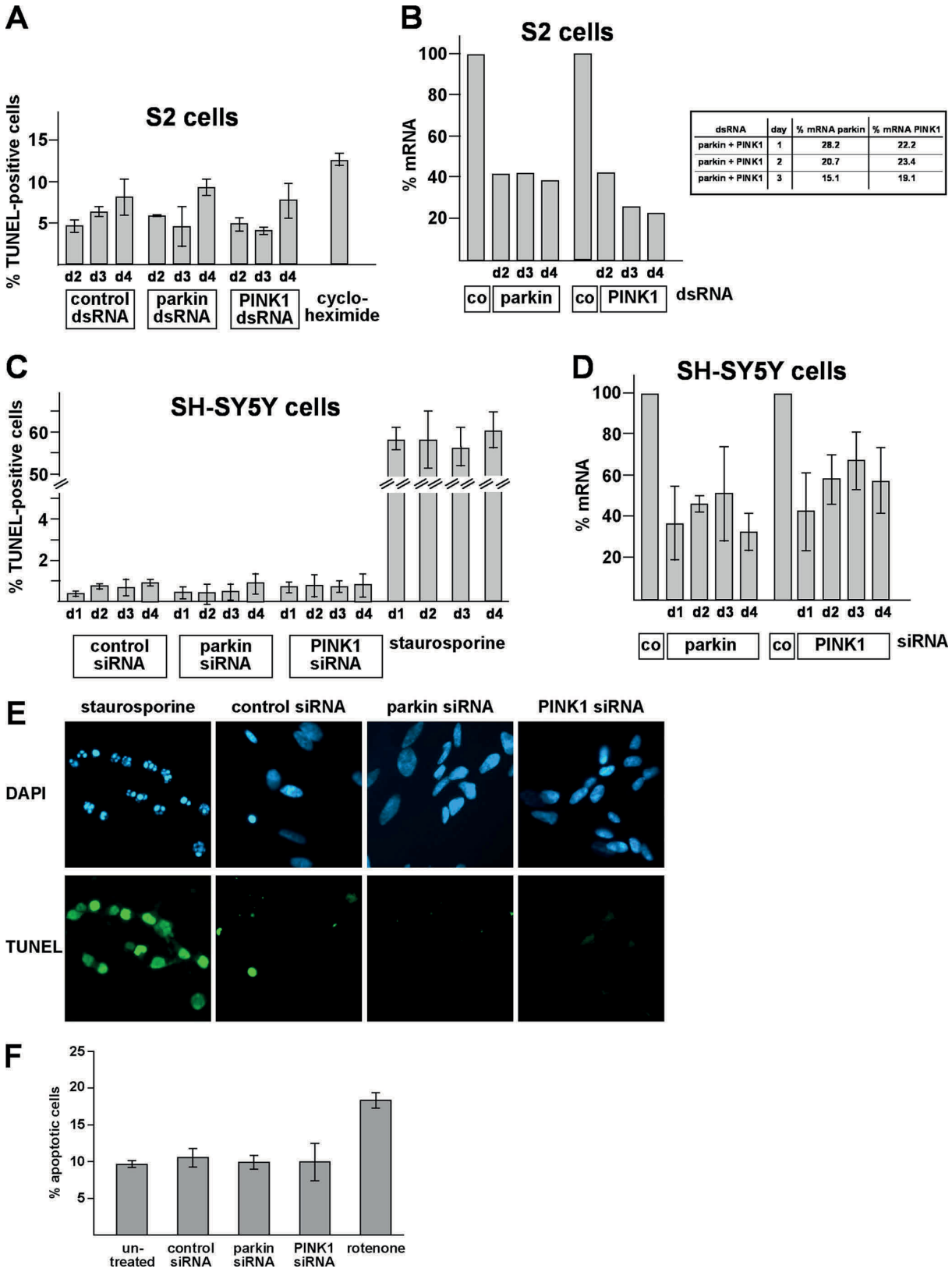

dsRNA	day	% mRNA parkin	% mRNA PINK1
parkin + PINK1	1	28.2	22.2
parkin + PINK1	2	20.7	23.4
parkin + PINK1	3	15.1	19.1

drial fragmentation can occur as a consequence of apoptosis, we analyzed apoptotic cell death in parkin- or PINK1-deficient SH-SY5Y or S2 cells over a period of 4 days after siRNA treatment. Importantly, mitochondrial fission induced by parkin or PINK1 deficiency was not associated with an increase in apoptosis. At the time we observed an increase in fragmented mitochondria in parkin- or PINK1-depleted SH-SY5Y or S2 cells, there was no activation of apoptosis as determined by a TUNEL assay (Fig. 6, *A–D*). An additional approach to analyze apoptotic cell death did not reveal SH-SY5Y cells positive for activated caspase-3 upon parkin/PINK1 down-regulation (Fig. 6*F*). In conclusion, our comparative analysis revealed that mitochondrial fission induced by parkin or PINK1 loss of function occurs both in human SH-SY5Y cells and insect S2 cells; however, in S2 cells this seems to be an early and transient phenotype.

In a next step we included primary mouse hippocampal neurons in our analysis and monitored mitochondrial morphology upon transducing primary neurons by a lentivirus expressing PINK1 shRNA and mito-EYFP (PINK1 shRNA) or mito-EYFP (control, Fig. 7*A*). 60% of the cells were transduced, and the overall PINK1 knockdown efficiency was 50% (determined by quantitative RT-PCR). First we determined the lengths of mitochondria in primary neurons. To consider possible differences in neuronal soma and processes, we assessed the length of mitochondria in both compartments separately. Primary hippocampal neurons deficient for PINK1 showed a significant decrease in the length of mitochondria both in soma (0.81 μm $\pm$ 0.01 in control to 0.68 $\pm$ 0.05 μm in PINK1 shRNA, $p = 0.014$) and processes (1.26 $\pm$ 0.04 μm in control to 1.16 $\pm$ 0.04 μm in PINK1 shRNA, $p = 0.006$) (Fig. 7*B*). Consequently, average mitochondrial length (soma and processes) was significantly decreased in PINK1 knockdown neurons (0.85 $\pm$ 0 μm) compared with neurons transduced with the control virus (1.02 $\pm$ 0.02 μm; $p < 0.001$). These differences in mitochondrial length were paralleled by an increase in the percentage of fragmented mitochondria (<0.5 μm; PINK1 shRNA, 15.0 $\pm$ 1.12%; control, 9.6 $\pm$ 1.03%; $p < 0.001$) and a decrease in the percentage of intermediate (0.5–5 μm; PINK1 shRNA, 84.9 $\pm$ 1.1%; control, 89.7 $\pm$ 1.03%; $p = 0.002$) and tubular mitochondria (>5 μm; PINK1 shRNA, 0.85 $\pm$ 0.07%; control, 1.03 $\pm$ 1.03%; $p = 0.005$) in PINK shRNA neurons in comparison to neurons transduced with control virus (Fig. 7*C*). Thus, our results in primary mouse hippocampal neurons demonstrated a subtle but highly significant mitochondrial phenotype that is consistent with that observed in SH-SY5Y and *Drosophila* S2 cells.

DISCUSSION

Several studies reported that loss of PINK1 function causes mitochondrial dysfunction (26, 30, 37–47). Parkin has been reported to compensate for PINK1 deficiency in the fly model, and we, therefore, addressed the question of whether parkin itself plays a role in maintaining mitochondrial integrity. We previously could show that parkin is a stress-responsive protein with a wide neuroprotective capacity and that pathogenic mutations and severe proteotoxic stress can induce inactivation of parkin (12, 14, 15, 23). We now present evidence that a loss of parkin function impairs mitochondrial morphology, dynamics, and function. Moreover, the mitochondrial phenotype of parkin-deficient cells is similar to that of PINK1-deficient cells. Parkin- or PINK1-deficient SH-SY5Y cells showed a significant increase in the percentage of cells with truncated or fragmented mitochondria along with a decrease in cellular ATP production. The mitochondrial phenotype could morphologically and functionally be prevented by the enhanced expression of Mfn2, OPA1, or dominant negative Drp1, suggesting that a decrease in mitochondrial fusion or an increase in fission is associated with a loss of parkin or PINK1 function. Several lines of evidence indicated that an increase in mitochondrial fragmentation is responsible for the alterations observed in parkin- or PINK1-deficient cells. First, the mitochondrial phenotype in parkin- or PINK1-deficient cells was not observed in Drp1-deficient cells. Second, parkin as well as PINK1 suppressed mitochondrial fission induced by Drp1. These results are consistent with a recent publication from Sandebring *et al.* (30) who observed an increase in Drp1-dependent mitochondrial fission in PINK1-deficient human neuroblastoma cells.

A possible role of parkin and PINK1 in modulating mitochondrial morphology/dynamics emerged from recent studies in *Drosophila* (33–36). In flies, the parkin or PINK1 flight muscle phenotype was suppressed by an increase in mitochondrial fission and a decrease in fusion, leading to the conclusion that the PINK1/parkin pathway promotes mitochondrial fission. Interestingly, we did not observe fragmentation of mitochondria upon overexpression of parkin or PINK1 in human cells; on

FIGURE 6. **The increase in mitochondrial fragmentation observed in parkin- or PINK1-deficient S2 or SH-SY5Y cells is not associated with an increase in apoptosis.** *A*, S2 cells were treated with control dsRNA and parkin-specific or PINK1-specific dsRNA. At days 2, 3, and 4 after treatment, cells were fixed and permeabilized. Apoptotic cells were detected by fluorescently labeling the free 3′-OH ends of DNA strand breaks (TUNEL). As a positive control, cells were treated with cycloheximide (10 μM, 6 h). Shown is the percentage of apoptotic cells, determined by the number of TUNEL-positive cells of at least 300 DAPI-stained cells. Quantifications were based on at least three independent experiments. *B*, parkin or PINK1 knockdown efficiencies in S2 cells corresponding to the experiments shown in Figs. 5*A* and 6*A*. Cells were harvested at days 2, 3, and 4 after treatment. Total cellular RNA was isolated and subjected to quantitative RT-PCR using parkin- and PINK1-specific primers. The amount of RNA of each sample was normalized with respect to the endogenous housekeeping gene Rp49. The efficiencies of the parkin/PINK1 double knockdown are shown in the *right panel*. *C*, SH-SY5Y cells were transfected with control siRNA and parkin-specific or PINK1-specific siRNA. At days 1, 2, 3, and 4 after transfection, cells were fixed and permeabilized. Apoptotic cells were detected by the TUNEL assay described in *A*. As a positive control, cells were treated with staurosporine (1 μM, 4 h). Shown is the percentage of apoptotic cells, determined by the number of TUNEL-positive cells of at least 300 DAPI-stained cells. Quantifications were based on at least three independent experiments. *D*, quantification of parkin or PINK1 knockdown efficiencies in SH-SY5Y cells corresponding to the experiment shown under *C*. SH-SY5Y cells were harvested at days 1, 2, 3, and 4 after siRNA transfection. Total cellular RNA was isolated and subjected to quantitative RT-PCR using parkin- and PINK1-specific primers. The amount of mRNA of each sample was normalized with respect to the endogenous housekeeping gene β-actin. *E*, examples of the direct immunofluorescence analysis described under *C*. Apoptotic cells (TUNEL-positive) were fluorescein-labeled (*green*), and nuclei were stained with DAPI (*blue*). *F*, in addition to the TUNEL assay, a single cell analysis for activated caspase-3 was performed in SH-SY5Y cells. Two days after transfection with siRNA, SH-SY5Y cells were fixed, permeabilized, and analyzed by indirect immunofluorescence. Activation of caspase-3 was detected using an anti-active caspase-3 antibody. As a positive control, cells were treated with rotenone (10 μM, 3 h). Shown is the percentage of apoptotic cells, determined by the number of activated caspase-3-positive cells of at least 300 DAPI-stained cells. Quantifications were based on triplicates of at least three independent experiments.

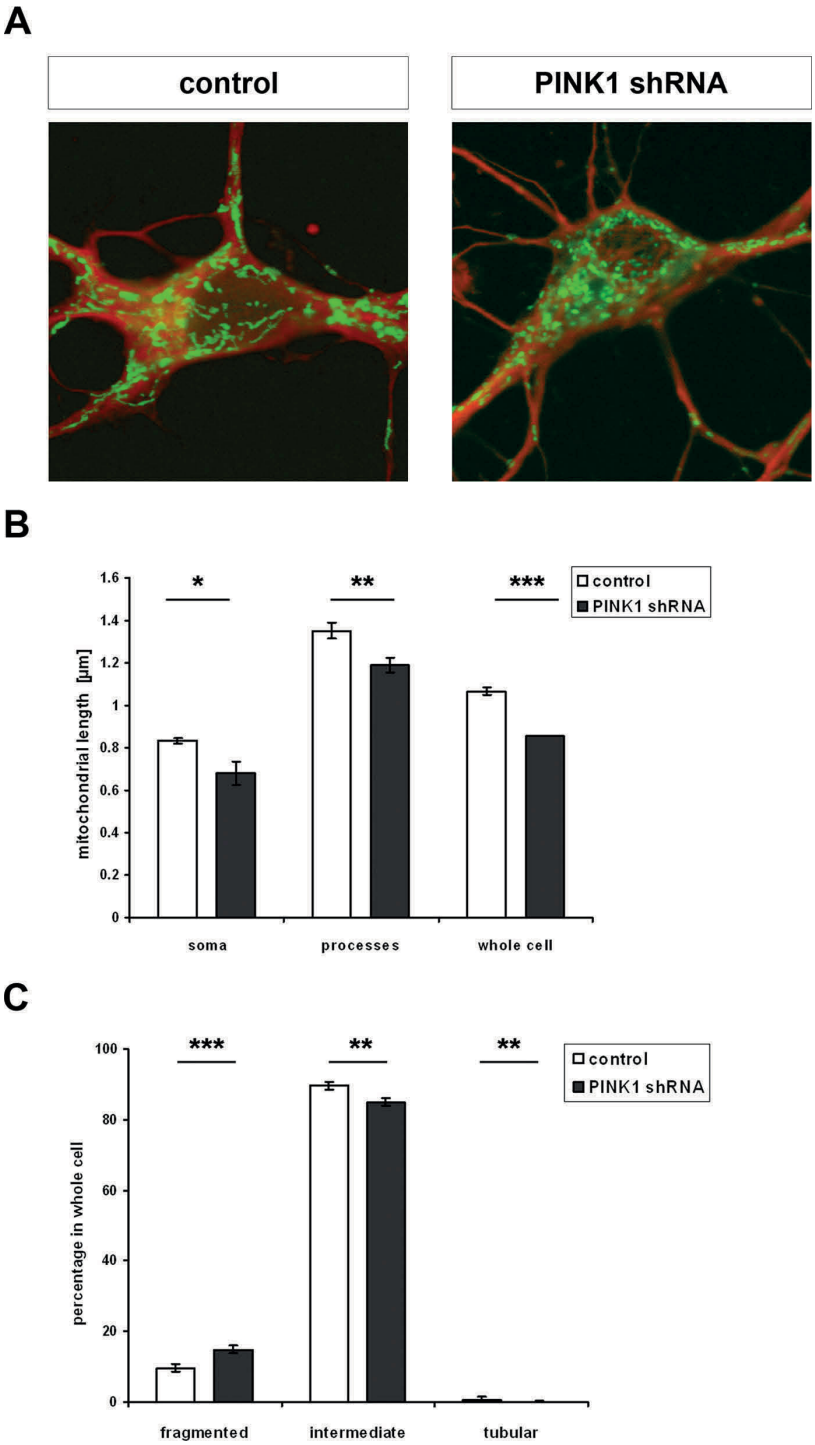

FIGURE 7. **PINK1-deficient primary mouse hippocampal neurons show a decrease in the length of mitochondria and an increase in mitochondrial fragmentation.** *A*, hippocampal cells of E15.5 C57/BL6 mice were transduced with pLL3.7 + mito-EYFP lentivirus for control or pLL.3.7 + PINK1 shRNA mito-EYFP for down-regulation of PINK1. Mito-EYFP expression was used to determine mitochondrial morphology (*green*). To visualize neurons, cells were detected with the anti-β III tubulin antibody by immunocytochemistry (*red*). *B*, for quantification, the lengths of mitochondria of 40 neurons per group were determined. Shown is the mean mitochondrial length with S.E. in the soma, processes, and in the whole neuron. Down-regulation of PINK1 by shRNA led to significant decrease in mitochondrial length throughout the neuronal cell (soma, $p = 0.014$; processes, $p = 0.006$; whole neuron, $p < 0.001$). *C*, mitochondria were categorized into fragmented (<0.5 μm), intermediate (0.5–5 μm), and tubular (>5 μm). Shown is the percentage ± S.E. of mitochondria in these categories in whole neurons ($n = 40$). PINK1 down-regulation via shRNA resulted in a significant increase in fragmented ($p < 0.001$) mitochondria at the expense of intermediate ($p = 0.002$) and tubular ($p = 0.005$) mitochondria.

the contrary, parkin and PINK1 prevented mitochondrial fragmentation induced by Drp1. In line with this observation, the parkin and PINK1 knockdown phenotype in human cells was rescued by increasing mitochondrial fusion and decreasing fission. The parkin/PINK1 studies in flies and mammalian cells appear controversial at first glance. However, our comparative analysis of the consequences of parkin or PINK1 down-regulation in human, mouse, and insect cells revealed that two aspects might be relevant to explain the discrepant findings. First, the time of phenotype analysis seems to be crucial, and second, there could be differences between arthropods and mammals in the regulation of mitochondrial dynamics and/or in the elimination of dysfunctional mitochondria, especially in highly specialized tissues such as flight muscles. Although we looked at an acute manifestation of parkin or PINK1 knockdown in cultured cells, the phenotype observed in adult flies might be influenced by compensatory effects. In support of this scenario, we did observe a significant increase in mitochondrial fragmentation upon parkin or PINK1 knockdown in cultured insect cells, but this was an early and transient phenomenon. Conceptually, flies might try to rescue the parkin/PINK1 null phenotype by activating fusion in an effort to dilute dysfunctional mitochondria. However, in tissues with high energy demands, such as flight muscles, this strategy might not be beneficial in the end, as increased fusion eventually leads to the contamination of the whole mitochondrial network with dysfunctional contents. This might explain why parkin/PINK1 null flies show a phenotype in such tissues that can be rescued by increasing fission, possibly favoring the elimination of dysfunctional mitochondria by mitophagy. In accordance with this concept, a recent study proposed that parkin can promote autophagic clearance of dysfunctional mitochondria (48). Moreover, regulation of the fusion machinery seems to be more complex in mammals compared with insects. Flies do not have the two mitofusins Mfn1 and Mfn2, but have only dmnf/Marf, whereas the expression of Fzo is restricted to the male germ line (49). In addition, regulation of OPA1 function might be different in flies. For example, the presenilin-associated rhomboid-like (PARL) protease, implicated in OPA1 processing, harbors a highly conserved N-terminal regulatory domain in mammals which is not found in insects (24). Phosphorylation of this vertebrate-specific domain inhibits mitochondrial fragmentation, a regulatory mechanism that obviously emerged during vertebrate evolution (24). Consequently, controversial reports on the effects of proteins influencing mitochondrial dynamics may be at least partially attributed to differences in the complex regulation of these proteins.

Our initial observation that PINK1 deficiency causes alterations in mitochondrial morphology in cultured human cells (11) has also been reported by other groups (26, 30, 45, 46), whereas others observed bioenergetic deficits but failed to detect morphological changes (39, 47). This can be explained by the fact that morphological alterations occur early upon parkin/PINK1 down-regulation and are more prominent in a transient knockdown in comparison to a stable knockdown. Accordingly, we observed a decrease in mitochondrial length and connectivity also in primary mouse neurons as an early response to PINK1 down-regulation that can be compensated at later stages, explaining why PINK1 knock-out mice do not show obvious morphological mitochondrial alterations. However, mitochondrial quality control and compensatory mechanisms might not be sufficient to fully restore mitochondrial function, especially in neuronal populations with a low bioenergetic threshold and a high oxidative burden, such as dopaminergic neurons in the substantia nigra.

The next important step will be to address the question of whether parkin/PINK1 play a direct role in the regulation of mitochondrial morphology or dynamics. Recent research revealed that the activity and subcellular localization of Drp1 is regulated by posttranslational modifications, such as phosphorylation, ubiquitylation, and sumoylation (for review, see Ref. 50); therefore, Drp1 would be a prime candidate for such direct regulatory effects. On the other hand, it is also conceivable that parkin or PINK1 exert an indirect effect on mitochondrial morphology by influencing mitochondrial functions, such as complex I activity, or mitochondrial quality control. In this context it will be important to understand the functional interplay between PINK1 and parkin and to focus on compensatory pathways that are induced after PINK1/parkin loss of function.

Acknowledgments—We thank Heidi M. McBride for providing the Drp1, Mfn2, and OPA1 plasmids and for helpful discussions, Roger Y. Tsien for providing the mCherry plasmid, and Anita Schlierf, Dominik Paquet, Dr. Richard Page, and Veronika Müller for experimental help. We are grateful to Gerhard Welzl for help with the statistical analysis.

REFERENCES

1. Abou-Sleiman, P. M., Muqit, M. M., and Wood, N. W. (2006) *Nat. Rev. Neurosci.* **7,** 207–219
2. Lin, M. T., and Beal, M. F. (2006) *Nature* **443,** 787–795
3. Schapira, A. H. (2008) *Lancet Neurol.* **7,** 97–109
4. Bogaerts, V., Theuns, J., and van Broeckhoven, C. (2008) *Genes Brain Behav.* **7,** 129–151
5. Dodson, M. W., and Guo, M. (2007) *Curr. Opin. Neurobiol.* **17,** 331–337
6. Mandemakers, W., Morais, V. A., and De Strooper, B. (2007) *J. Cell Sci.* **120,** 1707–1716
7. Greene, J. C., Whitworth, A. J., Kuo, I., Andrews, L. A., Feany, M. B., and Pallanck, L. J. (2003) *Proc. Natl. Acad. Sci. U.S.A.* **100,** 4078–4083
8. Clark, I. E., Dodson, M. W., Jiang, C., Cao, J. H., Huh, J. R., Seol, J. H., Yoo, S. J., Hay, B. A., and Guo, M. (2006) *Nature* **441,** 1162–1166
9. Park, J., Lee, S. B., Lee, S., Kim, Y., Song, S., Kim, S., Bae, E., Kim, J., Shong, M., Kim, J. M., and Chung, J. (2006) *Nature* **441,** 1157–1161
10. Yang, Y., Gehrke, S., Imai, Y., Huang, Z., Ouyang, Y., Wang, J. W., Yang, L., Beal, M. F., Vogel, H., and Lu, B. (2006) *Proc. Natl. Acad. Sci. U.S.A.* **103,** 10793–10798
11. Exner, N., Treske, B., Paquet, D., Holmström, K., Schiesling, C., Gispert, S., Carballo-Carbajal, I., Berg, D., Hoepken, H. H., Gasser, T., Krüger, R., Winklhofer, K. F., Vogel, F., Reichert, A. S., Auburger, G., Kahle, P. J., Schmid, B., and Haass, C. (2007) *J. Neurosci.* **27,** 12413–12418
12. Winklhofer, K. F., Henn, I. H., Kay-Jackson, P. C., Heller, U., and Tatzelt, J. (2003) *J. Biol. Chem.* **278,** 47199–47208
13. Duvezin-Caubet, S., Jagasia, R., Wagener, J., Hofmann, S., Trifunovic, A., Hansson, A., Chomyn, A., Bauer, M. F., Attardi, G., Larsson, N. G., Neupert, W., and Reichert, A. S. (2006) *J. Biol. Chem.* **281,** 37972–37979
14. Henn, I. H., Bouman, L., Schlehe, J. S., Schlierf, A., Schramm, J. E., Wegener, E., Nakaso, K., Culmsee, C., Berninger, B., Krappmann, D., Tatzelt, J., and Winklhofer, K. F. (2007) *J. Neurosci.* **27,** 1868–1878
15. Henn, I. H., Gostner, J. M., Lackner, P., Tatzelt, J., and Winklhofer, K. F. (2005) *J. Neurochem.* **92,** 114–122

16. Harder, Z., Zunino, R., and McBride, H. (2004) *Curr. Biol.* **14,** 340–345
17. Neuspiel, M., Zunino, R., Gangaraju, S., Rippstein, P., and McBride, H. (2005) *J. Biol. Chem.* **280,** 25060–25070
18. Rambold, A. S., Miesbauer, M., Rapaport, D., Bartke, T., Baier, M., Winklhofer, K. F., and Tatzelt, J. (2006) *Mol. Biol. Cell* **17,** 3356–3368
19. Shaner, N. C., Campbell, R. E., Steinbach, P. A., Giepmans, B. N., Palmer, A. E., and Tsien, R. Y. (2004) *Nat. Biotechnol.* **22,** 1567–1572
20. Consiglio, A., Quattrini, A., Martino, S., Bensadoun, J. C., Dolcetta, D., Trojani, A., Benaglia, G., Marchesini, S., Cestari, V., Oliverio, A., Bordignon, C., and Naldini, L. (2001) *Nat. Med.* **7,** 310–316
21. Ventura, A., Meissner, A., Dillon, C. P., McManus, M., Sharp, P. A., Van Parijs, L., Jaenisch, R., and Jacks, T. (2004) *Proc. Natl. Acad. Sci. U.S.A.* **101,** 10380–10385
22. Yang, Y., Nishimura, I., Imai, Y., Takahashi, R., and Lu, B. (2003) *Neuron* **37,** 911–924
23. Schlehe, J. S., Lutz, A. K., Pilsl, A., Lämmermann, K., Grgur, K., Henn, I. H., Tatzelt, J., and Winklhofer, K. F. (2008) *J. Biol. Chem.* **283,** 13771–13779
24. Jeyaraju, D. V., Xu, L., Letellier, M. C., Bandaru, S., Zunino, R., Berg, E. A., McBride, H. M., and Pellegrini, L. (2006) *Proc. Natl. Acad. Sci. U.S.A.* **103,** 18562–18567
25. Taguchi, N., Ishihara, N., Jofuku, A., Oka, T., and Mihara, K. (2007) *J. Biol. Chem.* **282,** 11521–11529
26. Weihofen, A., Thomas, K. J., Ostaszewski, B. L., Cookson, M. R., and Selkoe, D. J. (2009) *Biochemistry* **48,** 2045–2052
27. Darios, F., Corti, O., Lücking, C. B., Hampe, C., Muriel, M. P., Abbas, N., Gu, W. J., Hirsch, E. C., Rooney, T., Ruberg, M., and Brice, A. (2003) *Hum. Mol. Genet.* **12,** 517–526
28. Denison, S. R., Wang, F., Becker, N. A., Schüle, B., Kock, N., Phillips, L. A., Klein, C., and Smith, D. I. (2003) *Oncogene* **22,** 8370–8378
29. Zhou, C., Huang, Y., Shao, Y., May, J., Prou, D., Perier, C., Dauer, W., Schon, E. A., and Przedborski, S. (2008) *Proc. Natl. Acad. Sci. U.S.A.* **105,** 12022–12027
30. Sandebring, A., Thomas, K. J., Beilina, A., van der Brug, M., Cleland, M. M., Ahmad, R., Miller, D. W., Zambrano, I., Cowburn, R. F., Behbahani, H., Cedazo-Mínguez, A., and Cookson, M. R. (2009) *PLoS ONE* **4,** e5701
31. Ishihara, N., Fujita, Y., Oka, T., and Mihara, K. (2006) *EMBO J.* **25,** 2966–2977
32. Song, Z., Chen, H., Fiket, M., Alexander, C., and Chan, D. C. (2007) *J. Cell Biol.* **178,** 749–755
33. Poole, A. C., Thomas, R. E., Andrews, L. A., McBride, H. M., Whitworth, A. J., and Pallanck, L. J. (2008) *Proc. Natl. Acad. Sci. U.S.A.* **105,** 1638–1643
34. Yang, Y., Ouyang, Y., Yang, L., Beal, M. F., McQuibban, A., Vogel, H., and Lu, B. (2008) *Proc. Natl. Acad. Sci. U.S.A.* **105,** 7070–7075
35. Deng, H., Dodson, M. W., Huang, H., and Guo, M. (2008) *Proc. Natl. Acad. Sci. U.S.A.* **105,** 14503–14508
36. Park, J., Lee, G., and Chung, J. (2009) *Biochem. Biophys. Res. Commun.* **378,** 518–523
37. Gandhi, S., Wood-Kaczmar, A., Yao, Z., Plun-Favreau, H., Deas, E., Klupsch, K., Downward, J., Latchman, D. S., Tabrizi, S. J., Wood, N. W., Duchen, M. R., and Abramov, A. Y. (2009) *Mol. Cell* **33,** 627–638
38. Gautier, C. A., Kitada, T., and Shen, J. (2008) *Proc. Natl. Acad. Sci. U.S.A.* **105,** 11364–11369
39. Gegg, M. E., Cooper, J. M., Schapira, A. H., and Taanman, J. W. (2009) *PLoS ONE* **4,** e4756
40. Gispert, S., Ricciardi, F., Kurz, A., Azizov, M., Hoepken, H. H., Becker, D., Voos, W., Leuner, K., Müller, W. E., Kudin, A. P., Kunz, W. S., Zimmermann, A., Roeper, J., Wenzel, D., Jendrach, M., García-Arencíbia, M., Fernández-Ruiz, J., Huber, L., Rohrer, H., Barrera, M., Reichert, A. S., Rüb, U., Chen, A., Nussbaum, R. L., and Auburger, G. (2009) *PLoS ONE* **4,** e5777
41. Grunewald, A., Gegg, M. E., Taanman, J. W., King, R. H., Kock, N., Klein, C., and Schapira, A. H. (2009) *Exp. Neurol.*, in press
42. Hoepken, H. H., Gispert, S., Morales, B., Wingerter, O., Del Turco, D., Mülsch, A., Nussbaum, R. L., Müller, K., Dröse, S., Brandt, U., Deller, T., Wirth, B., Kudin, A. P., Kunz, W. S., and Auburger, G. (2007) *Neurobiol. Dis.* **25,** 401–411
43. Liu, W., Vives-Bauza, C., Acín-Peréz, R., Yamamoto, A., Tan, Y., Li, Y., Magrané, J., Stavarache, M. A., Shaffer, S., Chang, S., Kaplitt, M. G., Huang, X. Y., Beal, M. F., Manfredi, G., and Li, C. (2009) *PLoS ONE* **4,** e4597
44. Marongiu, R., Spencer, B., Crews, L., Adame, A., Patrick, C., Trejo, M., Dallapiccola, B., Valente, E. M., and Masliah, E. (2009) *J. Neurochem.* **108,** 1561–1574
45. Wood-Kaczmar, A., Gandhi, S., Yao, Z., Abramov, A. Y., Abramov, A. S., Miljan, E. A., Keen, G., Stanyer, L., Hargreaves, I., Klupsch, K., Deas, E., Downward, J., Mansfield, L., Jat, P., Taylor, J., Heales, S., Duchen, M. R., Latchman, D., Tabrizi, S. J., and Wood, N. W. (2008) *PLoS ONE* **3,** e2455
46. Dagda, R. K., Cherra, S. J., 3rd, Kulich, S. M., Tandon, A., Park, D., and Chu, C. T. (2009) *J. Biol. Chem.* **284,** 13843–13855
47. Morais, V. A., Verstreken, P., Roethig, A., Smet, J., Snellinx, A., Vanbrabant, M., Haddad, D., Frezza, C., Mandemakers, W., Vogt-Weisenhorn, D., Van Coster, R., Wurst, W., Scorrano, L., and De Strooper, B. (2009) *EMBO Mol. Med.* **1,** 99–111
48. Narendra, D., Tanaka, A., Suen, D. F., and Youle, R. J. (2008) *J. Cell Biol.* **183,** 795–803
49. Hwa, J. J., Hiller, M. A., Fuller, M. T., and Santel, A. (2002) *Mech. Dev.* **116,** 213–216
50. Santel, A., and Frank, S. (2008) *IUBMB life* **60,** 448–455

Human Molecular Genetics, 2010, Vol. 19, No. 19 **3734–3746**
doi:10.1093/hmg/ddq288
Advance Access published on July 16, 2010

Loss of the Parkinson's disease-linked gene DJ-1 perturbs mitochondrial dynamics

I. Irrcher[1], H. Aleyasin[1], E.L. Seifert[2], S.J. Hewitt[1], S. Chhabra[1], M. Phillips[1], A.K. Lutz[4], M.W.C. Rousseaux[1], L. Bevilacqua[2], A. Jahani-Asl[1], S. Callaghan[1], J.G. MacLaurin[1], K.F. Winklhofer[4], P. Rizzu[5], P. Rippstein[3], R.H. Kim[6], C.X. Chen[7], E.A. Fon[7], R.S. Slack[1], M.E. Harper[2], H.M. McBride[3], T.W. Mak[6] and D.S. Park[1,8,*]

[1]Department of Cellular and Molecular Medicine, [2]Department of Biochemistry, Microbiology, and Immunology and [3]Ottawa Heart Institute, University of Ottawa, Ottawa, Canada, [4]Adolf Butenandt Institute, Neurobiochemistry, Ludwig Maximillians University, Munich, Germany, [5]Department of Clinical Genetics, Medical Genomics VU University Medical Center, Amsterdam, The Netherlands, [6]The Campbell Family Institute for Breast Cancer Research, University of Toronto, Toronto, Canada, [7]Department of Biochemistry, McGill University, Montreal, Canada and [8]Department of Cogno-Mechatronics Engineering, Pusan National University, Korea

Received June 2, 2010; Revised and Accepted July 7, 2010

Growing evidence highlights a role for mitochondrial dysfunction and oxidative stress as underlying contributors to Parkinson's disease (PD) pathogenesis. DJ-1 (PARK7) is a recently identified recessive familial PD gene. Its loss leads to increased susceptibility of neurons to oxidative stress and death. However, its mechanism of action is not fully understood. Presently, we report that DJ-1 deficiency in cell lines, cultured neurons, mouse brain and lymphoblast cells derived from DJ-1 patients display aberrant mitochondrial morphology. We also show that these DJ-1-dependent mitochondrial defects contribute to oxidative stress-induced sensitivity to cell death since reversal of this fragmented mitochondrial phenotype abrogates neuronal cell death. Reactive oxygen species (ROS) appear to play a critical role in the observed defects, as ROS scavengers rescue the phenotype and mitochondria isolated from DJ-1 deficient animals produce more ROS compared with control. Importantly, the aberrant mitochondrial phenotype can be rescued by the expression of Pink1 and Parkin, two PD-linked genes involved in regulating mitochondrial dynamics and quality control. Finally, we show that DJ-1 deficiency leads to altered autophagy in murine and human cells. Our findings define a mechanism by which the DJ-1-dependent mitochondrial defects contribute to the increased sensitivity to oxidative stress-induced cell death that has been previously reported.

INTRODUCTION

Parkinson's disease (PD), the second most common neurodegenerative disorder, is characterized by the progressive loss of neurons within the substantia nigra *pars compacta* (1,2). Though the pathogenic mechanisms underlying PD are not well understood, growing evidence supports a role for mitochondrial dysfunction, oxidative stress and more recently autophagy.

Mitochondrial dysfunction was initially tied to PD in studies demonstrating the presence of aberrant mitochondrial function in idiopathic PD patients (3,4). Moreover, several dopaminergic toxins acted as mitochondrial toxins by inhibiting the electron transport chain, producing toxic-free radicals in the process (5,6). Since this time, several familial PD genes, including, Parkin (PARK2), Pink1 (PARK6) and DJ-1 (PARK7), have been linked to mitochondria. Their loss results in abnormal mitochondrial morphology (7,8). Interestingly, the interplay of Pink1 and Parkin dynamically regulates mitochondrial morphology via mitochondrial fission/fusion and also affects mitochondrial quality control (9–11). As the function of Pink1 and Parkin in these contexts continues to be elucidated, the role(s) of DJ-1 is less understood.

*To whom correspondence should be addressed at: Faculty of Medicine, Department Of Cellular and Molecular Medicine (CMM), University of Ottawa, 451 Smyth Road, Ottawa, Ontario, Canada K1H 8M5. Tel: +1 6135625800 ext. 8816; Fax: +1 6135625403; Email: dpark@uottawa.ca

Homozygous loss-of-function mutations in DJ-1 (PARK7) result in early onset PD (12). Several lines of evidence, including our own, indicate that DJ-1 protects neurons against oxidative stress-induced cell death (13,14). It has been postulated that DJ-1 exerts its protective function by regulating mitochondrial homeostasis or participating in the oxidative stress response either serving as an antioxidant scavenger or a redox sensor (14–17). More recently, DJ-1 was found to affect mitochondrial quality control (18,19). Given the importance of reactive oxygen species (ROS) in regulating mitochondrial dynamics and the observations that loss of Pink1 and Parkin has also been linked to mitochondrial dysfunction, we wanted to address whether DJ-1 also affects mitochondrial dynamics and function.

Here we examined mitochondrial morphology and function in DJ-1 deficient tissues and hypothesized that loss of DJ-1 would produce a fragmented mitochondrial phenotype, accounting increased sensitivity to cell death of DJ-1 deficient neurons previously reported (14). We demonstrate that DJ-1 deficiency leads to a fragmented mitochondrial phenotype in multiple contexts including neurons and human DJ-1 patient cells. Second, we provide evidence that ROS plays a critical role in this fragmentation phenotype and that DJ-1 deficiency results in elevated ROS levels. Third, we show that this mitochondrial phenotype is an important contributor to the sensitivity to oxidative stress caused by the loss of DJ-1. Fourth, we show that Pink1 and Parkin can rescue the mitochondrial fragmentation induced by the loss of DJ-1. Finally, we also show that the loss of DJ-1 results in increased autophagic activity.

RESULTS

Loss of DJ-1 alters mitochondrial morphology and dynamics

Based upon the growing evidence for mitochondrial morphology and dynamics as underlying contributors to PD, we first investigated a role for DJ-1 in mitochondrial remodeling. Primary cortical neurons and mouse embryonic fibroblasts (MEFs) from DJ-$1^{+/+}$ or DJ-$1^{-/-}$ embryos (E15.5) were cultured. Mitochondria were quantified and binned according to length, as done previously (20). As shown in Figure 1A and quantified in Figure 1B, mitochondrial lengths in DJ-$1^{+/+}$ primary cortical neurons at 3 days *in vitro* were significantly longer and less fragmented than in DJ-$1^{-/-}$ neurons. This fragmented mitochondrial phenotype was also evident in MEFs (Fig. 1C and D) and *in vivo* in the striatum of DJ-$1^{+/+}$ and DJ-$1^{-/-}$ mice (Fig. 1E and F). Thus, the fragmented morphology appears to be a more generalized phenomenon rather than restricted to a specific cell type, occurring both *in vitro* and *in vivo*. These data demonstrate that mitochondrial morphology is altered with the loss of DJ-1.

To address whether the DJ-1-dependent mitochondrial fragmentation was related to alterations in mitochondrial fusion rates, DJ-$1^{+/+}$ or DJ-$1^{-/-}$ MEFs were transduced with a matrix-targeted photoactivatable GFP lentivirus (PA-GFP). PA-GFP was activated in ~10% of the cell using a 405 nm laser line at 75% intensity (21). Upon photoactivation, the spread of the GFP signal throughout the mitochondrial reticulum was assessed immediately post-activation and following 20 min (Fig. 2A). The data in Figure 2B demonstrate that mitochondrial fusion in MEFs is decreased by 30% DJ-$1^{-/-}$ when compared with DJ-$1^{+/+}$. Steady-state levels of the mitochondrial fission and fusion proteins, Dynamin Related Protein-1 (Drp1) and mitofusin 1 (MFN1) were also measured to determine whether the loss of DJ-1 would result in altered expression. As shown in Figure 2C, Drp1 levels were not altered, while decreases in the levels of MFN1 were observed.

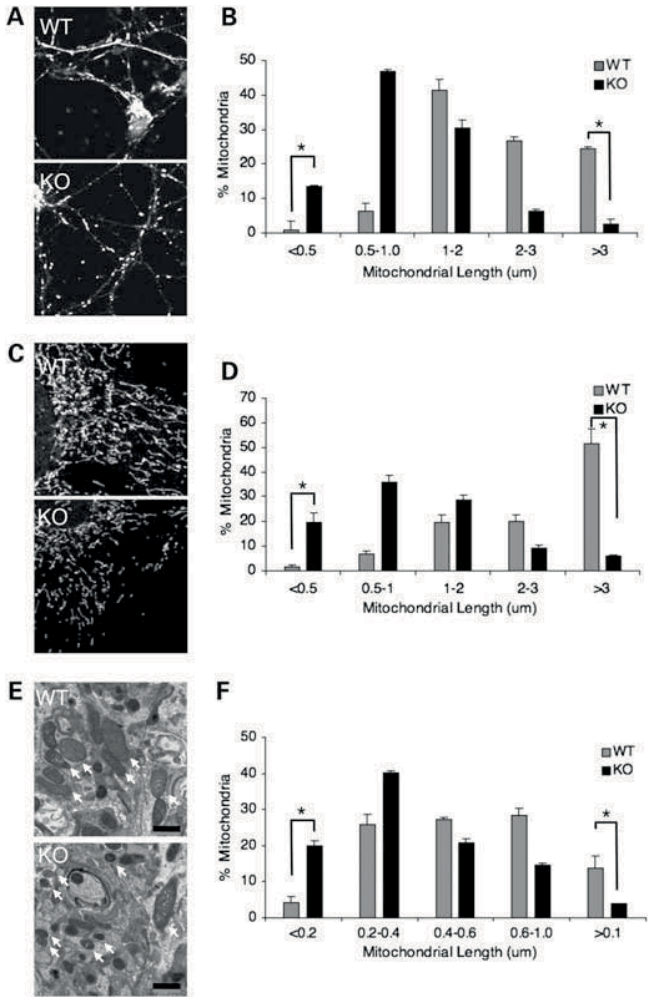

Figure 1. DJ-1 deficiency results in altered mitochondrial morphology *in vitro* and *in vivo*. (**A**) Primary cortical neurons (3 DIV) and (**C**) MEFs from wild-type (WT) and knockout (KO) DJ-1 embryos were harvested and fixed as described under Materials and Methods and immunostained with antibodies to Tom20 to visualize mitochondria. Quantification of mitochondrial lengths in (**B**) primary cortical neurons and (**D**) MEFs was done as described previously [Jahani-Asl *et al*. (20); $n = 4$ independent experiments with a minimum of 500 mitochondria/experiment counted]. Scale Bar = 2 μm. $^{*}P < 0.05$ versus respective +/+ control. (**E**) Electron microscopic images of WT and KO DJ-1 striatum prepared as described in Materials and Methods. (**F**) Quantification of mitochondrial diameters in the striatum of WT and KO DJ-1 mice from three mice/genotype. Scale bar = 500 nm. $^{*}P < 0.05$ versus respective WT DJ-1 control. DIV, days *in vitro*. White arrows in (E) depict mitochondria.

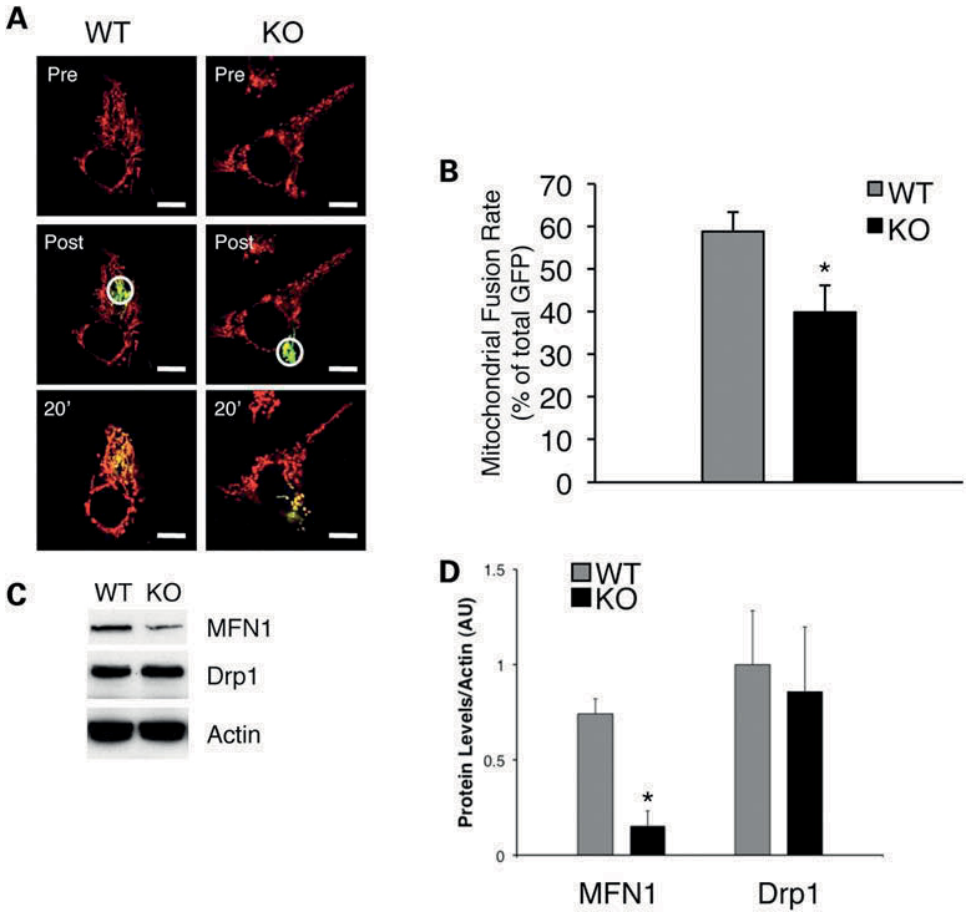

Figure 2. Mitochondrial fusion is decreased with DJ-1 deficiency. (**A**) Confocal images of mitochondria from DJ-$1^{+/+}$ (WT) and DJ-$1^{-/-}$ (KO) MEFs transduced with mitochondrial matrix-targeted DS-red and PA-GFP lentiviruses as described in the Supplementary Information. Images shown are from pre-activation (Pre), immediately following activation (Post) in a small region of interest (indicated by open white circles) as well as following 20 min (20′) of activation. (**B**) Quantification of mitochondrial fusion 20 min post-activation from DJ-$1^{+/+}$ ($n = 14$ cells) and DJ-$1^{-/-}$ ($n = 12$ cells) MEFs. (**C**) Protein extracts were made from DJ-$1^{+/+}$ and DJ-$1^{-/-}$ MEFs and subjected to western blotting for Drp-1, Mfn1 and actin (for loading control). Data shown are representative of at least three independent experiments. (**D**) Quantification of Drp1 and MFN1 protein levels, corrected with actin for loading in DJ-1 WT and KO MEFs. $^{*}P < 0.05$.

Rescue of mitochondrial length in DJ-$1^{-/-}$ neurons abrogates neuronal cell death

Our previous work has shown that overexpression of DJ-1 protects primary cortical neurons from oxidative stress (14). Here we report that DJ-1 deficiency promotes mitochondrial fragmentation. To determine whether these phenomena are linked, primary cortical neurons from DJ-$1^{+/+}$ and DJ-$1^{-/-}$ embryos were infected with dominant-negative dynamin-related protein 1 (DRP1K38E), a mutant form of the mitochondrial fission factor that promotes an elongated mitochondrial reticulum when expressed in cells. Expression levels of Drp1 K38E are shown in Figure 3A and were previously described (21). When primary cortical neurons were subjected to oxidative stress in the form of MPP^{+} (10 μM), a metabolite of the parkinsonism-inducing drug MPTP (22) for 48 h, the hypersensitive DJ-$1^{-/-}$ neurons showed an increase in cell death. However, DJ-$1^{-/-}$ cortical neurons infected with DRP1K38E were completely protected from the toxic effects of MPP^{+} suggesting that mitochondrial fragmentation contributes to oxidative stress-induced sensitivity to cell death (Fig. 3B).

NAC treatment rescues the mitochondrial phenotype in DJ-$1^{-/-}$ neurons

ROS can significantly influence mitochondrial morphology, producing a fragmented phenotype (23). Thus, to assess whether the DJ-1-dependent mitochondrial morphology is related to ROS, we determined whether quenching with N-acetyl-L-cysteine (NAC) might affect mitochondrial fragmentation observed in DJ-1 deficient cells. DJ-$1^{+/+}$ and DJ-$1^{-/-}$ primary cortical neurons were incubated with the ROS scavenger NAC (1 mM) for 48 h (Fig. 4A). Quantification of mitochondrial lengths in vehicle-treated (VEH) DJ-$1^{+/+}$ and DJ-$1^{-/-}$ neurons revealed a similar pattern of mitochondrial morphology deficits as described in Figure 1. While treatment with NAC did not significantly alter mitochondrial length in the DJ-$1^{+/+}$ neurons, treatment of DJ-$1^{-/-}$ neurons with NAC completely reversed the mitochondrial fragmentation where the percentage of mitochondria exhibiting lengths greater than 3 μm increased (i.e. $1.14 \pm 0.305\%$ in KO-VEH to $32.144 \pm 3.141\%$ in KO-NAC; Fig. 2B) and the percentage of fragmented mitochondria decreased (i.e.

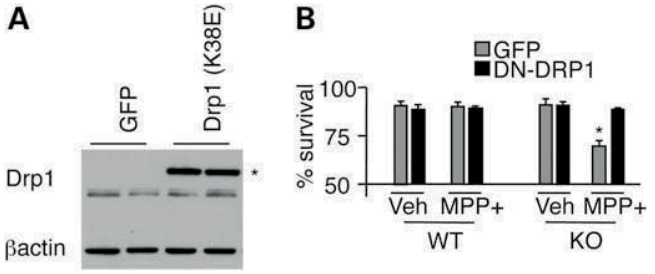

Figure 3. Mitochondrial length is critical for neuronal cell survival. (**A**) Primary cortical neurons infected with either GFP or DN-Drp1 were treated with vehicle (Veh) or MPP+ (10 μM) for 24 h. (**B**) Cell survival was assessed by counting infected cells with intact or dead nuclei plotting the ratio of live:dead cells in treated and untreated DJ-$1^{+/+}$ and DJ-$1^{-/-}$ ($n = 3$ independent experiments, each experiment was performed in triplicate).

<0.5 μm; $15.928 \pm 3.03\%$ in KO-VEH versus $0.198 \pm 0.038\%$ in KO-NAC; Fig. 4B), suggesting that elevated levels of ROS can cause mitochondrial fragmentation, which can be reversed if ROS levels are reduced.

Wild-type DJ-1 but not the DJ-1 C106A mutant rescue mitochondrial morphology defects

It has been previously reported that DJ-1 exerts its effect on oxidative stress via an isoelectric pH shift resulting in a more acidic molecule (24). Importantly, the residue that appears to be sensitive to oxidative modification, in particular hydrogen peroxide-induced oxidation, is a cysteine residue in position 106 (25,26). Thus, to provide additional relevance for the role of ROS and the importance of DJ-1 and oxidative stress in the regulation of mitochondrial morphology, we investigated whether DJ-1 itself actively regulates mitochondrial morphology and to further ascertain whether the DJ-1 mutant that is defective in handling ROS would fail to rescue the DJ-1 deficient phenotype. DJ-$1^{+/+}$ and DJ-$1^{-/-}$ cortical neurons were infected with adenoviruses encoding GFP (as a control), wild-type DJ-1 (DJ-1) or an oxidant mutant form of DJ-1 (C106A). This DJ-1 mutant harbors a cysteine to alanine point mutation at amino acid 106 rendering the oxidative capacity of DJ-1 non-functional. Expression levels of viruses are shown in Supplementary Material, Fig. S1. As shown in Figure 5A and quantified in Figure 5B, DJ-$1^{+/+}$ or DJ-$1^{-/-}$ cortical neurons infected with GFP virus alone display the wild-type mitochondrial phenotype as shown in Figure 1, demonstrating that viral expression of GFP alone does not significantly alter mitochondrial length. Next, while overexpression of DJ-1 had no effect on mitochondrial morphology in DJ-$1^{+/+}$ neurons, DJ-1 expression in DJ-$1^{-/-}$ neurons increased the percentage of mitochondria exhibiting lengths greater than 3 μm ($5.15 \pm 0.826\%$ in KO-GFP versus $47.97 \pm 12.51\%$ in KO DJ-1) and decreased the percentage of fragmented mitochondria ($42.00 \pm 2.56\%$ in KO-GFP versus $1.403 \pm 1.4\%$ in KO DJ-1) supporting the idea that wild-type DJ-1 plays a role in regulating mitochondrial morphology. On the other hand, the oxidant mutant C106A cannot recapitulate the full rescue displayed by WT DJ-1 indicating that the redox function of DJ-1 is critical in promoting a fused mitochondrial reticulum.

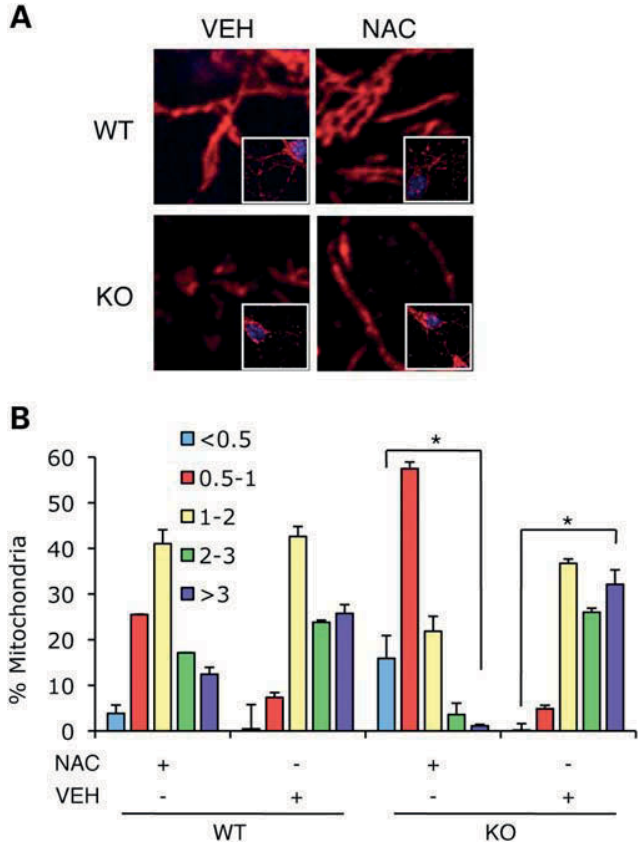

Figure 4. NAC rescues the mitochondrial morphology in DJ-1-deficient primary cortical neurons. (**A**) Confocal images of neurons taken from vehicle- (VEH) and NAC-treated (NAC) WT and KO neurons. Neurons were harvested and fixed 48 h post-treatment and immunostained with antibodies to Tom20 (red) to visualize mitochondria. Scale bar = 2 μm. Inset: lower magnification images. (**B**) Quantification of mitochondrial lengths as described previously [Jahani-Asl *et al*. (20); $n = 3$ independent experiments with a minimum of 500 mitochondria/experiment were counted]. Scale bar = 2 μm. $^{*}P < 0.05$ versus respective controls.

DJ-1 deficiency alters ROS production

If ROS were indeed important in promoting the fragmented mitochondrial phenotype induced by DJ-1 deficiency, we would expect that ROS production would be elevated in mitochondria isolated from DJ-$1^{-/-}$ mice when compared with DJ-$1^{+/+}$ controls. Accordingly, we isolated mitochondrial fractions from brain and skeletal muscle; tissues typically associated with high metabolic requirements and mitochondria and are therefore significant sources of ROS. As predicted, we observed that H_2O_2 production in mitochondria isolated from DJ-$1^{-/-}$ mice is increased 1.4-fold ($P < 0.05$) compared with DJ-$1^{+/+}$ controls in both brain (Fig. 6) and skeletal muscle (Supplementary Material, Fig. S2A), respectively. In either tissue, H_2O_2 production in the DJ-$1^{-/-}$ animals was not further increased with the addition of the mitochondrial Complex I inhibitor rotenone, suggesting that ROS production in DJ-1 deficient mitochondria is generated primarily via Complex I. Despite the increased H_2O_2 production, we did not observe gross differences in mitochondrial function

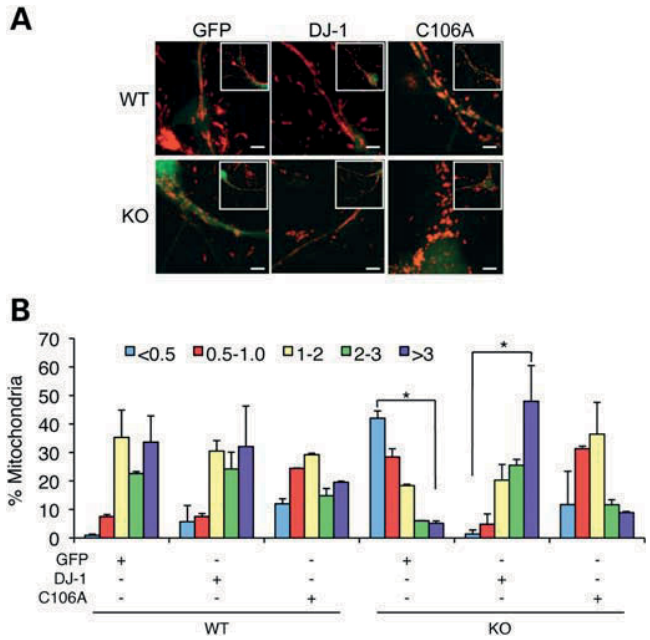

Figure 5. Restoration of wild-type mitochondrial phenotype upon re-expression of DJ-1 *in vitro*. (**A**) Confocal images from WT and KO DJ-1 primary cortical neurons infected with GFP, GFP-DJ-1 and GFP-DJ-1 C106A adenoviruses as described in Materials and Methods. Neurons were harvested and fixed 48 h post-infection and immunostained with antibodies to Tom20 (red) to visualize mitochondria. Inset: lower magnification images. (**B**) Quantification of mitochondrial lengths as described previously [Jahani-Asl *et al*. (20); $n = 3$ independent experiments with a minimum of 500 mitochondria/experiment that were counted per condition]. $^{*}P < 0.05$ versus respective controls.

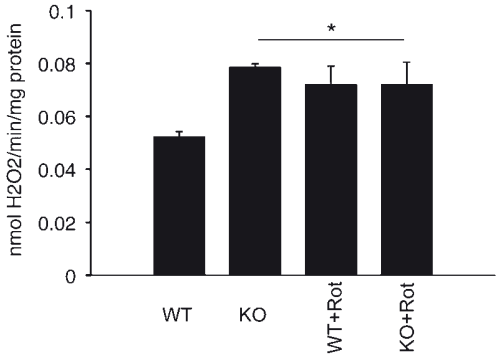

Figure 6. Brain mitochondria isolated from DJ-1 deficient animals produce more ROS. H_2O_2 production was measured in mitochondria isolated from WT and KO DJ-1 brains. $^{*}P < 0.05$ versus WT DJ-1 (P/M, pyruvate/malate; Rot, rotenone).

measurements that were performed such as mitochondrial respiration and citrate synthase activity in DJ-$1^{-/-}$ mice, at least in the brain (Supplementary Material, Fig. S2B and S2C). However, it should be noted that both mitochondrial respiration and citrate synthase activity were decreased in skeletal muscle (Supplementary Material, Fig. S2D and S2E).

Pink1 and Parkin rescue mitochondrial length in DJ-$1^{-/-}$ primary cortical neurons

Previous work conducted in *Drosophila* has demonstrated that Pink1 and Parkin participate in mitochondrial remodeling and are part of the same genetic pathway where Pink1 is upstream of Parkin (9–11,27–29). More recent evidence in mammalian cells is supportive of this notion and also implicates Parkin and Pink1 in the regulation of autophagy, a lysosomal degradation pathway responsible for the degradation of damaged proteins and organelles, including mitochondria (29–31). Thus, we determined whether Pink1 and Parkin could rescue the mitochondrial phenotype in DJ-$1^{-/-}$ primary cortical neurons. Accordingly, we infected DJ-$1^{+/+}$ and DJ-$1^{-/-}$ primary cortical neurons with Pink1 and Parkin viruses, and quantified mitochondrial length as before. Viral expression of Parkin was confirmed in Supplementary Material, Fig. S3. Viral expression of Pink1 was previously described (32). As shown in Figure 7A and C and quantified in Figure 7B and D, overexpression of either Pink1 or Parkin in DJ-$1^{-/-}$ primary cortical neurons promoted an increase in the percentage of mitochondria that were greater than 3 μm in length (5.151 ± 0.826% in KO-GFP versus 44.08 ± 1.646% in KO-Pink; Fig. 7B and 1.686 ± 0.133% in KO-GFP versus 30.126 ± 8.068% in KO-Parkin; Fig. 7D) and decreased the percentage of fragmented mitochondrial (i.e. <0.5 μm; 42.00 ± 2.562%; Fig. 7B in KO-GFP versus 0.948 ± .271% in KO-Pink1 and 34.108 ± 5.50% in KO-GFP versus 4.888 ± 2.924% in KO-Parkin; Fig. 7D) respectively, suggesting that both Pink1 and Parkin can rescue the fragmentation phenotype observed with the loss of DJ-1.

To further confirm these findings, we also quantified the percentage of cells that contained fragmented mitochondria a dopaminergic cell line (SH-5Y5Y) in which DJ-1 was transiently knocked down and subsequently overexpressed with Parkin or Pink1. Confirmation of DJ-1, Pink1 and Parkin overexpression is shown in Supplementary Material, Fig. S4A, S4B and S4C, respectively. As seen in DJ-$1^{-/-}$ primary cortical neurons, transient knockdown of DJ-1 produced a significant increase in cells exhibiting fragmented mitochondria and this phenotype could be prevented with overexpression of DJ-1, Pink1 or Parkin (Fig. 7E and F).

DJ-1 deficiency results in enhanced autophagic flux

As mentioned above, Pink1 and Parkin have both been implicated in the regulation of autophagy in response to mitochondrial damage (9–11,30,31). Our present data show that the loss of DJ-1 leads to increased mitochondrial ROS production and fragmentation. Since both of these parameters are linked with autophagy, we evaluated whether a downstream autophagic response might also be altered with DJ-1 deficiency. To this end, we employed conventional autophagy assays including the evaluation of steady-state microtubule-associated protein light chain 3-II (LC3-II) and the LC3-associated protein p62, under basal conditions as well as GFP-LC3 puncta formation (33). As shown in Figure 8A, the markers

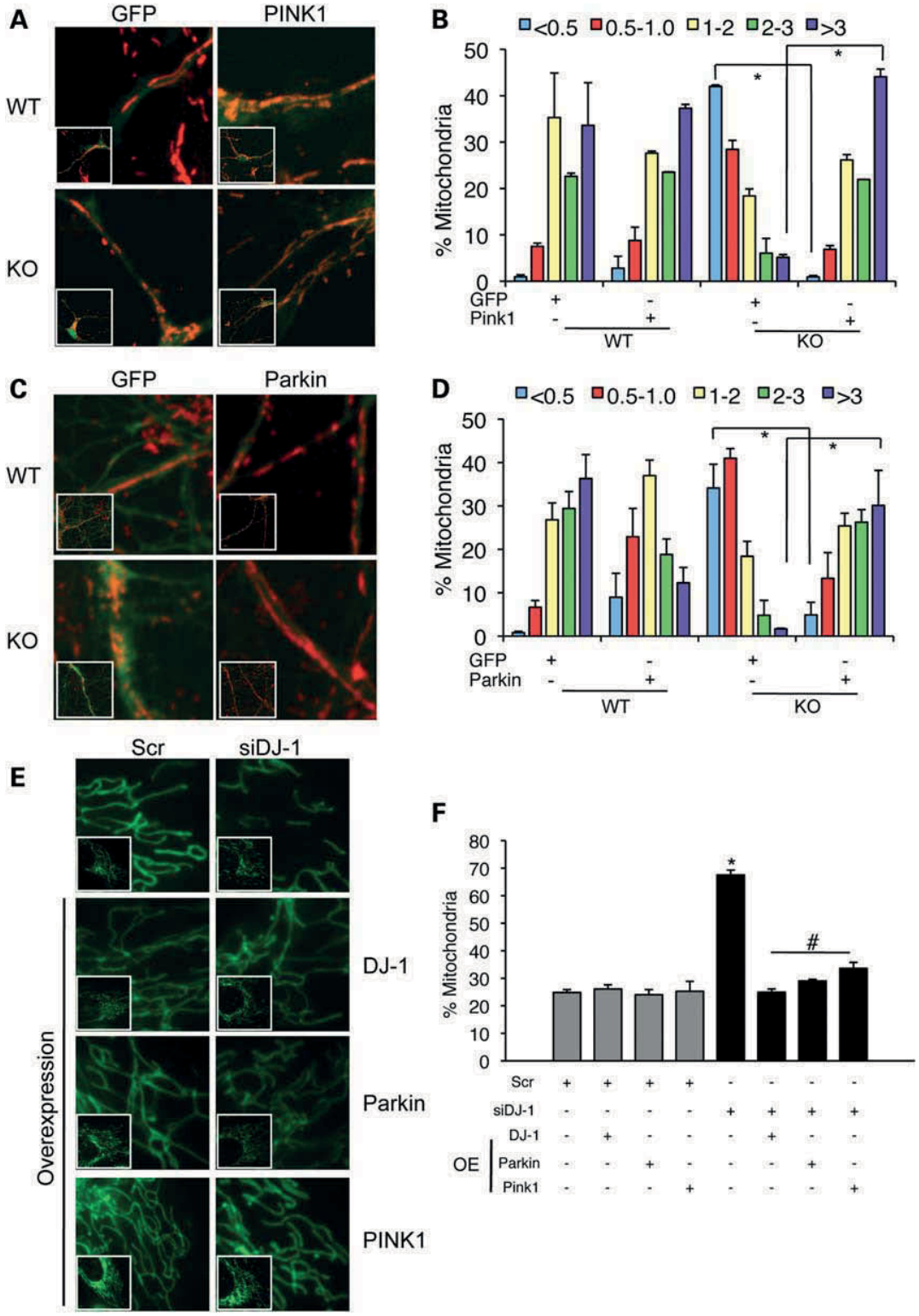

Figure 7. Rescue of mitochondrial morphology with Pink1 and Parkin in a DJ-1-deficient background. (**A**) Confocal images from WT and KO DJ-1 primary cortical neurons infected with GFP or GFP-PINK1 adenoviruses as described in Materials and Methods. Neurons were harvested and fixed 48 h post-infection and immunostained with antibodies to Tom20 (red) to visualize mitochondria. Inset: lower magnification images. (**B**) Quantification of mitochondrial lengths as described previously [Jahani-Asl *et al*. (20); $n = 3$ independent experiments with a minimum of 500 mitochondria/experiment that were counted per condition]. Scale bar = 5 μm. $^{*}P < 0.05$ versus respective controls. (**C**) Confocal images from WT and KO DJ-1 primary cortical neurons infected with eGFP or eGFP-Parkin adeno-associated viruses as described in Materials and Methods. Neurons were harvested and fixed 4 days post-infection and immunostained with

of autophagy p62 and LC3-II levels in DJ-1$^{-/-}$ mouse embryonic fibroblasts (MEFs) are decreased compared with DJ-1$^{+/+}$ controls, indicating that the loss of DJ-1 results in a reduction in autophagosomes since levels of LC3-II correlate with autophagosome number (34,35). This reduction can either be attributed to the downregulation of autophagosome formation or enhanced autophagic degradation (34). The use of bafilomycin A1, a late inhibitor of autophagy (34), restores steady-state p62 as well as LC3-II protein levels suggesting that the loss of DJ-1 enhances autophagic degradation, in other words autophagic activity is overactive. Next, we made use of the H1299 cell line in which GFP-LC3 is stably expressed and transiently reduced DJ-1 protein levels via siRNA to confirm the DJ-1-dependent perturbations in the autophagic pathway. As shown in Figure 8B, at 48 h post-transfection, the level of DJ-1 was significantly reduced upon transfection of a siRNA specifically targeted to DJ-1. The effect of DJ-1 knockdown was accompanied by a significant decrease in p62 levels, and an increased accumulation of cleaved GFP demonstrating that autophagic activity is enhanced by transient knockdown of DJ-1 (Fig. 8B). This was further observed with immunofluorescence where GFP puncta formation was increased by 1.5-fold ($P < 0.05$) with transient knockdown of DJ-1 (Fig. 8C and D). Given the recent involvement of Parkin and PINK1 in the regulation of mitochondria specific autophagy (mitophagy), we also assessed the steady-state levels of mitochondrial markers to determine whether DJ-1 may also play a role. As shown in Figure 8E, loss of DJ-1 does not induce significantly altering the expression of *cytochrome c* oxidase (COX) subunits of complex I or complex V. Furthermore, expression of the outer mitochondrial membrane marker Tom20 was also unchanged. This suggests that mitophagy, at least at a gross level, is not affected by the loss of DJ-1. This theory is supported by initial observations that Parkin is not significantly recruited to mitochondria in DJ-1 KO cells under basal conditions (Joselin *et al*., unpublished data).

Mitochondrial morphology and autophagy are also perturbed in human DJ-1-linked Parkinson's disease

Finally, to provide evidence that the DJ-1-dependent perturbations in mitochondrial homeostasis also extend to a human model of DJ-1-linked PD, we obtained human lymphoblasts isolated from control and PD patients. The PD lymphoblasts were obtained from an Italian and Dutch family, respectively (12). The previously described L166P pathogenic mutation found in the Italian family consists of a leucine to proline substitution at amino acid 166, while the Deletion (Del) mutation, found in a Dutch family, results from a complete loss of exons 1–5 (12). As shown in Figure 9A, similar to the pattern of mitochondrial morphology observed in DJ-1$^{+/+}$ and DJ-1$^{-/-}$ murine tissues, electron microscopic analysis of lymphoblasts isolated from human PD patients (L166P, DEL) contained a greater percentage of fragmented mitochondria compared with control lymphoblasts (i.e. <0.5 μm; $41.578 \pm 2.41\%$ and $48.316 \pm 6.02\%$ in PD versus $12.62 \pm 3.03\%$ and $9.755 \pm 2.23\%$ in controls) and a smaller percentage of mitochondria that were longer than >1.0 μm ($23.019 \pm 0.84\%$ and $23.997 \pm 0.94\%$ in PD versus $41.578 \pm 2.41\%$ and $48.316 \pm 6.02\%$ in controls; Fig. 9B). We also evaluated whether autophagy was similarly affected in human DJ-1-linked PD and observed that p62 was decreased in both PD patient cell lines when compared with CTRL lymphoblasts (Fig. 9C). These data confirm that the mitochondrial morphology as well as changes in autophagic markers observed in DJ-1$^{+/+}$ and DJ-1$^{-/-}$ are also present in human DJ-1-linked PD.

DISCUSSION

Mitochondrial dysfunction appears to contribute to the progression of sporadic PD and it has been postulated that excess ROS produced as the result of mitochondrial dysfunction may be an important reason for which neurons exhibit increased sensitivity to oxidative stress-induced neuronal cell death (36,37). Emerging evidence points to underlying defects in mitochondrial morphology and dynamics as a potential mechanism to explain this increased sensitivity (38). In PD, this relationship is significant since several PD-linked genes (DJ-1, Parkin, Pink1) have been found to reside or translocate to the mitochondrial compartments (7,8,29,39–42), participate in mitochondrial remodeling (7,9–11) and actively regulate mitochondrial quality control (18,19,41–43). Of the three PD-linked genes that have been associated with mitochondria, the least is known regarding the role of DJ-1.

Mitochondrial morphology, dynamics and ROS production are altered by the loss of DJ-1

We first began our investigation by characterizing the impact of DJ-1 deficiency on mitochondrial morphology and function under steady-state conditions in a variety of experimental systems. We demonstrated both *in vitro* and *in vivo* neuronal and non-neuronal cells, as well as in brain tissue that mitochondria are significantly more fragmented with the loss of DJ-1. Importantly, we also extended these findings to human DJ-1-linked PD to convincingly implicate that an aberrant DJ-1-dependent mitochondrial phenotype in a more disease relevant model. We also demonstrated that the mitochondrial phenotype produced by the loss of DJ-1 contributes to the

antibodies to Tom20 (red) to visualize mitochondria. Inset: lower magnification images. (**D**) Quantification of mitochondrial lengths as described previously [Jahani-Asl *et al*. (20); $n = 3$ independent experiments with a minimum of 500 mitochondria/experiment that were counted per condition]. Scale bar = 5 μm. $^{*}P < 0.05$ versus respective controls. (**E**) Confocal images from SH-5Y5Y cells in which DJ-1 has been knocked down via siRNA, and transfected with DJ-1, Parkin or PINK1 as described in the Materials and Methods. Inset: lower magnification images. (**F**) Quantification of at least 300 cells/condition was performed as described in the Materials and Methods. Data are representative of at least three independent experiments where each condition was done in triplicate. OE, overexpression. Scale bar = 5 μm. $^{*}P < 0.05$ versus siDJ-1- and $^{\#}P < 0.05$ versus siDJ-1.

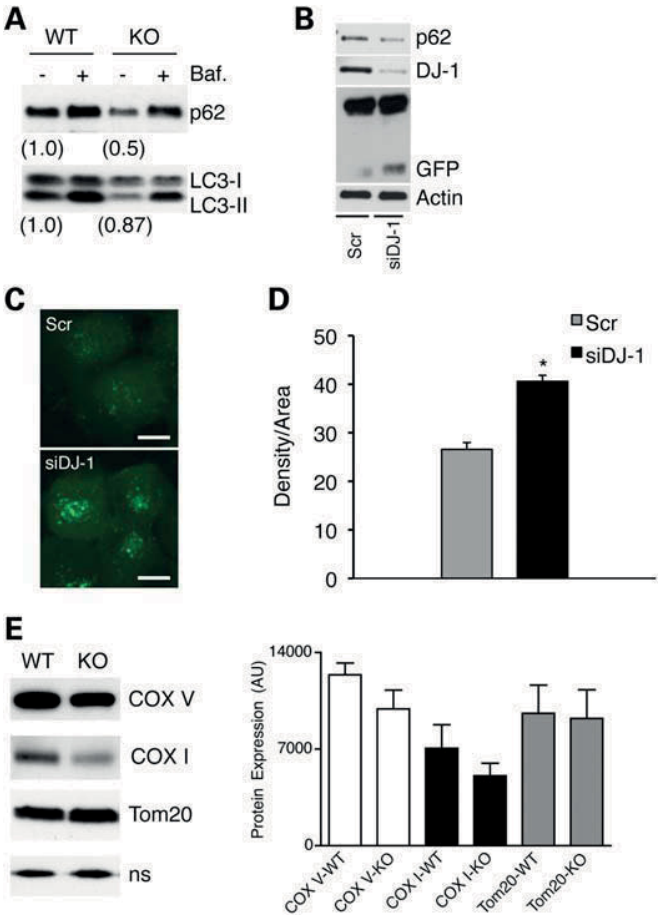

Figure 8. Cells deficient for DJ-1 undergo enhanced autophagic activity. (**A**) Proteins were extracted from WT and KO DJ-1 MEFs treated with (+) or without (−) Bafilomycin (10 μg/ml, 3 h) and subjected to western blotting for p62 and LC3-I and LC3-II levels. Numbers below representative images refer to fold changes versus WT (-Baf) after correction for actin. Data are representative of three independent experiments. (**B**) Total cell lysates from H1299 cells stably expressing GFP-LC3 and transfected with either scrambled (Scr) or a siRNA against DJ-1 (siDJ-1) were analyzed by western blotting for DJ-1, p62 and free GFP. Data are representative of at least three independent experiments. (**C**) Confocal images of H1299 cells stably expressing GFP-LC3 cells transfected with either scrambled (Scr) or a siRNA against DJ-1 (siDJ-1). (**D**) The density of GFP puncta in Scr versus siDJ-1 conditions was analyzed in at least 150 cells/condition. Data are representative of three independent experiments $^{*}P < 0.05$, siDJ-1 versus. Scr. control. Scale bar = 2 μm. (**E**) Total cell lysates from DJ-1 WT and KO MEFs were subjected to western blotting for COX V, COX I and Tom20 levels (n.s., non-specific band was used as a loading control). Data are representative of five to seven independent experiments.

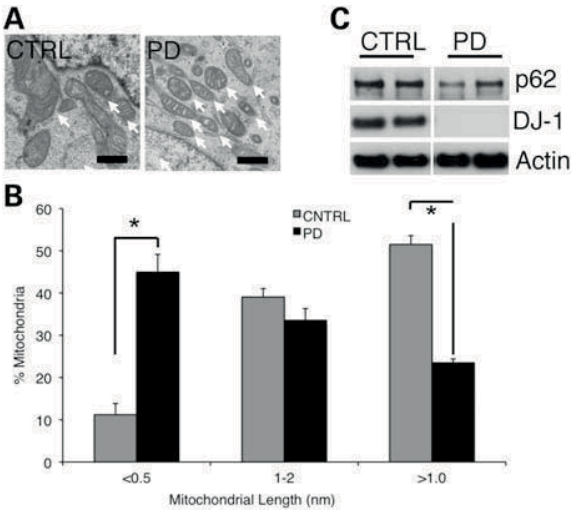

Figure 9. Mitochondrial morphology and autophagy are also perturbed in human DJ-1-linked PD. (**A**) EM images of mitochondria from human lymphoblasts isolated from healthy control (C48 and GEPA) and PD (L166P and Del) patients. (**B**) Quantification of mitochondrial diameters in human lymphoblasts ($n = 4$; at least 200 mitochondria/experiment were counted). Scale bar = 500 nm. $^{*}P < 0.05$, PD versus control. (**C**) Total protein was extracted from human control (CTRL), and PD (L166P and Del) lymphoblasts were subjected to western blotting for DJ-1, p62 and actin. Data are quantified as the relative changes in steady state protein levels corrected for loading using actin. Five independent experiments are represented. $^{*}P < 0.05$, PD versus control. White arrows in (A) depict mitochondria.

oxidative stress-induced sensitivity to cell death since reversal of the mitochondrial phenotype by overexpression of DN-Drp1 to rescue mitochondrial fragmentation abrogated neuronal cell death induced by MPP+. Is the fragmented phenotype a result of increased fission or decreased fusion? Since mitochondrial fusion rates and the steady state levels of the mitochondrial fusion protein MFN1 are decreased in DJ-1 deficient cells, we would be tempted to speculate that mitochondrial fusion is decreased. However, our results also do not rule out that an increase in mitochondrial fission is also a possibility. Indeed, during the preparation of this manuscript, Krebiehl *et al.* (44) demonstrated that altered mitochondrial morphology induced by the loss of DJ-1 could be attributed to changes in mitochondrial fission. The implications of decreased or increased mitochondrial fusion or fission that occurs with DJ-1 deficiency could readily explain the increased sensitivity of these cells to oxidative stress (14), as it is known that fragmented mitochondria precedes apoptosis, or alternatively renders mitochondria more susceptible to death-inducing stimuli (20,45–48).

ROS is important in establishing the DJ-1-dependent phenotype

Based on the known impact of excess ROS on mitochondrial morphology (23), we suspected that the increased ROS produced by mitochondria from DJ-$1^{-/-}$ animals could be responsible for the fragmented phenotype. Indeed, we confirmed this hypothesis by first demonstrating that scavenging ROS with the use of NAC or WT DJ-1 (itself a suspected free radical scavenger), but not an oxidant mutant of DJ-1 (C106A), was able to rescue the fragmented phenotype observed in DJ-1 deficient primary cortical neurons. Our data also show that while the excess H_2O_2 produced within mitochondria by the loss of DJ-1 is sufficient to alter mitochondrial morphology, they are not produced in sufficient concentrations to cause overt changes in mitochondrial oxygen consumption and citrate synthase activity, at least in the

brain. In all likelihood, these factors contribute to the lack of any gross neuronal abnormalities including dopaminergic neuron numbers in the substantia nigra, fiber densities and dopamine levels in the striatum and the absence of any behavioral deficits in untreated DJ-1 deficient mice (14). It is therefore more likely that DJ-1 deficiency compromises the sub-cellular milieu rendering them more vulnerable to additional stress. Indeed, the observation that DJ-1 deficiency does not seem to grossly affect mitophagy leading to the accumulation, instead of the removal of fragmented mitochondria further adds to this possibility. This theory is also supported by initial observations that Parkin is not significantly recruited to mitochondria in DJ-1 KO cells under basal conditions (Joselin *et al*., unpublished data).

Indeed, as we have previously demonstrated, DJ-1 deficient animals/cells are hypersensitive to MPTP or hydrogen peroxide treatment and this hypersensitization results in the previously described dopaminergic cell death and behavioral deficits, effectively recapitulating some pathological and clinical features of human PD (14).

Pink1 and Parkin can rescue DJ-1 deficient mitochondrial fragmentation

We also assessed the relationship of DJ-1 with Parkin and Pink1, two recessively linked PD genes, as they have all been implicated in regulating aspects of mitochondrial morphology and/or dynamics. Previous studies using the *Drosophila melanogaster* model have shown that the loss of Pink1 and Parkin independently compromise mitochondrial integrity (9,11,28,49). Since double mutants produce an identical phenotype to each mutant alone, and overexpression of Parkin rescues Pink1 deficits but not *vice versa*, it was postulated that they function in the same pathway with Pink1 positioned upstream of Parkin (9,11,28,49). More recently, it has been shown that Pink1 and Parkin actively participate in mitochondrial quality control (18,19,41–43). Given that DJ-1 deficiency induces oxidative stress and mitochondrial defects, we hypothesized that overexpression of these mitochondrial quality control factors would rescue the DJ-1 deficient mitochondrial phenotype. We confirmed this hypothesis using two different models. First, Pink1 and Parkin were overexpressed in DJ-1 deficient primary cortical neurons. In this model, overexpression of either Pink1 or Parkin rescued the fragmented mitochondrial phenotype in DJ-1 deficient cells. Second, we used a dopaminergic cell line to overexpress Pink1 and Parkin in cells where DJ-1 levels were reduced down by siRNA. Similar to our findings in primary cortical neurons, the DJ-1-induced fragmentation phenotype produced by knockdown of DJ-1 was reversed with overexpression of either Pink1 or Parkin. It is important to stress that the exact mechanistic link between DJ-1 and Pink/Parkin is not clear. However, we would propose that DJ-1 somehow modulates the actions or activity of Pink1 and/or Parkin, possibly via its effect on the ROS environment. Given the effects of Parkin and PINK1 deficiency on antioxidant capacity and ROS production (50–52), it is also tempting to speculate that overexpression of either gene could potentially ameliorate that ROS milieu of the DJ-1 deficient cells, thereby reversing the fragmented phenotype. Alternatively, a more direct regulation is also possible.

DJ-1 deficiency increases autophagic activity

Increasing evidence has implicated several PD-linked genes including Pink and Parkin in the process of autophagy (18,19,41–43). Two recently published studies have now implicated DJ-1 (19,44). We also pursued this phenomenon in the present manuscript and suggest that the loss of DJ-1 promotes enhanced autophagy resulting in increased turnover. According to Mizushima and Yoshimori (34) and Rubinsztein *et al*. (35), a loss in the levels of the autophagy markers LC3-II and p62 at a given time is either attributed to a downregulation of autophagosome formation or enhanced degradation. If the level of LC3-II or p62 rises following incubation with autophagy inhibitors such as Bafilomycin A1, as was seen in the present study, it is considered that during the course of the experimental time frame that the number of molecules degraded exceeds the number being produced. We further assessed the effect of transient DJ-1 knockdown on autophagic activity and found that within 48 h of DJ-1 knockdown, the autophagy was increased, as measured by the decrease in p62 levels and the increase in LC3 puncta formation. It has previously been shown that following acute starvation, autophagy is increased and that prolonged starvation leads to excessive activity and turnover (35). Acute starvation led to decreased p62 levels and LC3 puncta formation, whereas a complete loss of LC3-II levels was observed during prolonged starvation. By analogy, one could interpret that acute DJ-1 knockdown results increase autophagic activity, while germline deletion is associated with excessive autophagic activity resulting in increased turnover. In either condition, autophagic activity is enhanced with DJ-1 deficiency. Future studies will more carefully evaluate the nature of this phenomenon. Additionally, whether DJ-1 more directly regulates the autophagic response or merely influences the ROS environment leading to increased flux is unknown and warrants further study. The evidence suggesting that ROS triggers autophagy would be in keeping with the latter suggestion (53–55). Furthermore, the idea that DJ-1 participates in the Pink1/Parkin pathway temptingly suggests the possibility that DJ-1 could modulate Pink1/Parkin activity and thereby regulate autophagic activity. Alternatively, DJ-1 may more directly regulate additional upstream activators of autophagy, including mTOR and AMPK, which has been suggested previously (19). More careful analyses will be required to validate these possibilities.

In conclusion, this study demonstrates that DJ-1 plays an active role in the remodeling of mitochondria and regulation of autophagy. Cells lacking DJ-1 display a fragmented mitochondrial morphology that can be rescued with ROS scavengers, wild-type DJ-1, Parkin and Pink1. This DJ-1-dependent mitochondrial morphology contributes to oxidative stress-induced sensitivity to cell death since reversal of this mitochondrial phenotype abrogates neuronal cell death. Finally, we also show that DJ deficiency leads to altered autophagy in DJ-1-deficient murine and human cells. We propose that under conditions of oxidative stress, these derangements may account for the reported increased sensitivity to cell death of DJ-1 deficient neurons.

MATERIALS AND METHODS

Antibodies

The following antibodies were used in this study: mouse anti-Drp-1 (BD Transduction), chicken anti-MFN1 (Novus Biological), rabbit anti-MFN2 (Santa Cruz), mouse anti-COX V (Mitosciences), mouse anti-COX I (Mitosciences), rabbit anti-Tom20 (Santa Cruz), rabbit anti-LC3 (Novus Biologicals), guinea pig anti-p62 (ARP), mouse anti-p62 (Santa Cruz), mouse anti DJ-1 (Stressgen), mouse anti-parkin mouse PRK8 (Santa Cruz), anti-PINK1 polyclonal antibody (Novus Biologicals), anti-DJ1 polyclonal antibody (Abcam),mouse anti-&β-cactin (Sigma), horseradish peroxidase-conjugated secondary antibodies (Bio-Rad).

Cell lines, transfections, viral infections and plasmids

MEFs and primary cortical neurons were derived from E14.5–15.5 transgenic DJ-1 animals as previously described (14). Immortalized human lymphoblasts obtained from DJ-1-linked PD (Del or L166P) or healthy controls were cultured as described previously (56). H1299 cell line stably expressing GFP-LC3 cultured as previously described (57). SH-5Y5Y cells were cultivated as previously described (58). For RNA interference, SH-5Y5Y or H1299 cells were reverse-transfected with Stealth siRNA (Invitrogen) using Lipofectamine RNAiMAX (Invitrogen) or siRNA (Santa Cruz) using siLentFect (Bio-Rad), respectively, according to the manufacturer's instructions. *DNA Constructs (SH-5Y5Y cells)*: Human wild-type (wt) parkin and human wild-type PINK1 were described earlier (49,59). Human wild-type DJ was amplified from a human brain cDNA library and inserted into the pcDNA3.1 vector (Invitrogen). *Viral plasmids and infections (primary cortical neurons)*: for rescue studies, cortical neurons were harvested from DJ-$1^{+/+}$ or DJ-$1^{-/-}$ littermate embryos (produced by a heterozygote cross) at E15.5 and plated at a density of 150 000 cells per well (24-well dish) on glass cover slips coated with 1XPoly-D-Lysine. Viral particles expressing GFP, DJ-1, DJ-1 C106A, Pink1 or Parkin were administered at a multiplicity of infection (MOI) of 30 at the time of plating. Cortical neurons infected with DJ-1, DJ-1C106A and Pink1 were harvested 48 h following infection. Cortical neurons infected with Parkin were harvested 4 days post-infection and plating. For cell survival studies, cortical neurons harvested as described above were infected with either control (EGFP) adenovirus or dominant-negative Drp-1 (ECFP-C1 DLVP K38E) adenoviruses at MOI of 40 and then immediately seeded into 24-well plates at an approximate density of 350 000 neurons/well. Neurons were cultured for 3 days and then treated with 10 μM MPP^+ for 24 h.

Cell survival

Neuronal survival was evaluated by assessing nuclear integrity of GFP/CFP-positive neurons as done previously (14).

Citrate synthase activity

Maximal activity of citrate synthase (EC 4.1.3.7) was measured at 25°C in previously frozen homogenate and mitochondria from brain and skeletal as previously described (60).

Confocal microscopy/immunofluoresence/mitochondrial fusion rates

Confocal images were acquired with a 63× objective (1.4) by an inverted Laser Scanning Microscope (LSM510 META, Zeiss). Mitochondrial fusion rates were calculated as previously described (21).

Generation and genotyping of DJ-1 mice

The generation and genotype of the DJ-1 deficient mice has previously been described in detail (61).

H_2O_2 generation

Mitochondrial H_2O_2 production rate was determined in freshly isolated mitochondria from sketelal muscle and brain using the *p*-hydroxyphenylacetate (PHPA) fluorometric assay (62). Mitochondria (0.1 mg/ml) were incubated in standard incubation medium (IM: 120 mM KCl, 1 mM EGTA, 5 mM KH_2PO_4, 2 mM $MgCl_2$ and 3 mM HEPES; pH 7.4) supplemented with 0.3% defatted BSA. H_2O_2 production was monitored for up to 25 min using a temperature-controlled fluorimeter (BioTek, FLx800) at 37°C. Fluorescence readings were converted to H_2O_2 production rates by use of a standard curve.

Immunofluoresence (primary cortical neurons and MEFs)

Cortical neurons or MEFs were fixed with 4% PFA diluted in cell culture medium for 15 min at 37°C. Cells were then washed 3× with 1XPBS. Immediately following this, cells were permeabilized and blocked with 10% normal goat serum-0.1% Triton X/PBS for 1 h at room temperature. Cells were then stained with Tom-20 (1:100, a kind gift from Dr Gordon Shore or from Santa Cruz) or *cytochrome c* (1:100, BD Biosciences, in 5% normal goat serum overnight at 4°C) for the visualization of mitochondria. The following day, cells were washed 3× with 5% normal goat serum/PBS and then incubated for 1 h with the appropriate Alexa conjugated fluorophores in 5% normal goat serum/PBS. Cells were then washed 3× with 1XPBS, rinsed in sterile H_2O and mounted onto microscope slides using Gel Mount (Sigma).

Fluorescent staining of mitochondria and western blot analysis (SH-5Y5Y cells)

SH-5Y5Y cells were grown on 15 mm glass cover slips. Cells were fluorescently labeled with 0.1 μM $DiOC_6$ (3) in cell culture medium for 15 min. After washing the cover slips with medium, living cells were analyzed for mitochondrial morphology by fluorescence microscopy using a Leica DMRB microscope (Leica, Wetzlar, Germany). Cells were categorized in two classes according to their mitochondrial morphology: tubular or fragmented. Cells displaying an intact network of tubular mitochondria were classified as tubular. When this network was disrupted and mitochondria appeared predominantly spherical or rod-like, they were classified as fragmented. The mitochondrial morphology of at least 300 cells per plate was determined in a blinded manner, i.e. the researcher was blind to the transfection status.

Quantifications were based on triplicates of at least three independent experiments. Proteins were analyzed by SDS–PAGE and western blotting using polyvinylidene difluoride membranes (Millipore, Schwalbach, Germany). The membranes were blocked with 5% non-fat dry milk in TBS containing 0.1% Tween 20 (TBS-T) for 1 h at room temperature and then incubated with the primary antibody in blocking solution for 16 h at 4°C. After extensive washing with TBS-T, the membranes were incubated with HRP-conjugated secondary antibody for 60 min at room temperature. Following washing with TBS-T, the antigen was detected with the enhanced chemiluminescence (ECL) detection system or ECL plus detection system (Amersham Biosciences, Freiburg, Germany).

Immunoblotting

Cell lysis was carried out identically for both MEFs and neurons. Cells were washed twice with PBS, scraped in lysis buffer containing 50 mM Tris–HCl pH 7.5, 100 mM NaCl, 0.4% Triton X-100, 1 mM DTT and 1× protease inhibitor cocktail (Roche). Samples were kept on ice for 20 min and then spun with maximal speed at 20 000*g* at 4°C for 5 min. Protein quantification was carried out using both Bradford (Bio-Rad) and BCA (Pierce) methods. Fifteen micrograms of each lysate was electrophoresed on 12% SDS–polyacrylamide gels, or 4–20% gradient gels (Invitrogen) and transferred to polyvinylidene fluoride (PVDF) or nitrocellulose membranes (Millipore). For tissue lysates, 15 μg of each tissue lysate was electrophoresed on 12% SDS–PAGE gels and transferred to polyvinylidene fluoride (PVDF) or nitrocellulose membranes (Millipore).

Isolation of mitochondria

DJ-$1^{+/+}$ or DJ-$1^{-/-}$ mice (4–6 months old) were euthanized by decapitation for isolation of skeletal muscle and brain mitochondria. Isolation of skeletal muscle mitochondria was performed using a modified method of Chappell and Perry (63), as previously described in detail (64). Brain mitochondria were isolated as described (50).

Lentivirus production and transduction

Lentiviral vectors were generated by transient transfection in 293T cells using PEI. The constructs for manufacturing the lentiviruses were obtained from Addgene.org. Protocols used to manufacture and purify lentiviruses were done according to Tronolab's protocols (www.tronolab.com).

Oxygen consumption

Oxygen consumption was measured in isolated brain mitochondria (0.3 mg/ml) at 37°C using a Clark-type oxygen electrode (Hansatech, Norfolk, UK), incubated in standard incubation medium (IM: 120 mM KCl, 1 mM EGTA, 5 mM KH_2PO_4, 2 mM $MgCl_2$ and 3 mM HEPES; pH 7.4) containing 0.3% defatted BSA and assumed to contain 406 nmol O/ml at 37°C (65). State 3 (maximum phosphorylating) respiration was determined using 5 mM glutamate/5 mM malate as substrate, and 500 μM ADP. State 4 (non-phosphorylating or maximal leak-dependent respiration) was determined following addition of oligomycin (8 μg/ml). All measurements were performed in duplicate.

Statistical analyses

Unless otherwise described, data analysis was carried out using independent two-tailed *t*-tests. Significance was marked by * when $P < 0.05$. All data are presented as means ± SEM.

SUPPLEMENTARY MATERIAL

Supplementary Material is available at *HMG* online.

ACKNOWLEDGEMENTS

The authors would like to thank Dr Gordon Shore (McGill University, Montreal, Canada) for the provision of the GFP-LC3 stable cell line and the α-Tom20 antibody. The authors also wish to thank Paul Marcogliese and Viola Mugamba for technical assistance, and Dr Marc Germain for helpful insights on the manuscript.

Conflict of Interest statement. None declared.

FUNDING

This work was supported by grants from the Canadian Institutes of Health Research (CIHR), Heart and Stroke Foundation of Ontario (HSFO), Neuroscience Canada (Brain Repair Grant), Parkinson's Society Canada (PSC), Parkinson's Disease Foundation (PDF) and World Class University program through the National Research Foundation of Korea funded by the Ministry of Education, Science and Technology, South Korea (R31-2008-000-20004-0) to D.S.P. I.I. was supported by a CIHR Postdoctoral fellowship. H.A. was supported by a Heart and Stroke Foundation of Canada doctoral award. E.L.S. was supported by a Canadian Diabetes Association (CDA) Postdoctoral fellowship. A.J.-A. was supported by a CIHR doctoral award. M.W.C.R. was supported by a Heart and Stroke Foundation of Ontario Master's student award; S.C. was supported by a summer student award from the centre for stroke recovery (CSR); S.J.H. was supported by PSC Master's Student award.

REFERENCES

1. Abou-Sleiman, P.M., Muqit, M.M. and Wood, N.W. (2006) Expanding insights of mitochondrial dysfunction in Parkinson's disease. *Nat. Rev.*, **7**, 207–219.
2. Schapira, A.H. (1998) Mitochondrial dysfunction in neurodegenerative disorders. *Biochim. Biophys. Acta*, **1366**, 225–233.
3. Mann, V.M., Cooper, J.M., Krige, D., Daniel, S.E., Schapira, A.H. and Marsden, C.D. (1992) Brain, skeletal muscle and platelet homogenate mitochondrial function in Parkinson's disease. *Brain*, **115**, 333–342.
4. Bindoff, L.A., Birch-Machin, M.A., Cartlidge, N.E., Parker, W.D. Jr and Turnbull, D.M. (1991) Respiratory chain abnormalities in skeletal muscle from patients with Parkinson's disease. *J. Neurol. Sci.*, **104**, 203–208.

5. Drechsel, D.A. and Patel, M. (2008) Role of reactive oxygen species in the neurotoxicity of environmental agents implicated in Parkinson's disease. *Free Radic. Biol. Med.*, **44**, 1873–1886.
6. Cleeter, M.W., Cooper, J.M. and Schapira, A.H. (1992) Irreversible inhibition of mitochondrial complex I by 1-methyl-4-phenylpyridinium: evidence for free radical involvement. *J. Neurochem.*, **58**, 786–789.
7. Silvestri, L., Caputo, V., Bellacchio, E., Atorino, L., Dallapiccola, B., Valente, E.M. and Casari, G. (2005) Mitochondrial import and enzymatic activity of PINK1 mutants associated to recessive parkinsonism. *Hum. Mol. Genet.*, **14**, 3477–3492.
8. Zhou, C., Huang, Y., Shao, Y., May, J., Prou, D., Perier, C., Dauer, W., Schon, E.A. and Przedborski, S. (2008) The kinase domain of mitochondrial PINK1 faces the cytoplasm. *Proc. Natl Acad. Sci. USA*, **105**, 12022–12027.
9. Poole, A.C., Thomas, R.E., Andrews, L.A., McBride, H.M., Whitworth, A.J. and Pallanck, L.J. (2008) The PINK1/Parkin pathway regulates mitochondrial morphology. *Proc. Natl Acad. Sci. USA*, **105**, 1638–1643.
10. Deng, H., Dodson, M.W., Huang, H. and Guo, M. (2008) The Parkinson's disease genes pink1 and parkin promote mitochondrial fission and/or inhibit fusion in Drosophila. *Proc. Natl Acad. Sci. USA*, **105**, 14503–14508.
11. Clark, I.E., Dodson, M.W., Jiang, C., Cao, J.H., Huh, J.R., Seol, J.H., Yoo, S.J., Hay, B.A. and Guo, M. (2006) Drosophila pink1 is required for mitochondrial function and interacts genetically with parkin. *Nature*, **441**, 1162–1166.
12. Bonifati, V., Rizzu, P., van Baren, M.J., Schaap, O., Breedveld, G.J., Krieger, E., Dekker, M.C., Squitieri, F., Ibanez, P., Joosse, M. *et al.* (2003) Mutations in the DJ-1 gene associated with autosomal recessive early-onset parkinsonism. *Science*, **299**, 256–259.
13. Aleyasin, H., Rousseaux, M.W., Phillips, M., Kim, R.H., Bland, R.J., Callaghan, S., Slack, R.S., During, M.J., Mak, T.W. and Park, D.S. (2007) The Parkinson's disease gene DJ-1 is also a key regulator of stroke-induced damage. *Proc. Natl Acad. Sci. USA*, **104**, 18748–18753.
14. Kim, R.H., Smith, P.D., Aleyasin, H., Hayley, S., Mount, M.P., Pownall, S., Wakeham, A., You-Ten, A.J., Kalia, S.K., Horne, P. *et al.* (2005) Hypersensitivity of DJ-1-deficient mice to 1-methyl-4-phenyl-1,2,3,6-tetrahydropyrindine (MPTP) and oxidative stress. *Proc. Natl Acad. Sci. USA*, **102**, 5215–5220.
15. Andres-Mateos, E., Perier, C., Zhang, L., Blanchard-Fillion, B., Greco, T.M., Thomas, B., Ko, H.S., Sasaki, M., Ischiropoulos, H., Przedborski, S. *et al.* (2007) DJ-1 gene deletion reveals that DJ-1 is an atypical peroxiredoxin-like peroxidase. *Proc. Natl Acad. Sci. USA*, **104**, 14807–14812.
16. Taira, T., Saito, Y., Niki, T., Iguchi-Ariga, S.M., Takahashi, K. and Ariga, H. (2004) DJ-1 has a role in antioxidative stress to prevent cell death. *EMBO Rep.*, **5**, 213–218.
17. Park, J., Kim, S.Y., Cha, G.H., Lee, S.B., Kim, S. and Chung, J. (2005) Drosophila DJ-1 mutants show oxidative stress-sensitive locomotive dysfunction. *Gene*, **361**, 133–139.
18. Gonzalez-Polo, R., Niso-Santano, M., Moran, J.M., Ortiz-Ortiz, M.A., Bravo-San Pedro, J.M., Soler, G. and Fuentes, J.M. (2009) Silencing DJ-1 reveals its contribution in paraquat-induced autophagy. *J. Neurochem.*, **109**, 889–898.
19. Vasseur, S., Afzal, S., Tardivel-Lacombe, J., Park, D.S., Iovanna, J.L. and Mak, T.W. (2009) DJ-1/PARK7 is an important mediator of hypoxia-induced cellular responses. *Proc. Natl Acad. Sci. USA*, **106**, 1111–1116.
20. Jahani-Asl, A., Cheung, E.C., Neuspiel, M., MacLaurin, J.G., Fortin, A., Park, D.S., McBride, H.M. and Slack, R.S. (2007) Mitofusin 2 protects cerebellar granule neurons against injury-induced cell death. *J. Biol. Chem.*, **282**, 23788–23798.
21. Zunino, R., Schauss, A., Rippstein, P., Andrade-Navarro, M. and McBride, H.M. (2007) The SUMO protease SENP5 is required to maintain mitochondrial morphology and function. *J. Cell Sci.*, **120**, 1178–1188.
22. Kopin, I.J. and Markey, S.P. (1988) MPTP toxicity: implications for research in Parkinson's disease. *Annu. Rev. Neurosci.*, **11**, 81–96.
23. Barsoum, M.J., Yuan, H., Gerencser, A.A., Liot, G., Kushnareva, Y., Graber, S., Kovacs, I., Lee, W.D., Waggoner, J., Cui, J. *et al.* (2006) Nitric oxide-induced mitochondrial fission is regulated by dynamin-related GTPases in neurons. *EMBO J.*, **25**, 3900–3911.
24. Mitsumoto, A., Nakagawa, Y., Takeuchi, A., Okawa, K., Iwamatsu, A. and Takanezawa, Y. (2001) Oxidized forms of peroxiredoxins and DJ-1 on two-dimensional gels increased in response to sublethal levels of paraquat. *Free Radic. Res.*, **35**, 301–310.
25. Canet-Aviles, R.M., Wilson, M.A., Miller, D.W., Ahmad, R., McLendon, C., Bandyopadhyay, S., Baptista, M.J., Ringe, D., Petsko, G.A. and Cookson, M.R. (2004) The Parkinson's disease protein DJ-1 is neuroprotective due to cysteine-sulfinic acid-driven mitochondrial localization. *Proc. Natl Acad. Sci. USA*, **101**, 9103–9108.
26. Meulener, M.C., Xu, K., Thomson, L., Ischiropoulos, H. and Bonini, N.M. (2006) Mutational analysis of DJ-1 in Drosophila implicates functional inactivation by oxidative damage and aging. *Proc. Natl Acad. Sci. USA*, **103**, 12517–12522.
27. Whitworth, A.J. and Pallanck, L.J. (2009) The PINK1/Parkin pathway: a mitochondrial quality control system? *J. Bioenerg. Biomembr.*, **41**, 499–503.
28. Park, J., Lee, G. and Chung, J. (2009) The PINK1-Parkin pathway is involved in the regulation of mitochondrial remodeling process. *Biochem. Biophys. Res. Commun.*, **378**, 518–523.
29. Vives-Bauza, C., Zhou, C., Huang, Y., Cui, M., de Vries, R.L., Kim, J., May, J., Tocilescu, M.A., Liu, W., Ko, H.S. *et al.* (2010) PINK1-dependent recruitment of Parkin to mitochondria in mitophagy. *Proc. Natl Acad. Sci. USA*, **107**, 378–383.
30. Geisler, S., Holmstrom, K.M., Skujat, D., Fiesel, F.C., Rothfuss, O.C., Kahle, P.J. and Springer, W. (2010) PINK1/Parkin-mediated mitophagy is dependent on VDAC1 and p62/SQSTM1. *Nat. Cell Biol.*, **12**, 119–131.
31. Narendra, D.P., Jin, S.M., Tanaka, A., Suen, D.F., Gautier, C.A., Shen, J., Cookson, M.R. and Youle, R.J. (2010) PINK1 is selectively stabilized on impaired mitochondria to activate parkin. *PLoS Biol.*, **8**, e1000298.
32. Haque, M.E., Thomas, K.J., D'Souza, C., Callaghan, S., Kitada, T., Slack, R.S., Fraser, P., Cookson, M.R., Tandon, A. and Park, D.S. (2008) Cytoplasmic Pink1 activity protects neurons from dopaminergic neurotoxin MPTP. *Proc. Natl Acad. Sci. USA*, **105**, 1716–1721.
33. Klionsky, D.J., Abeliovich, H., Agostinis, P., Agrawal, D.K., Aliev, G., Askew, D.S., Baba, M., Baehrecke, E.H., Bahr, B.A., Ballabio, A. *et al.* (2008) Guidelines for the use and interpretation of assays for monitoring autophagy in higher eukaryotes. *Autophagy*, **4**, 151–175.
34. Mizushima, N. and Yoshimori, T. (2007) How to interpret LC3 immunoblotting. *Autophagy*, **3**, 542–545.
35. Rubinsztein, D.C., Cuervo, A.M., Ravikumar, B., Sarkar, S., Korolchuk, V., Kaushik, S. and Klionsky, D.J. (2009) In search of an 'autophagomometer'. *Autophagy*, **5**, 585–589.
36. Giasson, B.I., Ischiropoulos, H., Lee, V.M. and Trojanowski, J.Q. (2002) The relationship between oxidative/nitrative stress and pathological inclusions in Alzheimer's and Parkinson's diseases. *Free Radic. Biol. Med.*, **32**, 1264–1275.
37. Perkins, G., Bossy-Wetzel, E. and Ellisman, M.H. (2009) New insights into mitochondrial structure during cell death. *Exp. Neurol.*, **218**, 183–192.
38. Knott, A.B., Perkins, G., Schwarzenbacher, R. and Bossy-Wetzel, E. (2008) Mitochondrial fragmentation in neurodegeneration. *Nat. Rev.*, **9**, 505–518.
39. Lev, N., Ickowicz, D., Melamed, E. and Offen, D. (2008) Oxidative insults induce DJ-1 upregulation and redistribution: implications for neuroprotection. *Neurotoxicology*, **29**, 397–405.
40. Junn, E., Jang, W.H., Zhao, X., Jeong, B.S. and Mouradian, M.M. (2009) Mitochondrial localization of DJ-1 leads to enhanced neuroprotection. *J. Neurosci. Res.*, **87**, 123–129.
41. Narendra, D., Tanaka, A., Suen, D.F. and Youle, R.J. (2009) Parkin-induced mitophagy in the pathogenesis of Parkinson disease. *Autophagy*, **5**, 706–708.
42. Narendra, D., Tanaka, A., Suen, D.F. and Youle, R.J. (2008) Parkin is recruited selectively to impaired mitochondria and promotes their autophagy. *J. Cell Biol.*, **183**, 795–803.
43. Cherra, S.J. 3rd, Dagda, R.K., Tandon, A. and Chu, C.T. (2009) Mitochondrial autophagy as a compensatory response to PINK1 deficiency. *Autophagy*, **5**, 1213–1214.
44. Krebiehl, G., Ruckerbauer, S., Burbulla, L.F., Kieper, N., Maurer, B., Waak, J., Wolburg, H., Gizatullina, Z., Gellerich, F.N., Woitalla, D. *et al.* (2010) Reduced basal autophagy and impaired mitochondrial dynamics due to loss of Parkinson's disease-associated protein DJ-1. *PLoS ONE*, **5**, e9367.
45. Delivani, P., Adrain, C., Taylor, R.C., Duriez, P.J. and Martin, S.J. (2006) Role for CED-9 and Egl-1 as regulators of mitochondrial fission and fusion dynamics. *Mol. Cell*, **21**, 761–773.
46. Frank, S., Gaume, B., Bergmann-Leitner, E.S., Leitner, W.W., Robert, E.G., Catez, F., Smith, C.L. and Youle, R.J. (2001) The role of dynamin-related

protein 1, a mediator of mitochondrial fission, in apoptosis. *Dev. Cell*, **1**, 515–525.
47. Karbowski, M., Arnoult, D., Chen, H., Chan, D.C., Smith, C.L. and Youle, R.J. (2004) Quantitation of mitochondrial dynamics by photolabeling of individual organelles shows that mitochondrial fusion is blocked during the Bax activation phase of apoptosis. *J. Cell Biol.*, **164**, 493–499.
48. Lee, Y.J., Jeong, S.Y., Karbowski, M., Smith, C.L. and Youle, R.J. (2004) Roles of the mammalian mitochondrial fission and fusion mediators Fis1, Drp1 and Opa1 in apoptosis. *Mol. Biol. Cell*, **15**, 5001–5011.
49. Exner, N., Treske, B., Paquet, D., Holmstrom, K., Schiesling, C., Gispert, S., Carballo-Carbajal, I., Berg, D., Hoepken, H.H., Gasser, T. *et al.* (2007) Loss-of-function of human PINK1 results in mitochondrial pathology and can be rescued by parkin. *J. Neurosci.*, **27**, 12413–12418.
50. Palacino, J.J., Sagi, D., Goldberg, M.S., Krauss, S., Motz, C., Wacker, M., Klose, J. and Shen, J. (2004) Mitochondrial dysfunction and oxidative damage in parkin-deficient mice. *J. Biol. Chem.*, **279**, 18614–18622.
51. Wood-Kaczmar, A., Gandhi, S., Yao, Z., Abramov, A.Y., Miljan, E.A., Keen, G., Stanyer, L., Hargreaves, I., Klupsch, K., Deas, E. *et al.* (2008) PINK1 is necessary for long term survival and mitochondrial function in human dopaminergic neurons. *PLoS ONE*, **3**, e2455.
52. Gegg, M.E., Cooper, J.M., Schapira, A.H. and Taanman, J.W. (2009) Silencing of PINK1 expression affects mitochondrial DNA and oxidative phosphorylation in dopaminergic cells. *PLoS ONE*, **4**, e4756.
53. Chen, Y. and Gibson, S.B. (2008) Is mitochondrial generation of reactive oxygen species a trigger for autophagy? *Autophagy*, **4**, 246–248.
54. Martindale, J.L. and Holbrook, N.J. (2002) Cellular response to oxidative stress: signaling for suicide and survival. *J. Cell Physiol.*, **192**, 1–15.
55. Scherz-Shouval, R., Shvets, E., Fass, E., Shorer, H., Gil, L. and Elazar, Z. (2007) Reactive oxygen species are essential for autophagy and specifically regulate the activity of Atg4. *EMBO J.*, **26**, 1749–1760.
56. Macedo, M.G., Anar, B., Bronner, I.F., Cannella, M., Squitieri, F., Bonifati, V., Hoogeveen, A., Heutink, P. and Rizzu, P. (2003) The DJ-1L166P mutant protein associated with early onset Parkinson's disease is unstable and forms higher-order protein complexes. *Hum. Mol. Genet.*, **12**, 2807–2816.
57. Chang, N.C., Nguyen, M., Germain, M. and Shore, G.C. (2010) Antagonism of Beclin 1-dependent autophagy by BCL-2 at the endoplasmic reticulum requires NAF-1. *EMBO J.*, **29**, 606–618.
58. Lutz, A.K., Exner, N., Fett, M.E., Schlehe, J.S., Kloos, K., Lammermann, K., Brunner, B., Kurz-Drexler, A., Vogel, F., Reichert, A.S. *et al.* (2009) Loss of parkin or PINK1 function increases Drp1-dependent mitochondrial fragmentation. *J. Biol. Chem.*, **284**, 22938–22951.
59. Winklhofer, K.F., Henn, I.H., Kay-Jackson, P.C., Heller, U. and Tatzelt, J. (2003) Inactivation of parkin by oxidative stress and C-terminal truncations: a protective role of molecular chaperones. *J. Biol. Chem.*, **278**, 47199–47208.
60. Matlib, M.A., Shannon, W.A. Jr and Srere, P.A. (1979) Measurement of matrix enzyme activity in situ in isolated made permeable with toluene. *Methods Enzymol.*, **56**, 544–550.
61. Kim, R.H., Peters, M., Jang, Y., Shi, W., Pintilie, M., Fletcher, G.C., DeLuca, C., Liepa, J., Zhou, L., Snow, B. *et al.* (2005) DJ-1, a novel regulator of the tumor suppressor PTEN. *Cancer Cell*, **7**, 263–273.
62. Hyslop, P.A. and Sklar, L.A. (1984) A quantitative fluorimetric assay for the determination of oxidant production by polymorphonuclear leukocytes: its use in the simultaneous fluorimetric assay of cellular activation processes. *Anal. Biochem.*, **141**, 280–286.
63. Chappell, J.B. and Perry, S.V. (1954) Biochemical and osmotic properties of skeletal muscle mitochondria. *Nature*, **173**, 1094–1095.
64. Seifert, E.L., Bezaire, V., Estey, C. and Harper, M.E. (2008) Essential role for uncoupling protein-3 in mitochondrial adaptation to fasting but not in fatty acid oxidation or fatty acid anion export. *J. Biol. Chem.*, **283**, 25124–25131.
65. Reynafarje, B., Costa, L.E. and Lehninger, A.L. (1985) O2 solubility in aqueous media determined by a kinetic method. *Anal. Biochem.*, **145**, 406–418.

The EMBO Journal (2010) 29, 3571–3589 | © 2010 European Molecular Biology Organization | All Rights Reserved 0261-4189/10
www.embojournal.org

THE EMBO JOURNAL

Inhibition of mitochondrial fusion by α-synuclein is rescued by PINK1, Parkin and DJ-1

Frits Kamp[1,2,7,*], Nicole Exner[1,2,7], Anne Kathrin Lutz[3,7], Nora Wender[4], Jan Hegermann[4], Bettina Brunner[1,2], Brigitte Nuscher[1,2], Tim Bartels[2], Armin Giese[5], Klaus Beyer[2,6], Stefan Eimer[4], Konstanze F Winklhofer[3] and Christian Haass[1,2,*]

[1]DZNE-German Center for Neurodegenerative Diseases, Munich, Germany, [2]Adolf-Butenandt-Institute, Biochemistry, Ludwig-Maximilians-University, Munich, Germany, [3]Adolf-Butenandt-Institute, Neurobiochemistry, Ludwig-Maximilians-University, Munich, Germany, [4]European Neuroscience Institute Goettingen and DFG Research Center for Molecular Physiology of the Brain (CMPB), Goettingen, Germany, [5]Center for Neuropathology and Prion Research, Ludwig-Maximilians-University, Munich, Germany and [6]Department of Chemistry, The University of Arizona, Tucson, AZ, USA

Aggregation of α-synuclein (αS) is involved in the pathogenesis of Parkinson's disease (PD) and a variety of related neurodegenerative disorders. The physiological function of αS is largely unknown. We demonstrate with *in vitro* vesicle fusion experiments that αS has an inhibitory function on membrane fusion. Upon increased expression in cultured cells and in *Caenorhabditis elegans*, αS binds to mitochondria and leads to mitochondrial fragmentation. In *C. elegans* age-dependent fragmentation of mitochondria is enhanced and shifted to an earlier time point upon expression of exogenous αS. In contrast, siRNA-mediated downregulation of αS results in elongated mitochondria in cell culture. αS can act independently of mitochondrial fusion and fission proteins in shifting the dynamic morphologic equilibrium of mitochondria towards reduced fusion. Upon cellular fusion, αS prevents fusion of differently labelled mitochondrial populations. Thus, αS inhibits fusion due to its unique membrane interaction. Finally, mitochondrial fragmentation induced by expression of αS is rescued by coexpression of PINK1, parkin or DJ-1 but not the PD-associated mutations PINK1 G309D and parkin Δ1–79 or by DJ-1 C106A.

The EMBO Journal (2010) **29,** 3571–3589. doi:10.1038/emboj.2010.223; Published online 14 September 2010
Subject Categories: membranes & transport; neuroscience
Keywords: α-synuclein; mitochondria; neurodegeneration; Parkinson's disease

*Corresponding authors. F Kamp or C Haass, DZNE-German Center for Neurodegenerative Diseases, Adolf Butenandt-Institute, Biochemistry, Ludwig-Maximilians-University, Schillerstrasse 44, 80336, Munich, Germany. Tel.: +49 89 2180 75472; Fax: +49 89 2180 75415; E-mails: fkamp@med.uni-muenchen.de or chaass@med.uni-muenchen.de
[7]These authors contributed equally to this work

Received: 16 February 2010; accepted: 12 August 2010; published online: 14 September 2010

Introduction

A characteristic feature of Parkinson's disease (PD) is the intracellular deposition of Lewy bodies, which are predominantly composed of α-synuclein (αS). This 140 amino acid protein is widely distributed throughout the brain and expressed at high levels in neurons where it can reach concentrations of 0.5–1% of total protein (i.e. 30–60 μM) (Iwai *et al*, 1995; Spillantini *et al*, 1997; Bodner *et al*, 2009). In Lewy bodies, αS is arranged in fibrils with a β-sheet like structure (Der-Sarkissian *et al*, 2003; Chen *et al*, 2007). It is assumed that the pathogenicity of αS is associated with aggregation of the protein, which involves formation of small neurotoxic oligomers that eventually mature to larger insoluble deposits (Lee *et al*, 2004a; Haass and Selkoe, 2007; Kramer and Schulz-Schaeffer, 2007; Kostka *et al*, 2008; Kayed *et al*, 2009). A similar cascade of protein aggregation and precipitation is causative for the onset of other neurodegenerative diseases, such as Alzheimer's disease (Dobson, 2003; Haass and Selkoe, 2007).

A remarkable property of αS is its structural flexibility (Davidson *et al*, 1998; Beyer, 2007; Uversky, 2007). The protein is essentially unstructured in dilute aqueous solution (Uversky, 2002), whereas α-helical folding occurs upon binding to lipid surfaces. The NMR-derived structure of SDS-micelle-bound αS revealed two anti-parallel aligned amphipathic α-helices, the 'N-helix' spanning residues 3 through 37 and the 'C-helix' spanning residues 45 through 92. The C-terminal domain, which contains approximately 40 amino acids of which 14 are negatively charged and 2 positively charged, remains unstructured (Lee *et al*, 2004b; Ulmer and Bax, 2005; Ulmer *et al*, 2005). The structure of membrane-bound αS cannot be resolved by NMR as the rotation of vesicles is too slow. However, other biophysical techniques including electron spin resonance and circular dichroism (CD) revealed that α-helical folding also occurs for the N-terminal region when αS binds to membranes (Nuscher *et al*, 2004; Beyer, 2007; Jao *et al*, 2008; Drescher *et al*, 2008a). However, whether membrane-bound αS assumes a single extended α-helix, a broken helix or multiple structures (including oligomers) is unclear (Drescher *et al*, 2008a, b; Bodner *et al*, 2009; Ferreon *et al*, 2009; Perlmutter *et al*, 2009; Trexler and Rhoades, 2009). It has also been reported that αS binds to synaptic vesicles (Maroteaux *et al*, 1988; Jensen *et al*, 1998; Abeliovich *et al*, 2000; Kahle *et al*, 2000; Murphy *et al*, 2000; Cabin *et al*, 2002; Chandra *et al*, 2004, 2005; Jo *et al*, 2004; Yavich *et al*, 2004; Larsen *et al*, 2006; Ben Gedalya *et al*, 2009) as well as to mitochondria (Martin *et al*, 2006; Nakamura *et al*, 2008; Shavali *et al*, 2008). Biophysical studies from our laboratory revealed that binding of αS to highly curved bilayers leads to a stabilization of defects in the lipid packing (Nuscher *et al*, 2004; Cornell and Taneva, 2006; Kamp and Beyer, 2006). This motivated us to investigate whether αS could have an impact on membrane fusion.

So far little is known about the biological consequences of binding of αS to intracellular membranes. Studies in yeast

revealed that overexpression of αS leads to cellular toxicity by interfering with vesicular transport between the endoplasmic reticulum and the Golgi complex (Cooper *et al*, 2006). Fragmentation of the Golgi apparatus was also reported in neurons containing Pale bodies, pathological deposits known as early stages of Lewy bodies (Gosavi *et al*, 2002; Fujita *et al*, 2006; Lee *et al*, 2006). Moreover, functional impairment of mitochondria was caused by expression of wild type or mutant αS (Hsu *et al*, 2000; Orth *et al*, 2003; Smith *et al*, 2005; Parihar *et al*, 2008, 2009).

Although one of the well-described biochemical properties of αS is membrane binding associated with a structural switch, the biological function of the membrane-associated variant is unclear. Here, we demonstrate for the first time that αS inhibits fusion of model membranes. Biophysical studies led us to investigate the consequences of enhanced αS levels on membrane fusion *in vivo*. Life imaging in cultured cells and *Caenorhabditis elegans* demonstrates that expression of αS induces mitochondrial fragmentation, whereas down-regulation of αS leads to elongation of mitochondria. Strikingly, the mitochondrial phenotype caused by expression of αS could be rescued by coexpression of three recessive PD-associated genes, PINK1, parkin and DJ-1, but not the corresponding familial PD-associated mutants PINK1 G309D, and parkin Δ1–79 or by the synthetic mutant DJ-1 C106A (Waak *et al*, 2009).

Results

αS inhibits membrane fusion in vitro

We tested the effect of αS in several 'classic' fusion assays using protein-free model membranes. In our first protocol, we used small unilamellar vesicles (SUVs) consisting of dipalmitoyl-phosphatidylcholine (DPPC), which are known to fuse below the chain-melting temperature T_m, increasing their diameter from 30 to 70 nm (Schullery *et al*, 1980a, b; Gaber and Sheridan, 1982). This spontaneous fusion is a very slow process (Supplementary Figure S1). Trace amounts of non-ionic detergent $C_{12}E_8$ accelerate the fusion of DPPC-SUV, particularly at temperatures just below T_m (the gel to liquid–crystalline phase transition of bilayers of DPPC occurs at $T_m = 41°C$). We measured vesicle fusion by following changes in the static light scattering. At 36°C a suspension of DPPC-SUV reached maximal light scattering values within 10 min after detergent addition (Figure 1A). Fusion was suppressed when the experiment was performed in the presence of increasing amounts of αS and was blocked completely at lipid/αS ratios $\leqslant$200 mole/mole (3 μM αS), that is at concentrations where αS binding to vesicles saturates (Nuscher *et al*, 2004). We also applied dynamic light scattering (DLS) experiments, which demonstrated the increase in diameter of fusing vesicles (Supplementary Figure S2). To confirm that the increase in light scattering of fusing vesicles was not an aggregation artifact, we used two fluorescent membrane fusion assays. In a lipid-mixing assay, NBD fluorescence of 'donor' vesicles was completely quenched prior to addition of detergent. Upon fusion of donor vesicles and vesicles without fluorescent probes, lipid mixing abolishes the quenching effect. Membrane fusion, monitored by this technique could be reduced by increasing amounts of αS (Figure 1B). Alternatively, in a contents-mixing assay we repeated the $C_{12}E_8$-induced fusion of DPPC-SUV by mixing equal amounts of vesicles with trapped Tb^{3+}-citrate with vesicles containing dipicholinic acid (DPA). Formation of the Tb^{3+}–DPA complex led to a strong increase in fluorescence (Figure 1C). Almost no fluorescence increase was observed after addition of αS at a lipid/protein molar ratio 200:1, indicating that fusion was effectively inhibited. Together, these independent experiments support the inhibition of membrane fusion by αS.

Considering the domain structure of lipid-bound αS, the question arises whether its anti-fusogenic behaviour is due to stabilization of packing defects in the bilayer (Kamp and Beyer, 2006), or rather to membrane repulsion caused by the negatively charged C-terminal domain. To distinguish between these two possibilities, the fusion assay was repeated using an αS mutant lacking the last 24 amino acids of the C-terminus. This fragment (αS1–116) was still capable of completely suppressing membrane fusion (Figure 1D). On the contrary, a peptide composed of 25 amino acids of the C-terminus of αS (αS116–140), as well as a peptide comprised of 25 amino acids of the centre region of αS (αS41–65), was not capable of inhibiting membrane fusion (Figure 1D). We also compared the anti-fusogenic effect of αS with other membrane-binding proteins. Cytochrome c and lysozyme have similar molecular weights as αS. Both are globular proteins with a net positive charge known to bind to membrane surfaces. Cytochrome c and lysozyme did not significantly slow down the fusion of DPPC-SUV (Figure 1E). Exchangeable apolipoproteins have structural similarities to αS and share stabilization of lipid packing because of the binding of a 'sided' helix to the lipid surface (Derksen *et al*, 1996; Nuscher *et al*, 2004; Cornell and Taneva, 2006; Beyer, 2007). Interestingly, apolipoprotein A-I (ApoA-I) blocked the fusion completely, just like αS (Figure 1E). These findings indicate that the folding and membrane interaction of the N-terminal domain rather than the negative charges of the C-terminal domain are responsible for the anti-fusogenic effect of αS.

To test whether the effect of αS also applies to vesicles composed of other lipids, we investigated fusion of vesicles composed of negatively charged palmitoyl-oleoyl-phosphatidylserine (POPS), triggered by Ca^{2+}-ions (Wilschut *et al*, 1980). Fusion was initiated by adding $CaCl_2$ and was complete within 10 min after the addition (Figure 1F). When αS was added after the addition of Ca^{2+}, the fusion rate was reduced >10 times. Again, we compared the anti-fusogenic effect of αS with other membrane-binding proteins. In this case, we used cytochrome c and poly-lysine. Poly-lysine, like cytochrome c, is expected to bind to negatively charged membranes (Zhang and Rowe, 1994). Cytochome c had no effect even at a 10-fold higher molar concentration than αS. Poly-lysine reduced the fusion rate about five times (Figure 1F). Having established the suppression of membrane fusion by αS in classic fusion assays of vesicles composed of only one kind of lipid, we wondered whether αS would also suppress fusion of membranes of lipid mixtures mimicking compositions of biological membranes. The effect of αS on polyethyleneglycol (PEG)-mediated fusion of vesicles composed of a lipid mixture with reported optimal fusion potential (Haque *et al*, 2001) is shown in Figure 1G. The suppression of fusion by αS was significant, although higher amounts of αS were required compared with the DPPC-SUV and POPS-SUV, probably because of a lower affinity of αS to

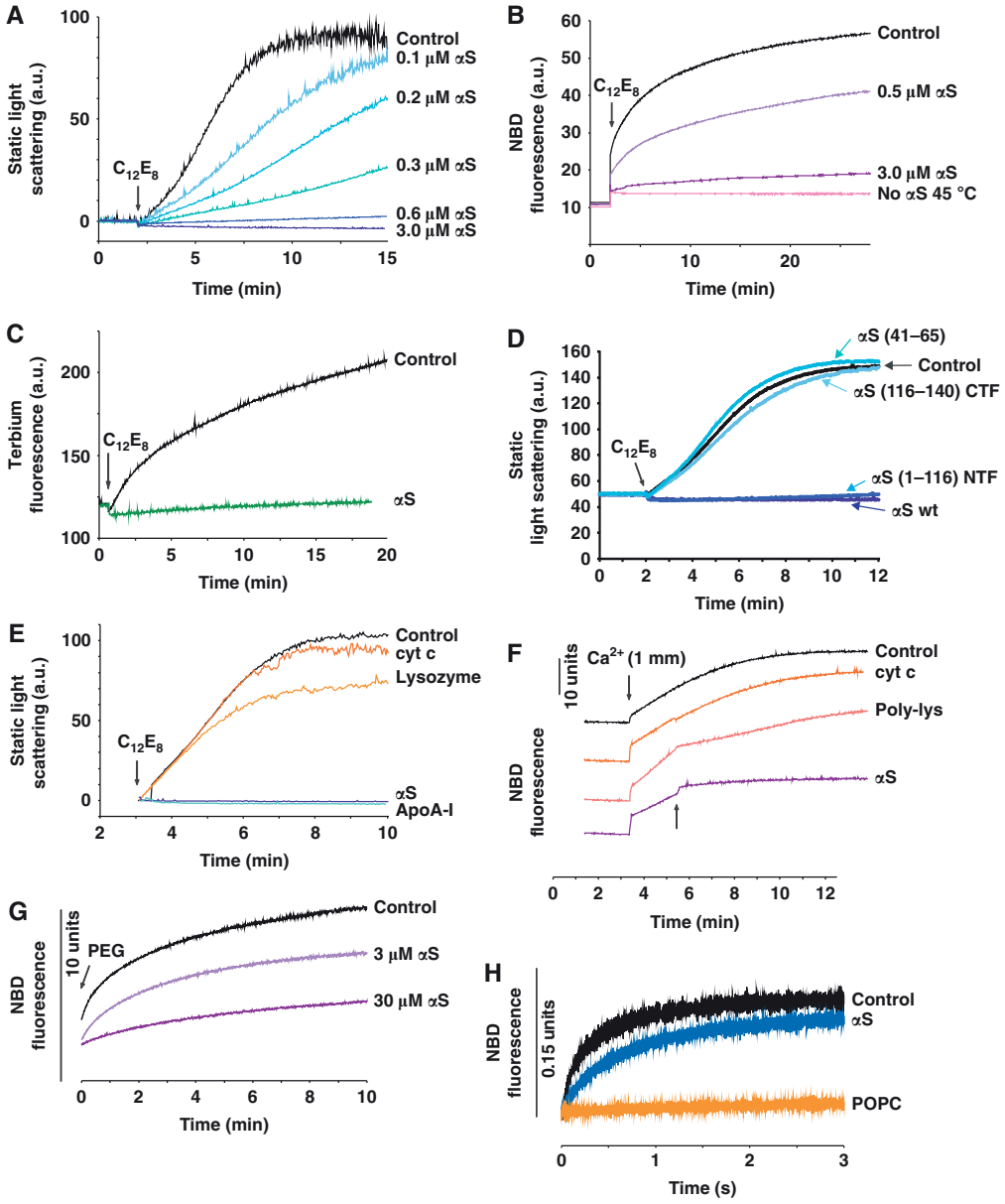

Figure 1 αS inhibits membrane fusion *in vitro*. (**A**) Fusion of DPPC-SUV was monitored by the increase in static light scattering upon addition of an aliquot of $C_{12}E_8$. Increasing amounts of αS inhibit membrane fusion (blue lines). Lipid concentration 600 μM, $T = 36°C$. (**B**) Lipid-mixing assay of DPPC-SUV. αS inhibited fusion completely at lipid/αS = 200 mole/mole (purple line). $T = 35°C$. Pink line: no fusion occurred at 45°C, that is at temperature above T_m. (**C**) Contents-mixing assay carried out in the presence and absence of αS (lipid/αS = 200 mole/mole, green line). $T = 30°C$. (**D**) An N-terminal fragment mutant of αS, αS(1–116) (blue line), lacking the negatively charged C-terminal domain was capable of completely suppressing the fusion of DPPC-SUV, like wt-αS (dark blue line); whereas peptides comprised of the C-terminal fragment, αS(116–140), or the central domain of αS, αS(41–65), failed to inhibit fusion (blue lines). Lipid/protein = 100 mole/mole. $T = 25°C$. (**E**) Comparison of inhibition of membrane fusion by αS with cytochrome c, lysozyme and Apolipoprotein A-I (ApoA-I). For all proteins: lipid/protein = 200 mole/mole. $T = 36°C$. (**F**) Ca^{2+}-induced fusion of POPS-SUV. Fusion was initiated by adding an aliquot of $CaCl_2$ and monitored by the lipid-mixing assay. αS, added 2 min after the addition of Ca^{2+} (arrow), blocked fusion almost completely (lipid/αS = 200 mole/mole). Control experiments: cytochrome c (lipid/protein = 20 mole/mole) or poly-lysine (lipid/protein 200 mole/mole) was added instead of αS. $T = 25°C$. (**G**) SUV of a mixture of lipids with reported optimal fusion potential (DOPC/DOPE/BBSM/cholesterol, 35:30:15:20 molar ratio) (Haque *et al*, 2001). Fusion was initiated by addition of 4% PEG and followed using the lipid-mixing assay. Total lipid concentration was 300 μM. When the experiment was repeated with αS, fusion was slowed. $T = 37°C$. (**H**) Spontaneous rapid fusion of SUV composed of lipids with opposite charges (POPS-SUV and PC^+-SUV). Lipid-mixing assay performed in stop-flow fluorimetry. Lipid concentration was 60 μM. αS (1.2 μM) inhibited the fusion. When POPS was replaced by POPC (uncharged) no fusion occurred, as expected. $T = 25°C$.

the membranes comprised of the chosen lipid mixture. Finally, rapid spontaneous fusion can be achieved upon mixing of vesicles with opposite interfacial net charges (Pantazatos and MacDonald, 1999; Lei and MacDonald, 2003). In this assay, fusion was complete after about 3 sec (Figure 1H). Again fusion was reduced by αS. Taken together, these findings demonstrate that αS selectively blocks membrane fusion in a number of independent *in vitro* fusion assay systems.

αS impairs mitochondrial fusion in cultured cells

Mitochondria change their morphology because of continuous fusion and fission (Detmer and Chan, 2007; Westermann, 2008). In addition, mitochondrial morphology and function is affected by loss of parkin or PINK1 function, which are both associated with familial PD (Kitada *et al*, 1998; Valente *et al*, 2004; Exner *et al*, 2007; Dagda *et al*, 2009; Lutz *et al*, 2009; Morais *et al*, 2009; Sandebring *et al*, 2009). To prove whether enhanced levels of αS, as observed in sporadic PD (Sharon *et al*, 2003; Chiba-Falek *et al*, 2006; Grundemann *et al*, 2008) as well as in familial PD associated with a triplication of the αS gene (Singleton *et al*, 2003), influence the balance between mitochondrial fission and fusion, we overexpressed αS in neuronal SH-SY5Y cells. This was particularly interesting as αS has been reported to bind to intracellular membranes including mitochondria (Nakamura *et al*, 2008; Shavali *et al*, 2008). Changes in mitochondrial morphology were monitored by imaging of cells, transfected with mito-GFP. When wild-type αS was overexpressed in SH-SY5Y cells, increased mitochondrial fragmentation was observed (Figure 2A). Quantification of the relative amounts of cells with fragmented mitochondria revealed that upon overexpression of αS, the number of cells that display fragmented mitochondria increased from 34% under control conditions to 46% (Figure 2B). Expression of similar amounts of mutant αS-A30P or A53T led to fragmentation of mitochondria to the same extent as the wild-type protein (Figures 2A–C). This is consistent with the finding that mutants of αS also bind to model membranes (Nuscher *et al*, 2004; Ramakrishnan *et al*, 2006; Giannakis *et al*, 2008; Karpinar *et al*, 2009; Perlmutter *et al*, 2009). β-Synuclein (βS) shares a number of biological and biophysical properties with αS, including binding to lipid surfaces (Nuscher *et al*, 2004; Beyer, 2007). We therefore investigated if βS may also affect mitochondrial fusion/fission. Indeed, both orthologs lead to the formation of fragmented mitochondria (Figures 2D–F), suggesting a redundant function of αS and βS.

To further address the question whether the increase in mitochondrial fragmentation observed in αS-expressing SH-SY5Y cells is due to alterations in mitochondrial fusion, we performed a PEG fusion assay (Niemann *et al*, 2005; Malka *et al*, 2007) (Figure 3). A first set of cells was transiently cotransfected with mito-GFP and αS or empty vector as a control. Another set of cells was cotransfected with mito-DsRed and αS or vector. At 8 h after transfection, both sets of cells were mixed and plated on coverslips. After 16 h, fusion of cocultured cells was induced by a 90-s treatment with PEG and fused cells were further incubated in the presence of cycloheximide for 5 h. Mitochondria of fused cells were analysed by confocal microscopy. Mitochondrial fusion is indicated by extensive colocalization of mito-GFP and mito-DsRed in control cells (Figures 3A and B). In contrast, upon overexpression of αS colocalization was dramatically reduced demonstrating that αS blocks mitochondrial fusion.

Mitochondria are known to fragment in stress situations (Westermann, 2008; Cho *et al*, 2010). To exclude that the changes in mitochondrial phenotype caused by αS overexpression are due to a secondary stress response, we performed control experiments to prove whether mitochondrial function was impaired by the expression of αS. The membrane potential in SH-SY5Y cells expressing mito-GFP was evaluated by TMRM fluorescence intensity of the mitochondria. There was no difference in TMRM fluorescence intensity when we compared the vector control cells with cells expressing αS (Figures 4A and B). In addition, no reduction of ATP production was observed in cells expressing wt-αS, αS A30P or αS A53T compared with the control-transfected cells (Figures 4C and D).

αS enhances age-dependent mitochondrial fragmentation in C. elegans

In line with our observations in cultured cells, when expressed in *C. elegans* body wall muscles (BWMs) wt-αS led to dramatic alterations of mitochondrial morphology and also to mitochondrial fragmentation (Figure 5). As *C. elegans* BWMs contain a highly stereotyped planar arrangement of mitochondria (Figure 5A) they are particularly suited for the analysis of mitochondrial morphology. To visualize mitochondria, we used the transmembrane domain of the outer mitochondrial membrane protein TOM70 fused to CFP (Labrousse *et al*, 1999). Moderate expression of αS led to the formation of extremely thin and highly interconnected mitochondria (Figures 5B and D) in about 20–40% of the transgenic BWMs. However, the majority, 50–70% of αS-expressing BWMs contained highly fragmented mitochondria that are roundish in their appearance (Figures 5C and D) in all independent transgenic strains analysed. Strikingly, a similar mitochondrial fragmentation was observed in aged 7-day-old worms in the absence of exogenous αS expression (Figure 5E), suggesting that mitochondrial fragmentation also happens during the normal ageing process of the BWM tissue. *C. elegans* BWMs are particularly susceptible to ageing and have been shown to gradually and progressively deteriorate with age (Herndon *et al*, 2002). *C. elegans* mean life span is about 12–18 days. After reaching adulthood, *C. elegans* hermaphrodites lay all their eggs within approximately 3 days and then persist through a post-reproductive period were senescent decline is evident (Herndon *et al*, 2002). As *C. elegans* animals still grow after reaching adulthood, aged BWMs were bigger in size (Figure 5E). Interestingly, ectopic expression of αS accelerated the mitochondrial aging phenotype (Figures 5E and F).

αS expression also led to mitochondrial fragmentation in neurons (Figures 5G–I). In neuronal cell bodies, we distinguished three categories of mitochondrial morphology: ring-like [R], tubular [T] or fragmented [F] mitochondria. Wild-type neurons mostly contained ring-like and long tubular mitochondria, whereas αS-expressing neurons showed mostly fragmented mitochondria. These observations confirmed that αS expression in living organisms leads to mitochondrial fragmentation in a tissue-independent manner.

αS is enriched at the mitochondrial outer membrane

To assess whether the increased mitochondrial fragmentation seen upon αS overexpression is caused by a direct binding of αS to mitochondrial membranes, we analysed mitochondrial morphology and the subcellular localization of αS by high pressure freeze (HPF) immuno-electron microscopy (EM). We did not observe any changes in the morphology of the mitochondrial cristae by αS expression as seen in the HPF-EM images (Figure 6A). We detected αS by using polyclonal αS antibodies on 90 nm thin immuno-EM sections of plastic embedded and HPF fixed SH-SY5Y cells. Label density was

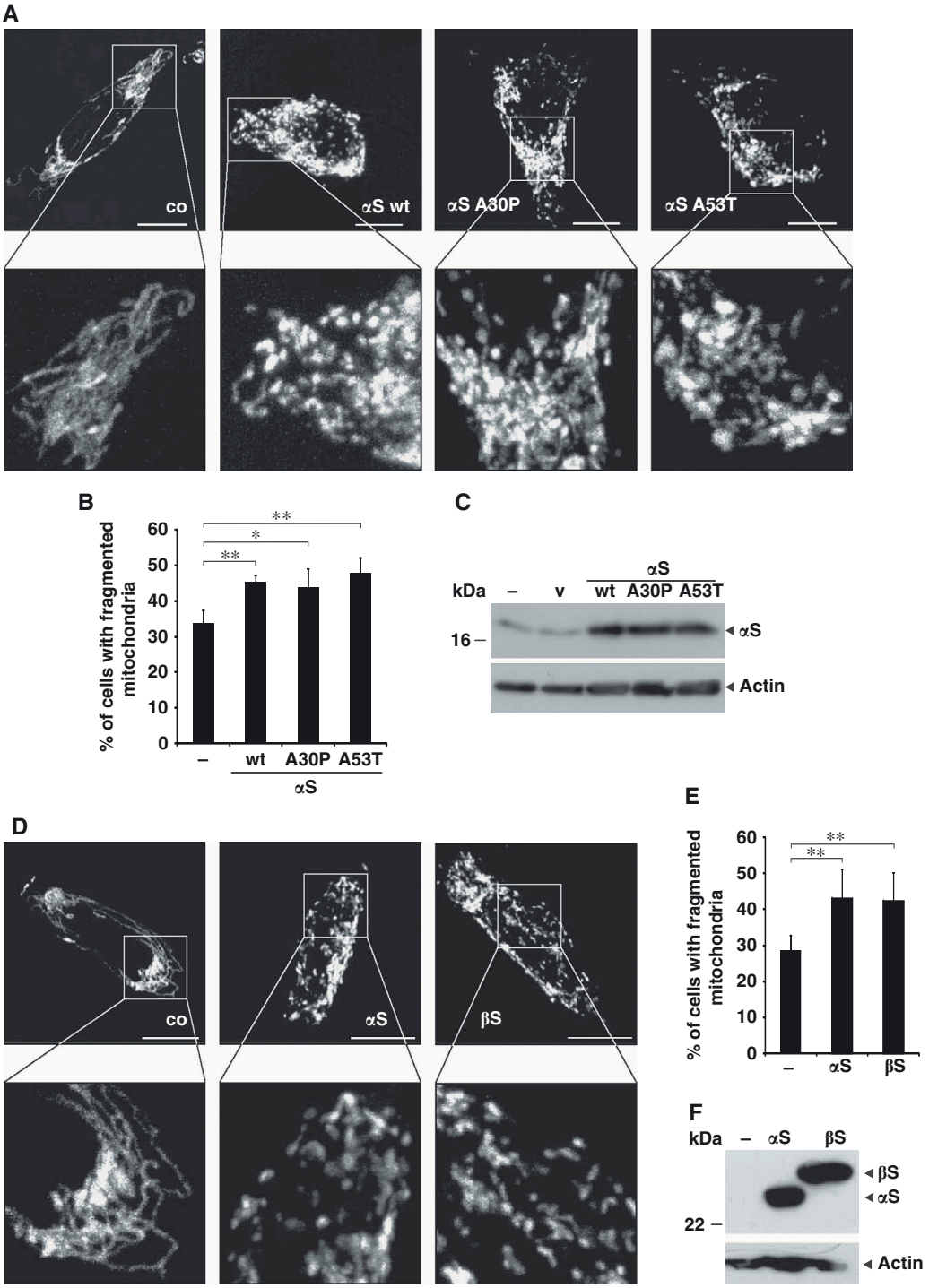

Figure 2 Mitochondrial fragmentation imaged in SH-SY5Y cells expressing αS. (**A**) Images of fluorescently labelled mitochondria. The panels display representative individual cells either control transfected (co) or transfected with wild-type αS (αS-wt), αS A30P or αS A53T. Scale bars = 10 μm. (**B**) Statistical analyses of mitochondrial morphology of cells from the experiments shown in (**A**). Approximately 250 cells of each experiment were counted, and the relative amount of transfected cells with altered mitochondrial morphology (i.e. fragmentation) was determined. (**C**) Expression levels of αS were analysed by western blotting using β-actin as loading control (v, vector). (**D**) Images of fluorescently labelled mitochondria. The panels display representative individual cells either untransfected (co) or transfected with αS-V5 (αS) or β-synuclein-V5 (βS). Scale bars = 10 μm. (**E**) Statistical analyses of mitochondrial morphology of cells from the experiments shown in (**D**). Approximately 300 cells of each experiment were counted, and the relative amount of transfected cells with altered mitochondrial morphology (i.e. fragmentation) was determined. Error bars indicate s.d. (**F**) Expression levels of αS and βS were analysed by western blotting with a V5-antibody using β-actin as loading control. $*P \leqslant 0.05$, $**P \leqslant 0.01$.

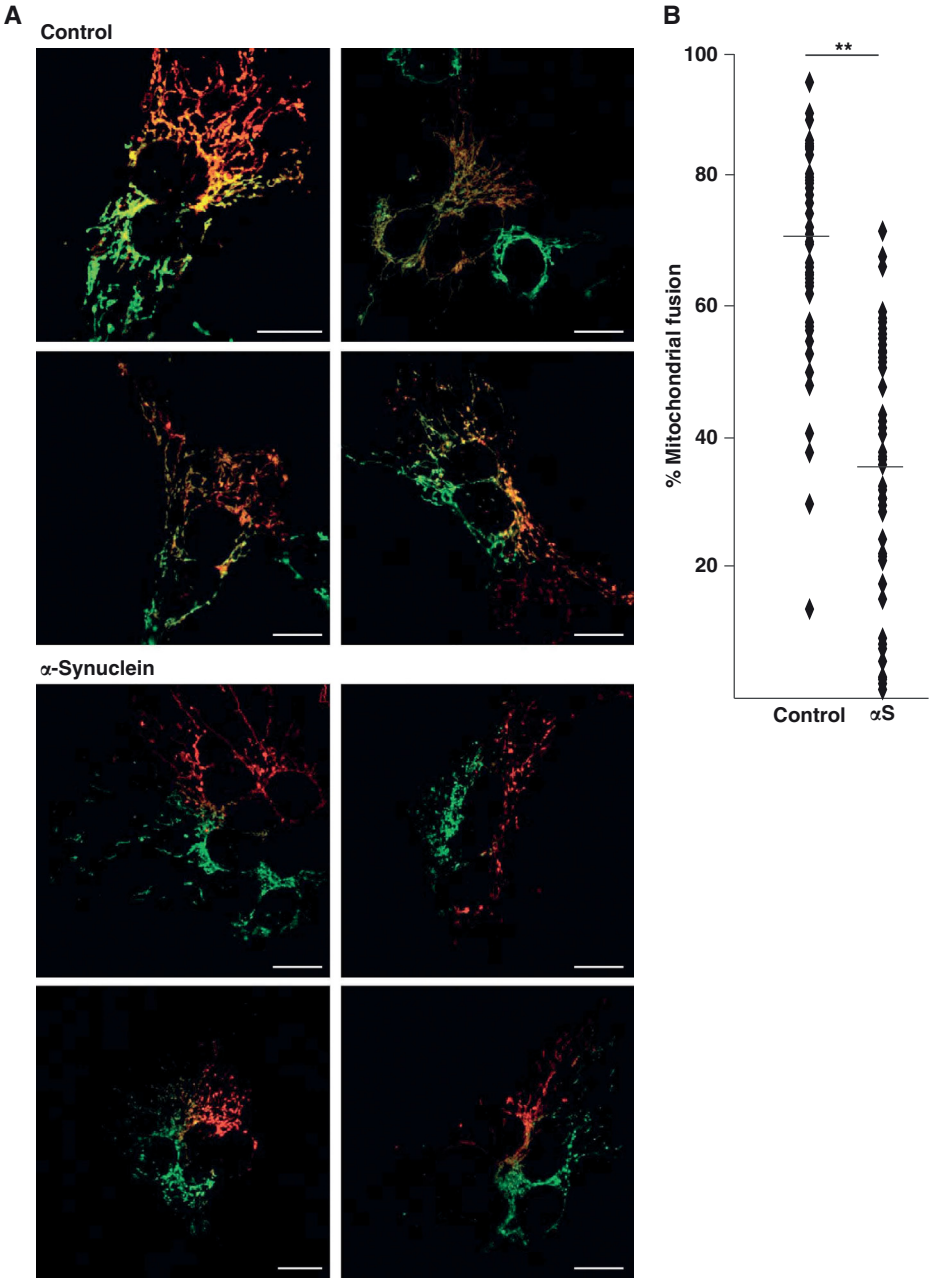

Figure 3 αS decreases fusion of differentially labelled mitochondrial populations. Cells expressing mito-GFP or mito-DsRed were fused with PEG in the presence or absence of exogenous αS. (**A**) Confocal images of representative polykaryons are shown. Fusion was monitored by the extent of mito-GFP and mito-DsRed colocalization. Scale bars = 15 μm. Upper panel: vector transfected (control); lower panel: αS transfected. (**B**) Quantification of mitochondrial fusion in αS and control cells. Each dot represents one measured value. Mean values are indicated by horizontal bars. Asterisks indicate significant differences in the percentage of cell hybrids with fused mitochondria compared with the vector control. Expression controls are provided in Supplementary Figure S3.

estimated by calculating the number of gold particles per μm^2 of the EM image. Three different areas were measured: the cytosol, the inside of mitochondria and the mitochondrial membrane. The mitochondrial membrane area was calculated as length of the membrane (μm) multiplied with 0.03 μm, because of possible shift of the gold particle of 15 nm in both directions of the membrane (Hoppert, 2003). When αS was overexpressed, it was detected at the mitochondrial membrane, whereas no αS signal was found inside mitochondria (Figures 6B and C). The amount of αS bound to the mitochondrial membrane was evaluated statistically (Figure 6C). About 38 gold particles were detected per μm^2 mitochondrial membrane area, whereas less than one αS signal was detected per μm^2 of cytosol. Because of the fact that HPF immuno-EM is a post-embedding labelling technique, the labelling intensity is usually lower than with classical fixation pre-embedding techniques. Therefore, endogenous αS was near the detection limit. These findings suggest that αS induces mitochondrial fragmentation by direct binding to the outer mitochondrial membrane.

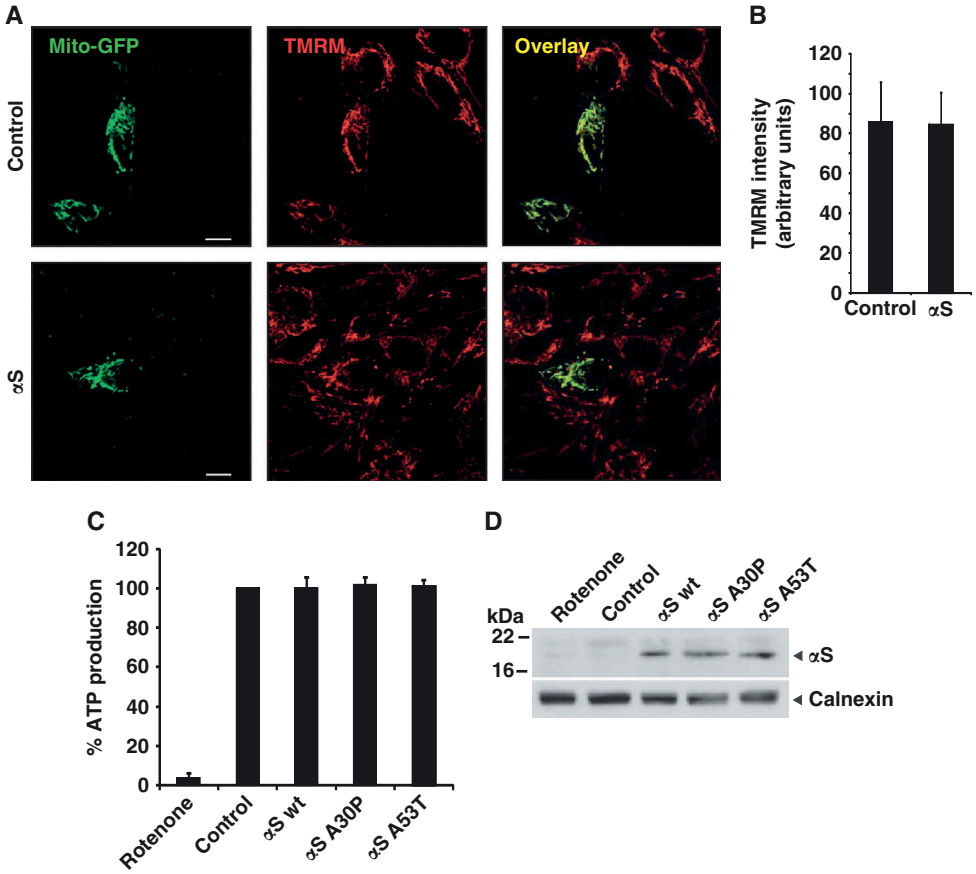

Figure 4 Mitochondrial function is not impaired by low level expression of αS. (**A**) SH-SY5Y cells were cotransfected with mito-GFP and vector (control) or αS. Living cells were stained with TMRM and colocalization was determined by overlay. (**B**) Quantification of TMRM fluorescence intensity. For each condition, $n = 30$ pictures as shown in (**A**) were quantified. (**C**) Steady-state cellular ATP levels were measured in SH-SY5Y cells transfected with either vector (control), αS wt, αS A30P or αS A53T. (**D**) Expression levels of αS were analysed by western blotting using calnexin as loading control. Error bars indicate s.d.

Pink-1, parkin and DJ-1 rescue αS-induced changes in mitochondrial morphology

Previously it was shown that familial PD-associated genes can confer stress protection (Palacino *et al*, 2004; Clark *et al*, 2006; Park *et al*, 2006). We therefore investigated whether Pink-1, parkin and DJ-1 protect from αS-induced mitochondrial fragmentation. Strikingly, coexpression of wild-type PINK1, wild-type parkin, wild-type DJ-1 with αS rescued the morphological phenotype caused by αS (Figure 7A). However, the mitochondrial fragmentation caused by αS overexpression could not be rescued by coexpression of the familial PD-associated mutants PINK1 G309D or by a parkin mutant lacking the N-terminal ubiquitin-like domain (Δ1–79), which is impaired in its ubiquitylation activity and neuroprotective capacity (Henn *et al*, 2007). The synthetic loss of function DJ-1–1 C106A mutant that prevents oxidation at the active centre (Waak *et al*, 2009) also failed to rescue the mitochondrial fragmentation (Figure 7A). Expression of wild-type PINK1, wild-type parkin and wild-type DJ-1 and each mutant alone did not affect mitochondrial morphology (Figure 7B).

Downregulation of αS forces mitochondrial fusion

To further substantiate the physiological relevance of the involvement of αS in modulating mitochondrial morphology, we used a siRNA knockdown approach to study physiological consequences of αS loss-of-function. As αS binds to mitochondria (Figure 6) (Li *et al*, 2007; Cole *et al*, 2008; Devi *et al*, 2008; Nakamura *et al*, 2008; Parihar *et al*, 2008), we assumed that a loss of αS may lead to the opposite effect as observed upon overexpression, namely to an increase of cells with elongated mitochondria (Figure 8). Knockdown of αS by siRNA considerably reduced αS protein levels (Figure 8C). Under these conditions, a significant increase in the number of cells with elongated mitochondria (13%) was observed (Figures 8A and B). Mitochondrial tubules were extended through the entire cell, which was rarely observed in control transfected (4%) or untransfected cells. Expression of siRNA resistant αS reverted this phenotype to control levels (5%), demonstrating the specificity of the knockdown effect. In these experiments, mitochondrial morphology was monitored using the fluorescent dye DiOC6(3). Similar results were obtained when we imaged mitochondria labelled with mito-GFP (Supplementary Figure S5).

To independently confirm that αS suppresses mitochondrial fusion, we induced fragmentation via the addition of the respiratory chain uncoupler CCCP (Ishihara *et al*, 2003). After 1 h, CCCP was removed and the recovery of mitochondrial morphology was monitored over the next 45 min in the presence of endogenous αS or upon siRNA-mediated

knockdown of αS. After CCCP treatment, the number of mitochondria with normal morphology was dramatically reduced (Figure 8D). Over the next 45 min in the absence of CCCP physiological mitochondrial morphology recovered significantly faster upon reduction of αS as in the presence of normal αS levels. Similarly, the amount of fragmented mitochondria dramatically increased during the 1-h treatment with CCCP. The number of fragmented mitochondria then

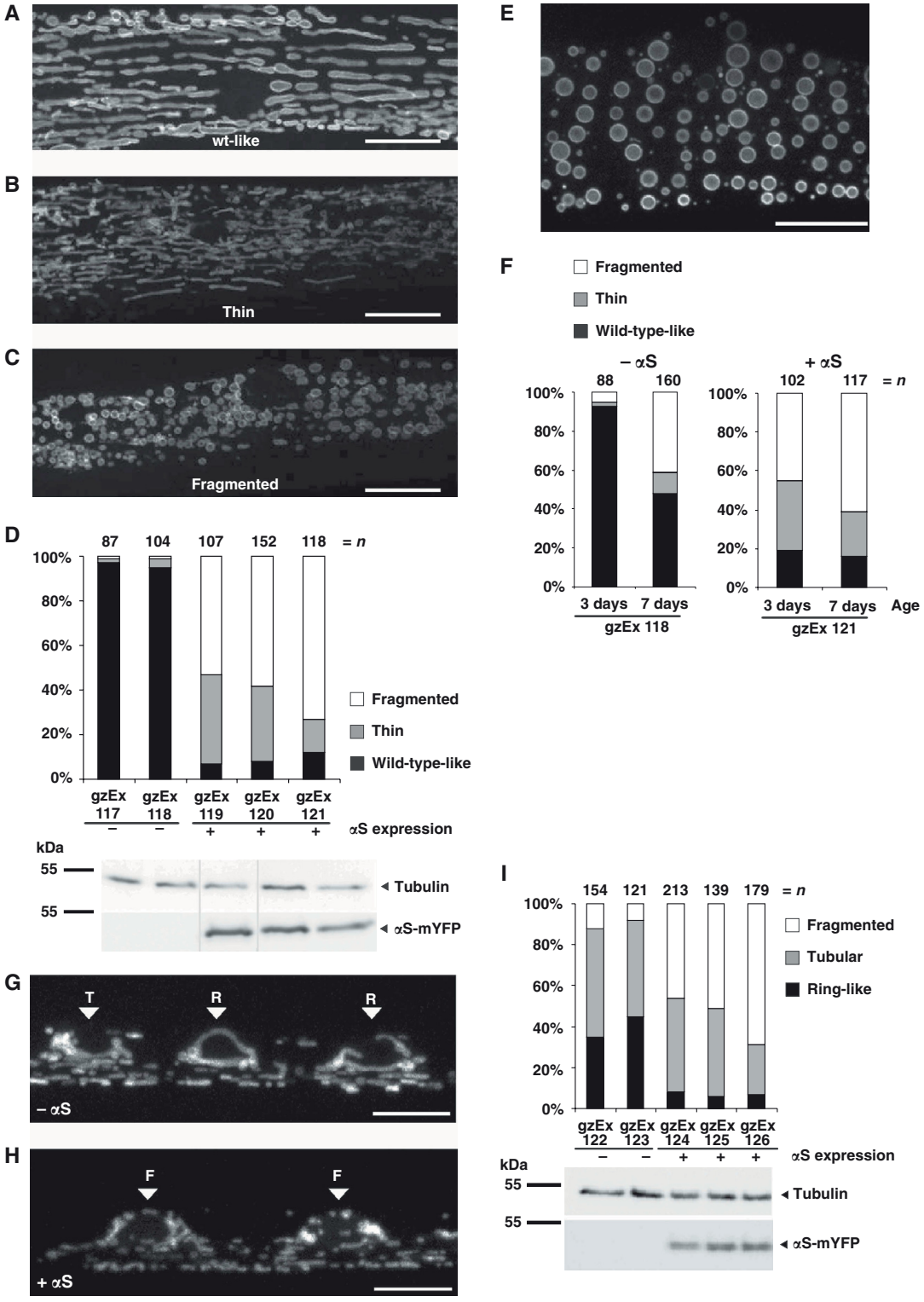

declined significantly faster in cells with reduced αS levels. These findings therefore further support that αS directly inhibits mitochondrial fusion.

αS-mediated mitochondrial fragmentation is independent of mitochondrial fusion and fission proteins

We next shifted the dynamic equilibrium of mitochondria towards increased fusion and investigated whether this can be antagonized by addition of αS. This was done on the one hand by expression of the fusion-promoting proteins Mfn1, Mfn2 and Opa1 or on the other hand by downregulation of the fission-promoting protein Drp1. Overexpression of αS did not affect expression levels or subcellular localization of Mfn1, Mfn2, Opa1 or Drp1. Furthermore, no aberrant processing of Opa1 was observed (Duvezin-Caubet *et al*, 2006) (Supplementary Figure S7). Nevertheless, the appearance of a higher number of cells with elongated and highly connected mitochondria, as observed upon expression of Mfn1, Mfn2 or Opa1 alone was reduced by coexpression of αS (Figure 9A). Moreover, expression of Mfn2 together with the downregulation of αS had an additive effect in inducing mitochondrial elongation (Figure 9B). Likewise, knockdown of Drp1 with siRNA leads to an increase in elongated mitochondria, indicating reduced mitochondrial fission. This increase was significantly less when αS was overexpressed. Similarly, elongation of mitochondria was induced by expression of the dominant-negative Drp1 K38E mutant. Again, coexpression with αS reduced the number of cells with elongated mitochondria (Figures 9C and D).

Discussion

Familial PD is not only caused by missense mutations within the αS gene, but also by a gene duplication/triplication, which leads to enhanced protein levels of αS (Singleton *et al*, 2003; Ibanez *et al*, 2004). Moreover, in patients with sporadic PD, an increase of αS mRNA and oligomers was observed (Sharon *et al*, 2003; Chiba-Falek *et al*, 2006; Grundemann *et al*, 2008). A polymorphism in the SNCA promoter increases gene expression and PD susceptibility (Maraganore *et al*, 2006). Two recent large genome-wide association studies concordantly revealed that common variants in SNCA increase the risk of PD (Satake *et al*, 2009; Simon-Sanchez *et al*, 2009). αS has a high propensity to bind to lipid membranes *in vitro* and multiple evidence exists that αS may affect vesicular trafficking, Golgi structure and mitochondrial function, although a unifying cellular mechanism behind these observations is not known (Cooper *et al*, 2006; Fujita *et al*, 2006; Larsen *et al*, 2006; Gitler *et al*, 2008; Parihar *et al*, 2009). On the basis of biophysical studies, our hypothesis has been that αS inhibits membrane fusion. Undoubtedly, proteins and Ca^{2+} ions have an essential role in the regulation, targeting and triggering of fusing membranes *in vivo* (Weber *et al*, 1998; Nickel *et al*, 1999; Tamm *et al*, 2003; Liu *et al*, 2005; Chen *et al*, 2006; Dennison *et al*, 2006; Takamori *et al*, 2006). However, a necessary requirement for any membrane fusion is *mixing of the lipids* (Chernomordik *et al*, 1995; Chernomordik and Kozlov, 2003; Lentz, 2007; Weinreb and Lentz, 2007; Piomelli *et al*, 2007). High curvature of membranes causes defects in the packing of the lipids, which are necessary to trigger the formation of a fusion stalk (Chernomordik *et al*, 1995; Dennison *et al*, 2006). As αS seals defects in stressed bilayers (Kamp and Beyer, 2006), we expected that αS might inhibit membrane fusion (see model in Figure 10). Although we recognize that the *in vitro* fusion assays do not fully represent *in vivo* membrane fusion events, the biophysical experiments provided the basis for the *in vivo* experiments. We therefore first studied the influence of αS binding to lipid vesicles *in vitro* and in a next step investigated the effects of αS expression in the living cell and in an animal model. In this study, αS inhibited fusion in all *in vitro* fusion assays applied. Differential scanning calorimetry experiments further supported our hypothesis that αS suppresses fusion due to its unique interaction with the membrane (Supplementary Figure S1). In control experiments, no significant decrease in the fusion rate was found with cytochrome c and lysozyme. Thus, partial coating of the lipid/water interface by proteins with a net positive charge affected the fusion only marginally. Poly-lysine inhibited fusion but to a much lesser extent compared with αS. One poly-lysine molecule contains about 500 lysine residues. At the lipid/protein molar ratio used, a large fraction of the outer surface would be coated by poly-lysine. In this case, the fusion would be inhibited by charge repulsion. In contrast, ApoA-I inhibited fusion as efficiently as αS. As the biological function of apolipoproteins is to stabilize plasma lipoproteins (Gursky, 2005; Cornell and Taneva, 2006), we conclude that ApoA-I suppresses fusion of membranes probably by a similar mechanism as αS. Finally, fusion was also blocked with a truncated αS, lacking the charged C-terminal domain. These observations support our hypothesis that αS inhibits membrane fusion by stabilizing the lipid packing of stressed bilayers, independently of other protein factors that might be involved in the fusion machinery of membranes.

Investigating *in vivo* effects of αS on mitochondrial fusion was particularly interesting, as morphological changes and

Figure 5 αS expression leads to mitochondrial fragmentation in *C. elegans* muscles and neurons. (**A**) In wild-type muscles without expression of αS, mitochondria are forming regular tubular structures. (**B**, **C**) Expression of human αS leads to changes in mitochondrial morphology, which can be classified into two categories: (**B**) very thin and highly interconnected tubules and (**C**) fragmented vesicular mitochondria. Scale bars = 10 μm. (**D**) Quantification of the relative appearance of wild-type-like, fragmented, and thin mitochondria in independent transgenic lines expressing αS-mYFP. Expression levels of αS-mYFP were analysed by western blot using tubulin as a loading control. All lanes originate from the same gel. Only the lanes of those transgenic lines, which were chosen for imaging due to good penetrance and fluorescent signal, are shown here. (**E**) Mitochondrial fragmentation is also observed in aged 7-day-old wild-type body wall muscles. Scale bar = 10 μm. (**F**) Mitochondrial morphologies are compared between 3 day versus 7-day-old muscles without (right graph) and with αS-mYFP expression (left graph). (**G**, **H**) Images show TOM70-CFP-labelled mitochondria in motoneurons of young adult *C. elegans*. Arrowheads label neuronal cell bodies, indicating the morphological category. The mitochondrial morphology in neuronal cell bodies was grouped into three categories: ring-like [R], tubular [T] or fragmented [F] mitochondria. Wild-type neurons mostly contain ring-like and long tubular mitochondria (**G**), whereas αS-expressing neurons show mostly fragmented mitochondria in cell bodies as well as in the axons (**H**). Scale bars = 5 μm. (**I**) Quantification of relative occurrence of ring-like, tubular and fragmented mitochondria and αS-mYFP expression levels.

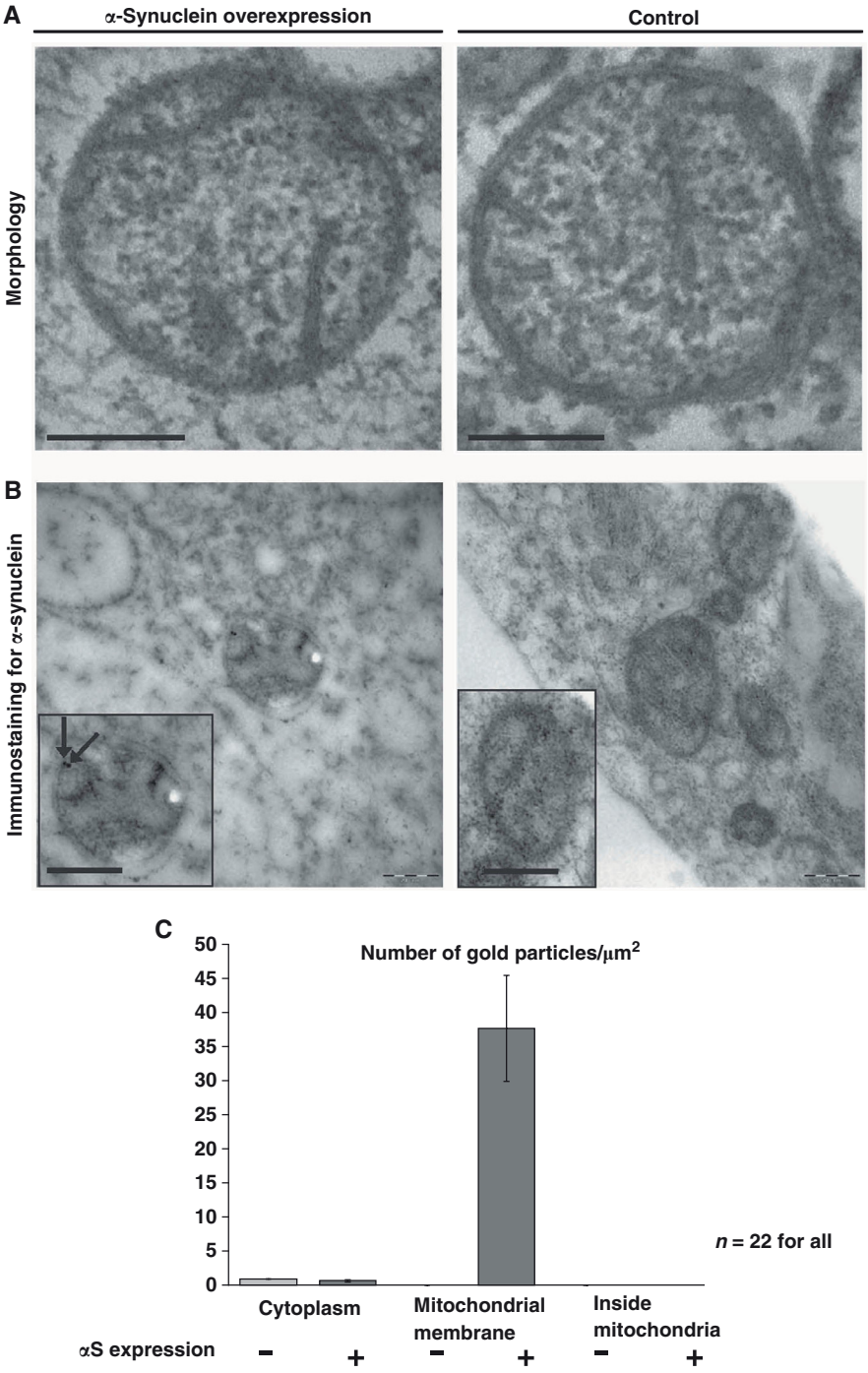

Figure 6 αS binds to mitochondrial outer membranes. (**A**) Electron microscopy of mitochondria in cells overexpressing αS (left panel) and without overexpression (control, right panel). Scale bars = 200 nm. (**B**) Immunostaining for αS. Insets: Mitochondria in high magnification. Arrows indicate localization of αS. Scale bars = 200 nm. (**C**) Statistical analysis of the density of immunogold labelling in the cytosol, at the mitochondrial membrane and inside the mitochondria, comparing αS overexpressing cells (+) and the control without overexpression (−). No label inside the mitochondria was detected in both samples. Error bars indicate s.d.

dysfunction of mitochondria have frequently been reported as a consequence of a loss of function of familial PD-associated genes such as PINK1 and parkin (Exner *et al*, 2007; Dagda *et al*, 2009; Lutz *et al*, 2009; Sandebring *et al*, 2009). Moreover, localization of αS to mitochondria has also been reported (Li *et al*, 2007; Cole *et al*, 2008; Devi *et al*, 2008; Nakamura *et al*, 2008; Parihar *et al*, 2008) and was confirmed in this study. We found evidence that αS is functionally involved in fusion of mitochondrial membranes. This was demonstrated by different approaches: (i) when cells were transfected with αS, a significantly larger amount of the cells displayed fragmented mitochondria (Figure 2). Similarly,

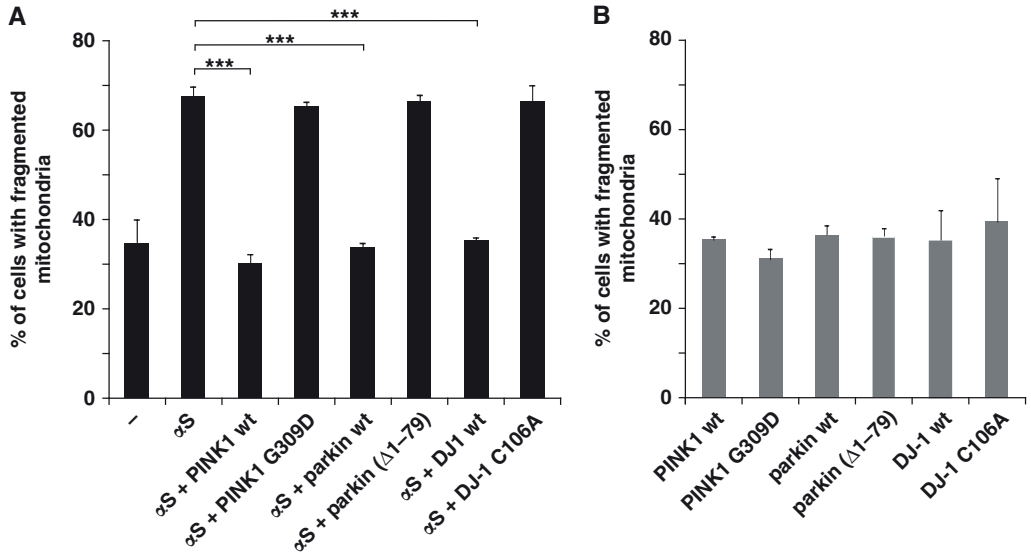

Figure 7 Expression of three familial PD-associated genes rescues mitochondrial fragmentation caused by αS. (**A**) Coexpression of PINK1, parkin or DJ-1 with αS rescues fragmentation of mitochondria, whereas their loss-of-function mutants do not. Cells were transfected as indicated and mitochondrial morphology was quantitated as in Figure 2B. (**B**) Single expression of PINK1, parkin or DJ-1 or each mutant alone does not affect mitochondrial morphology. Error bars indicate s.d. Expression controls are provided in Supplementary Figure S4. $***P \leqslant 0.001$.

increased fragmentation of mitochondria was observed, when αS was expressed in BWMs and neurons of *C. elegans* (Figure 5). Interestingly, overexpression of αS accelerated a mitochondrial phenotype associated with physiological aging (Figure 5). As aging is a major risk factor for PD, this finding may have fundamental implications for the understanding of disease progression. (ii) The opposite phenotype, namely an elongation of mitochondria, occurred upon siRNA-mediated knockdown of αS (Figure 8). (iii) The experiment from Figure 8D showed that re-elongation of mitochondria upon CCCP-induced fragmentation was faster when αS levels were suppressed by αS siRNA. (iv) Specific enrichment of αS at mitochondrial outer membranes was visualized by immuno-EM. Notably, under conditions of mitochondrial fragmentation, cristae structure and length was unchanged and morphology was not affected on the level of EM. These experiments support the idea that αS binds to the outer membrane of mitochondria and inhibits or reduces their fusion. (v) When the plasma membranes of two populations of cells with differently coloured mitochondria were fused, subsequent mitochondrial fusion was significantly reduced when αS was overexpressed (Figure 3). (vi) When fusion was elevated by overexpression of the fusion-promoting proteins Mfn1, Mfn2 and Opa1, by downregulation of the fission-promoting protein Drp1 or by expression of the dominant-negative mutant Drp1-K38E, we observed a backshift of the equilibrium towards reduced fusion by coexpression of αS. Together, these data indicated that αS is not interacting directly with proteins involved in fusion or fission machineries. We propose that the influence of αS on mitochondrial dynamics is based on its interaction with membrane lipids, preventing the necessary formation of a fusion stalk, an idea that is strongly supported by our *in vitro* fusion experiments. Moreover, αS could inhibit lipid fusion events in protein-assisted mitochondrial fusion.

An alternative explanation for the observed effects of αS on mitochondrial dynamics would be that αS enhances mitochondrial fission. This is unlikely as the free-energy change involved with the structural switch of αS upon membrane binding (Nuscher *et al*, 2004) is not enough to cause fission and mitochondrial fission is a GTP requiring event (Westermann, 2008). The experiment of Figure 3, in which fusion of red and green labelled mitochondria in fused cells was slower when αS was overexpressed, can only be explained by an inhibitory effect of αS on fusion. Furthermore, the experiment from Figure 8D showed that re-elongation of mitochondria upon CCCP-induced fragmentation was faster when cytosolic αS levels were suppressed by αS siRNA. As during the re-elongation phase hardly any mitochondrial fission occurs, the slower re-elongation in the presence of αS can only be explained by a specific inhibitory effect of αS on the fusion of mitochondrial membranes. Another alternative explanation for the observed effects of αS on mitochondrial dynamics would be that αS expression alters the levels of expression of fission or fusion proteins, their subcellular localizations and/or post-translational modifications. However, no such effects were observed (Supplementary Figure S7).

We suggest that αS may have a general protective role preventing spontaneous membrane fusion. A rather unselective lipid membrane binding of αS independent of the individual fusion machineries suggests a pleiotropic function of αS. Indeed, there is evidence that αS directly affects Golgi morphology as well as priming of synaptic vesicles (Gosavi *et al*, 2002; Fujita *et al*, 2006; Larsen *et al*, 2006). Interestingly, a recent genome-wide screen for yeast genes that rescue αS-mediated toxicity revealed several conserved genes involved in vesicular trafficking including the evolutionarily conserved Rab1 GTPase Ypt1 (Cooper *et al*, 2006). In subsequent experiments, the authors were also able to show that Rab1 overexpression in the model systems *C. elegans* and *Drosophila melanogaster* were similarly effective to ameliorate αS-induced cellular toxicity. In combination with *in vitro* ER-to-Golgi transport assays, this strongly indicates that

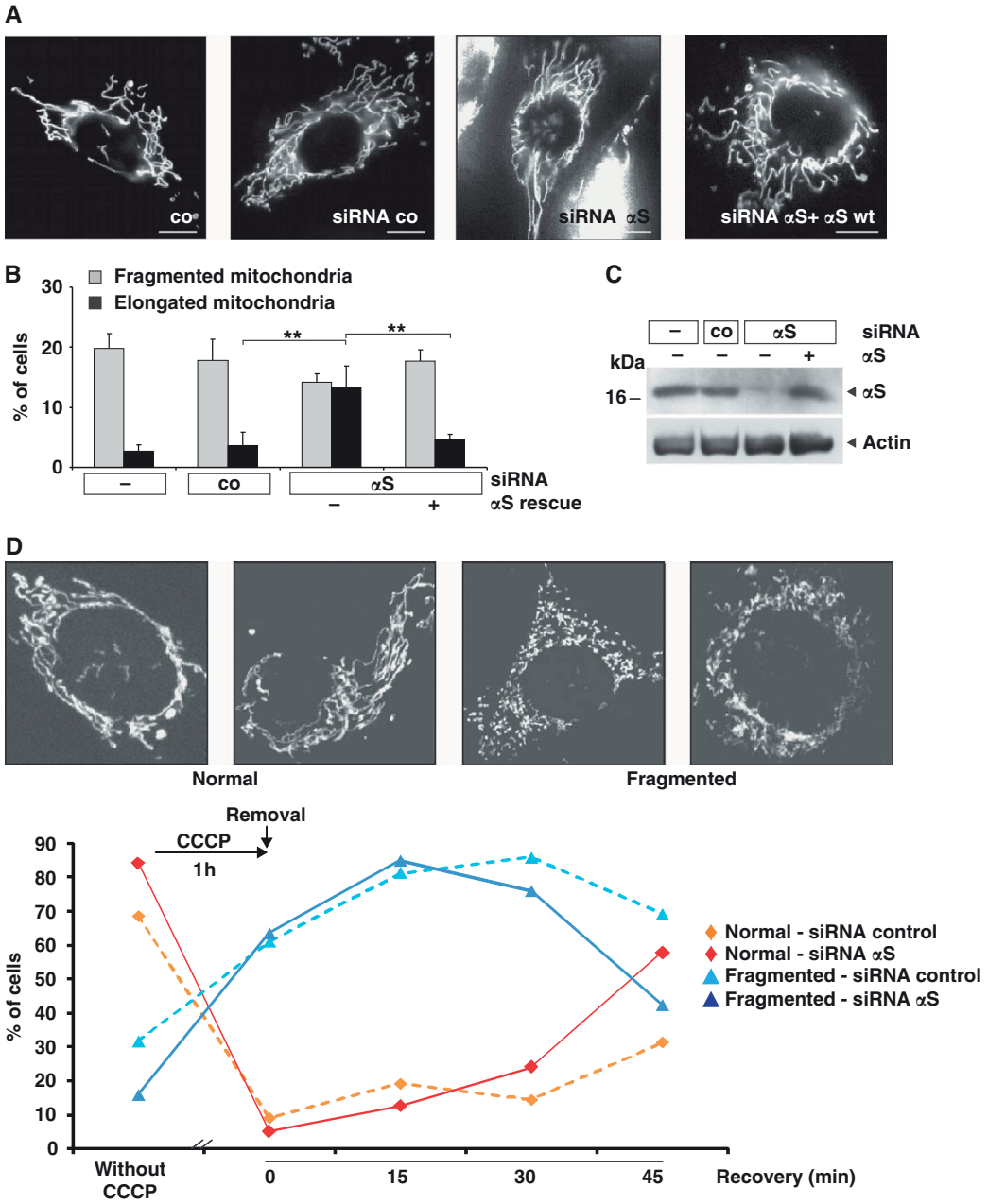

Figure 8 Loss of αS induces elongation of mitochondria. (**A**) Images of fluorescently labelled mitochondria. The panels display representative individual cells either untransfected (co) or transfected with control-siRNA, αS-siRNA, and αS-siRNA + αS-cDNA. Scale bar = 10 μm. (**B**) Statistical analyses of mitochondrial morphology of cells from the experiments shown in (**A**). Approximately 300 cells of each experiment were counted, and the relative amount of cells with changed mitochondrial morphology (i.e. fragmentation or elongation) was determined. Error bars indicate s.d. (**C**) Downregulation of αS in SH-SY5Y cells and retransfection with wild-type αS was monitored by western blotting using β-actin as a loading control. (**D**) Analyses of mitochondrial morphology of cells transfected with a control siRNA or an siRNA against αS before exposure to 10 μM CCCP for 1 h and at different recovery times after removal of CCCP. Insets show images of fluorescently labelled mitochondria. The panels display representative mitochondrial phenotypes as observed before (normal) and after (fragmented) exposure to CCCP. Scale bars = 10 μm. Approximately 60 cells of each experiment were counted, and the relative amount of transfected cells with normal or fragmented mitochondrial morphology was determined. $^{**}P \leqslant 0.01$.

overexpression of αS affects vesicle fusion at the Golgi and not vesicle budding at the ER (Gitler *et al*, 2008). According to our data, these observations may now be attributed to the lipid membrane-binding properties of αS rather than a genetic interaction of αS and the Rab GTPase Ypt1. However, in a cellular context, some organelles might be preferentially bound by αS and binding might depend on αS expression levels. Indeed, in our cell system, a preferential binding to mitochondria was observed. In contrast, in embryonic hippocampal neurons a mild overexpression of αS reduced reclustering of synaptic vesicles, with no apparent change in the rate of fusion (Nemani *et al*, 2010). However, it was unclear if binding of αS to synaptic vesicles was directly affected. Interestingly, our study revealed that the inhibition

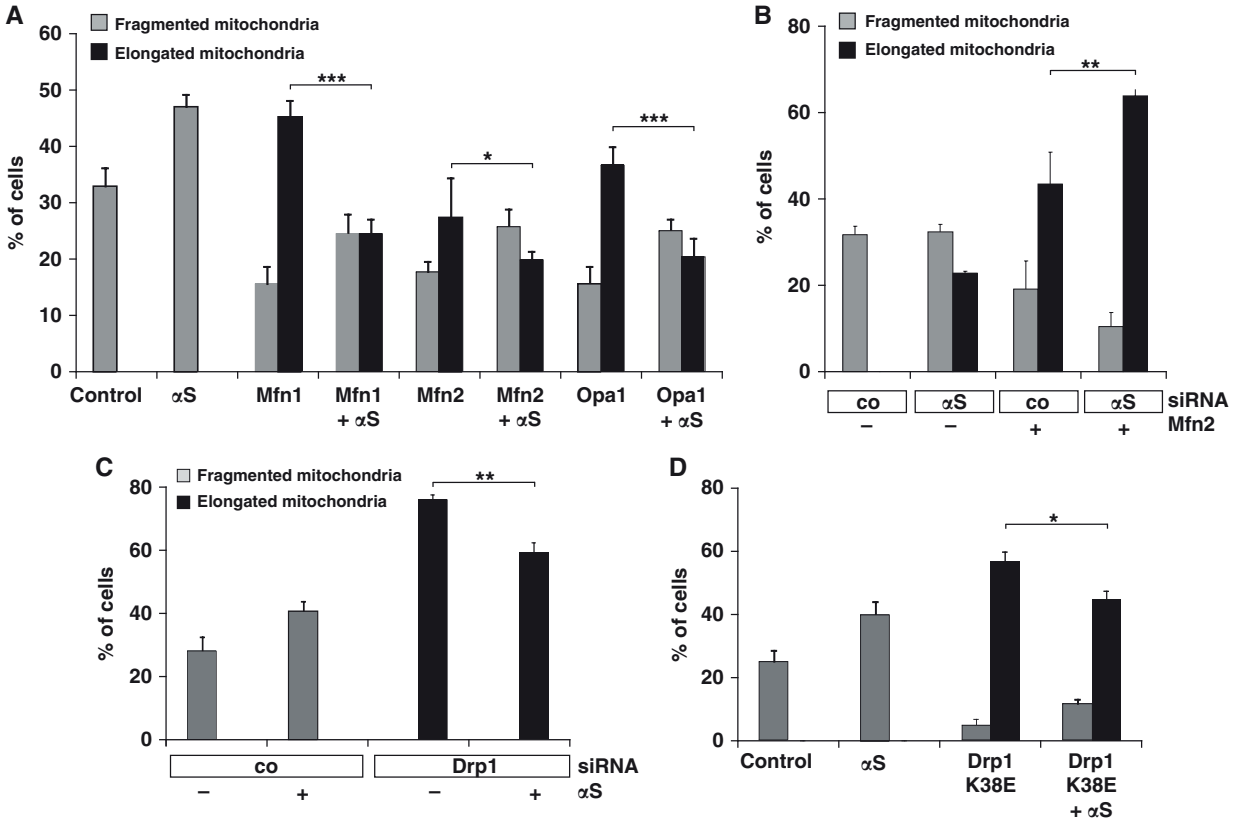

Figure 9 αS-mediated mitochondrial fragmentation is independent of the fusion and fission machinery. (**A**) Cells were transfected with Mfn1, Mfn2, Opa1 and αS as indicated. The relative amounts of cells with changed mitochondrial morphology (i.e. fragmentation or elongation) were determined. (**B**) Cells were transfected with control siRNA or siRNA directed against αS and cotransfected with Mfn2 where indicated. The relative amounts of cells with altered mitochondrial morphology (i.e. fragmentation or elongation) were determined. (**C**) Cells were transfected with control siRNA or Drp1-specific siRNA and cotransfected with αS where indicated, fluorescently labelled and the relative amounts of cells with fragmented or elongated mitochondria were determined. (**D**) Cells were transfected with vector (control), αS and Drp1 K38E where indicated, and the relative amounts of cells with fragmented or elongated mitochondria were determined. Error bars indicate s.d. Expression controls are provided in Supplementary Figure S6. $*P \leqslant 0.05$, $**P \leqslant 0.01$, $***P \leqslant 0.001$.

of mitochondrial fusion by αS could be rescued by coexpression of PINK1, Parkin or DJ-1 but not by the PD related PINK1 G309D and parkin Δ(–79), or by DJ-1 C106A. As PINK1, parkin and DJ-1 have no homologues in *S. cerevisiae*, they could not be found in the extended genome-wide screen (Cooper *et al*, 2006; Gitler *et al*, 2009). Our findings are in line with data from *D. melanogaster*, where αS-induced loss of climbing activity and degeneration of the retina was rescued by PINK1 or parkin (Haywood and Staveley, 2006; Todd and Staveley, 2008). So far, it can only be speculated how this beneficial effect of PINK1 and parkin could be mediated. Obviously, PINK1, parkin and DJ-1 can functionally interact to maintain mitochondrial morphology and function and to protect against adverse effects of αS overexpression. This functional interaction does not necessarily involve a direct interaction between these proteins, it is rather conceivable that different pathways converge at the level of mitochondrial integrity. As PINK1, parkin and DJ-1 are known to protect cells against mitochondrial stress (Canet-Aviles *et al*, 2004; Palacino *et al*, 2004; Kim *et al*, 2005; Clark *et al*, 2006; Park *et al*, 2006; Exner *et al*, 2007; Henn *et al*, 2007; Wood-Kaczmar *et al*, 2008) they could exert a protective effect on mitochondria that counteracts negative effects of αS accumulation. Our data do not exclude that the rescuing effects of the recessive PD-associated genes may work via interaction with the fusion/fission machinery.

Taken together, our findings suggest that αS gene duplications or triplications may lead to increased amounts of αS binding to mitochondria, which inhibits mitochondrial fusion and would therefore trigger disease pathology. In contrast, the missense mutations may rather affect other cellular pathways such as aggregation (Karpinar *et al*, 2009; Tsika *et al*, 2010). Further support to our finding that altered mitochondrial dynamics induced by αS might contribute to PD pathology comes from a recent finding that Pink1 and Parkin affect mitophagy in an ubiquitination-dependent manner (Geisler *et al*, 2010). Therefore, the changes in mitochondrial dynamics and turnover might render neurons susceptible to degeneration in PD.

Materials and methods

Chemicals

Phospholipids (1-palmityl-2-oleoyl-*sn*-glycero-3-phospho-choline (POPC), dipalmitoyl-*sn*-glycero-3-phospho-choline (DPPC), dioleoyl-*sn*-glycero-3-phosphocholine (DOPC), 1-palmityl-2-oleoyl-*sn*-glycero-3-phospho-serine (POPS), dioleoyl-*sn*-glycero-3-phospho-ethanolamine (DOPE) and 1-palmityl-2-oleoyl-*sn*-glycero-3-ethyl-phosphocholine (PC^+)) were purchased from Avanti Polar Lipids (Alabaster, AL).

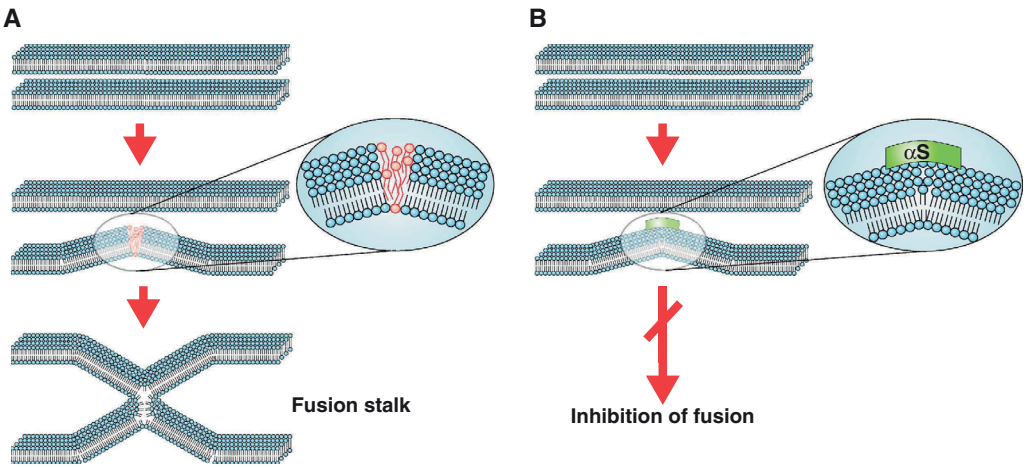

Figure 10 A model of inhibition of membrane fusion by αS. (**A**) Formation of a fusion stalk in the absence of αS. Two membranes achieve close proximity, possibly assisted by a docking machine (not drawn). Curvature in at least one of the fusing membranes causes stress in the packing of the lipids (see inset, the red lipids are not ideally packed), which is necessary to enable fusion of the leaflets of the two fusing membranes and the formation of a fusion stalk. (**B**) Binding of αS to curved membranes seals the packing defects and therefore inhibits the formation of a fusion stalk.

N-(7-nitrobenz-2-oxa-1,3-diazol-4-yl)-1,2-dihexadecanoyl-*sn*-glycero-3-phospho-ethanolamine (NBD-PE) and rhodamine-B 1,2-dihexadecanoyl-*sn*-glycero-3-phosphoethanolamine (Rh-PE) were purchased from Invitrogen. Bovine Brain Sphingomyelin (BBSM), cholesterol, Cytochrome c (MW 13 kDa), Poly-L-lysine (MW 67 kDa), lysozyme (MW 14.3 kDa) and ApoA-I (MW 28.3 kDa) were purchased from Sigma. PEG octa-*n*-dodecylether detergent ($C_{12}E_8$) was purchased from Fluka.

Protein preparations

Recombinant αS (wt-αS) was prepared, purified and desalted as described before (Kahle *et al*, 2001). Lyophilized aliquots were kept at −20°C. Stock solutions of 0.1–0.2 mg/ml αS were kept at 4°C for not longer than 1 week. CD and DLS showed that the protein was in random-coil conformation and that no aggregates were present. The construct αS1–116, lacking the last 24 amino acids from the C-terminus was generated by PCR amplification of the αS gene with the 5′-oligonucleotide primer GGAATTCCATATGGATGTATTCATGA AAGGACTT, and the 3′-oligonucleotide primer GGAATTCCATATG TTACATATCTTCCAGAATTCCTTCCTG containing the *Nde*I restriction site. Amplimers were subcloned into the *Nde*I site of pET-5a (Novagen, San Diego, CA), and constructs used to transform *Escherichia coli* BL21 (DE3). The construct was confirmed by DNA sequencing and the expressed mutant checked by mass spectrometry. Peptides αS (41–65) and αS (116–140) were purchased from PANATecs GmbH.

A cytochrome c stock solution (1 mM) in water was prepared and calibrated with a spectrophotometer using $\varepsilon_{550-539} = 20.1\,mM^{-1}$ for reduced cytochrome c.

Vesicle preparation

SUVs were prepared by sonicating the hydrated lipids 20 min (pulsed mode 20%) under Argon at >5°C above the phase transition temperature of the lipids. SUV were usually diluted to a final lipid concentration of <1 mM to slow down spontaneous fusion. For SUV containing a mixture of lipids, the lipids were first mixed in chloroform. Chloroform was evaporated with nitrogen gas and 1 h vacuum. For cholesterol-containing vesicles, the lipids were mixed in 1 ml of *tert*-butanol. After overnight lyophilization, buffer was added to the lipids. Lipids were always vortexed and hydrated at least 1 h prior to sonication.

Fusion experiments using static light scattering

DPPC-SUV in phosphate buffer (20 mM Na-Phosphate, 100 mM KCl, pH 7.4) were prepared as described above and diluted in a temperature controlled, stirred fluorescence cuvet (2.5 ml) to a final lipid concentration of 600 μM. Static light scattering was measured with a Jasco FP-6300 Fluorimeter with excitation and emission both at 500 nm. Aliquots of protein were added using a Hamilton Syringe through a pinhole in the lid of the instrument. Fusion was initiated by mixing quickly 15 μl of a 5 mM $C_{12}E_8$ stock solution (final $C_{12}E_8$: 30 μM, lipid/detergent ratio = 20 mole/mole).

Lipid-mixing assay

We incorporated 2 mole % NBD-PE and 2 mole % Rhodamine-PE in the vesicles of DPPC-SUV. In these 'donor' vesicles, the fluorescence of NBD was completely quenched by Rhodamine. However, when these vesicles fuse with a 10-fold excess of vesicles without fluorescent probes, lipid-mixing results in dilution of the probes, which neutralizes the quenching effect, that is the NBD-fluorescence increases (Struck *et al*, 1981). Excitation was at 450 nm and emission at 530 nm. Experiments were done at a total lipid concentration of 625 μM, and fusion was triggered with $C_{12}E_8$ (lipid/detergent ratio = 20 mole/mole).

Contents-mixing assay

Vesicles A: 8 mg DPPC hydrated in 1 ml DPA buffer (100 mM KCl, 20 mM Hepes-NaOH, 75 mM DPA, pH 7.4) were sonicated at 45°C for 20 min under Argon. External buffer was replaced by Hepes buffer (20 mM Hepes-NaOH, 150 mM KCl, pH 7.4) using a Sephadex G75 Column, at 45°C, eluting with Hepes buffer. Final lipid concentration was about 5 mM. Vesicles were stored at 45°C to prevent fusion. Vesicles B were prepared as vesicles A, except that Terbium buffer was trapped (100 mM KCl, 20 mM Hepes-NaOH, 75 mM Citrate, 7.5 mM $TbCl_3$, pH 7.4). Fusion experiment: stirred cuvet at 30°C with 1.75 ml Hepes buffer + 2 μl 1 M EDTA (final EDTA concentration 1 mM) + 125 μl Vesicles A + 125 μl vesicles B (final total lipid concentration about 625 μM). Fusion was induced by adding 12.5 μl $C_{12}E_8$ stock solution (final lipid/$C_{12}E_8$ = 20 mole/mole). Formation of the Tb^{3+}–DPA complex due to mixing of the contents of the SUV was revealed by the Terbium fluorescence (λ_{em} = 454 nm, excitation at 276 nm). Any Tb^{3+} that had leaked to the external buffer was bound to EDTA resulting in total suspension of the Terbium fluorescence. The experiment was repeated in the presence of αS (lipid/αS = 200 mole/mole).

Calcium-induced fusion

Fusion assay: donor vesicles (POPS-SUV with 2 mole % NBD-PE and 2 mole % Rhodamine PE) were mixed with a 10-fold excess of acceptor vesicles (POPS-SUV) in 2.5 ml stirred Hepes buffer (20 mM Hepes-NaOH, 100 mM KCl, pH 7.4.) at RT (final donor lipid concentration: 2 μM, acceptor lipid concentration: 20 μM). Fusion was initiated after 2 min by adding 25 μl of a 100 mM $CaCl_2$ stock solution (final $CaCl_2$: 1 mM).

Spontaneous fusion of vesicles with opposite charges measured with stop-flow fluorescence

Experiments were carried out with a Jasco J-810 CD Spectrometer equipped with a BioLogic μSFM-20 stop-flow extension. Fluorescence was measured by setting the photomultiplier at 90 degree angle and placing a 500 nm cutoff filter in front of it. Excitation was at 450 nm with open slit (20 nm). Donor vesicles (SUV of PC^+ with 2% NBD-PE and 2% Rh-PE) were put into one syringe and acceptor vesicles (POPS-SUV) in the other. Equal volumes of both syringes were rapidly mixed and subsequent fluorescence changes monitored after the dead time of mixing (about 8 μs). Final lipid concentration of POPS-SUV was 50 μM and PC^+-SUV was 10 μM.

PEG-induced vesicle fusion

SUV composed of DOPC:DOPE:BBSM:cholesterol (molar ratio 35:30:15:20) were prepared in phosphate buffer (20 mM Na-Phosphate, 100 mM KCl, pH 7.4) by sonication. Fusion of 'donor' vesicles (including 2 mole % NBD-PE and 2 mole % Rh-PE) with a 10-fold excess of 'acceptor' vesicles (containing no fluorescent lipids) was initiated by addition of 4% (w/w) of PEG (Polyethyleneglycol 8000).

Cell culture and transfection

SH-SY5Y human neuroblastoma cells were cultured in DMEM F-12 with glutamine (Lonza) supplemented with 15% (v/v) fetal calf serum, non-essential amino acids (Invitrogen) and penicillin/streptomycin. Transfection was performed with Lipofectamine/Plus (Invitrogen) according to the manufacturer's instructions. Vectors for expression of αS wt, A30P and A53T mutants as described (Hasegawa *et al*, 2004) and for expression of DJ-1 C106A as described (Waak *et al*, 2009) were kindly provided by P Kahle (Laboratory of Functional Neurogenetics, Hertie Institute for Clinical Brain Research, Tübingen, Germany). The following DNA constructs have been described before: PINK1 wt and PINK1 G309D (Exner *et al*, 2007), parkin wt and parkin Δ1–79 (Winklhofer *et al*, 2003; Henn *et al*, 2005), DJ-1 wt (Gorner *et al*, 2004), Mfn2, Opa1, Drp1(K38E)-ECFP (Harder *et al*, 2004; Neuspiel *et al*, 2005), mito-DsRED (Okita *et al*, 2004). The human Mfn1 cDNA sequence (BC040557) was obtained from Open Biosystems and subcloned into pcDNA6A/V5-His (Invitrogen) using *Nhe*I and *Xho*I. βS was subcloned into pcDNA6A/V5 using *Hin*dIII and *Xho*I. Mito-GFP was purchased from Invitrogen. For RNA interference, cells were transfected with HP-validated siRNA directed against the 3′UTR of αS or non-targeting control siRNA (Qiagen). Downregulation of Drp1 was performed as described (Lutz *et al*, 2009).

Fluorescent staining of mitochondria

For visualization of mitochondria, SH-SY5Y cells were cotransfected with mito-GFP (Invitrogen), fixed for 15 min in 4% paraformaldehyde in phosphate-buffered saline (PBS) at room temperature. Coverslips were mounted onto glass slides using ProLong Gold Antifade Reagent (Invitrogen) for analysis. A series of images along the *z* axis were taken with an inverted laser scanning confocal microscope (Zeiss Axiovert 200 M), with a ×100/1.4 DIC oil immersion lens and projected into a single image using the maximal projection tool of the LSM 510 confocal software (Zeiss). For life-cell imaging, SH-SY5Y cells were seeded on poly-L-lysine-coated coverslips. On the day after transfection, cells were fluorescently labelled with 0.1 μM DiOC6(3) (Molecular Probes) in medium for 15 min. Coverslips were rinsed in PBS and living cells were analysed for mitochondrial morphology by fluorescence microscopy using a Leica DMRB microscope. Transfected cells were identified by coexpression of mCherry for life-cell imaging or by coexpression of mito-GFP. Cells that displayed a network of filamentous mitochondria (see Figures 2A and D and 8A; control transfected) were classified as normal, cells with a disrupted network of mitochondria (see Figure 2A; αS wt, A30P and A53T and Figure 2D αS and βS) were classified as fragmented, cells with much extended mitochondrial tubules were classified as elongated (see Figure 8A; siRNA αS). Data are mean values of at least three independent experiments. Fragmentation was induced by incubation of cells in 10 μM carbonyl cyanide 3-chlorophenylhydrazone (CCCP) for 1 h. The medium was replaced by fresh medium without CCCP and after different time points cells were fixed and mounted onto glass slides. Cells that displayed a network of filamentous mitochondria were classified as normal, cells with fragmented or partially re-elongated mitochondria were classified as fragmented.

Measurement of mitochondrial membrane potential with TMRM

SH-SY5Y cells were seeded on poly-L-lysine-coated coverslips. On the day after transfection, cells were fluorescently labelled with 20 nM TMRM (Molecular Probes) in imaging buffer (116 mM NaCl, 5.4 mM KCl, 0.4 mM $MgSO_4$, 20 mM HEPES, 0.9 mM Na_2HPO_4, 1.2 mM $CaCl_2$, 10 mM glucose, 20 mM taurine, 5 mM pyruvate, pH 7.4) for 60 min at room temperature as described (Davidson *et al*, 2007). Pictures were taken with an inverted laser scanning confocal microscope (Zeiss LSM 510 Meta) with a ×100/1.4 DIC oil immersion lens at lowest setting of the HeNe (543 nm) laser. The intensity of the TMRM signal in the area of mito-GFP and TMRM signal colocalization was measured in life cells using the LSM 510 confocal software (Zeiss).

Measurement of cellular ATP levels

Cellular steady-state ATP levels were measured using the ATP Bioluminescence assay kit HS II (Roche Applied Science) according to the manufacturer's instructions. SH-SY5Y cells were plated on six-well plates. After 24 h, cells were transfected using Lipofectamine/Plus (Invitrogen) with the indicated DNA constructs. At 20 h before harvesting cells, the culture medium was replaced by medium containing 3 mM glucose. Cells were washed twice with PBS, scraped off the plate, and lysed according to the provided protocol. Bioluminescence of the samples was determined using an LB96V luminometer (Berthold Technologies), analysed with WinGlow Software (Berthold Technologies) and normalized to total protein levels. Each transfection was performed in duplicate, and all experiments were repeated at least five times.

PEG cellular fusion assay

SH-SY5Y cells were transiently transfected with either mitochondrially targeted green fluorescent protein (mito-GFP) or mitochondrially targeted DsRED (mito-RFP) and either empty vector or αS. At 8 h after transfection, cells were coplated (ratio 1:1) on coverslips and cocultivated for 16 h. Then, fusion of cocultured cells was induced by a 90-s treatment with a pre-warmed solution of 50% (w/v) PEG 3350 in PBS, followed by extensive washing with pre-warmed PBS. After additional cocultivation for 5 h in cell culture medium, cells were fixed with 3.7% (v/v) formaldehyde in PBS. After two washes with PBS, coverslips were mounted and then analysed using confocal microscopy (Zeiss LSM 510 Meta) in a blinded manner. To inhibit *de novo* synthesis of fluorescent proteins, 30 min before PEG treatment cells were incubated with the protein synthesis inhibitor cyclohexymide (40 μg/ml), which was subsequently added to all solutions and tissue culture media until the cells were fixed. Cell hybrids from two independent experiments were analysed in a blinded manner for mitochondrial fusion using Zeiss LSM 510 Meta Software. Per experiment at least 40 cell hybrids were analysed. The percent mitochondrial fusion indicates the rate of overlap between green and red mitochondrially targeted fluorescent proteins expressed in one cell hybrid.

Antibodies

Protein expression was controlled by separation of 0.25% Triton X-100 cell lysates on SDS gels, followed by immunoblotting with the following antibodies: αS rat monoclonal antibody against human αS (116–131) peptide MPVDPDNEAYEMPSEE, (Kahle *et al*, 2000), PINK1 polyclonal antibody BC100–494 (Novus Biologicals), parkin polyclonal antibody 2132 (Cell Signaling), DJ-1 rabbit polyclonal antiserum 3407 (Gorner *et al*, 2007), Mfn1 polyclonal antibody (Novus Biologicals), Mfn2 polyclonal antibody (Sigma), Opa1 polyclonal antibody (Duvezin-Caubet *et al*, 2006) Drp1 monoclonal antibody (BD Transduction Laboratories), Tim23 monoclonal antibody (BD Bioscience), calreticulin polyclonal antibody (Calbiochem), V5 monoclonal antibody (Invitrogen), calnexin polyclonal antibody (StressGen), GFP mouse monoclonal (Roche) and β-actin monoclonal antibody (Sigma). Bound antibodies were detected with the enhanced chemiluminescence detection system (Amersham) or the Immobilon western chemoluminescent HRP substrate (Millipore).

Statistical analysis

Statistical analysis was carried out using ANOVA ($^*P \leqslant 0.05$; $^{**}P \leqslant 0.01$; $^{***}P \leqslant 0.001$).

C. elegans: generation of transgenic animals, fluorescence microscopy

C. elegans strains were cultured at 20°C as described previously (Karpinar *et al*, 2009). To express human αS in *C. elegans* BWMs, αS was fused to mYFP citrine at the C-terminus and cloned under the control of the *myo-3*-promoter in the expression vector pPD115.62 (*Pmyo-3*::*gfp*, kindly provided by A Fire) replacing *gfp* (Karpinar *et al*, 2009). C-terminal fusion of αS with YFP has been used before and it has been shown that it does not significantly change the structure of the protein or its aggregation properties (van Ham *et al*, 2010). To create transgenic *C. elegans* expressing the mitochondrial marker TOM70-CFP in muscle cells, an injection mix containing *Pmyo-3*::*tom70-cfp* (5 ng/μl, kindly provided by A van der Bliek, UCLA) and the coinjection-marker pRF4 (*rol-6(su1006sd)*; 40 ng/μl) was injected into the gonads of young adults as described (Mello *et al*, 1991). To create transgenic worms expressing αS-YFP in addition to the mitochondrial marker, worms were injected with a plasmid mix additionally containing *Pmyo-3*::*αS-yfp* (55 ng/μl for gzEx119 and 30 ng/μl for gzEx120 and gzEx121). All injection mixes were adjusted to a total DNA concentration of 100 ng/μl by addition of pBluescript II (Stratagene). Transgenic animals were imaged on the first day of adulthood while being anaesthetized with 50 mM NaN_3 in M9 buffer and mounted on 2% agarose pads. Imaging was performed using an UltraviewVox spinning disk microscope (Perkin Elmer) with a ×100/1.40 oil immersion objective. The morphological appearance of mitochondria in BWMs of transgenic strains were classified into three categories: (i) wild-type like, (ii) fragmented or (iii) thin and highly interconnected. The classification was done on *z*-stacks, which were projected into a single plane using the extended focus tool of the Volocity software (Perkin Elmer).

In order to analyse the changes in mitochondrial morphology occurring during aging, we compared the mitochondrial morphology in muscle cells of young adult worms (3 days after hatching) with that of worms in the post-reproductive stage (7 days after hatching).

For neuronal expression, the *myo3*-promoter in was replaced by the neuronal *rab-3*-promoter creating *Prab-3*::*tom70-cfp* (5 ng/μl) and *Prab-3*::*αS-yfp* (30 ng/μl), respectively (the respective plasmid concentrations in the injection mixes are indicated). Motor neurons were imaged as described previously for BWMs. Mitochondrial appearance in neuronal cell bodies was classified into three categories: as (i) ring-like, (ii) tubular or (iii) highly fragmented. αS expression levels were determined by western blotting using either a polyclonal rabbit αS antibody (Anaspec) or monoclonal rat αS antibody 15G7 and normalized against α-tubulin using the monoclonal mouse antibody 12G10 (DSHB).

Electron microscopy

Culture cells were grown on Thermonox discs and mounted between two 10 μm deep aluminium platelets (Microscopy Services, Flintbek) and immediately frozen using a BalTec HPM 10. Freeze substitution was carried out in a Leica AFS2. For morphological investigations, incubations were at −90°C for 100 h in 0.1% tannic acid, 7 h in 2% OsO_4, and at −20°C for 16 h in 2% OsO_4, followed by embedding in EPON at RT. For immunostaining, incubations were at −90°C for 100 h in 1.5% uranyl acetate, followed by embedding in Lowicryl HM20 at −45°C (Rostaing *et al*, 2004) (all solutions w/v in dry acetone). EPON sections were 50 nm, Lowicryl sections 90 nm. Lowicryl sections were stained with anti-synuclein antibodies (rabbit, AnaSpec Inc.) and 10 nm Goat-anti-rabbit-gold. Washing was done on 50 mM PBS with 0.05% Tween20. In all, 50 nm EPON sections were post-stained with saturated uranyl acetate in 75% methanol and 4% lead citrate (Reynolds, 1963). In all, 90 nm Lowicryl sections were post-stained with 6% phoshotungstic acid. Micrographs were taken with a 1024 × 1024 CCD detector (Proscan CCD HSS 512/1024; Proscan Electronic Systems, Scheuring, Germany) in a Zeiss EM 902A, operated in the bright field mode.

Supplementary data

Supplementary data are available at *The EMBO Journal* Online (http://www.embojournal.org).

Acknowledgements

This work was supported by the Collaborative Research Center SFB 596 (Projects A14, B10, B13 and B9), the Lüneburg Foundation, the Leibniz Award of the Deutsche Forschungs Gemeinschaft, the German Ministry for Education and Research (NGFN plus 'Functional Genomics of Parkinson's Disease'), the Helmholtz Alliance 'Mental Health in an Ageing Society' and the Center for Integrated Protein Science Munich (CIPSM). C Haass is supported by a 'Forschungsprofessur' of the LMU. N Wender is funded by the Dorothea-Schlözer-Programm of the Georg-August-Universität Göttingen. We thank Sabine Odoy for excellent technical assistance, P Kahle and H McBride for providing plasmids, the Hans and Ilse Breuer Foundation for the confocal microscope and M Klingenberg and H Steiner for critical discussions of the manuscript.

Conflict of interest

The authors declare that they have no conflict of interest.

References

Abeliovich A, Schmitz Y, Farinas I, Choi-Lundberg D, Ho WH, Castillo PE, Shinsky N, Verdugo JM, Armanini M, Ryan A, Hynes M, Phillips H, Sulzer D, Rosenthal A (2000) Mice lacking alpha-synuclein display functional deficits in the nigrostriatal dopamine system. *Neuron* **25:** 239–252

Ben Gedalya T, Loeb V, Israeli E, Altschuler Y, Selkoe DJ, Sharon R (2009) Alpha-synuclein and polyunsaturated fatty acids promote clathrin-mediated endocytosis and synaptic vesicle recycling. *Traffic* **10:** 218–234

Beyer K (2007) Mechanistic aspects of Parkinson's disease. α-synuclein and the biomembrane. *Cell Biochem Biophys* **47:** 285–299

Bodner CR, Dobson CM, Bax A (2009) Multiple tight phospholipid-binding modes of alpha-synuclein revealed by solution NMR spectroscopy. *J Mol Biol* **390:** 775–790

Cabin DE, Shimazu K, Murphy D, Cole NB, Gottschalk W, McIlwain KL, Orrison B, Chen A, Ellis CE, Paylor R, Lu B, Nussbaum RL (2002) Synaptic vesicle depletion correlates with attenuated synaptic responses to prolonged repetitive stimulation in mice lacking alpha-synuclein. *J Neurosci* **22:** 8797–8807

Canet-Aviles RM, Wilson MA, Miller DW, Ahmad R, McLendon C, Bandyopadhyay S, Baptista MJ, Ringe D, Petsko GA, Cookson MR (2004) The Parkinson's disease protein DJ-1 is neuroprotective due to cysteine-sulfinic acid-driven mitochondrial localization. *Proc Natl Acad Sci USA* **101:** 9103–9108

Chandra S, Fornai F, Kwon HB, Yazdani U, Atasoy D, Liu X, Hammer RE, Battaglia G, German DC, Castillo PE, Sudhof TC (2004) Double-knockout mice for alpha- and beta-synucleins: effect on synaptic functions. *Proc Natl Acad Sci USA* **101:** 14966–14971

Chandra S, Gallardo G, Fernandez-Chacon R, Schluter OM, Sudhof TC (2005) Alpha-synuclein cooperates with CSPalpha in preventing neurodegeneration. *Cell* **123:** 383–396

Chen M, Margittai M, Chen J, Langen R (2007) Investigation of alpha-synuclein fibril structure by site-directed spin labeling. *J Biol Chem* **282:** 24970–24979

Chen X, Arac D, Wang TM, Gilpin CJ, Zimmerberg J, Rizo J (2006) SNARE-mediated lipid mixing depends on the physical state of the vesicles. *Biophys J* **90:** 2062–2074

Chernomordik L, Kozlov MM, Zimmerberg J (1995) Lipids in biological membrane fusion. *J Membr Biol* **146:** 1–14

Chernomordik LV, Kozlov MM (2003) Protein-lipid interplay in fusion and fission of biological membranes. *Annu Rev Biochem* **72:** 175–207

Chiba-Falek O, Lopez GJ, Nussbaum RL (2006) Levels of alpha-synuclein mRNA in sporadic Parkinson disease patients. *Mov Disord* **21:** 1703–1708

Cho DH, Nakamura T, Lipton SA (2010) Mitochondrial dynamics in cell death and neurodegeneration. *Cell Mol Life Sci* (in press)

Clark IE, Dodson MW, Jiang C, Cao JH, Huh JR, Seol JH, Yoo SJ, Hay BA, Guo M (2006) Drosophila pink1 is required for mitochondrial

function and interacts genetically with parkin. *Nature* **441:** 1162–1166

Cole NB, Dieuliis D, Leo P, Mitchell DC, Nussbaum RL (2008) Mitochondrial translocation of alpha-synuclein is promoted by intracellular acidification. *Exp Cell Res* **314:** 2076–2089

Cooper AA, Gitler AD, Cashikar A, Haynes CM, Hill KJ, Bhullar B, Liu K, Xu K, Strathearn KE, Liu F, Cao S, Caldwell KA, Caldwell GA, Marsischky G, Kolodner RD, Labaer J, Rochet JC, Bonini NM, Lindquist S (2006) Alpha-synuclein blocks ER-Golgi traffic and Rab1 rescues neuron loss in Parkinson's models. *Science* **313:** 324–328

Cornell RB, Taneva SG (2006) Amphipathic helices as mediators of the membrane interaction of amphitropic proteins, and as modulators of bilayer physical properties. *Curr Protein Pept Sci* **7:** 539–552

Dagda RK, Cherra III SJ, Kulich SM, Tandon A, Park D, Chu CT (2009) Loss of PINK1 function promotes mitophagy through effects on oxidative stress and mitochondrial fission. *J Biol Chem* **284:** 13843–13855

Davidson SM, Yellon D, Duchen MR (2007) Assessing mitochondrial potential, calcium, and redox state in isolated mammalian cells using confocal microscopy. *Methods Mol Biol* **372:** 421–430

Davidson WS, Jonas A, Clayton DF, George JM (1998) Stabilization of α-synuclein secondary structue upon bindung to synthetic membranes. *J Biol Chem* **273:** 9443–9449

Dennison SM, Bowen ME, Brunger AT, Lentz BR (2006) Neuronal SNAREs do not trigger fusion between synthetic membranes but do promote PEG-mediated membrane fusion. *Biophys J* **90:** 1661–1675

Der-Sarkissian A, Jao CC, Chen J, Langen R (2003) Structural organization of α-synuclein fibrils studied by site-directed spin labeling. *J Biol Chem* **278:** 37530–37535

Derksen A, Gantz D, Small DM (1996) Calorimetry of apolipoprotein-A1 binding to phosphatidylcholine-triolein-cholesterol emulsions. *Biophys J* **70:** 330–338

Detmer SA, Chan DC (2007) Functions and dysfunctions of mitochondrial dynamics. *Nat Rev Mol Cell Biol* **8:** 870–879

Devi L, Raghavendran V, Prabhu BM, Avadhani NG, Anandatheerthavarada HK (2008) Mitochondrial import and accumulation of {alpha}-sy. *J Biol Chem* **283:** 9089–9100

Dobson CM (2003) Protein folding and misfolding. *Nature* **426:** 884–890

Drescher M, Godschalk F, Veldhuis G, van Rooijen BD, Subramaniam V, Huber M (2008a) Spin-label EPR on alpha-synuclein reveals differences in the membrane binding affinity of the two antiparallel helices. *Chembiochem* **9:** 2411–2416

Drescher M, Veldhuis G, van Rooijen BD, Milikisyants S, Subramaniam V, Huber M (2008b) Antiparallel arrangement of the helices of vesicle-bound alpha-synuclein. *J Am Chem Soc* **130:** 7796–7797

Duvezin-Caubet S, Jagasia R, Wagener J, Hofmann S, Trifunovic A, Hansson A, Chomyn A, Bauer MF, Attardi G, Larsson NG, Neupert W, Reichert AS (2006) Proteolytic processing of OPA1 links mitochondrial dysfunction to alterations in mitochondrial morphology. *J Biol Chem* **281:** 37972–37979

Exner N, Treske B, Paquet D, Holmstrom K, Schiesling C, Gispert S, Carballo-Carbajal I, Berg D, Hoepken HH, Gasser T, Kruger R, Winklhofer KF, Vogel F, Reichert AS, Auburger G, Kahle PJ, Schmid B, Haass C (2007) Loss-of-function of human PINK1 results in mitochondrial pathology and can be rescued by parkin. *J Neurosci* **27:** 12413–12418

Ferreon AC, Gambin Y, Lemke EA, Deniz AA (2009) Interplay of alpha-synuclein binding and conformational switching probed by single-molecule fluorescence. *Proc Natl Acad Sci USA* **106:** 5645–5650

Fujita Y, Ohama E, Takatama M, Al-Sarraj S, Okamoto K (2006) Fragmentation of Golgi apparatus of nigral neurons with alpha-synuclein-positive inclusions in patients with Parkinson's disease. *Acta Neuropathol* **112:** 261–265

Gaber BP, Sheridan JP (1982) Kinetic and thermodynamic studies of the fusion of small unilamellar phospholipid vesicles. *Biochim Biophys Acta* **685:** 87–93

Geisler S, Holmstrom KM, Skujat D, Fiesel FC, Rothfuss OC, Kahle PJ, Springer W (2010) PINK1/Parkin-mediated mitophagy is dependent on VDAC1 and p62/SQSTM1. *Nat Cell Biol* **12:** 119–131

Giannakis E, Pacifico J, Smith DP, Hung LW, Masters CL, Cappai R, Wade JD, Barnham KJ (2008) Dimeric structures of alpha-synuclein bind preferentially to lipid membranes. *Biochim Biophys Acta* **1778:** 1112–1119

Gitler AD, Bevis BJ, Shorter J, Strathearn KE, Hamamichi S, Su LJ, Caldwell KA, Caldwell GA, Rochet JC, McCaffery JM, Barlowe C, Lindquist S (2008) The Parkinson's disease protein alpha-synuclein disrupts cellular Rab homeostasis. *Proc Natl Acad Sci USA* **105:** 145–150

Gitler AD, Chesi A, Geddie ML, Strathearn KE, Hamamichi S, Hill KJ, Caldwell KA, Caldwell GA, Cooper AA, Rochet JC, Lindquist S (2009) Alpha-synuclein is part of a diverse and highly conserved interaction network that includes PARK9 and manganese toxicity. *Nat Genet* **41:** 308–315

Gorner K, Holtorf E, Odoy S, Nuscher B, Yamamoto A, Regula JT, Beyer K, Haass C, Kahle PJ (2004) Differential effects of Parkinson's disease-associated mutations on stability and folding of DJ-1. *J Biol Chem* **279:** 6943–6951

Gorner K, Holtorf E, Waak J, Pham TT, Vogt-Weisenhorn DM, Wurst W, Haass C, Kahle PJ (2007) Structural determinants of the C-terminal helix-kink-helix motif essential for protein stability and survival promoting activity of DJ-1. *J Biol Chem* **282:** 13680–13691

Gosavi N, Lee HJ, Lee JS, Patel S, Lee SJ (2002) Golgi fragmentation occurs in the cells with prefibrillar alpha-synuclein aggregates and precedes the formation of fibrillar inclusion. *J Biol Chem* **277:** 48984–48992

Grundemann J, Schlaudraff F, Haeckel O, Liss B (2008) Elevated alpha-synuclein mRNA levels in individual UV-laser-microdissected dopaminergic substantia nigra neurons in idiopathic Parkinson's disease. *Nucleic Acids Res* **36:** e38

Gursky O (2005) Apolipoprotein structure and dynamics. *Curr Opin Lipidol* **16:** 287–294

Haass C, Selkoe DJ (2007) Soluble protein oligomers in neurodegeneration: lessons from the Alzheimer's amyloid beta-peptide. *Nat Rev Mol Cell Biol* **8:** 101–112

Haque ME, McIntosh TJ, Lentz BR (2001) Influence of lipid composition on physical properties and PEG-mediated fusion of curved and uncurved model membrane vesicles: 'nature's own fusogenic lipid bilayer'. *Biochemistry* **40:** 4340–4348

Harder Z, Zunino R, McBride H (2004) Sumo1 conjugates mitochondrial substrates and participates in mitochondrial fission. *Curr Biol* **14:** 340–345

Hasegawa T, Matsuzaki M, Takeda A, Kikuchi A, Akita H, Perry G, Smith MA, Itoyama Y (2004) Accelerated alpha-synuclein aggregation after differentiation of SH-SY5Y neuroblastoma cells. *Brain Res* **1013:** 51–59

Haywood AF, Staveley BE (2006) Mutant alpha-synuclein-induced degeneration is reduced by parkin in a fly model of Parkinson's disease. *Genome* **49:** 505–510

Henn IH, Bouman L, Schlehe JS, Schlierf A, Schramm JE, Wegener E, Nakaso K, Culmsee C, Berninger B, Krappmann D, Tatzelt J, Winklhofer KF (2007) Parkin mediates neuroprotection through activation of IkappaB kinase/nuclear factor-kappaB signaling. *J Neurosci* **27:** 1868–1878

Henn IH, Gostner JM, Lackner P, Tatzelt J, Winklhofer KF (2005) Pathogenic mutations inactivate parkin by distinct mechanisms. *J Neurochem* **92:** 114–122

Herndon LA, Schmeissner PJ, Dudaronek JM, Brown PA, Listner KM, Sakano Y, Paupard MC, Hall DH, Driscoll M (2002) Stochastic and genetic factors influence tissue-specific decline in ageing C. elegans. *Nature* **419:** 808–814

Hoppert M (2003) *Microscopic Techniques in Biotechnology*. Weinheim: Wiley-VCH

Hsu LJ, Sagara Y, Arroyo A, Rockenstein E, Sisk A, Mallory M, Wong J, Takenouchi T, Hashimoto M, Masliah E (2000) alpha-synuclein promotes mitochondrial deficit and oxidative stress. *Am J Pathol* **157:** 401–410

Ibanez P, Bonnet AM, Debarges B, Lohmann E, Tison F, Pollak P, Agid Y, Durr A, Brice A (2004) Causal relation between alpha-synuclein gene duplication and familial Parkinson's disease. *Lancet* **364:** 1169–1171

Ishihara N, Jofuku A, Eura Y, Mihara K (2003) Regulation of mitochondrial morphology by membrane potential, and DRP1-dependent division and FZO1-dependent fusion reaction in mammalian cells. *Biochem Biophys Res Commun* **301:** 891–898

Iwai A, Masliah E, Yoshimoto M, Ge N, Flanagan L, de Silva HA, Kittel A, Saitoh T (1995) The precursor protein of non-A beta

component of Alzheimer's disease amyloid is a presynaptic protein of the central nervous system. *Neuron* **14:** 467–475

Jao CC, Hegde BG, Chen J, Haworth IS, Langen R (2008) Structure of membrane-bound alpha-synuclein from site-directed spin labeling and computational refinement. *Proc Natl Acad Sci USA* **105:** 19666–19671

Jensen PH, Nielsen MS, Jakes R, Dotti CG, Goedert M (1998) Binding of alpha-synuclein to brain vesicles is abolished by familial Parkinson's disease mutation. *J Biol Chem* **273:** 26292–26294

Jo E, Darabie AA, Han K, Tandon A, Fraser PE, McLaurin J (2004) alpha-Synuclein-synaptosomal membrane interactions: implications for fibrillogenesis. *Eur J Biochem* **271:** 3180–3189

Kahle PJ, Neumann M, Ozmen L, Muller V, Jacobsen H, Schindzielorz A, Okochi M, Leimer U, van Der Putten H, Probst A, Kremmer E, Kretzschmar HA, Haass C (2000) Subcellular localization of wild-type and Parkinson's disease-associated mutant alpha-synuclein in human and transgenic mouse brain. *J Neurosci* **20:** 6365–6373

Kahle PJ, Neumann M, Ozmen L, Müller V, Odoy S, Okamoto N, Jacobsen H, Iwatsubo T, Trojanowski JQ, Takahashi H, Wakabayashi K, Bogdanovic N, Riederer P, Kreschmar HA, Haass C (2001) Selective insolubility of alpha-synuclein in human Lewy Body diseases is recapitulated in a transgenic mouse model. *Am J Pathol* **159:** 2215–2225

Kamp F, Beyer K (2006) Binding of α-synuclein affects the lipid packing in bilayers of small vesicles. *J Biol Chem* **281:** 9251–9259

Karpinar DP, Balija MB, Kugler S, Opazo F, Rezaei-Ghaleh N, Wender N, Kim HY, Taschenberger G, Falkenburger BH, Heise H, Kumar A, Riedel D, Fichtner L, Voigt A, Braus GH, Giller K, Becker S, Herzig A, Baldus M, Jackle H *et al* (2009) Pre-fibrillar alpha-synuclein variants with impaired beta-structure increase neurotoxicity in Parkinson's disease models. *EMBO J* **28:** 3256–3268

Kayed R, Pensalfini A, Margol L, Sokolov Y, Sarsoza F, Head E, Hall J, Glabe C (2009) Annular protofibrils are a structurally and functionally distinct type of amyloid oligomer. *J Biol Chem* **284:** 4230–4237

Kim RH, Smith PD, Aleyasin H, Hayley S, Mount MP, Pownall S, Wakeham A, You-Ten AJ, Kalia SK, Horne P, Westaway D, Lozano AM, Anisman H, Park DS, Mak TW (2005) Hypersensitivity of DJ-1-deficient mice to 1-methyl-4-phenyl-1,2,3,6-tetrahydropyrindine (MPTP) and oxidative stress. *Proc Natl Acad Sci USA* **102:** 5215–5220

Kitada T, Asakawa S, Hattori N, Matsumine H, Yamamura Y, Minoshima S, Yokochi M, Mizuno Y, Shimizu N (1998) Mutations in the parkin gene cause autosomal recessive juvenile parkinsonism. *Nature* **392:** 605–608

Kostka M, Hogen T, Danzer KM, Levin J, Habeck M, Wirth A, Wagner R, Glabe CG, Finger S, Heinzelmann U, Garidel P, Duan W, Ross CA, Kretzschmar H, Giese A (2008) Single-particle characterization of iron-induced pore-forming alpha -synuclein oligomers. *J Biol Chem* **283:** 10992–11003

Kramer ML, Schulz-Schaeffer WJ (2007) Presynaptic alpha-synuclein aggregates, not Lewy bodies, cause neurodegeneration in dementia with Lewy bodies. *J Neurosci* **27:** 1405–1410

Labrousse AM, Zappaterra MD, Rube DA, VanderBliek AM (1999) C. elegans dynamin-related protein DRP-1 controls severing of the mitochondrial outer membrane. *Mol Cell* **4:** 815–826

Larsen KE, Schmitz Y, Troyer MD, Mosharov E, Dietrich P, Quazi AZ, Savalle M, Nemani V, Chaudhry FA, Edwards RH, Stefanis L, Sulzer D (2006) α-Synuclein overexpression in PC12 and chromaffin cells impairs catecholamine release by interfering with a late step in exocytosis. *J Neurosci* **26:** 11915–11922

Lee HJ, Khoshaghideh F, Lee S, Lee SJ (2006) Impairment of microtubule-dependent trafficking by overexpression of alpha-synuclein. *Eur J Neurosci* **24:** 3153–3162

Lee HJ, Khoshaghideh F, Patel S, Lee SJ (2004a) Clearance of alpha-synuclein oligomeric intermediates via the lysosomal degradation pathway. *J Neurosci* **24:** 1888–1896

Lee JC, Langen R, Hummel PA, Gray HB, Winkler JR (2004b) Alpha-synuclein structures from fluorescence energy-transfer kinetics: implications for the role of the protein in Parkinson's disease. *Proc Natl Acad Sci USA* **101:** 16466–16471

Lei G, MacDonald RC (2003) Lipid bilayer vesicle fusion: intermediates captured by high-speed microfluorescence spectroscopy. *Biophys J* **85:** 1585–1599

Lentz BR (2007) PEG as a tool to gain insight into membrane fusion. *Eur Biophys J* **36:** 315–326

Li WW, Yang R, Guo JC, Ren HM, Zha XL, Cheng JS, Cai DF (2007) Localization of alpha-synuclein to mitochondria within midbrain of mice. *Neuroreport* **18:** 1543–1546

Liu T, Tucker WC, Bhalla A, Chapman ER, Weisshaar JC (2005) SNARE-driven, 25-millisecond vesicle fusion *in vitro*. *Biophys J* **89:** 2458–2472

Lutz AK, Exner N, Fett ME, Schlehe JS, Kloos K, Laemmermann K, Brunner B, Kurz-Drexler A, Vogel F, Reichert AS, Bouman L, Vogt-Weisenhorn D, Wurst W, Tatzelt J, Haass C, Winklhofer KF (2009) Loss of parkin or PINK1 function increases DRP1-dependent mitochondrial fragmentation. *J Biol Chem* **284:** 22938–22951

Malka F, Aure K, Goffart S, Spelbrink JN, Rojo M (2007) The mitochondria of cultured mammalian cells: I. Analysis by immunofluorescence microscopy, histochemistry, subcellular fractionation, and cell fusion. *Methods Mol Biol* **372:** 3–16

Maraganore DM, de Andrade M, Elbaz A, Farrer MJ, Ioannidis JP, Kruger R, Rocca WA, Schneider NK, Lesnick TG, Lincoln SJ, Hulihan MM, Aasly JO, Ashizawa T, Chartier-Harlin MC, Checkoway H, Ferrarese C, Hadjigeorgiou G, Hattori N, Kawakami H, Lambert JC *et al* (2006) Collaborative analysis of alpha-synuclein gene promoter variability and Parkinson disease. *JAMA* **296:** 661–670

Maroteaux L, Campanelli JT, Scheller RH (1988) Synuclein: a neuron-specific protein localized to the nucleus and presynaptic nerve terminal. *J Neurosci* **8:** 2804–2815

Martin LJ, Pan Y, Price AC, Sterling W, Copeland NG, Jenkins NA, Price DL, Lee MK (2006) Parkinson's disease alpha-synuclein transgenic mice develop neuronal mitochondrial degeneration and cell death. *J Neurosci* **26:** 41–50

Mello CC, Kramer JM, Stinchcomb D, Ambros V (1991) Efficient gene transfer in C. elegans: extrachromosomal maintenance and integration of transforming sequences. *EMBO J* **10:** 3959–3970

Morais VA, Verstreken P, Roethig A, Smet J, Snellinx A, Vanbrabant M, Haddad D, Frezza C, Mandemakers W, Vogt-Weisenhorn D, Van Coster R, Wurst W, Scorrano L, De Strooper B (2009) Parkinson's disease mutations in PINK1 result in decreased complex I activity and deficient synaptic function. *EMBO Mol Med* **1:** 99–111

Murphy DD, Rueter SM, Trojanowski JQ, Lee VM (2000) Synucleins are developmentally expressed, and alpha-synuclein regulates the size of the presynaptic vesicular pool in primary hippocampal neurons. *J Neurosci* **20:** 3214–3220

Nakamura K, Nemani VM, Wallender EK, Kaehlcke K, Ott M, Edwards RH (2008) Optical reporters for the conformation of alpha-synuclein reveal a specific interaction with mitochondria. *J Neurosci* **28:** 12305–12317

Nemani VM, Lu W, Berge V, Nakamura K, Onoa B, Lee MJ, Chaudhry FA, Nicoli RA, Edwards RH (2010) Increased expression of alpha-synuclein reduces neurotransmitter release by inhibiting synaptic vesicle reclustering after endocytosis. *Neuron* **65:** 66–79

Neuspiel M, Zunino R, Gangaraju S, Rippstein P, McBride H (2005) Activated mitofusin 2 signals mitochondrial fusion, interferes with Bax activation, and reduces susceptibility to radical induced depolarization. *J Biol Chem* **280:** 25060–25070

Nickel W, Weber T, McNew JA, Parlati F, Sollner TH, Rothman JE (1999) Content mixing and membrane integrity during membrane fusion driven by pairing of isolated v-SNAREs and t-SNAREs. *Proc Natl Acad Sci USA* **96:** 12571–12576

Niemann A, Ruegg M, La Padula V, Schenone A, Suter U (2005) Ganglioside-induced differentiation associated protein 1 is a regulator of the mitochondrial network: new implications for Charcot-Marie-Tooth disease. *J Cell Biol* **170:** 1067–1078

Nuscher B, Kamp F, Mehnert T, Odoy S, Haass C, Kahle PJ, Beyer K (2004) α-synuclein has a high affinity for packing defects in a bilayer membrane. A thermodynamics study. *J Biol Chem* **21:** 21966–21975

Okita C, Sato M, Schroeder T (2004) Generation of optimized yellow and red fluorescent proteins with distinct subcellular localization. *Biotechniques* **36:** 418–422, 424

Orth M, Tabrizi SJ, Schapira AH, Cooper JM (2003) Alpha-synuclein expression in HEK293 cells enhances the mitochondrial sensitivity to rotenone. *Neurosci Lett* **351:** 29–32

Palacino JJ, Sagi D, Goldberg MS, Krauss S, Motz C, Wacker M, Klose J, Shen J (2004) Mitochondrial dysfunction and oxidative damage in parkin-deficient mice. *J Biol Chem* **279:** 18614–18622

Pantazatos DP, MacDonald RC (1999) Directly observed membrane fusion between oppositely charged phospholipid bilayers. *J Membr Biol* **170:** 27–38

Parihar MS, Parihar A, Fujita M, Hashimoto M, Ghafourifar P (2008) Mitochondrial association of alpha-synuclein causes oxidative stress. *Cell Mol Life Sci* **65:** 1272–1284

Parihar MS, Parihar A, Fujita M, Hashimoto M, Ghafourifar P (2009) Alpha-synuclein overexpression and aggregation exacerbates impairment of mitochondrial functions by augmenting oxidative stress in human neuroblastoma cells. *Int J Biochem Cell Biol* **41:** 2015–2024

Park J, Lee SB, Lee S, Kim Y, Song S, Kim S, Bae E, Kim J, Shong M, Kim JM, Chung J (2006) Mitochondrial dysfunction in Drosophila PINK1 mutants is complemented by parkin. *Nature* **441:** 1157–1161

Perlmutter JD, Braun AR, Sachs JN (2009) Curvature dynamics of α-synuclein familial Parkinson disease mutants: molecular simulations of the micelle- and bilayer-bound forms. *J Biol Chem* **284:** 7177–7189

Piomelli D, Astarita G, Rapaka R (2007) A neuroscientist's guide to lipidomics. *Nat Rev* **8:** 743–754

Ramakrishnan M, Jensen PH, Marsh D (2006) Association of alpha-synuclein and mutants with lipid membranes: spin-label ESR and polarized IR. *Biochemistry* **45:** 3386–3395

Reynolds ES (1963) The use of lead citrate at high pH as an electron-opaque stain in electron microscopy. *J Cell Biol* **17:** 208–212

Rostaing P, Weimer RM, Jorgensen EM, Triller A, Bessereau JL (2004) Preservation of immunoreactivity and fine structure of adult C. elegans tissues using high-pressure freezing. *J Histochem Cytochem* **52:** 1–12

Sandebring A, Thomas KJ, Beilina A, van der Brug M, Cleland MM, Ahmad R, Miller DW, Zambrano I, Cowburn RF, Behbahani H, Cedazo-Minguez A, Cookson MR (2009) Mitochondrial alterations in PINK1 deficient cells are influenced by calcineurin-dependent dephosphorylation of dynamin-related protein 1. *PLoS One* **4:** e5701

Satake W, Nakabayashi Y, Mizuta I, Hirota Y, Ito C, Kubo M, Kawaguchi T, Tsunoda T, Watanabe M, Takeda A, Tomiyama H, Nakashima K, Hasegawa K, Obata F, Yoshikawa T, Kawakami H, Sakoda S, Yamamoto M, Hattori N, Murata M *et al* (2009) Genome-wide association study identifies common variants at four loci as genetic risk factors for Parkinson's disease. *Nat Genet* **41:** 1303–1307

Schullery SE, Schmidt CF, Felgner P, Tillack TW, Thompson TE (1980a) Fusion of dipalmitoylphosphatidylcholine vesicles. *Biochemistry* **19:** 3919–3923

Schullery SE, Schmidt CF, Felgner P, Tillack TW, Thompson TE (1980b) Fusion of dipalmitoylphosphatidylcholine vesicles. *Biochemistry* **19:** 3919–3923

Sharon R, Bar-Joseph I, Frosch MP, Walsh DM, Hamilton JA, Selkoe DJ (2003) The formation of highly soluble oligomers of α-synuclein is regulated by fatty acids and enhanced in Parkinson's disease. *Neuron* **37:** 583–595

Shavali S, Brown-Borg HM, Ebadi M, Porter J (2008) Mitochondrial localization of alpha-synuclein protein in alpha-synuclein overexpressing cells. *Neurosci Lett* **439:** 125–128

Simon-Sanchez J, Schulte C, Bras JM, Sharma M, Gibbs JR, Berg D, Paisan-Ruiz C, Lichtner P, Scholz SW, Hernandez DG, Kruger R, Federoff M, Klein C, Goate A, Perlmutter J, Bonin M, Nalls MA, Illig T, Gieger C, Houlden H *et al* (2009) Genome-wide association study reveals genetic risk underlying Parkinson's disease. *Nat Genet* **41:** 1308–1312

Singleton AB, Farrer M, Johnson J, Singleton A, Hague S, Kachergus J, Hulihan M, Peuralinna T, Dutra A, Nussbaum R, Lincoln S, Crawley A, Hanson M, Maraganore D, Adler C, Cookson MR, Muenter M, Baptista M, Miller D, Blancato J *et al* (2003) alpha-Synuclein locus triplication causes Parkinson's disease. *Science* **302:** 841

Smith WW, Jiang H, Pei Z, Tanaka Y, Morita H, Sawa A, Dawson VL, Dawson TM, Ross CA (2005) Endoplasmic reticulum stress and mitochondrial cell death pathways mediate A53T mutant alpha-synuclein-induced toxicity. *Hum Mol Genet* **14:** 3801–3811

Spillantini MG, Schmidt ML, Lee VM, Trojanowski JQ, Jakes R, Goedert M (1997) Alpha-synuclein in Lewy bodies. *Nature* **388:** 839–840

Struck DK, Hoekstra D, Pagano RE (1981) Use of resonance energy transfer to monitor membrane fusion. *Biochemistry* **20:** 4093–4099

Takamori S, Holt M, Stenius K, Lemke EA, Gronborg M, Riedel D, Urlaub H, Schenck S, Brugger B, Ringler P, Muller SA, Rammner B, Grater F, Hub JS, De Groot BL, Mieskes G, Moriyama Y, Klingauf J, Grubmuller H, Heuser J *et al* (2006) Molecular anatomy of a trafficking organelle. *Cell* **127:** 831–846

Tamm LK, Crane J, Kiessling V (2003) Membrane fusion: a structural perspective on the interplay of lipids and proteins. *Curr Opin Struct Biol* **13:** 453–466

Todd AM, Staveley BE (2008) Pink1 suppresses alpha-synuclein-induced phenotypes in a Drosophila model of Parkinson's disease. *Genome* **51:** 1040–1046

Trexler A, Rhoades E (2009) α-Synuclein binds large unilamellar vesicles as an extended helix. *Biochemistry* **48:** 2304–2306

Tsika E, Moysidou M, Guo J, Cushman M, Gannon P, Sandaltzopoulos R, Giasson BI, Krainc D, Ischiropoulos H, Mazzulli JR (2010) Distinct region-specific alpha-synuclein oligomers in A53T transgenic mice: implications for neurodegeneration. *J Neurosci* **30:** 3409–3418

Ulmer TS, Bax A (2005) Comparison of structure and dynamics of micelle-bound human alpha-synuclein and Parkinson disease variants. *J Biol Chem* **280:** 43179–43187

Ulmer TS, Bax A, Cole NB, Nussbaum RL (2005) Structure and dynamics of micelle-bound human alpha-synuclein. *J Biol Chem* **280:** 9595–9603

Uversky VN (2002) What does it mean to be natively unfolded? *Eur J Biochem* **269:** 2–12

Uversky VN (2007) Neuropathology, biochemistry, and biophysics of alpha-synuclein aggregation. *J Neurochem* **103:** 17–37

Valente EM, Abou-Sleiman PM, Caputo V, Muqit MM, Harvey K, Gispert S, Ali Z, Del Turco D, Bentivoglio AR, Healy DG, Albanese A, Nussbaum R, Gonzalez-Maldonado R, Deller T, Salvi S, Cortelli P, Gilks WP, Latchman DS, Harvey RJ, Dallapiccola B *et al* (2004) Hereditary early-onset Parkinson's disease caused by mutations in PINK1. *Science* **304:** 1158–1160

van Ham TJ, Esposito A, Kumita JR, Hsu ST, Kaminski Schierle GS, Kaminski CF, Dobson CM, Nollen EA, Bertoncini CW (2010) Towards multiparametric fluorescent imaging of amyloid formation: studies of a YFP model of alpha-synuclein aggregation. *J Mol Biol* **395:** 627–642

Waak J, Weber SS, Gorner K, Schall C, Ichijo H, Stehle T, Kahle PJ (2009) Oxidizable residues mediating protein stability and cytoprotective interaction of DJ-1 with apoptosis signal-regulating kinase 1. *J Biol Chem* **284:** 14245–14257

Weber T, Zemelman BV, McNew JA, Westermann B, Gmachl M, Parlati F, Sollner TH, Rothman JE (1998) SNAREpins: minimal machinery for membrane fusion. *Cell* **92:** 759–772

Weinreb G, Lentz BR (2007) Analysis of membrane fusion as a two-state sequential process: evaluation of the stalk model. *Biophys J* **92:** 4012–4029

Westermann B (2008) Molecular machinery of mitochondrial fusion and fission. *J Biol Chem* **283:** 13501–13505

Wilschut J, Düzgünes N, Fraley R, Papahadjopoulos D (1980) Studies on the mechanism of membrane fusion: kinetics of calcium ion induced fusion of phosphatidylserine vesicles followed by a new assay for mixing of aqueous vesicles contents. *Biochemistry* **1980:** 6011–6021

Winklhofer KF, Henn IH, Kay-Jackson PC, Heller U, Tatzelt J (2003) Inactivation of parkin by oxidative stress and C-terminal truncations: a protective role of molecular chaperones. *J Biol Chem* **278:** 47199–47208

Wood-Kaczmar A, Gandhi S, Yao Z, Abramov AY, Miljan EA, Keen G, Stanyer L, Hargreaves I, Klupsch K, Deas E, Downward J, Mansfield L, Jat P, Taylor J, Heales S, Duchen MR, Latchman D, Tabrizi SJ, Wood NW (2008) PINK1 is necessary for long term survival and mitochondrial function in human dopaminergic neurons. *PLoS One* **3:** e2455

Yavich L, Tanila H, Vepsalainen S, Jakala P (2004) Role of alpha-synuclein in presynaptic dopamine recruitment. *J Neurosci* **24:** 11165–11170

Zhang F, Rowe ES (1994) Calorimetric studies of the interactions of cytochrome c with dioleoylphosphatidylglycerol extruded vesicles: ionic strength effects. *Biochim Biophys Acta* **1193:** 219–225

TITLE: The Mitochondrial Chaperone Protein TRAP1 Mitigates α-Synuclein Toxicity

RUNNING HEAD: TRAP1 mitigates α-Synuclein toxicity

Erin K. Butler[1,2,3,*], Aaron Voigt[1,*], A. Kathrin Lutz[4], Jane P. Toegel[1], Ellen Gerhardt[2], Peter Karsten[1], Björn Falkenburger[1], Andrea Reinartz[5], Konstanze F. Winklhofer[4], Jörg B. Schulz[1,6]

[1]Department of Neurology, University Medical Center, RWTH Aachen, Pauwelsstraße 30, D-52074 Aachen, Germany

[2]Department of Neurodegeneration and Restorative Research, Center Molecular Physiology of the Brain (CMPB), Georg-August University Göttingen, Waldweg 33, D-37073 Göttingen, Germany

[3]Göttingen Graduate School for Neurosciences and Molecular Biology (GGNB)

[4]Adolf Butenandt Institute, Neurobiochemistry, Ludwig Maximilians University, Schillerstr. 44, D-80336 Munich, Germany

[5]Department of Pathology, University Medical Center, RWTH Aachen, Pauwelsstraße 30, D-52074 Aachen, Germany

[6]Jülich-Aachen Research Alliance (JARA) Brain
*EKB and AV join first authorship.

Corresponding Author: Jörg B. Schulz
Department of Neurology
University Hospital

RWTH Aachen

Pauwelsstrasse 30

D-52074 Aachen

Germany

Tel.: +49-241-808-9600

Fax: +49-241-808-2582
E-mail: jschulz@ukaachen.de

ABSTRACT:
Overexpression or mutation of α-Synuclein is associated with protein aggregation and interferes with a number of cellular processes, including mitochondrial integrity and function. We used a whole-genome screen in the fruit fly *Drosophila melanogaster* to search for novel genetic modifiers of human [A53T]α-Synuclein-induced neurotoxicity. Decreased expression of the mitochondrial chaperone protein tumor necrosis factor receptor associated protein-1 (TRAP1) was found to enhance age-dependent loss of fly head dopamine (DA) and DA neuron number resulting from [A53T]α-Synuclein expression. In addition, decreased TRAP1 expression in [A53T]α-Synuclein-expressing flies resulted in enhanced loss of climbing ability and sensitivity to oxidative stress. Overexpression of human TRAP1 was able to rescue these phenotypes. Similarly, human TRAP1 overexpression in rat primary cortical neurons rescued [A53T]α-Synuclein-induced sensitivity to rotenone treatment. In human (non)neuronal cell lines, small interfering RNA directed against TRAP1 enhanced [A53T]α-Synuclein-induced sensitivity to oxidative stress treatment. [A53T]α-Synuclein directly interfered with mitochondrial function, as its expression reduced Complex I activity in HEK293 cells. These effects were blocked by TRAP1 overexpression. Moreover, TRAP1 was able to prevent alteration in mitochondrial morphology caused by [A53T]α-Synuclein overexpression in human SH-SY5Y cells. These results indicate that [A53T]α-Synuclein toxicity is intimately connected to mitochondrial dysfunction and that toxicity reduction in fly and rat primary neurons and human cell lines can be achieved using overexpression of the mitochondrial chaperone TRAP1. Interestingly, TRAP1 has previously been shown to be phosphorylated by the serine/threonine kinase PINK1, thus providing a potential link of PINK1 via TRAP1 to α-Synuclein.

AUTHOR SUMMARY:
Parkinson's disease (PD) is a progressive neurodegenerative disorder, pathologically characterized by loss of dopaminergic neurons in the substantia nigra pars compacta brain region. Mutations in α-Synuclein or gene duplication or triplication result in autosomal-dominant inherited PD. Indeed, aggregated and insoluble α-Synuclein is found in Lewy bodies, a pathological hallmark common to both sporadic and hereditary forms of PD. In order to better define α-Synuclein's pathogenic mechanism, we first used a fly genetic screen to search for novel genetic modifiers of mutant human [A53T]α-Synuclein neurotoxicity. We identified the mitochondrial chaperone protein TRAP1 as a novel modifier of the toxicity induced by [A53T]α-Synuclein. [A53T]α-Synuclein-induced toxicity was enhanced when TRAP1 expression was decreased, while overexpression of human TRAP1 (hTRAP1) provided a rescue.
Cell culture experiments further demonstrated that [A53T]α-Synuclein directly interferes with a number of mitochondrial functions, including Complex I ATP production, mitochondrial fragmentation and sensitivity to oxidative stress. These effects could be blocked by TRAP1 overexpression. As mitochondrial dysfunction has previously been linked to mutations in several other genes associated with genetic PD, these data provide further evidence of a common mitochondrial-centric mechanism of PD pathogenesis.

INTRODUCTION:

Parkinson's disease (PD) is the second most prevalent neurodegenerative disease behind Alzheimer's disease (AD), with an incidence rate of approximately 110 - 300 per 100,000 persons above the age of 50 [1]. The movement disorder is characterized by the selective death of dopaminergic neurons in the substantia nigra pars compacta (SNc) [2]. Death of SNc neurons results in a reduction of dopamine (DA) levels within their key efferent target, the striatum [3]. Mitochondrial Complex I activity deficit and evidence of enhanced oxidative stress within affected brain regions are also observed in PD [4-6]. Age and pesticide/herbicide exposure are the most important disease risk factors [7-9]. Importantly, there is no clinical therapy available that has been shown to slow or reverse PD.

While the majority of PD is diagnosed as idiopathic, 5 - 10 % of cases are attributable to familial forms of PD [10]. Although genetic PD represents only a small percentage of patients, mutations in these genes point to underlying biochemical pathways that could also be relevant to sporadic PD patients. Three missense mutations in the small pre-synaptic protein α-Synuclein (SNCA/PARK1/4; GenBank ID 6622) have been shown to result in autosomal-dominant PD. A critical effect of protein dose on pathology is implicated by disease-causing gene duplication and triplication [11-14]. α-Synuclein is also a major protein component of the Lewy Bodies (LB), the key histologic feature of dopaminergic and non-dopaminergic neurons found in PD patients [15]. Thus, α-Synuclein is strongly suggested to be a causal factor in PD pathogenesis.

Human α-Synuclein mutation or overexpression results in cytotoxicity, with [A53T]α-Synuclein being the most toxic variant known. Direct cell loss can be induced in both *in vitro* and *in vivo* models of yeast, *C. elegans*, *Drosophila,* rat, mouse, and non-human primate [16-23]. The formation of α-Synuclein oligomers from their native unfolded state is linked to cell membrane damage and results in dysfunction of multiple cell systems such as the ubiquitin proteasome system, the endoplasmic reticulum and lysosomes [24-31]. Recent data also suggests that α-Synuclein plays a role in modulating both mitochondrial function and damage. α-Synuclein-overexpressing cells exhibit multiple markers of mitochondrial dysfunction, including increased protein oxidation, increased ROS production, loss of mitochondrial membrane potential and reduced Complex I activity [32-38]. Several groups have demonstrated that α-Synuclein's entry in mitochondria is mediated via an N-terminal mitochondrial targeting sequence, with localization at the inner membrane [37,38]. Moreover, PD patient brain histology shows α-Synuclein accumulation within mitochondria of the SNc and striatum, a feature absent in control brains [38]. Mitochondrial dysfunction associated with adenosine triphosphate (ATP) depletion and electron transport chain (ETC) defects reduces the cell's ability to handle oxidative protein damage and cellular tasks, suggesting a possible reason for cell death.

In PD patient brains, early DA reduction indicates the withdrawal of SNc striatal projections, finally resulting in DA neuron loss and PD-related symptoms of rigidity and akinesia. In flies, expression of [A53T]α-Synuclein is accompanied by an age-dependent loss of DA and DA neurons, respectively. Thus, fly head DA levels provide an indirect readout for [A53T]α-Synuclein-induced toxicity. To further investigate the mechanism and identify novel modifiers of α-Synuclein toxicity, we performed a genome-wide genetic screen in *Drosophila*. In this screen, we identified, among other gene products, the mitochondrial chaperone protein TRAP1 (GenBank ID 10131) as a novel modifier of [A53T]α-Synuclein-induced DA loss. TRAP1 has

previously been shown to function downstream of the PD-related serine/threonine kinase PINK1 (GenBank ID 65018). PINK1-induced phosphorylation of TRAP1 seems to be necessary for the protein's protective effects against oxidative stress [39]. In our report we further characterize the functional consequences of TRAP1 reduction or overexpression in *Drosophila*, in primary neurons and dopaminergic cell lines and the effects on mitochondrial morphology and function.

RESULTS:

Expression of Human [A53T]α-Synuclein in Fly Heads and Genetic Screening for Modification of [A53T]α-Synuclein Toxicity

Expression of α-Synuclein in *Drosophila* is established as a useful model of PD [21]. As the fly lacks an α-Synuclein homolog, this model relies on ectopic expression of human α-Synuclein using the *UAS/GAL4* system [40]. We have previously analyzed DA neuron number in aged flies, expressing different mutant variants of α-Synuclein. Compared to controls, wild type α-Synuclein did not cause a decline in DA neuron number. Moreover, locomotion was not impaired in aged wild type α-Synuclein-expressing flies [41]. Based on these results, we chose [A53T]α-Synuclein for our screening. With single copy expression of a *UAS:[A53T]α-Synuclein* transgene (*A53T*) in aminergic neurons (*dopa decarboxylase-GAL4* driver, *ddc-GAL4*) (Figure 1A), no difference to overall fly fitness, as assessed by longevity, was observed (Figure 1B). In contrast, expression of two transgene copies, resulting in higher expression levels (Figure 1A), caused earlier lethality compared to controls (Figure 1B). However, when we measured DA levels of flies expressing one copy of [A53T]α-Synuclein under control of *ddc-GAL4* (*ddc>A53T*), we noticed a significant decrease in DA levels with aging (Figure 1C). Thus, measuring DA levels using high performance liquid chromatography represents a sensitive system to address DA levels in fly heads. After carefully addressing sensitivity, specificity and reproducibility of our readout marker (Figure 1D, Figure S1), we decided to perform a genome-wide screen to identify modifiers of [A53T]α-Synuclein-induced DA loss *in vivo.* Thus, flies with expression of [A53T]α-Synuclein in aminergic neurons were crossbred to fly lines carrying chromosomal deletions (deficiencies), utilizing the “Bloomington Deficiency Kit”. Progeny were screened for changes in DA loss over time (a summary of the screen results is given in Supporting Information). Although detailed single gene analysis is still ongoing, we identified a large number of genes coding for proteins involved in mitochondrial function within the candidate deficiencies. Therefore, we additionally cross-referenced our data with results from a genome-wide RNAi-screen, set to identify modulators of mitochondrial function [42]. Common genes were screened for alteration of [A53T]α-Synuclein-toxicity with respect to viability and DA loss.

TRAP1 Modification of [A53T]α-Synuclein Toxicity in the Fly

Among the deficiencies screened, *Df(2R)nap9* caused the greatest enhancement of [A53T]α-Synuclein-induced DA loss of all non-lethal interacting deficiencies. Of the 153 genes deleted by *Df(2R)nap9*, we found TRAP1 reduction to enhance [A53T]α-Synuclein-induced DA loss. The loss-of-function allele *TRAP1[KG06242]* (hereafter referred to as *TRAP1[KG]*, Figure S2) caused a reduction of fly head DA levels similar to those of *Df(2R)nap9* (data not shown). However, *TRAP1[KG]* did not alter DA levels (Figure 1D). Thus, flies with reduced TRAP1 in combination with the *ddc-GAL4* driver (*TRAP1[KG]/+; ddc/+*) served as controls in later analysis. TRAP1 is a mitochondrial chaperone, recently reported as a downstream phosphorylation target

of the PD protein PINK1 in rat and human cell lines [39]. As both fly and human TRAP1 share high sequence homology, we generated a UAS-transgenic fly to express human TRAP1 (hTRAP1). Interestingly, overexpression of hTRAP1 in fly heads was able to provide a rescue effect against [A53T]α-Synuclein-induced DA loss (Figure 2A). The effects of TRAP1 on DA levels were also reflected by its effect on tyrosine hydroxylase (TH)-positive neurons. *ddc>A53T* expressing flies showed increased loss of TH-positive neurons if TRAP1 levels were reduced (Figure 2B). In contrast, hTRAP1 overexpression was able to restore [A53T]α-Synuclein-induced loss of TH-positive neurons to control levels. Interestingly, *ddc*-driven overexpression of hTRAP1 did not increase longevity of *ddc>A53T* heterozygous flies (not shown). In PD patients, a reduction in brain DA content is later followed by neuronal decline. The same seems to hold true for flies. Although no reduction in longevity of *ddc>A53T/+* flies is observed, these flies display a significant reduction in DA content. A more pronounced dopamine reduction (*ddc>A53T/ddc>A53T*) results in neuronal decline, eventually leading to early death, reflected by a significantly shortened lifespan (Figure 1B). This might explain why TRAP1 will still provide 100% protection against loss of neurons (Figure 2B), even if DA levels have already started to decline (Figure 2A).

PD is clinically defined as a movement disorder. Thus, key to an animal disease model recapitulating this phenotype is loss of locomotor ability. Locomotion in flies is measurable using the negative geotaxis assay. In agreement with previous reports, *ddc>A53T* flies showed an age-related deficit in climbing ability [21,43]. Notably, *ddc*-driven hTRAP1 expression was able to significantly rescue the locomotion deficit in *ddc>A53T* flies (Figure 2C). Therefore, taken together, these data indicate that the rescue of head DA content is sufficient to restore motor ability.
Our data suggest that TRAP1 protects from toxic effects induced by [A53T]α-Synuclein. However, TRAP1 might also provide protection to any toxic insult. To address this possibility, we examined if TRAP1 provides protection against toxicity induced by the expression of other well-known toxic proteins/peptides.

Eye-specific expression (GMR-GAL4) of either human Tau or SCA3-derived polyglutamine stretches (PolyQ) in the fly eye result in a rough eye phenotype (REP). These REPs are sensitive to genetic modifiers and have successfully been used for screening [44,45]. Interestingly, overexpression of TRAP1 did not show a rescue of the PolyQ-induced REP. Moreover, silencing of TRAP1 by RNAi did not enhance the REP (Figure 2D). Similar results were obtained with Tau-expressing flies (not shown). A general protective role of TRAP1 in any toxic trigger is therefore unlikely but appears to be specific for α-Synuclein toxicity.

Modification of [A53T]α-Synuclein Toxicity by TRAP1 in Rat Primary Cortical Neuron Culture

In flies, overexpression of hTRAP1 was able to reduce [A53T]α-Synuclein-induced loss of DA in fly heads and loss of DA neurons, respectively. Thus, to additionally confirm that overexpression of hTRAP1 is able to rescue [A53T]α-Synuclein-induced sensitivity in vertebrate neurons, we used terminally-differentiated rat primary neuron cultures. Lentiviral infection specificity and efficacy in these cells was first verified (Figure 3A, B). As the neurons did not display robust toxicity upon [A53T]α-Synuclein expression alone, cells were exposed to low doses of the mitochondrial Complex I inhibitor rotenone. Compared to GFP-virus infected cells (control), co-expression of [A53T]α-Synuclein significantly enhanced cell loss (Figure 3C). In agreement with fly

data, coincident overexpression of TRAP1 restored survival to control values. Interestingly, expression of TRAP1 alone enhanced survival beyond that of control cells, indicative of a protective effect of TRAP1 on neurons independent of effects on [A53T]α-Synuclein-induced toxicity.

Modification of [A53T]α-Synuclein Toxicity by TRAP1 in Human HEK293 Cell Culture

To study the functional role of TRAP1, we used both TRAP1 overexpression and specific knockdown by small interfering RNA (siRNA) in HEK293 cells. Two different siRNAs directed against TRAP1 were first compared for efficacy. Both were able to reduce endogenous TRAP1 expression in HEK293 cells (Figure S3). The most efficient siRNA was used for all further investigations.

To confirm whether treatment of HEK293 cells mimicked the *in vivo* fly and *in vitro* rat neuron data concerning TRAP1 and stress sensitivity, HEK293 cells were treated overnight with a low dose of either hydrogen peroxide (Figure 4A) or the Complex I inhibitor rotenone (Figure 4B). [A53T]α-Synuclein expression enhanced cell sensitivity to both stressors. Reduction in TRAP1 expression further reduced survival in the presence of [A53T]α-Synuclein. For both, rotenone and hydrogen peroxide treatment, overexpression of TRAP1 in the context of [A53T]α-Synuclein expression attenuated the decrease in cell survival. The magnitude of the rescue effect was greatest when cells were exposed to rotenone (Figure 4A, B). In cells without [A53T]α-Synuclein expression, reduction of TRAP1 also caused stress sensitization. These data corroborate the reported function of TRAP1 as a protective mitochondrial chaperone [46-48].

Previous reports have indicated that [A53T]α-Synuclein may interfere with mitochondrial respiration, in particular with Complex I function [34]. Given the noted rescue effect of TRAP1 on rotenone-treated cells with or without [A53T]α-Synuclein expression, we hypothesized that the TRAP1 effect on [A53T]α-Synuclein may in part be related to altered ETC function. Thus, ATP production via Complex I was assayed in cells without oxidative stress, to evaluate the general effects of [A53T]α-Synuclein on ETC in combination with altered TRAP1 levels. Expression of [A53T]α-Synuclein reduced Complex I activity in HEK293 cells (Figure 4C). TRAP1-silencing enhanced this reduction, while TRAP1 overexpression rescued the [A53T]α-Synuclein-induced defect. In light of the defects observed in [A53T]α-Synuclein-induced Complex I ATP production (Figure 4C), total ATP levels in the cell were also investigated. Only cells expressing [A53T]α-Synuclein in combination with siTRAP1 showed a reduction of total ATP levels (Figure 4D). Although [A53T]α-Synuclein alone significantly reduced Complex I activity, overall ATP levels were unchanged.

Loss of mitochondrial membrane potential predisposes cells to apoptosis. [A53T]α-Synuclein has been suggested to adopt an alpha-helical conformation that could perforate membranes. At the same time, TRAP1 protection against apoptosis has been suggested to act via inhibition of opening mitochondrial permeability transition pore (PTP) [49]. The mitochondrial membrane potential is thought to indirectly reflect the state of the PTP. Cells were thus assessed for mitochondrial membrane potential using the mitochondrial membrane dye, JC-1. Only cells expressing [A53T]α-Synuclein in combination with siTRAP1 showed a loss of mitochondrial membrane potential (Figure 4E).

Finally, to exclude the possibility that altered Complex I ATP production might be due to varying quantites of mitochondria within the cells, instead of a functional deficit in the ETC, cell samples were probed for two mitochondrial proteins, VDAC1 and COX4. No major differences were observed for expression of VDAC1 and COX4

(Figure S4A). This suggests the detected decrease in Complex I ATP production resulted from a functional ETC deficit. JC-1 is an excellent dye to measure mitochondrial membrane potential and because of the color switch following depolarization, it makes it easy to normalize to cell density. However, JC-1 has been superseded by other dyes, like TMRM, with respect to the potential artifact of local concentration changes. With regard to this potential problem, we repeated mitochondrial membrane potential measurements using TMRM. In addition, we wanted to exclude potential off-target effects by siRNA treatment. Therefore, we generated HEK293 cells with stable expression of shTRAP1 constructs resulting in a roughly 90 % loss of TRAP1 protein levels (Figure S5A). In stable TRAP1-silenced cells, a significant reduction in membrane potential was observed after [A53T]α-Synuclein expression. This effect was absent in cells expressing scrambled shRNA, again indicating that TRAP1-silencing in combination with [A53T]α-Synuclein expression causes opening of mitochondrial PTP (Figure S5B).

Effect of TRAP1 Mutation on [A53T]α-Synuclein-Induced Toxicity

The human TRAP1 ATPase domain shares high homology with both other HSP90 proteins and TRAP1 orthologs found in other species (Figure S6). Recently, the ATPase domain of yeast HSP90 has been shown to be required for its HSP90 function. The mutation of a specific amino acid within the ATPase domain was sufficient to inhibit ATP binding [50]. This amino acid is highly conserved in both HSP90 and TRAP1 proteins (Figure S6). We therefore exchanged the aspartic acid at position 158 for asparagine (TRAP1[D158N]), creating a putative non-functional ATPase domain. Introducing the D158N mutation did not interfere with TRAP1 protein turnover, as expression in HEK293 cells resulted in similar abundance of TRAP1[D158N] and TRAP1[WT] proteins (Figure 5A).

Next, we asked if TRAP1[D158N] is as effective as TRAP1[WT] in protecting [A53T]α-Synuclein-expressing cells from oxidative stress. Cells overexpressing [A53T]α-Synuclein treated overnight with rotenone displayed a robust reduction in cell survival, which was rescued by TRAP1[WT] overexpression (Figure 4B). In contrast, overexpression of TRAP1[D158N] was less effective (Figure 5B). Similar results were observed when we tested ATP production by Complex I. In the context of [A53T]α-Synuclein expression without oxidative stress, TRAP1[WT] rescued [A53T]α-Synuclein-induced decrease in Complex I ATP production (Figure 5C), while TRAP1[D158N] showed significantly lower degree of rescue ability. Finally, cell lysates were again analyzed for abundance of the mitochondrial proteins VDAC1 and COX4. No changes in VDAC1 or COX4 protein levels were observed in cell lysates expressing either TRAP1[WT] or mutant TRAP1[D158N] (Figure S4B). These data thus indicate that mutant TRAP1 expression does not alter the overall mitochondrial content, arguing in favor of a functional ETC Complex deficit, rather than a deficit due to diminished numbers of mitochondrial/ETC components in the cell.

Recent data show that α-Synuclein impairs mitochondrial fusion, leading to fragmented mitochondria. Interestingly, the α-Synuclein-induced mitochondrial fragmentation can be attenuated by co-expression of PINK1, Parkin and DJ-1, but not by PD-linked mutant variants of these proteins [51]. Therefore, we sought to determine if TRAP1 is also able of attenuating α-Synuclein-induced mitochondrial fragmentation in SH-SY5Y cells. The [A53T]α-Synuclein-induced punctate mitochondrial staining was reversed to a tubular mitochondrial network by TRAP1[WT] co-expression. In contrast, co-expression of TRAP1[D158N] showed no effect (Figure 6A, B). The expression of both TRAP1 variants alone had no impact

on mitochondrial integrity. Verification of protein expression levels revealed robust α-Synuclein and TRAP1 expression after transfection with respective plasmids (Figure 6C). Thus, the impaired rescue ability of TRAP1[D158N] in comparison to TRAP1[WT] cannot be explained by the lower abundance of TRAP1[D158N] protein. It is rather the consequence of an altered function of the inherent ATPase function of TRAP1[D158N]. In addition, we asked if reduced TRAP1 levels might enhance mitochondrial fragmentation induced by [A53T]α-Synuclein expression. We noticed that TRAP1-silencing increased the number of cells with fragmented mitochondria. Combining TRAP1-silencing with [A53T]α-Synuclein expression enhanced fragmentation of mitochondria even further (Figure 7A, B). Effective TRAP1-silencing and [A53T]α-Synuclein expression was confirmed by Western blot analysis (Figure 7C).

Localization of [A53T]α-Synuclein to Mitochondria and Protein-Protein Interaction with TRAP1 in HEK293 Cell Culture

TRAP1 is defined as a mitochondrial molecular chaperone and has been shown to be protective against oxidative stress-induced cell death via multiple postulated mechanisms including cytochrome c release inhibition, interference with caspase-3 activation and attenuation of ROS production [39,46,48,52-54]. We thus hypothesized that TRAP1 might directly antagonize α-Synuclein mitochondrial-related toxicity. Confirming that TRAP1 is indeed found in the mitochondria, co-localization studies in HEK293 cells revealed a strong overlap between TRAP1 staining with “Mitotracker Orange”-labeled mitochondria (Figure S7A). Therefore, it was interesting to see if α-Synuclein might also localize with mitochondria, as previously reported [33,37,38]. To determine this, we performed cell fractionation experiments to separate cytoplasmic and mitochondrial enriched fractions. Using Western blotting, these fractions and input control were compared for the content of endogenous, VDAC1 (mitochondrial outer membrane protein), β-Tubulin (cytosol) and α-Synuclein proteins. Whereas the input showed abundance of all tested proteins, the cytosolic fraction displayed expected cytosolic proteins β-Tubulin and α-Synuclein. In the mitochondria enriched fraction, no contaminating protein from β-Tubulin could be detected. Importantly, exogenous [A53T]α-Synuclein protein was found within the mitochondria enriched fraction (Figure S7B).

Given the strong rescue effect of TRAP1 on toxicity induced by [A53T]α-Synuclein in various systems (flies, primary rat neurons, and human cells), this implies at least a genetic interaction of these proteins. Whether there is a direct interaction of [A53T]α-Synuclein and TRAP1 awaits further analysis.

DISCUSSION:

α-Synuclein plays an important role in PD pathogenesis. However, the mechanisms that actually lead to α-Synuclein-induced neurotoxicity remain unresolved. To gain insights into the disease mechanisms triggered by α-Synuclein, we performed a genome-wide modifier screen on [A53T]α-Synuclein-induced toxicity in flies. We used [A53T]α-Synuclein for our screen because its overexpression in flies results in a robust Parkinsonian phenotype [21,55-57]. Toxicity induced by α-Synuclein or its mutant variants is rather low and eye-specific expression of A53T does not cause rough eye phenotypes (REPs). Such REPs induced by eye-specific expression of toxic proteins provide an excellent tool for screens and have successfully been used in the past to identify genetic interactions applying alterations in eye morphology due to photoreceptor degeneration as an endpoint. Given the low toxicity of [A53T]α-

Synuclein, such screening approaches could not be conducted with regard to α-Synuclein-induced toxicity in flies. Our genetic screen fulfilled two important requirements: it utilized (i) an age-dependent model of [A53T]α-Synuclein toxicity, and (ii) an endpoint that is relevant to PD, this being the loss of dopamine. However, apart of being used as a neurotransmitter, DA in flies is also used for cuticle tanning. Thus, we cannot exclude the possibility that cuticle-derived DA might contribute to the overall DA in fly heads. Therefore, the measured decline is not only connected to DA loss in neurons. Nevertheless, secondary readouts like locomotion measurements or DA neuron counts indicate a strong correlation between decreased head DA content and proper function of DA neurons.

One of the candidates identified in our screen was the mitochondrial chaperone TRAP1. Consistent with our results, a genetic screen for alteration of α-Synuclein aggregation, conducted in *C. elegans*, identified *R151.7, a* homologue to *Drosophila* and human *TRAP1,* as a candidate worm gene. Knockdown of *R151.7* resulted in premature α-Synuclein aggregation [58]. Although aggregation was not assayed in our screen, this finding acts as an external confirmation that TRAP1 genetically interacts with α-Synuclein in different *in vivo* systems.
In multiple cell culture systems, TRAP1 has been shown to provide anti-apoptotic functions [48,52,53] as high levels of TRAP1 reduce the release of key factors involved in apoptosis, including Apoptosis Inducing Factor-1 and Cytochrome c, and additionally prevents Caspase-3 cleavage [39,46,48,59]. The direct mechanisms by which TRAP1 might inhibit apoptosis were not examined in this study. However, given that overexpression of TRAP1 in both rat primary neurons and HEK293 cells was able to enhance cell survival after rotenone treatment, we hypothesize that anti-apoptotic mechanisms might in part be responsible for rescue of [A53T]α-Synuclein toxicity by TRAP1. This is in agreement with the observation that PD-associated neuronal death involves apoptotic cell death [60-63]. In addition, the effects of TRAP1 modulation on ATP synthesis and activities of the ETC support a mitochondrial function. For more than two decades, biochemical studies, the 1-methyl-4-phenyl-1,2,3,6-tetrahydropyridine (MPTP) and transgenic animal models have implicated mitochondrial dysfunction in the pathogenesis of PD [5,64-71]. Genetic data, including mutations in PINK-1, Parkin, DJ-1, and HtrA2, have now specifically linked PD to both dysfunction and morphological change of the mitochondria [72-80]. However, the relationship of α-Synuclein pathology and mitochondrial dysfunction has been less clear. Our data are compatible with a localization of [A53T]α-Synuclein either in mitochondria or in mitochondrial membranes. Recent findings, though, have indicated that α-Synuclein may be localized to the outer mitochondrial membrane in pathological conditions and induce morphological changes of mitochondria by inhibiting mitochondrial fusion and enhancing mitochondrial fragmentation [51]. These morphological changes were rescued by overexpression of wild type PINK1, Parkin, and DJ-1 [51]. We show here that TRAP1 overexpression is also able to reverse [A53T]α-Synuclein-induced mitochondrial fragmentation.
Interestingly, TRAP1 has been identified as a substrate of the serine/threonine kinase PINK1. Phosphorylation of TRAP1 by PINK1 seems to be required for the protective effects mediated by PINK1. Combining these data with our findings leads to a potential pathogenic model, in which [A53T]α-Synuclein induces mitochondrial stress impairing, most likely, Complex I of the ECT by an as yet unidentified mechanism. Overexpression of TRAP1 counteracts this effect in flies, primary

neurons and human neuronal as well as non-neuronal cells. TRAP1[D158N] is less effective in protecting from [A53T]α-Synuclein-induced detrimental effects. The finding suggests that a functional ATPase domain is required for TRAP1 function.

METHODS:

Fly Stocks

Flies were raised and maintained on standard cornmeal-yeast-molasses-agar food at 25°C unless otherwise noted. Non-RNAi stocks were obtained from the Bloomington *Drosophila* Stock Centre, UAS-RNAi stocks either from the Vienna *Drosophila* RNAi Center (VDRC) or from National Institute of Genetics (NIG-fly, Japan). Bloomington lines used were: Wild type flies (*Oregon R*; referred to as + in text), w^{1118}*;; P{Ddc-GAL4.L}4.36* (BL7009; ddc: dopa decarboxylase, aminergic neuron specific driver, referred to in text as *ddc-GAL4*), w^{*}*; P{UAS-lacZ.B}Bg4-2-4b* (BL1777; referred to in text as UAS-LacZ), $y^{1}w^{67c23}$*; P{SUPor-P}Trap1*^{KG06242} (BL14032; referred to in text as TRAP1[KG]), *w[*]; P{w[+mC]=longGMR-GAL4}* (BL8605; referred to as GMR-GAL4 in text), *w[1118]; P{w[+mC]=UAS-HsapHSPA1L.W}53.1* (BL7455; expresses HSPA1L, the human homolog of HSP70 under GAL4 control; referred to as HSP70 in text), *w[1118]; P{w[+mC]=UAS-mitoGFP.AP}* (BL8443; expresses GFP with a mitochondrial import signal; referred to as mito-GFP in text) and *w[*]; P{w[+mC]=UAS-Hsap\MJD.tr-Q78}c211.2* (BL8150; expresses a HA-tagged C-terminal fragment of the human Machado-Joseph Disease/Spinocerebellar Ataxia 3 protein with a 78 repeat polyglutamine tract; referred to in text as PolyQ). For stable eye-specific expression of PolyQ, GMR-GAL4 driver was recombined with PolyQ transgene (GMR>PolyQ in text). Fly lines suitable for GFP (*yw;; UAS-GFP*) or human [A53T]α-Synuclein (*yw;; UAS-[A53T]α-Synuclein* [41]) expression (referred to in text as GFP or A53T, respectively). Stable expression under control of the ddc driver (*w[*];; ddc-GAL4>UAS-GFP*; *w[*];; ddc-GAL4>UAS-GFP*) were generated by recombination (flies referred to in text as *ddc>GFP* or *ddc>A53T*).

Transgenic flies expressing human TRAP1 (hTRAP1) were generated by BestGene Inc. In brief, human TRAP1 cDNA was sub-cloned from pcDNA3.1+ vector into pUASattB using *KpnI* and *XbaI* restriction sites. hTRAP1 expression in these transgenic flies (*w;; UAS-hTRAP1/TM3, Sb*; referred to in text as hTRAP1) was verified by Western blotting.

Genetic Deficiency Screen Breeding

The Bloomington Deficiency Kit was utilized for screening purposes (http://flystocks.bio.indiana.edu/Browse/df/dfkit_retired_July2009.htm). In general, a specific deficiency line was crossbred with *ddc>A53T* flies. Male offspring (*ddc>A53T* flies in combination with the respective deficiency) was selected and aged. At ages 1 and 4 weeks, a minimum of 9 flies was collected for later measurement of head DA using HPLC.

Measurement of Fly Head Dopamine (DA) using HPLC

Liquid nitrogen flash frozen fly heads were homogenized (Precellys 24 homogenizer) in homogenization buffer (0.1 M perchloric acid/ 3 % trichloric acid solution). 50 µl of supernatant from each sample were used for HPLC analysis (Dionex Ultimate 3000; running buffer: 57 mM citric acid, 43 mM sodium acetate, 0.1 mM EDTA, 1 mM octane sulfonic acid, 20 % methanol). Samples were separated on a chromatographic column (Dionex Acclaim C18, 5 µm, 2.1x 150 mm column, at 25°C), and DA was electrochemically detected on a graphite electrode (Dionex ED50 Electrochemical detector with following conditions: disposable carbon electrode at 0.8 V, flow rate 0.2 ml/min). DA (Sigma-Aldrich) standards of 0.1 µM, 0.25 µM and

0.4 µM were used for creation of a standard curve. Chromeleon 6.6 software was used for HPLC data analysis.

Fly Longevity and Oxidative Stress Assays

Longevity assays were performed as previously described [81]. For oxidative stress assays a minimum of 20 male flies (2-3 days of age) was kept on filter papers soaked with paraquat (20 mM paraquat dichloride in 5 % sucrose). Survival of flies was scored on a daily base. Fresh paraquat/sucrose solution was supplied daily.

Negative Geotaxis Assay

Fly climbing was assessed in accordance with previously published protocols [21,43,82]. Flies were aged on normal yeast medium. At ages 1 and 4 weeks, climbing was assessed (20 flies per genotype). Flies were individually placed in a graduated cylinder, and allowed to climb for 15 s. Maximum height attained was recorded, and analysis was repeated 3 times per time point, with 3 trials at one minute intervals recorded at each time point.

Immunohistochemistry

Fly brains were dissected in cold PBS, washed in a PBS/ 0.1 % Triton X (PBT), fixed in 4 % PFA (30 min, 4°C), and blocked in PBT containing 5 % normal goat serum (overnight, 4°C). For TH staining, brains were incubated with primary anti-TH antibody (1:100; rabbit polyclonal, AB152, Chemicon International/ Millipore) for 2 days, 4°C, and subsequently with fluorescent secondary anti-rabbit antibody (1:200; AlexaFluor-555 or Cy3; Invitrogen/Jackson Immunological Research) for 3.5 hours. Afterwards, brains were mounted in Vectashield (Vector Labs). The number of TH-positive neurons was determined on Z-stacked confocal sections (1 µm, Leica DM IRE2, Laser) [83]. At least 15 brains were analyzed per genotype.

Protein Collection and Western Blotting

Fly heads were homogenized in RIPA buffer (50 mM Tris, pH 8.0, 0.15 M NaCl, 0.1 % SDS, 1.0 % NP-40, 0.5 % Na-Deoxycholate, 2 mM EDTA, Complete™ Protease Inhibitors (Roche Applied Sciences), pH 7.4), centrifuged, and the supernatant was collected.

Cell culture protein samples were collected after washing cells in ice cold PBS, followed by lysis in RIPA buffer for 30 min on ice. Cell debris was removed by centrifugation, and supernatants were collected.

For Western blot analysis, protein samples were separated via SDS-PAGE gel and then transferred onto nitrocellulose membrane. Blocking in skim milk was followed by overnight primary antibody incubation. The primary antibodies used were as follows: mouse anti-α-Synuclein (1:1000; Cell Signaling); mouse anti-*Drosophila* Syntaxin (1:2000 Developmental Studies Hybridoma Bank (DSHB)), mouse anti-β-Tubulin (1:500, DSHB); mouse anti-δ Tubulin (1:10,000; Sigma-Aldrich); mouse anti-TRAP1 (1:1000; BD Biosystems); mouse anti-phospho-tyrosine (PY99) (1:200; Santa Cruz Biotechnology); mouse anti-phospho-threonine (H2) (1:200: Santa Cruz Biotechnology); mouse anti-phospho-serine (16B4) (1:200; Santa Cruz Biotechnology); mouse anti-Cytochrome c (1:500; Santa Cruz Biotechnology); rabbit anti-VDAC1 (0.3 µg/ml; Abcam); mouse anti-COX IV (2 µg/ml; Abcam); rabbit anti-GFP polyclonal (1:1000; Santa Cruz Biotechnology).

Appropriate secondary anti-mouse or rabbit horseradish peroxidase-linked antibodies (1:10,000) were obtained from GE Healthcare. Membranes were incubated with the secondary antibody for one hour, followed by signal detection using the Chemiglow substrate (Biozym).

Total RNA isolation, cDNA preparation and Real Time PCR

Method for fly head RNA isolation was adapted from the following link: http://www.ou.edu/journals/dis/DIS84/Tec2%20Bertucci/Bertucci.htm. 20 fly heads per tube were used for RNA isolation. RNA samples were treated with DNase following manufacturer's instructions (Promega RQ1 RNase-Free DNase kit). Total RNA from cultured cells was prepared from cells using Qiagen RNeasy Mini kit (Qiagen). RNA was used for cDNA production via reverse transcription using the iScript cDNA Synthesis Kit (BioRad). Real-time PCR measurements were performed using the SYBR Green (Thermo Fisher Scientific) reagent following manufacturer's instructions for preparation of PCR samples. Gene of interest signal was compared to that of control gene expression (β-Actin5c for fly samples and 18S for human samples) using the $2^{-\Delta\Delta Ct}$ method [84]. No-RT controls were performed to exclude for genomic DNA sample contamination. PCR reactions were followed by generation of a dissociation curve to check for side product generation.
Amplification conditions for fly samples were as follows: 5 min at 95°C, 40 cycles of: 30 s at 95°C, 30 s at 58°C, 60 s at 72°C, followed by 10 min at 72°C. Gene of interest was normalized to control β-Actin5c signal.
The primers used were as follows:
Fly β-Actin5c: for: 5′-ccagtcattcctttcaaacc-3′,
rev: 5′-gcaacttcttcgtcacacatt-3′
Fly TRAP1: for: 5′-aggcagagtcaccgatcc-3′,
rev: 5′-tgatgcctgcttggtctc-3′
Amplification conditions for cell culture samples were as follows: 5 min at 95°C, 40 cycles of: 30 s at 94°C, 30 s at 60°C, 60 s at 72°C, followed by 10 min at 72°C. Gene of interest was normalized to control 18S signal.
Primers were as follows:
Human 18S: Quantitect primers (Qiagen, Germany).
Human TRAP1: for: 5'-cagaccaatgccgagaaag-3'
rev: 5'-caccagctcttcctgtgtca-3'

Cell culture

Cloning and *in vitro* mutagenesis

Full length human α-Synuclein cDNA (423 bp), carrying the [A53T] mutation (cDNA a gift from Dr. Felipe Opazo, European Neuroscience Institute, Göttingen, Germany) was subcloned into the pcDNA3.1+ expression vector (Invitrogen) using *HindIII* and *EcoRV* restriction sites. Full length human TRAP1 cDNA (2115 bp) was amplified from human HEK293 cell cDNA samples. *BglII* and *XhoI* restriction sites were introduced using following primers:

for: 5'-gaagatctatggcgcgcgagctgcgggcgctgctgc-3',
rev: 5'- ccgctcgagtcagtgtcgctccagggccttgaca-3'.

TRAP1 cDNA was then cloned into the pcDNA3.1+ vector using the *BglII*, *XhoI* sites.
In vitro mutagenesis of human TRAP1 in pcDNA3.1+ was carried out using the QuickChange Site-Directed Mutagenesis kit (Stratagene) following manufacturer's instructions. Sites for mutagenesis were based on conserved sites found in the ATPase domain (see Figure S6 for sequence homology). PCR cycling parameters were used as suggested by Stratagene, with a specific extension time of 8 min and 16 cycles for all reactions. Primers used for generating the mutants were as follows:
TRAP1[D158N]: for: 5´- ggcaccatcaccatccagaatactggtatcggg-3`
rev: 5´- cccgataccagtattctggatggtgatggtgcc-3`

Lentivirus preparation

Full length human TRAP1 or [A53T]α-Synuclein cDNA was subcloned into a third generation lentiviral vector pRRLsin.cPPT.PGK/GFP.WPRE (Tronolab), excluding the GFP cassette. The GFP-expressing virus served as a control [85].

Cells, plasmid transfection and viral infection

Human HEK293 cells were grown in Dulbecco's modified Eagle's medium (DMEM), supplemented with 10 % fetal calf serum, 100 units/ml penicillin, and 100 mg/ml streptomycin. Transfection of plasmids and small interfering RNA (siRNA) into HEK293 cells was completed using Metafectene (Biontex) following manufacturer's instructions. siRNAs used for gene knockdown experiments were obtained from Qiagen: MAPK1 control siRNA (Qiagen 1027277); 2 different TRAP1 siRNAs (Flexitube siRNA SI03066364 and siRNA SI00115150); a scrambled siRNA for control (Allstars Negative Control, 1027280). Final concentration of siRNA used was 10 nM. Cells were seeded on poly-L lysine (PLL) coated plates (35,000 cells/cm^2) and then transfected 48 hours before experimentation.

Primary cortical rat neurons were prepared from E18 rat embryos, following previously published procedures [65]. Neurons were seeded on poly-ornithin-coated 24-well plates at a density of 125,000 cells/cm^2. Cells were maintained in Neurobasal medium (Gibco/Invitrogen), supplemented with 5 µg/ml transferrin, 1 % PSN, 0.5 mM L-Glutamine, 2 % B27 supplement. Primary neurons were infected equimolarly with lentiviruses one day after isolation and then cultured for 6 days before experimental use.

SH-SY5Y cells (DSMZ number ACC 209) were cultured in DMEM F-12 with glutamine (Lonza) supplemented with 15 % (v/v) fetal calf serum, non-essential amino acids (Invitrogen) and penicillin/streptomycin. Transfections were performed using Lipofectamine Plus (Invitrogen) according to the manufacturer's instructions. The following plasmids were described earlier: [A53T]α-Synuclein and mito-DsRed [51]. For downregulation of TRAP1, SH-SY5Y cells were reversely transfected with the indicated siRNA and co-transfected with mito-DsRed and empty vector or [A53T]α-Synuclein using Lipofectamin RNAiMax (Invitrogen) according to the manufacturers instruction. 24 hours after transfection, fresh medium was added. Cells were analyzed 48 h after transfection.

Fluorescent staining of mitochondria

SH-SY5Y cells were plated on 15 mm glass coverslips and co-transfected with mito-DsRed and the indicated DNA constructs. At 24 h after transfection, cells were washed twice with ice-cold PBS, fixed with 3.7 % paraformaldehyde for 10 minutes at room temperature and washed twice with PBS before mounting the coverslips. Transfected cells were identified by co-expression of mito-DsRed. Cells were categorized in two classes according to their mitochondrial morphology [75]. Cells displaying an intact network of tubular mitochondria were classified as tubular. When this network was disrupted and mitochondria appeared predominantly spherical or rod-like, they were classified as fragmented. The mitochondrial morphology of at least 300 cells per coverslip was determined in a blinded manner using a Leica DMRB microscope. Quantifications were based on triplicates of at least three independent experiments. Confocal images of representative cells were obtained using a Zeiss LSM 510 microscope. α-Synuclein was detected using a monoclonal anti-rat antibody described previously [51]. β-Actin was detected using a monoclonal antibody from Sigma.

Cell Culture Oxidative Stress Testing and Measurement of Cell Viability

Cells were incubated for 16 hours in the presence of either hydrogen peroxide (100 μM) or rotenone in DMSO (HEK293: 200 μM, rat cortical: 1 μM rotenone). Rotenone control cells were treated with equivalent amount of DMSO alone. After overnight oxidative stress treatment, cells were fixed in 4 % PFA for 10 min, before permeabilization in PBT for 10 min. Cells were incubated with Hoechst nuclear stain for 30 min before imaging on a fluorescent microscope (Leica DMI6000B). Using a macro within the Leica Qwin V3 quantification software, cell number remaining in each well was assessed by counting total fluorescent nuclei (6 images per well at 10X, with minimum 6 wells per genotype in a 24-well culture dish).

ATP Synthesis Assay

Method was adapted from [86]. Cells were trypsinized and washed three times in cold PBS. Cells were then resuspended in incubation medium ($2x10^5$ cells/ml, 25 mM Tris, 125 mM KCl, 2 mM K+EDTA, 10 mM KH_2PO_4, pH 7.4) and permeabilized with digitonin (40 μg/ml). To measure ATP produced via complexes I, III, IV, $2x10^4$ cells (minimum of 8 replicates per experiment) were resuspended in a complex incubation medium supplemented with 1 mg/ml BSA, 2 mM ADP, 10 mM glutamate, 2 mM malate. After incubation for 20 min at 37°C, the reaction was stopped by addition of 6 % perchloric acid, and samples were neutralized with 3 M K_2CO_3. ATP in each sample was measured in a plate reader using the CellTiter-Glo Luminescent reagent (Promega) following manufacturer-provided instructions. Total ATP levels were obtained using an ATP standard curve (ATP from Sigma), with final calculation expressing ATP as pmoles ATP per minute per 1 million cells, and plotted as percentage of control values.

Measurement of Steady State Cellular ATP

$2x10^4$ HEK293 cells/well were seeded (12 replicates per experiment) in an opaque white 96-well plate. Total ATP levels were measured as stated above.

Assessment of Mitochondrial Membrane Potential

Following manufacturer-provided instructions, cells (6 replicates per experiment) in a 96-well plate (black sided, clear bottom) were incubated with the mitochondrial probe JC-1 (3 μg/ml; Invitrogen) in full medium for 30 min at 37°C. After washing in PBS, JC-1 mitochondrial aggregates were measured in a plate reader (excitation: 530 nm, emission: 590 nm). As a control, JC-1 fluorescence was measured in the presence of the mitochondrial membrane potential inhibitor CCCP (Carbonyl cyanide *m*-chlorophenylhydrazone, 50 μM). Protein content per well was quantified using the Bradford assay. Fluorescence in relation to total protein was displayed as percentage of control values.

Immunocytochemistry

Cells were plated on PLL-coated glass slips. 48 hours after transfection, cells were fixed in 4 % PFA for 10 min, permeabilized in PBT for 10 min, followed by blocking in 1 % BSA and overnight incubation with the primary antibody at 4°C. Antibodies used: monoclonal rat anti-α-Synuclein (1:500, Alexis Biochemicals/Enzo Life Sciences); monoclonal mouse anti-NeuN (1:500, Chemicon); monoclonal mouse anti-TRAP1 (1:300, Alexis Biochemicals). For visualization of mitochondria cells pretreated for 4 hours with 1 μM rotenone, the cells were incubated with Mitotracker Orange CMTMRos (300 nM, following manufacturer's instructions, Invitrogen) for 30 min at 37°C prior to fixation. Cells were incubated with respective secondary antibodies for one hour (all secondary antibodies 1:1000, anti-mouse or rat AlexaFluor-488, 543, 633, Invitrogen), and mounted using Mowiol (Calbiochem), with or without the anti-bleaching agent DABCO or nuclear stain Hoechst (Sigma-Aldrich).

Immunoprecipitation (IP)

Protein was collected from HEK293 cells over-expressing α-Synuclein alone or both α-Synuclein and TRAP1, using the above described method for protein isolation and quantification from cell culture, with or without a 4 hour pre-treatment with 1 μM rotenone. IP procedure followed the general procedure supplied with the Protein A Agarose beads (Roche). To reduce background due to unspecific binding, protein samples were first pre-incubated with Protein A Agarose beads for 4 hours at 4°C. After removal of agarose beads by centrifugation, protein samples were incubated overnight at 4°C with either mouse anti-α-Synuclein monoclonal (Cell Signaling) or mouse anti-TRAP1 monoclonal (BD Biosystems) antibody. Incubation of samples with rabbit anti-GFP polyclonal served as a negative control. Protein A agarose beads were then added to the samples and incubated for 2 hours at 4°C. Agarose-antibody-antigen complexes were collected by centrifugation and washed three times in ice-cold RIPA buffer before running the samples on polyacrylamide gels and proceeding with Western botting.

Mitochondrial isolation

Mitochondria were isolated from HEK293 cells transfected with [A53T]α-Synuclein using the following protocol: Cells were suspended in MB buffer (70 mM sucrose, 10 mM HEPES, 1 mM EDTA, 210 nM Mannitol (pH 7.5) and protease inhibitors), homogenized with an injection needle (27G ¾“ 19mm, 5-6 strokes) and centrifuged at 750 xg for 7 min. After centrifugation the pellet was resuspended in MB buffer, homogenized using the same injection needle and centrifuged. This procedure was repeated four times. The resulting supernatants were pooled and centrifuged at 10000 xg for 30 min. This mitochondria-containing pellet was resuspended in MB buffer and further centrifugated at 1500 xg for 20 min. The purity of the resulting mitochondrial pellet was examined by Western blotting using specific antibodies directed against β-Tubulin, VDAC and α-Synuclein.

Statistics

Data was analyzed using GraphPad Prism 4.0 (GraphPad Software Inc.), using 1-way ANOVA followed by Newman-Keuls post testing. Use of a 2-way ANOVA was noted in the text. Survival data were analyzed with the Kaplan-Meier analysis method and the Log Rank Test for curve statistical comparison analysis. Statistical significance referred to as: *$p<0.05$; **$p<0.01$; ***$p<0.001$. All data is presented as mean ± SEM.

ACKNOWLEDGEMENTS: The authors would like to thank: Christiane Fahlbusch (Dept. of Neurodegeneration and Restorative Research, Georg-August University Göttingen, Germany) for excellent technical assistance and the laboratory of Dr. Sebastian Kügler and technician Ulrike Schoel (Dept. of Neurology, Viral Vector Laboratory, Georg-August University Göttingen, Germany) for preparation of rat cortical neurons used in the study. EKB was supported by a European Union Marie Curie Action doctoral stipend, Neuroscience Early Stage Research Training (NEUREST).

CONTRIBUTIONS:The author(s) have made the following declarations about their contributions: Conceived and designed the experiments: EKB, AV, KFW and JBS. Performed the experiments: EKB, EG, AKL, JPT, AR, BF and PK. Analyzed the data: EKB, AV and JBS. Wrote the manuscript: EKB, AV and JBS.

FINANCIAL DISCLOSURES: The authors have declared that there are no financial disclosures to be made.

COMPETING INTERESTS: The authors have declared that no competing interests exist.

ABBREVIATIONS

Parkinson's disease - PD; tumor necrosis factor receptor associated protein-1 - TRAP1; dopamine - DA; adenosine triphosphate - ATP; electron transport chain - ETC; substantia nigra pars compacta - SNc; human embryonic kidney cells-293 - HEK293; dopa decarboxylase - ddc; small interfering RNA – siRNA.

REFERENCES:

1. Mayeux R (2003) Epidemiology of neurodegeneration. Annu Rev Neurosci 26: 81-104.
2. Marsden CD (1983) Neuromelanin and Parkinson's disease. J Neural Transm Suppl 19: 121-141.
3. Lee FJ, Liu F (2008) Genetic factors involved in the pathogenesis of Parkinson's disease. Brain Res Rev 58: 354-364.
4. Keeney PM, Xie J, Capaldi RA, Bennett JP, Jr. (2006) Parkinson's disease brain mitochondrial complex I has oxidatively damaged subunits and is functionally impaired and misassembled. J Neurosci 26: 5256-5264.
5. Schapira AH, Cooper JM, Dexter D, Clark JB, Jenner P, et al. (1990) Mitochondrial complex I deficiency in Parkinson's disease. J Neurochem 54: 823-827.
6. Mizuno Y, Ikebe S, Hattori N, Nakagawa-Hattori Y, Mochizuki H, et al. (1995) Role of mitochondria in the etiology and pathogenesis of Parkinson's disease. Biochim Biophys Acta 1271: 265-274.
7. Semchuk KM, Love EJ, Lee RG (1992) Parkinson's disease and exposure to agricultural work and pesticide chemicals. Neurology 42: 1328-1335.
8. Liou HH, Tsai MC, Chen CJ, Jeng JS, Chang YC, et al. (1997) Environmental risk factors and Parkinson's disease: a case-control study in Taiwan. Neurology 48: 1583-1588.
9. Costello S, Cockburn M, Bronstein J, Zhang X, Ritz B (2009) Parkinson's disease and residential exposure to maneb and paraquat from agricultural applications in the central valley of California. Am J Epidemiol 169: 919-926.
10. Wood-Kaczmar A, Gandhi S, Wood NW (2006) Understanding the molecular causes of Parkinson's disease. Trends in Molecular Medicine 12: 521-528.
11. Singleton AB, Farrer M, Johnson J, Singleton A, Hague S, et al. (2003) alpha-Synuclein locus triplication causes Parkinson's disease. Science 302: 841.
12. Chartier-Harlin MC, Kachergus J, Roumier C, Mouroux V, Douay X, et al. (2004) Alpha-synuclein locus duplication as a cause of familial Parkinson's disease. Lancet 364: 1167-1169.
13. Farrer M, Kachergus J, Forno L, Lincoln S, Wang DS, et al. (2004) Comparison of kindreds with parkinsonism and alpha-synuclein genomic multiplications. Ann Neurol 55: 174-179.
14. Fuchs J (2007) Phenotypic variation in a large Swedish pedigree due to SNCA duplication and triplication. Neurology 68: 916-922.
15. Spillantini MG, Schmidt ML, Lee VM, Trojanowski JQ, Jakes R, et al. (1997) Alpha-synuclein in Lewy bodies. Nature 388: 839-840.
16. Lakso M, Vartiainen S, Moilanen AM, Sirvio J, Thomas JH, et al. (2003) Dopaminergic neuronal loss and motor deficits in Caenorhabditis elegans overexpressing human alpha-synuclein. J Neurochem 86: 165-172.
17. Smith WW, Jiang H, Pei Z, Tanaka Y, Morita H, et al. (2005) Endoplasmic reticulum stress and mitochondrial cell death pathways mediate A53T mutant alpha-synuclein-induced toxicity. Hum Mol Genet 14: 3801-3811.
18. Norris EH, Uryu K, Leight S, Giasson BI, Trojanowski JQ, et al. (2007) Pesticide exposure exacerbates alpha-synucleinopathy in an A53T transgenic mouse model. Am J Pathol 170: 658-666.

19. Martin LJ, Pan Y, Price AC, Sterling W, Copeland NG, et al. (2006) Parkinson's Disease {alpha}-Synuclein Transgenic Mice Develop Neuronal Mitochondrial Degeneration and Cell Death. J Neurosci 26: 41-50.
20. Hsu LJ, Sagara Y, Arroyo A, Rockenstein E, Sisk A, et al. (2000) {alpha}-Synuclein Promotes Mitochondrial Deficit and Oxidative Stress. Am J Pathol 157: 401-410.
21. Feany MB, Bender WW (2000) A Drosophila model of Parkinson's disease. Nature 404: 394-398.
22. Lo Bianco C, Ridet JL, Schneider BL, Deglon N, Aebischer P (2002) alpha -Synucleinopathy and selective dopaminergic neuron loss in a rat lentiviral-based model of Parkinson's disease. Proc Natl Acad Sci U S A 99: 10813-10818.
23. Eslamboli A, Romero-Ramos M, Burger C, Bjorklund T, Muzyczka N, et al. (2007) Long-term consequences of human alpha-synuclein overexpression in the primate ventral midbrain. Brain 130: 799-815.
24. Conway KA, Lee SJ, Rochet JC, Ding TT, Williamson RE, et al. (2000) Acceleration of oligomerization, not fibrillization, is a shared property of both alpha-synuclein mutations linked to early-onset Parkinson's disease: implications for pathogenesis and therapy. Proc Natl Acad Sci U S A 97: 571-576.
25. Volles MJ, Lansbury JPT (2007) Relationships between the Sequence of [alpha]-Synuclein and its Membrane Affinity, Fibrillization Propensity, and Yeast Toxicity. Journal of Molecular Biology 366: 1510-1522.
26. Cuervo AM, Stefanis L, Fredenburg R, Lansbury PT, Sulzer D (2004) Impaired degradation of mutant alpha-synuclein by chaperone-mediated autophagy. Science 305: 1292-1295.
27. Martinez-Vicente M, Talloczy Z, Kaushik S, Massey AC, Mazzulli J, et al. (2008) Dopamine-modified alpha-synuclein blocks chaperone-mediated autophagy. J Clin Invest 118: 777-788.
28. Petrucelli L, O'Farrell C, Lockhart PJ, Baptista M, Kehoe K, et al. (2002) Parkin protects against the toxicity associated with mutant alpha-synuclein: proteasome dysfunction selectively affects catecholaminergic neurons. Neuron 36: 1007-1019.
29. Stefanis L, Larsen KE, Rideout HJ, Sulzer D, Greene LA (2001) Expression of A53T mutant but not wild-type alpha-synuclein in PC12 cells induces alterations of the ubiquitin-dependent degradation system, loss of dopamine release, and autophagic cell death. J Neurosci 21: 9549-9560.
30. Snyder H, Mensah K, Theisler C, Lee J, Matouschek A, et al. (2003) Aggregated and monomeric alpha-synuclein bind to the S6' proteasomal protein and inhibit proteasomal function. J Biol Chem 278: 11753-11759.
31. Tanaka Y, Engelender S, Igarashi S, Rao RK, Wanner T, et al. (2001) Inducible expression of mutant alpha-synuclein decreases proteasome activity and increases sensitivity to mitochondria-dependent apoptosis. Hum Mol Genet 10: 919-926.
32. Li WW, Yang R, Guo JC, Ren HM, Zha XL, et al. (2007) Localization of alpha-synuclein to mitochondria within midbrain of mice. Neuroreport 18: 1543-1546.
33. Liu G, Zhang C, Yin J, Li X, Cheng F, et al. (2009) alpha-Synuclein is differentially expressed in mitochondria from different rat brain regions and dose-dependently down-regulates complex I activity. Neurosci Lett 454: 187-192.
34. Loeb V, Yakunin E, Saada A, Sharon R The Transgenic Overexpression of Î±-Synuclein and Not Its Related Pathology Associates with Complex I Inhibition. Journal of Biological Chemistry 285: 7334-7343.
35. Parihar MS, Parihar A, Fujita M, Hashimoto M, Ghafourifar P (2008) Mitochondrial association of alpha-synuclein causes oxidative stress. Cell Mol Life Sci 65: 1272-1284.
36. Parihar MS, Parihar A, Fujita M, Hashimoto M, Ghafourifar P (2009) Alpha-synuclein overexpression and aggregation exacerbates impairment of mitochondrial functions by augmenting oxidative stress in human neuroblastoma cells. The International Journal of Biochemistry & Cell Biology 41: 2015-2024.

37. Shavali S, Brown-Borg HM, Ebadi M, Porter J (2008) Mitochondrial localization of alpha-synuclein protein in alpha-synuclein overexpressing cells. Neurosci Lett 439: 125-128.
38. Devi L, Raghavendran V, Prabhu BM, Avadhani NG, Anandatheerthavarada HK (2008) Mitochondrial import and accumulation of alpha-synuclein impair complex I in human dopaminergic neuronal cultures and Parkinson disease brain. J Biol Chem 283: 9089-9100.
39. Pridgeon JW, Olzmann JA, Chin L-S, Li L (2007) PINK1 Protects against Oxidative Stress by Phosphorylating Mitochondrial Chaperone TRAP1. PLoS Biol 5: e172.
40. Muqit MM, Feany MB (2002) Modelling neurodegenerative diseases in Drosophila: a fruitful approach? Nat Rev Neurosci 3: 237-243.
41. Karpinar DP, Balija MB, Kugler S, Opazo F, Rezaei-Ghaleh N, et al. (2009) Pre-fibrillar alpha-synuclein variants with impaired beta-structure increase neurotoxicity in Parkinson's disease models. EMBO J 28: 3256-3268.
42. Chen J, Shi X, Padmanabhan R, Wang Q, Wu Z, et al. (2008) Identification of novel modulators of mitochondrial function by a genome-wide RNAi screen in Drosophila melanogaster. Genome Res 18: 123-136.
43. Du G, Liu X, Chen X, Song M, Yan Y, et al. Drosophila Histone Deacetylase 6 Protects Dopaminergic Neurons Against {alpha}-Synuclein Toxicity by Promoting Inclusion Formation. Mol Biol Cell: E10-03-0200.
44. Bilen J, Bonini NM (2007) Genome-wide screen for modifiers of ataxin-3 neurodegeneration in Drosophila. PLoS Genet 3: 1950-1964.
45. Shulman JM, Feany MB (2003) Genetic modifiers of tauopathy in Drosophila. Genetics 165: 1233-1242.
46. Hua G, Zhang Q, Fan Z (2007) Heat shock protein 75 (TRAP1) antagonizes reactive oxygen species generation and protects cells from granzyme M-mediated apoptosis. J Biol Chem 282: 20553-20560.
47. Im CN, Lee JS, Zheng Y, Seo JS (2007) Iron chelation study in a normal human hepatocyte cell line suggests that tumor necrosis factor receptor-associated protein 1 (TRAP1) regulates production of reactive oxygen species. J Cell Biochem 100: 474-486.
48. Masuda Y, Shima G, Aiuchi T, Horie M, Hori K, et al. (2004) Involvement of Tumor Necrosis Factor Receptor-associated Protein 1 (TRAP1) in Apoptosis Induced by Î²-Hydroxyisovalerylshikonin. Journal of Biological Chemistry 279: 42503-42515.
49. Xiang F, Huang YS, Shi XH, Zhang Q Mitochondrial chaperone tumour necrosis factor receptor-associated protein 1 protects cardiomyocytes from hypoxic injury by regulating mitochondrial permeability transition pore opening. FEBS J 277: 1929-1938.
50. Panaretou B, Prodromou C, Roe SM, O'Brien R, Ladbury JE, et al. (1998) ATP binding and hydrolysis are essential to the function of the Hsp90 molecular chaperone in vivo. EMBO J 17: 4829-4836.
51. Kamp F, Exner N, Lutz AK, Wender N, Hegermann J, et al. (2010) Inhibition of mitochondrial fusion by alpha-synuclein is rescued by PINK1, Parkin and DJ-1. EMBO J 29: 3571-3589.
52. Leav I, Plescia J, Goel HL, Li J, Jiang Z, et al. Cytoprotective Mitochondrial Chaperone TRAP-1 As a Novel Molecular Target in Localized and Metastatic Prostate Cancer. Am J Pathol 176: 393-401.
53. Costantino E, Maddalena F, Calise S, Piscazzi A, Tirino V, et al. (2009) TRAP1, a novel mitochondrial chaperone responsible for multi-drug resistance and protection from apoptotis in human colorectal carcinoma cells. Cancer letters 279: 39-46.
54. Gesualdi NM, Chirico G, Pirozzi G, Costantino E, Landriscina M, et al. (2007) Tumor necrosis factor-associated protein 1 (TRAP-1) protects cells from oxidative stress and apoptosis. Stress: The International Journal on the Biology of Stress 10: 342-350.

55. Takahashi M, Kanuka H, Fujiwara H, Koyama A, Hasegawa M, et al. (2003) Phosphorylation of [alpha]-synuclein characteristic of synucleinopathy lesions is recapitulated in [alpha]-synuclein transgenic Drosophila. Neuroscience Letters 336: 155-158.
56. Botella JA, Bayersdorfer F, Schneuwly S (2008) Superoxide dismutase overexpression protects dopaminergic neurons in a Drosophila model of Parkinson's disease. Neurobiol Dis 30: 65-73.
57. Shaltiel-Karyo R, Frenkel-Pinter M, Egoz-Matia N, Frydman-Marom A, Shalev DE, et al. Inhibiting Î±-Synuclein Oligomerization by Stable Cell-Penetrating Î²-Synuclein Fragments Recovers Phenotype of Parkinson's Disease Model Flies. PLoS ONE 5: e13863.
58. van Ham TJ, Thijssen KL, Breitling R, Hofstra RMW, Plasterk RHA, et al. (2008) C. elegans Model Identifies Genetic Modifiers of Î±-Synuclein Inclusion Formation During Aging. PLoS Genetics 4: e1000027.
59. Montesano Gesualdi N, Chirico G, Pirozzi G, Costantino E, Landriscina M, et al. (2007) Tumor necrosis factor-associated protein 1 (TRAP-1) protects cells from oxidative stress and apoptosis. Stress 10: 342-350.
60. Choi WS, Eom DS, Han BS, Kim WK, Han BH, et al. (2004) Phosphorylation of p38 MAPK induced by oxidative stress is linked to activation of both caspase-8- and -9-mediated apoptotic pathways in dopaminergic neurons. J Biol Chem 279: 20451-20460.
61. Hwang S, Kim D, Choi G, An SW, Hong YK, et al. (2010) Parkin suppresses c-Jun N-terminal kinase-induced cell death via transcriptional regulation in Drosophila. Mol Cells 29: 575-580.
62. Novikova L, Garris BL, Garris DR, Lau YS (2006) Early signs of neuronal apoptosis in the substantia nigra pars compacta of the progressive neurodegenerative mouse 1-methyl-4-phenyl-1,2,3,6-tetrahydropyridine/probenecid model of Parkinson's disease. Neuroscience 140: 67-76.
63. Singh S, Kumar S, Dikshit M (2010) Involvement of the mitochondrial apoptotic pathway and nitric oxide synthase in dopaminergic neuronal death induced by 6-hydroxydopamine and lipopolysaccharide. Redox Rep 15: 115-122.
64. Abou-Sleiman PM, Muqit MM, Wood NW (2006) Expanding insights of mitochondrial dysfunction in Parkinson's disease. Nat Rev Neurosci 7: 207-219.
65. Büeler H (2009) Impaired mitochondrial dynamics and function in the pathogenesis of Parkinson's disease. Experimental Neurology 218: 235-246.
66. Parker WD, Jr., Boyson SJ, Parks JK (1989) Abnormalities of the electron transport chain in idiopathic Parkinson's disease. Ann Neurol 26: 719-723.
67. Patki G, Che Y, Lau YS (2009) Mitochondrial dysfunction in the striatum of aged chronic mouse model of Parkinson's disease. Front Aging Neurosci 1: 3.
68. Schapira AHV (2008) Mitochondria in the aetiology and pathogenesis of Parkinson's disease. The Lancet Neurology 7: 97-109.
69. Song DD, Shults CW, Sisk A, Rockenstein E, Masliah E (2004) Enhanced substantia nigra mitochondrial pathology in human alpha-synuclein transgenic mice after treatment with MPTP. Exp Neurol 186: 158-172.
70. Vila M, Ramonet D, Perier C (2008) Mitochondrial alterations in Parkinson's disease: new clues. J Neurochem 107: 317-328.
71. Winklhofer KF, Haass C (2010) Mitochondrial dysfunction in Parkinson's disease. Biochim Biophys Acta 1802: 29-44.
72. Dagda RK, Chu CT (2009) Mitochondrial quality control: insights on how Parkinson's disease related genes PINK1, parkin, and Omi/HtrA2 interact to maintain mitochondrial homeostasis. J Bioenerg Biomembr 41: 473-479.
73. Exner N, Treske B, Paquet D, Holmstrom K, Schiesling C, et al. (2007) Loss-of-function of human PINK1 results in mitochondrial pathology and can be rescued by parkin. J Neurosci 27: 12413-12418.

74. Kitada T, Asakawa S, Hattori N, Matsumine H, Yamamura Y, et al. (1998) Mutations in the parkin gene cause autosomal recessive juvenile parkinsonism. Nature 392: 605-608.
75. Lutz AK, Exner N, Fett ME, Schlehe JS, Kloos K, et al. (2009) Loss of parkin or PINK1 function increases Drp1-dependent mitochondrial fragmentation. J Biol Chem 284: 22938-22951.
76. Morais VA, Verstreken P, Roethig A, Smet J, Snellinx A, et al. (2009) Parkinson's disease mutations in PINK1 result in decreased Complex I activity and deficient synaptic function. EMBO Mol Med 1: 99-111.
77. Sandebring A, Dehvari N, Perez-Manso M, Thomas KJ, Karpilovski E, et al. (2009) Parkin deficiency disrupts calcium homeostasis by modulating phospholipase C signalling. FEBS J 276: 5041-5052.
78. Sandebring A, Thomas KJ, Beilina A, van der Brug M, Cleland MM, et al. (2009) Mitochondrial alterations in PINK1 deficient cells are influenced by calcineurin-dependent dephosphorylation of dynamin-related protein 1. PLoS One 4: e5701.
79. Strauss KM, Martins LM, Plun-Favreau H, Marx FP, Kautzmann S, et al. (2005) Loss of function mutations in the gene encoding Omi/HtrA2 in Parkinson's disease. Hum Mol Genet 14: 2099-2111.
80. Valente EM, Salvi S, Ialongo T, Marongiu R, Elia AE, et al. (2004) PINK1 mutations are associated with sporadic early-onset parkinsonism. Ann Neurol 56: 336-341.
81. Voigt A, Herholz D, Fiesel FC, Kaur K, Muller D, et al. (2010) TDP-43-mediated neuron loss in vivo requires RNA-binding activity. PLoS One 5: e12247.
82. Auluck PK, Chan HY, Trojanowski JQ, Lee VM, Bonini NM (2002) Chaperone suppression of alpha-synuclein toxicity in a Drosophila model for Parkinson's disease. Science 295: 865-868.
83. Bayersdorfer F, Voigt A, Schneuwly S, Botella JA Dopamine-dependent neurodegeneration in Drosophila models of familial and sporadic Parkinson's disease. Neurobiology of Disease In Press, Corrected Proof.
84. Livak KJ, Schmittgen TD (2001) Analysis of Relative Gene Expression Data Using Real-Time Quantitative PCR and the 2-[Delta][Delta]CT Method. Methods 25: 402-408.
85. Reich A, Spering C, Gertz K, Harms C, Gerhardt E, et al. (2011) Fas/CD95 Regulatory Protein Faim2 Is Neuroprotective after Transient Brain Ischemia. J Neurosci 31: 225-233.
86. Gegg ME, Cooper JM, Schapira AHV, Taanman J-W (2009) Silencing of PINK1 Expression Affects Mitochondrial DNA and Oxidative Phosphorylation in DOPAMINERGIC Cells. PLoS ONE 4: e4756.

FIGURE LEGENDS

Figure 1. [A53T]α-Synuclein expression in fly heads results in age-dependent loss of DA. (A) Western blot showing abundance of human [A53T]α-Synuclein after aminergic neuron (*ddc-GAL4*)-specific expression in lysates of fly heads. While flies without [A53T]α-Synuclein transgene do not show any detectable signal for [A53T]α-Synuclein in Western blot, an increase of [A53T]α-Synuclein protein levels was observed by increasing the copy number of transgenes. Syntaxin served as a loading control and molecular weight markers are indicated. (B) Whereas *ddc>A53T/+* flies displayed no significant difference in longevity as compared to *ddc/+* flies, flies homozygous for *ddc>A53T* showed a significant decrease ($p<0.001$, Log rank test). (C) Compared to controls (*ddc/+*), *ddc>A53T/+* flies showed a significant age-dependent loss of DA at 3 and 4 weeks post eclosion (*$p<0.05$ vs. control). (D) Only *ddc>A53T* flies showed a significant decrease (***$p<0.001$) in DA concentration in fly heads at 4 weeks. Comparisons of multiple controls were not significant (4 week values as per cent of 1 week values; ANOVA followed by Newman-Keuls Multiple Comparison Test).

Figure 2. TRAP1 overexpression mitigates detrimental effects induced by neuronal [A53T]α-Synuclein expression. (A) Overexpression of [A53T]α-Synuclein under control of *ddc-GAL4* resulted in reduction of DA in fly heads at 4 weeks, which was potentiated by TRAP1 deficiency (*TRAP1[KG]/+;ddc>A53T/+*), but mitigated by TRAP1 overexpression (*ddc>A53T/hTRAP1*). (B) *ddc>A53T* flies display a reduction of TH-positive neurons, which was potentiated by TRAP1 deficiency, but rescued to control levels by TRAP1 overexpression. (C) In negative geotaxis assays *ddc>A53T* flies displayed a time-dependent decline in locomotion. Reduction of TRAP1 enhanced the inability to climb (although not significant), while overexpression of hTRAP1 provided a significant rescue effect (comparison of *ddc>A53T/+* vs *ddc>A53T/hTRAP1* at 4 weeks: $p<0.05$). Statistics in (A, B): ANOVA followed by Newman-Keuls Multiple Comparison Test; (C): 2-way ANOVA followed by Bonferroni post-hoc tests. Displayed are biologically relevant comparisons. *$p<0.05$; **$p<0.01$; ***$p<0.001$; ns = not significant. (D) Alterations in TRAP1 levels did not influence PolyQ-induced rough eye phenotypes. Light micrographs of external eye structures show that PolyQ-induced REP was suppressed by parallel expression of HSP70. In contrast, neither overexpression of hTRAP1 or silencing of endogenous TRAP1 by RNAi had an obvious impact on external eye structure. Expression of mitochondrial localized GFP (mito-GFP) served as control.

Figure 3. TRAP1 overexpression protects rat cortical neurons from [A53T]α-Synuclein-induced sensitivity to rotenone. (A) Western blot analysis of cells infected with lentivirus promoting either GFP, TRAP1 or [A53T]α-Synuclein expression. For visualization, the blot was probed with either TRAP1- or α-Synuclein specific antibodies, respectively. ß-Actin was used for normalization. (B) Rat cortical neurons infected with lentivirus promoting GFP expression were stained for neuronal marker NeuN (red) and DNA (Hoechst, blue). A high percentage of cells showed co-localization between GFP and the neuronal marker NeuN, indicative for high infection efficacy. Scale bar indicates 43 µm. (C) Quantification of cell survival after 16 h of rotenone treatment of cells infected with viruses mediating expression of indicated protein. Significant differences compared to control (GFP) are indicated. All other comparisons revealed highly significant differences ($p<0.001$) in statistical

analysis (ANOVA followed by Newman-Keuls multiple comparison test). **p<0.01; ***p<0.001; ns = not significant.

Figure 4. Alterations in TRAP1 levels influence [A53T]α-Synuclein-induced sensitivity to oxidative stress and mitochondrial effects in HEK293 cells. HEK293 cells were transfected with plasmids promoting [A53T]α-Synuclein or TRAP1 expression. Empty vector transfection served as control. In addition, RNAi-mediated silencing of endogenous TRAP1 was induced (siTRAP1). Cells transfected with indicated plasmid combinations were treated with (A) hydrogen peroxide (100 µm) or (B) rotenone (200 µM) to induce oxidative stress. Cell numbers were analyzed to monitor survival. (C-E) HEK293 without oxidative stress treatment overexpressing the indicated proteins, or with RNAi-mediated silencing of TRAP1 were analyzed for (C) ATP production via Complex I, (D) total ATP content, and (E) mitochondrial membrane potential. Statistical analysis of displayed bar graphs was performed using ANOVA followed by Newman-Keuls multiple comparison test. (A, B) Biologically relevant comparisons are indicated in bar graphs. (C) Differences compared to control are indicated. (A, B, C) A detailed summary of all comparisons is summarized in Figure S8. (D, E) Only cells with [A53T]α-Synuclein expression and TRAP1 reduction displayed significant differences in statistical analysis as indicated in graph. All other comparisons were not significant. *p<0.05; **p<0.01; ***p<0.001; ns = not significant.

Figure 5. Effect of TRAP1 mutation on modification of [A53T]α-Synuclein toxicity. (A) Western blot analysis of HEK293 lysates transfected with indicated constructs showed similar expression levels of TRAP1[WT] and TRAP1[D158N] and a reduction of endogenous TRAP1 by siTRAP1. Blot was probed with TRAP1-specific antibody. ß-Actin served as loading control. (B, C) Effect of TRAP1[WT] and TRAP1[D158N] on [A53T]α-Synuclein-induced effects in HEK293 cells. (B) Effect of TRAP1[D158N] on [A53T]α-Synuclein-induced toxicity. Cell survival after rotenone (200 µM) treatment was monitored. Compared to TRAP1[WT], cells expressing TRAP1[D158N] displayed a significant reduction in survival (t-test, **p<0.01). (C) Assessment of ATP production via Complex I in unstressed cells with [A53T]α-Synuclein expression revealed a significant reduction of ATP levels in TRAP1[D158N] versus TRAP1[WT] expressing cells (t-test, ***p<0.001).

Figure 6. Inhibition of mitochondrial fusion by [A53T]α-Synuclein is rescued by TRAP1. SH-SY5Y cells were co-transfected with the indicated constructs and mito-DsRed to visualize mitochondria. The mitochondrial morphology of transfected cells was analyzed by fluorescence microscopy. (A) Confocal images of representative cells displaying either an intact tubular mitochondrial network (control) or a fragmentation of this network (A53T). Co-expression of TRAP1[WT] prevented [A53T]α-Synuclein-induced mitochondrial fragmentation, whereas the TRAP1[D158N] mutant did not show rescue activity. Overexpression of either wild type or mutant TRAP1 alone did not influence mitochondrial morphology under steady state conditions. (B) For quantification, the mitochondrial morphology of at least 300 transfected cells per coverslip was determined in a blinded manner. Quantifications were based on triplicates of at least three independent experiments. Shown is the percentage of cells with fragmented mitochondria. (C) Expression levels of [A53T]α-Synuclein and TRAP1 were analyzed by Western blotting. β-Actin served as a loading control. ***p<0.001 (ANOVA).

Figure 7. Transient siRNA-mediated knockdown of TRAP1 increases [A53T]α-Synuclein-induced mitochondrial fragmentation. SH-SY5Y cells were co-transfected with the siRNAs and plasmids indicated. Mitochondria were visualized by DsRed targeted to mitochondria (mito-DsRed). (A) Confocal images taken of representative cells displaying either an intact tubular mitochondrial network (control siRNA) or a fragmentation of the network (control siRNA + A53T). Transient knockdown of TRAP1 causes mitochondrial fragmentation itself (TRAP1 siRNA), additional co-expression of [A53T]α-Synuclein aggravated this phenotype and led to an overall increase in cells showing a fragmented mitochondrial network (TRAP1 siRNA + A53T). (B) For quantification, at least 300 transfected cells per coverslip were analyzed. The mitochondrial morphology was determined in a blinded manner. Quantifications are based on triplicates of three independent experiments. (C) Expression levels of [A53T]α-Synuclein and TRAP1 were analyzed by Western Blotting. β-Actin was used as a loading control. **$p<0.01$; ***$p<0.001$ (ANOVA).

Figure legends Supplementary Information

Figure S1. Validation, specificity and sensitivity of HPLC to measure fly head DA. (A) Number of fly heads for single measurement varied from 3 - 30 and absolute DA amounts measured by HPLC were analyzed via linear regression; $r^2 = 0.997$ (n = 3). (B) Fly heads collected at indicated time of day were analyzed for DA using HPLC. Significant difference (ANOVA followed by Newman-Keuls Multiple Comparison Test) between time points noted: *p<0.05 vs. 10:30 and 16:30 (n = 3). (C) Wild type flies (one day post eclosion) were daily treated with tyrosine hydroxylase inhibitor α-methyltyrosine (α-MT). Fly heads were collected at 2-day intervals for measurement of DA using HPLC: Significant differences (t-test): *p<0.05 for Control (untreated) vs. 5 mM α-MT (n = 3).

Figure S2. Determination of TRAP1 transcript abundance. Flies heterozygous for P-element insertion TRAP1[KG] displayed a significant reduction in *trap1* transcript levels normalized to *actin5C* independent of *[A53T]α-Synuclein* expression (t-test, compared to respective control; **p<0.01; ***p<0.001).

Figure S3. Immunocytochemistry of [A53T]α-Synuclein-expressing HEK293 cells with overexpression or downregulation of TRAP1. (A) HEK293 cells transfected with [A53T]α-Synuclein were stained for TRAP1 (red), α-Synuclein (green) and DNA (blue). Merged picture is shown (right column). Upper panel: [A53T]α-Synuclein expressing cells co-transfected with empty vector. Middle panel: [A53T]α-Synuclein expressing cells with siTRAP1. Lower panel: Cells with [A53T]α-Synuclein and TRAP1 overexpression (scale bar = 24 µm). (B) Transfection with siTRAP1 reduced endogenous TRAP1 transcripts (in relation to β-Actin). (C) Both siTRAP1-1 and siTRAP1-2 resulted in significant knockdown of TRAP1 expression (ANOVA followed by Newman-Keuls Multiple Comparison Test; n = 3; ***p<0.001; ns = not significant).

Figure S4. Assessment of mitochondrial proteins. Changes in mitochondrial function by (A) alterations of TRAP1 levels or (B) expression of mutant TRAP1[D158N] are not caused by a decrease in overall mitochondrial load. Western blot analysis of HEK293 transfected with indicated constructs were assayed for abundance of the mitochondrial proteins VDAC1 and COX4. β-Actin served as loading control.

Figure S5. Stable silencing of TRAP1 causes a reduction in membrane potential of [A53T]α-Synuclein-expressing cells. We stably silenced TRAP1 in HEK293 cells using Lentiviruses-expressing short hairpin RNA (shRNA). (A) Silencing of TRAP1 was verified by Western blot. In contrast to HEK cells with stable expression of a scrambled shRNA construct, TRAP1-silenced cells displayed a strong reduction of TRAP1 protein load. Quantification of Western blots ($n \geq 3$) normalized with either VDAC or Tubulin revealed a strong reduction of TRAP1 in cells expressing shTRAP1 (95.43 +/-1.25 %). The presence of similar amounts of VDAC in relation to Tubulin between scrambled shRNA-expressing and TRAP1-silenced cells indicates that mitochondrial load is not effected by shTRAP1. (B) Membrane potential was measured using the dye TMRM. Cells with stable expression of either of scrambled shRNA or TRAP1 shRNA were co-transfected with pEPFP-N1, in combination with pCDNA3.1 or pCDNA3.1-[A53T]α-Synuclein. 2 days after transfection cells were treated with 200 nM TMRM for 30 minutes at 37°C. Fluorescence was measured at 573 nm (TMRM) and 509 nm (EGFP) and plotted as relative intensity (TMRM/GFP). Cells expressing scrambled shRNA displayed non-significant (ns) changes in membrane potential with or without [A53T]α-Synuclein-expression. In contrast, expression of [A53T]α-Synuclein caused a significant reduction in membrane potential of TRAP1-silenced cells (***$p<0.001$). Statistic: 2-way ANOVA followed by Bonferroni post-hoc tests.

Figure S6. Protein sequence data for TRAP1 used for mutant generation. (A) Protein sequence alignment showing conserved aspartic acid in HSP90 ATPase domains. The indicated conserved amino acid is reported to be critical for ATPase function in yeast Hsp82. Moreover, this aspartic acid is conserved in ATPase domains of human TRAP1 (position 158). (B) Multiple sequence comparison of TRAP1 proteins from different species showed a high degree of conservation of this aspartic acid in the ATPase domain. Alignments were performed using ClustalW2 (http://www.ebi.ac.uk/Tools/msa/clustalw2/).

Figure S7. Localization of TRAP1 and [A53T]α-Synuclein to the mitochondria. (A) Mitochondrial localization of TRAP1. Confocal section of HEK293 cells stained with the mitochondrial marker “Mitotracker Orange” (red), hTRAP1-specific antibody (green) and Hoechst nuclear stain (blue). A high degree of co-localization of red and green fluorescent signals is apparent in overlay. Scale bar indicates 27 µm. (B) Cell fractionation assay indicates localization of [A53T]α-Synuclein in mitochondria-enriched fraction. Samples derived after fractionation were used for Western blot analysis. Blots were probed with specific antibodies detecting α-Synuclein, VDAC1 and ß-Tubulin. Fractions analyzed (input, cytoplasmic and mitochondrial-enriched fraction) are indicated.

Figure S8. Detailed statistical analysis of the data shown in Figure 4. Summary of statistical analysis of bar graphs in Figure 4A, B & C (ANOVA followed by Newman-Keuls multiple comparison test). *$p<0.05$; **$p<0.01$; ***$p<0.001$; ns = not significant.

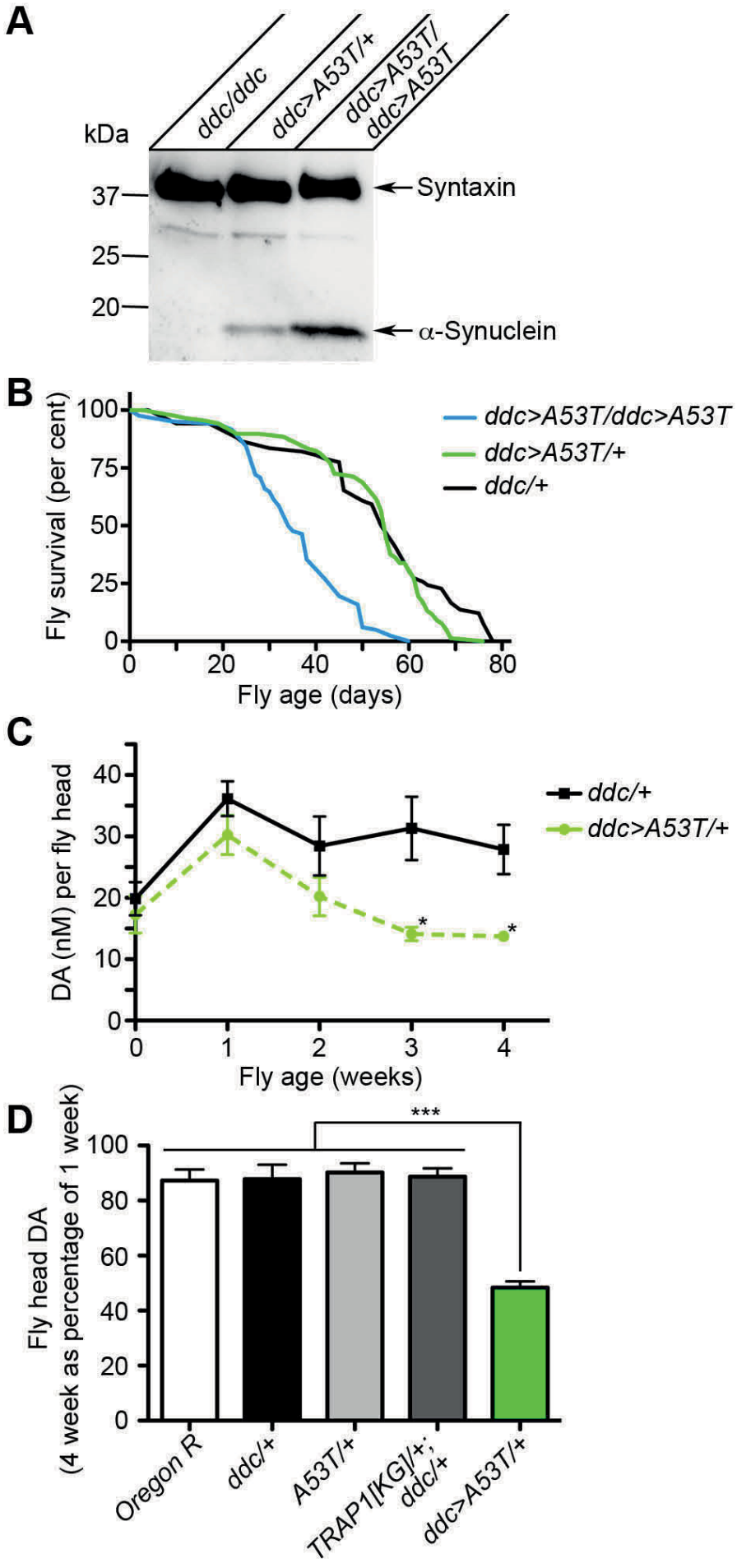
A
ddc/ddc
ddc>A53T/+
ddc>A53T/ ddc>A53T
kDa
37
25
20
Syntaxin
α-Synuclein
B
Fly survival (per cent)
100
75
50
25
0
0
20
40
60
80
Fly age (days)
ddc>A53T/ddc>A53T
ddc>A53T/+
ddc/+
C
DA (nM) per fly head
40
30
20
10
0
0
1
2
3
4
Fly age (weeks)
ddc/+
ddc>A53T/+
*
*
D
Fly head DA
(4 week as percentage of 1 week)
100
80
60
40
20
0
***
Oregon R
ddc/+
A53T/+
TRAP1[KG]/+; ddc/+
ddc>A53T/+

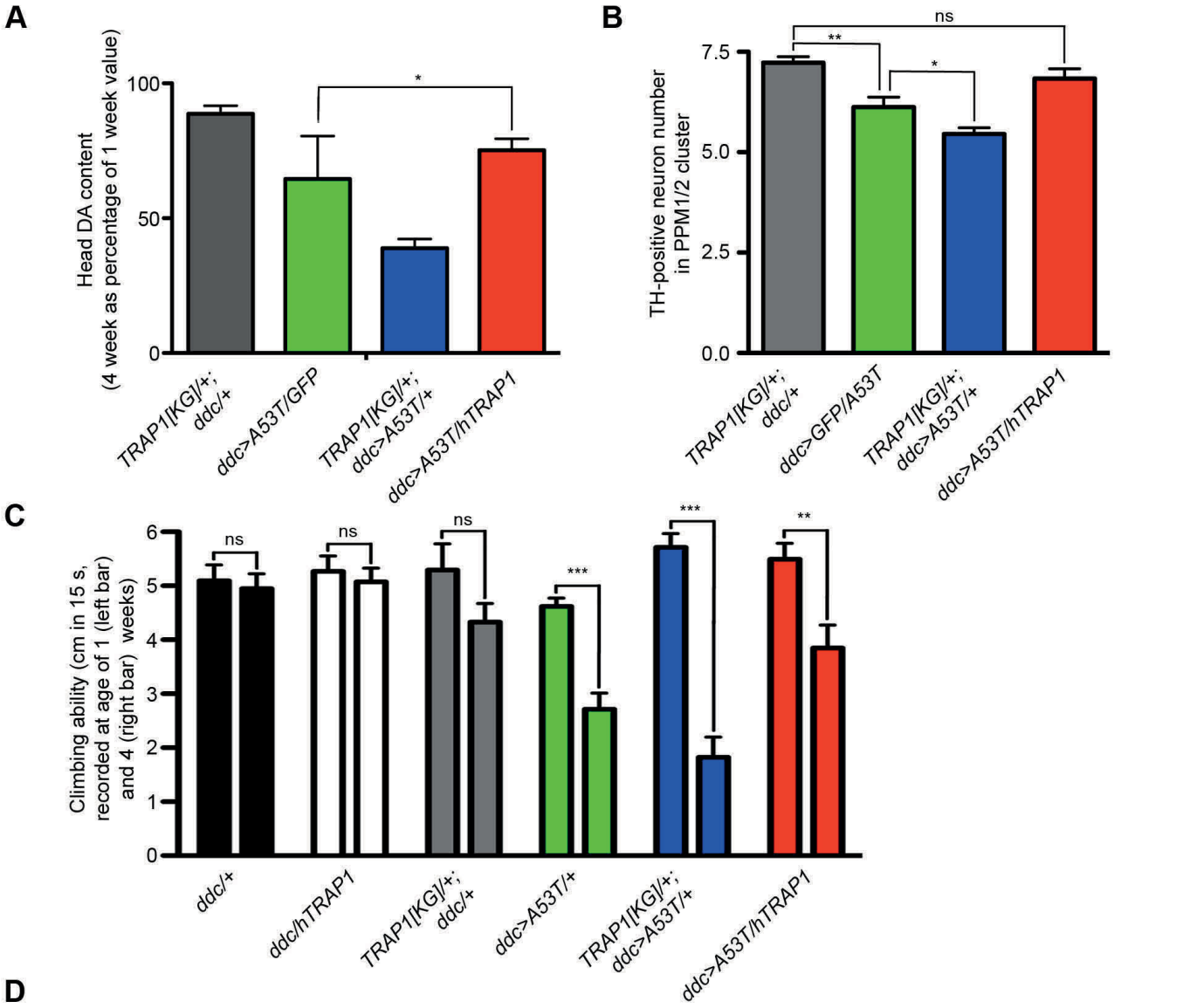
A
Head DA content
(4 week as percentage of 1 week value)
100
50
0
*
TRAP1[KG]/+;
ddc/+
ddc>A53T/GFP
TRAP1[KG]/+;
ddc>A53T/+
ddc>A53T/hTRAP1
B
TH-positive neuron number
in PPM1/2 cluster
7.5
5.0
2.5
0.0
ns
**
*
TRAP1[KG]/+;
ddc/+
ddc>GFP/A53T
TRAP1[KG]/+;
ddc>A53T/+
ddc>A53T/hTRAP1
C
Climbing ability (cm in 15 s,
recorded at age of 1 (left bar)
and 4 (right bar) weeks)
6
5
4
3
2
1
0
ns
ns
ns
***
***
**
ddc/+
ddc/hTRAP1
TRAP1[KG]/+;
ddc/+
ddc>A53T/+
TRAP1[KG]/+;
ddc>A53T/+
ddc>A53T/hTRAP1

D

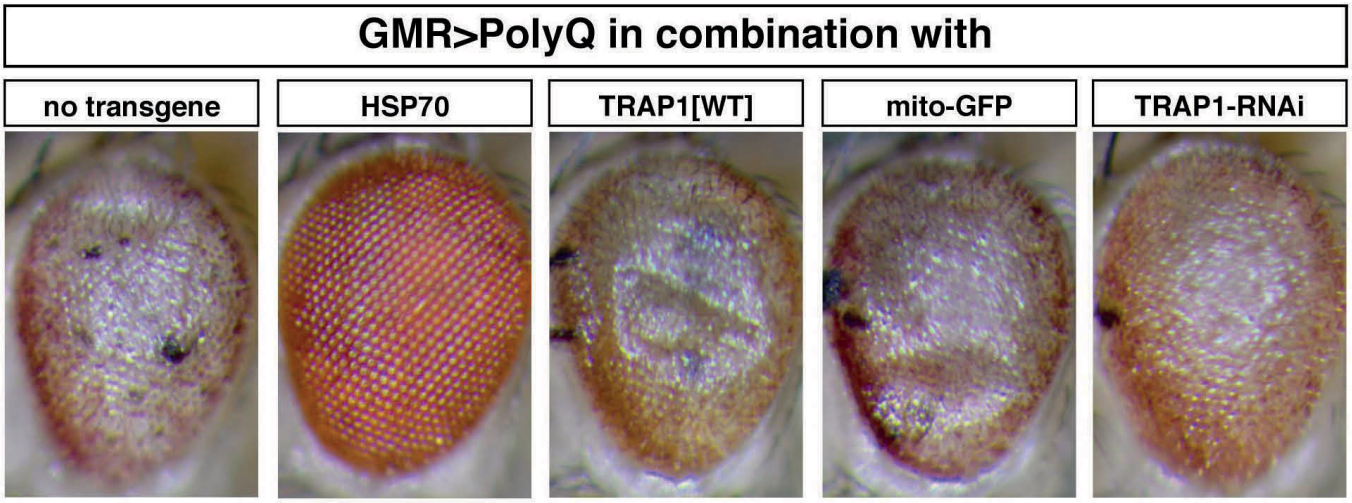
GMR>PolyQ in combination with
no transgene
HSP70
TRAP1[WT]
mito-GFP
TRAP1-RNAi

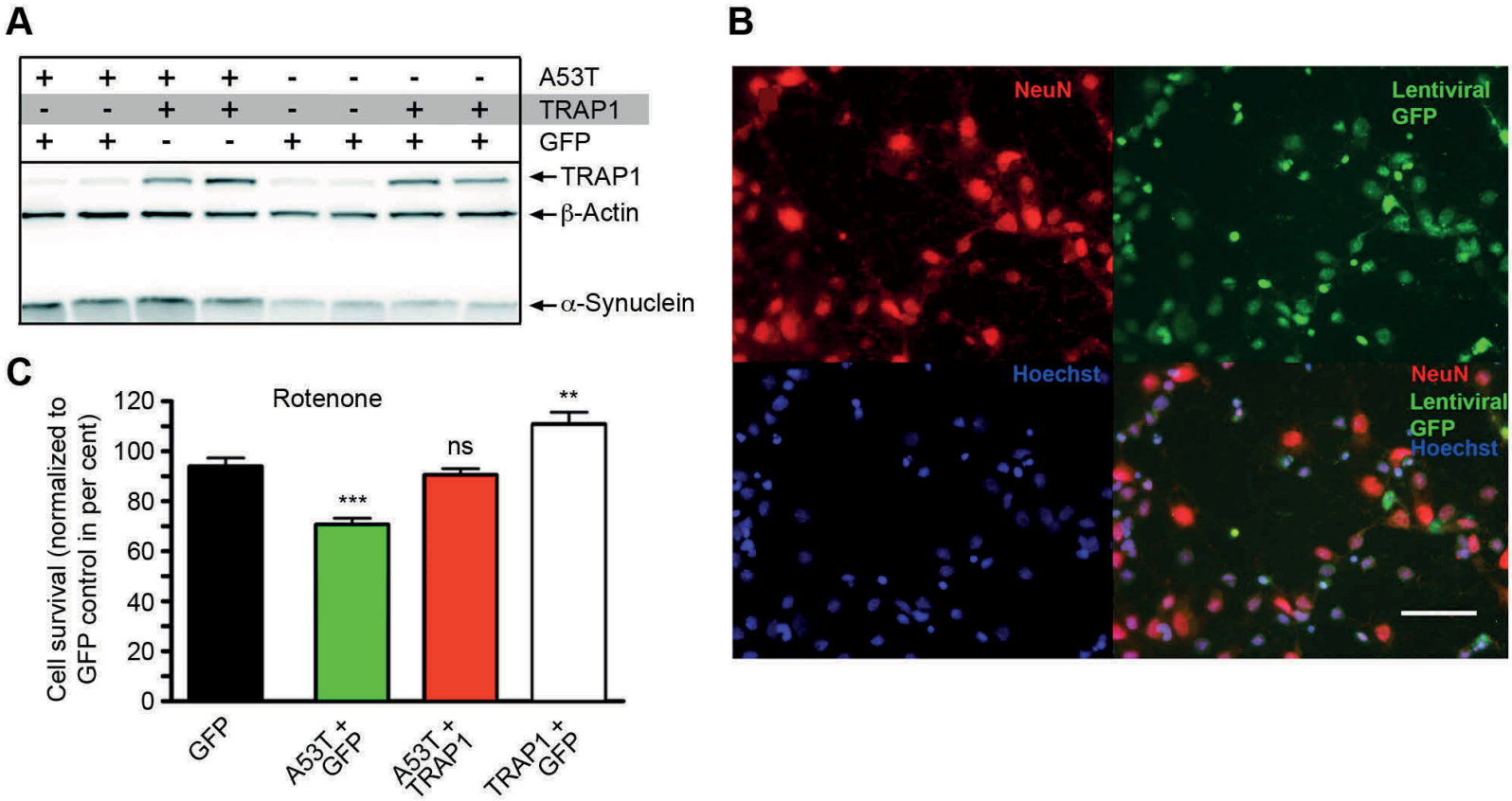
A
+ + + + - - - - A53T
- - + + - - + + TRAP1
+ + - - + + + + GFP
TRAP1
β-Actin
α-Synuclein
B
NeuN
Lentiviral GFP
Hoechst
NeuN
Lentiviral GFP
Hoechst
C
Rotenone
Cell survival (normalized to GFP control in per cent)
120
100
80
60
40
20
0
***
ns
**
GFP
A53T + GFP
A53T + TRAP1
TRAP1 + GFP

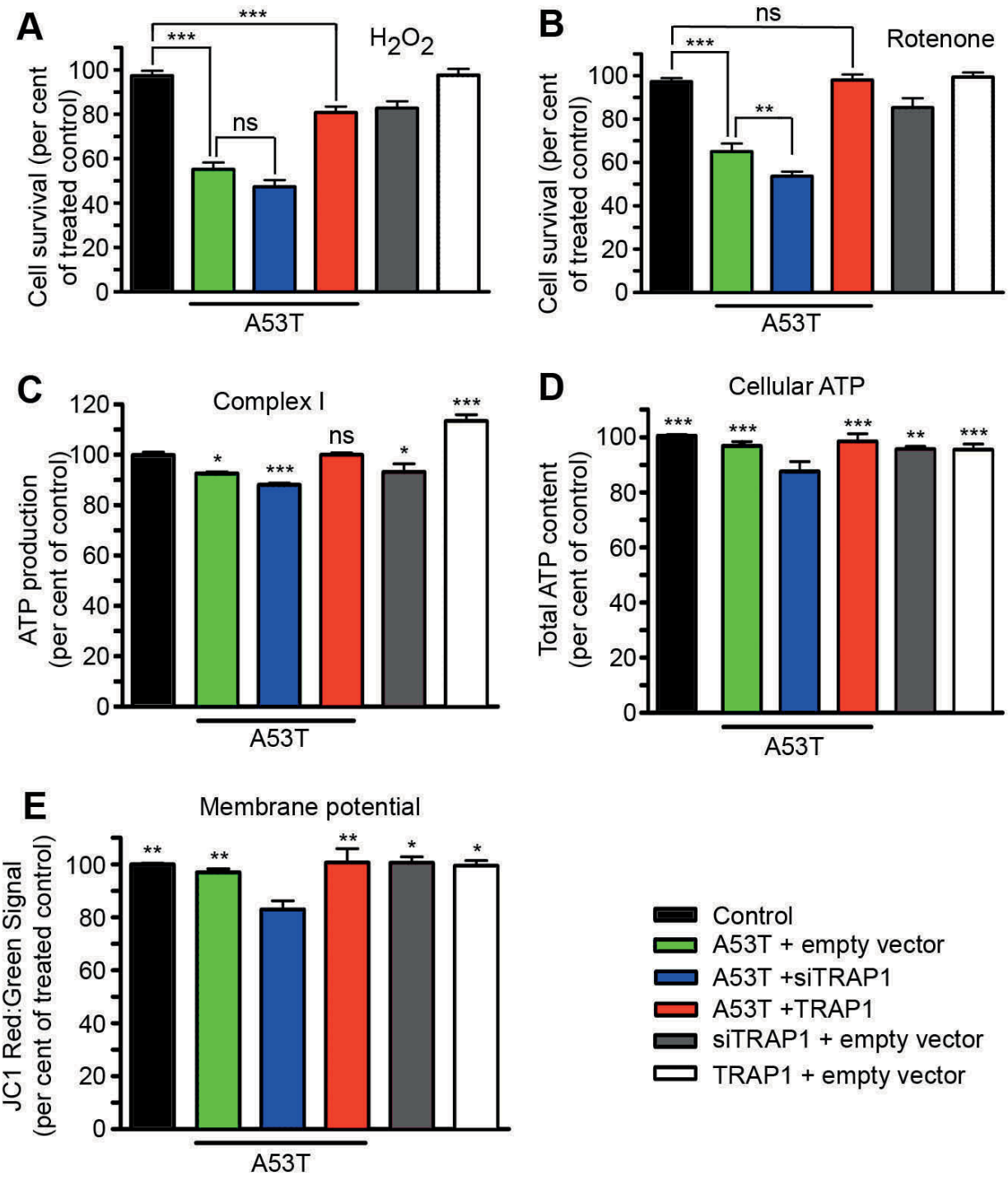
A
H_2O_2
Cell survival (per cent of treated control)
***
***
ns
A53T
B
Rotenone
ns
***
**
C
Complex I
ATP production (per cent of control)
D
Cellular ATP
Total ATP content (per cent of control)
E
Membrane potential
JC1 Red:Green Signal (per cent of treated control)
Control
A53T + empty vector
A53T +siTRAP1
A53T +TRAP1
siTRAP1 + empty vector
TRAP1 + empty vector

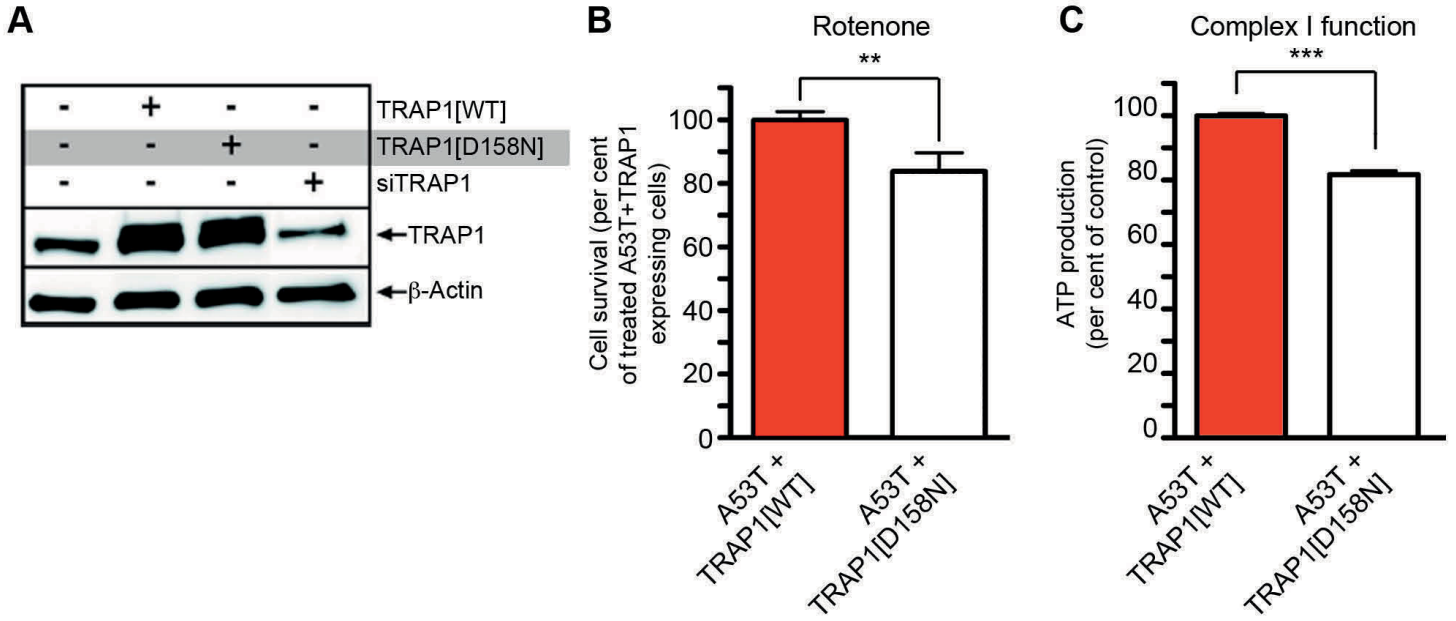
A
TRAP1[WT]
TRAP1[D158N]
siTRAP1
TRAP1
β-Actin
B
Rotenone
**
Cell survival (per cent of treated A53T+TRAP1 expressing cells)
100
80
60
40
20
0
A53T + TRAP1[WT]
A53T + TRAP1[D158N]
C
Complex I function
***
ATP production (per cent of control)
100
80
60
40
20
0
A53T + TRAP1[WT]
A53T + TRAP1[D158N]

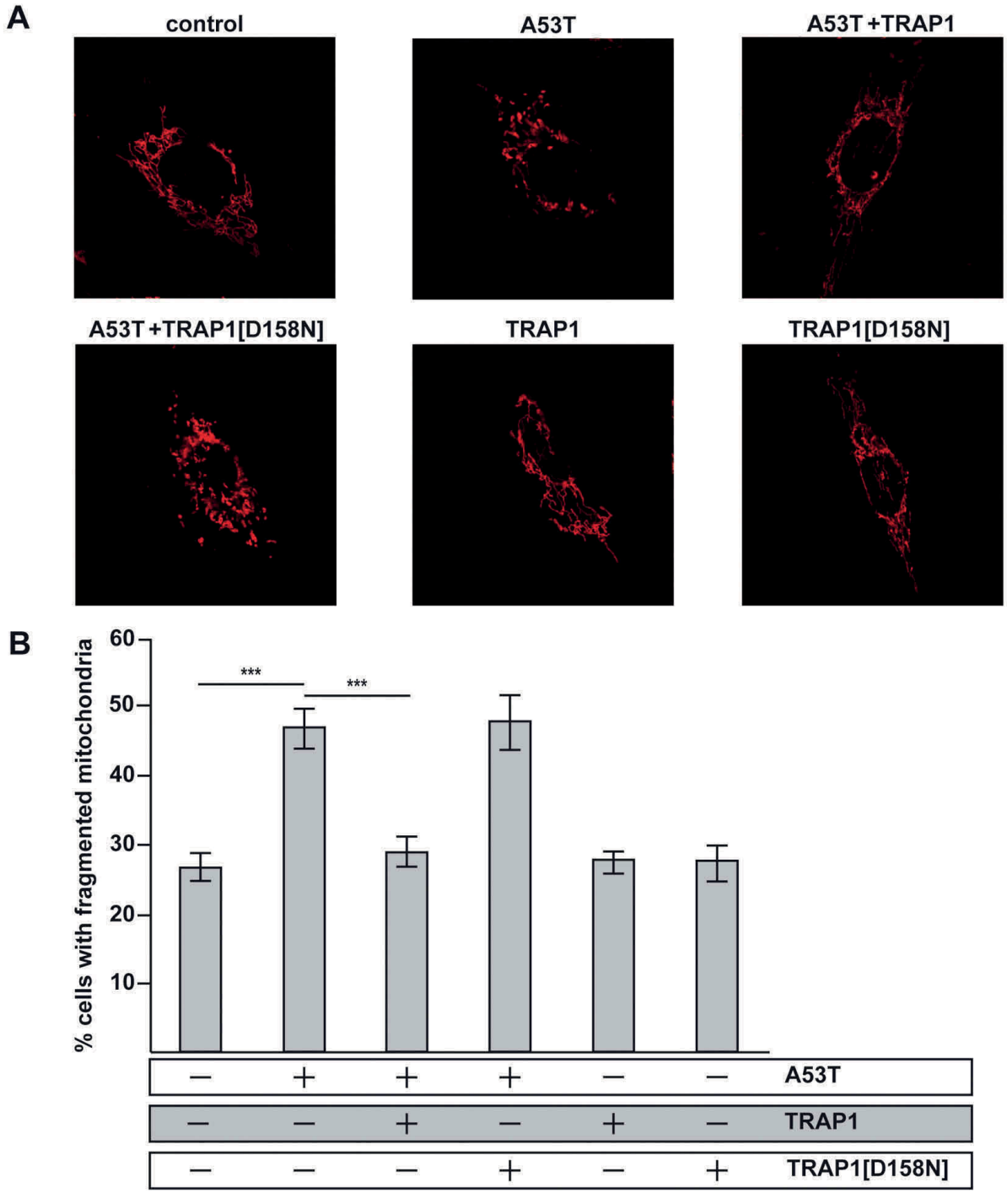
A
control
A53T
A53T +TRAP1
A53T +TRAP1[D158N]
TRAP1
TRAP1[D158N]
B
% cells with fragmented mitochondria
60
50
40
30
20
10
***
***
A53T
TRAP1
TRAP1[D158N]
C
α-Synuclein
TRAP1
β-actin
A53T
TRAP1
TRAP1[D158N]

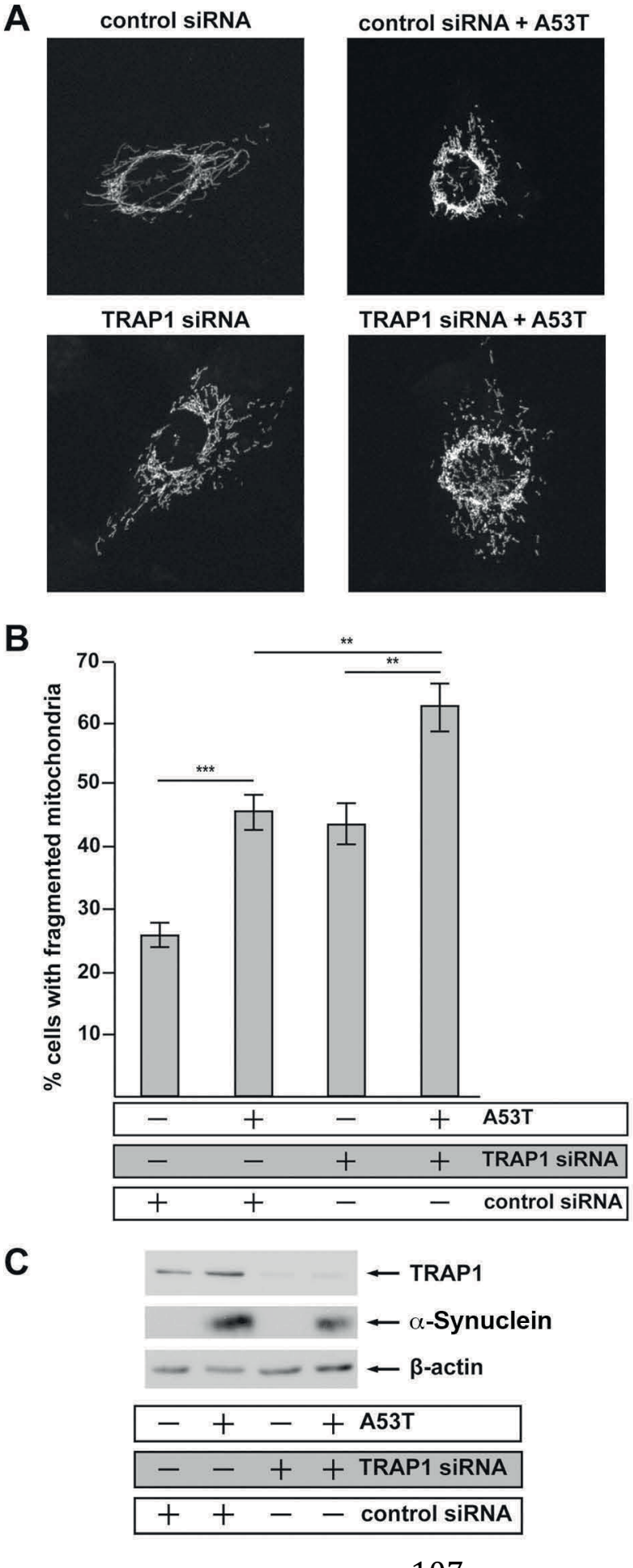
A
control siRNA
control siRNA + A53T
TRAP1 siRNA
TRAP1 siRNA + A53T
B
% cells with fragmented mitochondria
70
60
50
40
30
20
10
***
**
**
A53T
TRAP1 siRNA
control siRNA
C
TRAP1
α-Synuclein
β-actin
A53T
TRAP1 siRNA
control siRNA

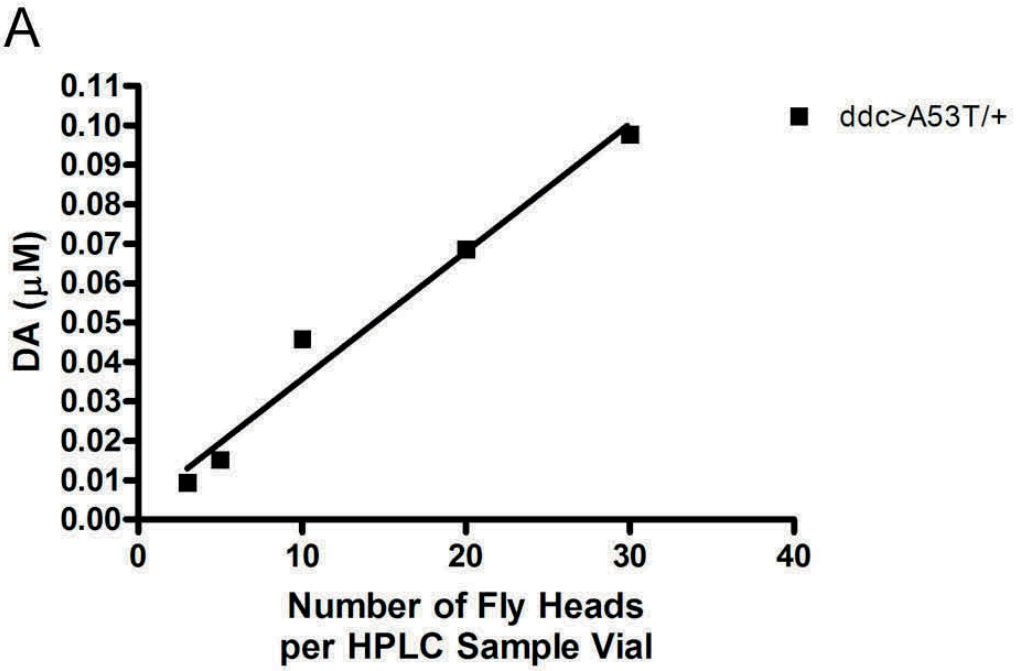
A
0.11
0.10
0.09
0.08
0.07
0.06
0.05
0.04
0.03
0.02
0.01
0.00
DA (μM)
0
10
20
30
40
Number of Fly Heads
per HPLC Sample Vial
ddc>A53T/+

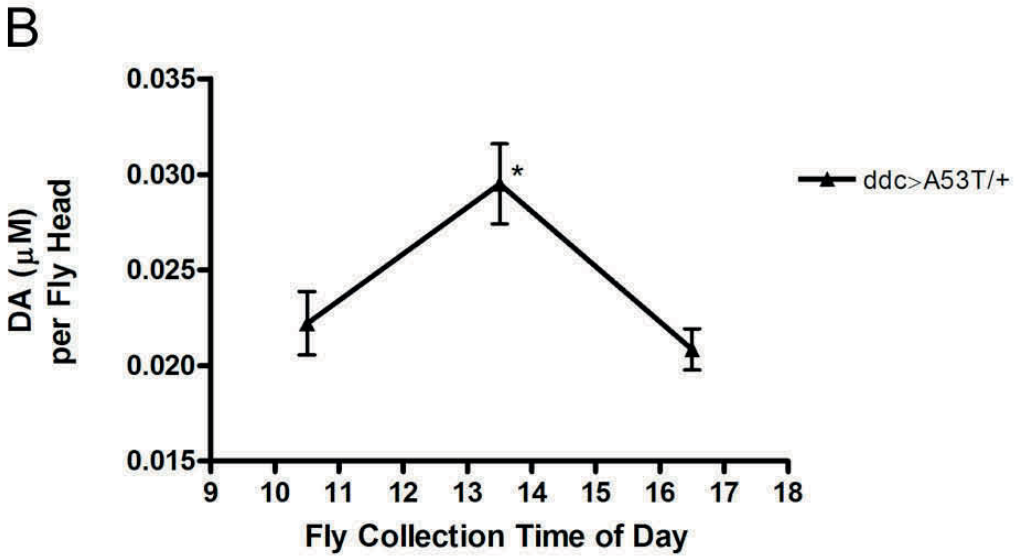
B
0.035
0.030
0.025
0.020
0.015
DA (μM)
per Fly Head
*
9
10
11
12
13
14
15
16
17
18
Fly Collection Time of Day
ddc>A53T/+

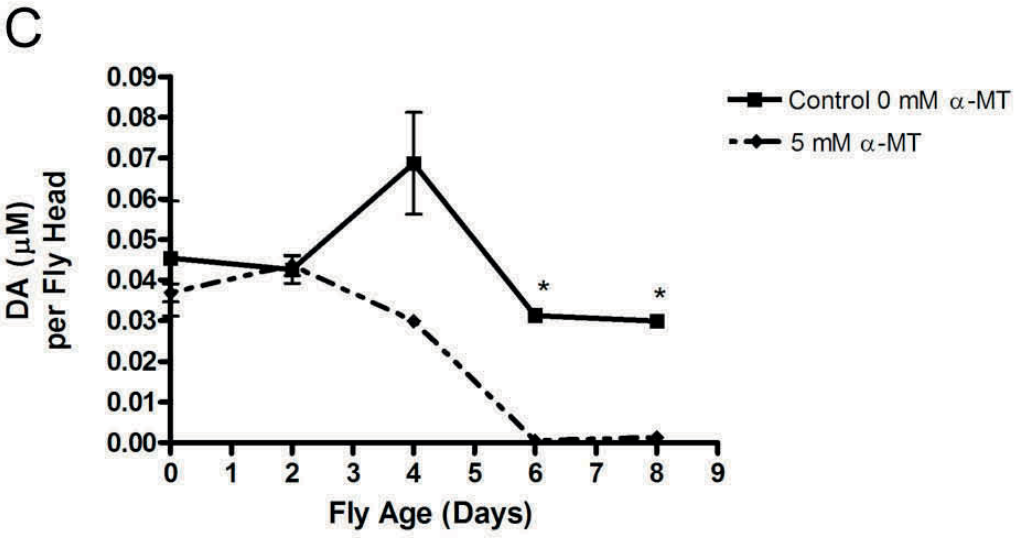
C
0.09
0.08
0.07
0.06
0.05
0.04
0.03
0.02
0.01
0.00
DA (μM)
per Fly Head
*
*
0
1
2
3
4
5
6
7
8
9
Fly Age (Days)
Control 0 mM α-MT
5 mM α-MT

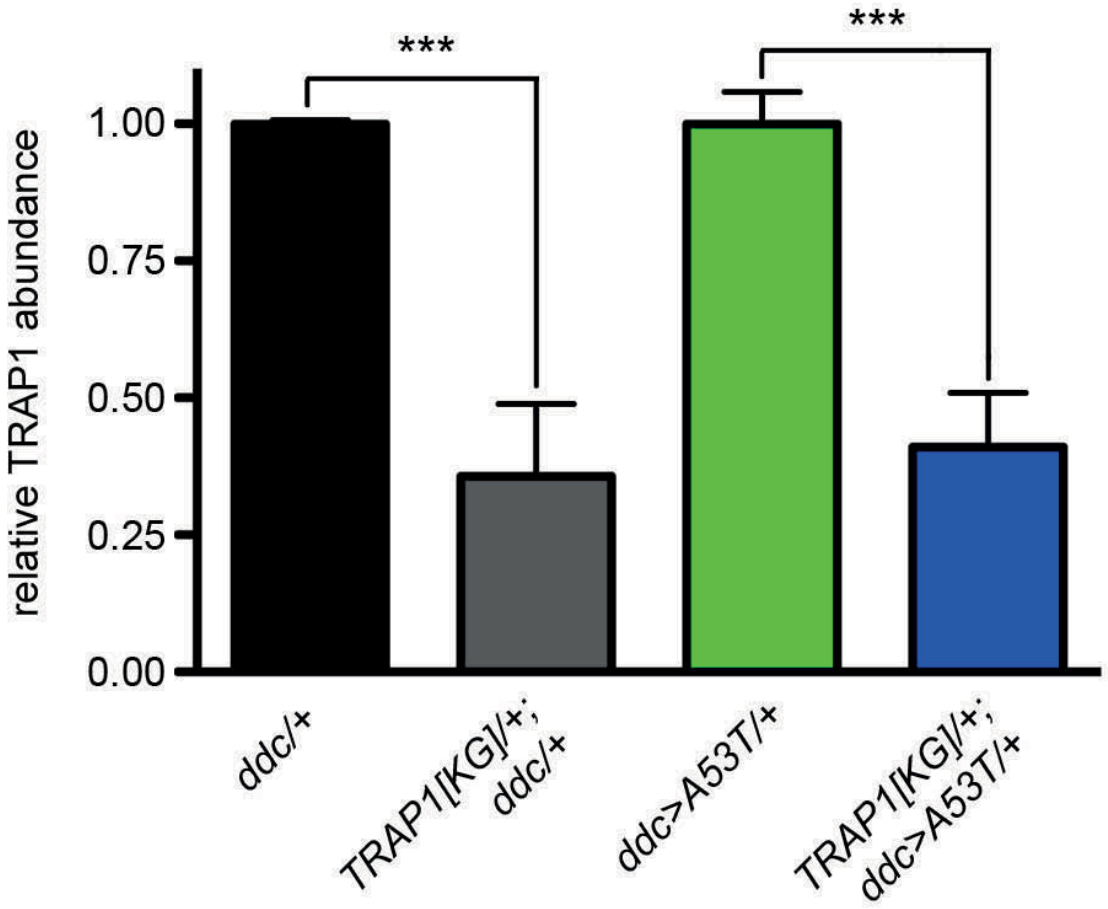
***
***
relative TRAP1 abundance
1.00
0.75
0.50
0.25
0.00
ddc/+
TRAP1[KG]/+; ddc/+
ddc>A53T/+
TRAP1[KG]/+; ddc>A53T/+

A

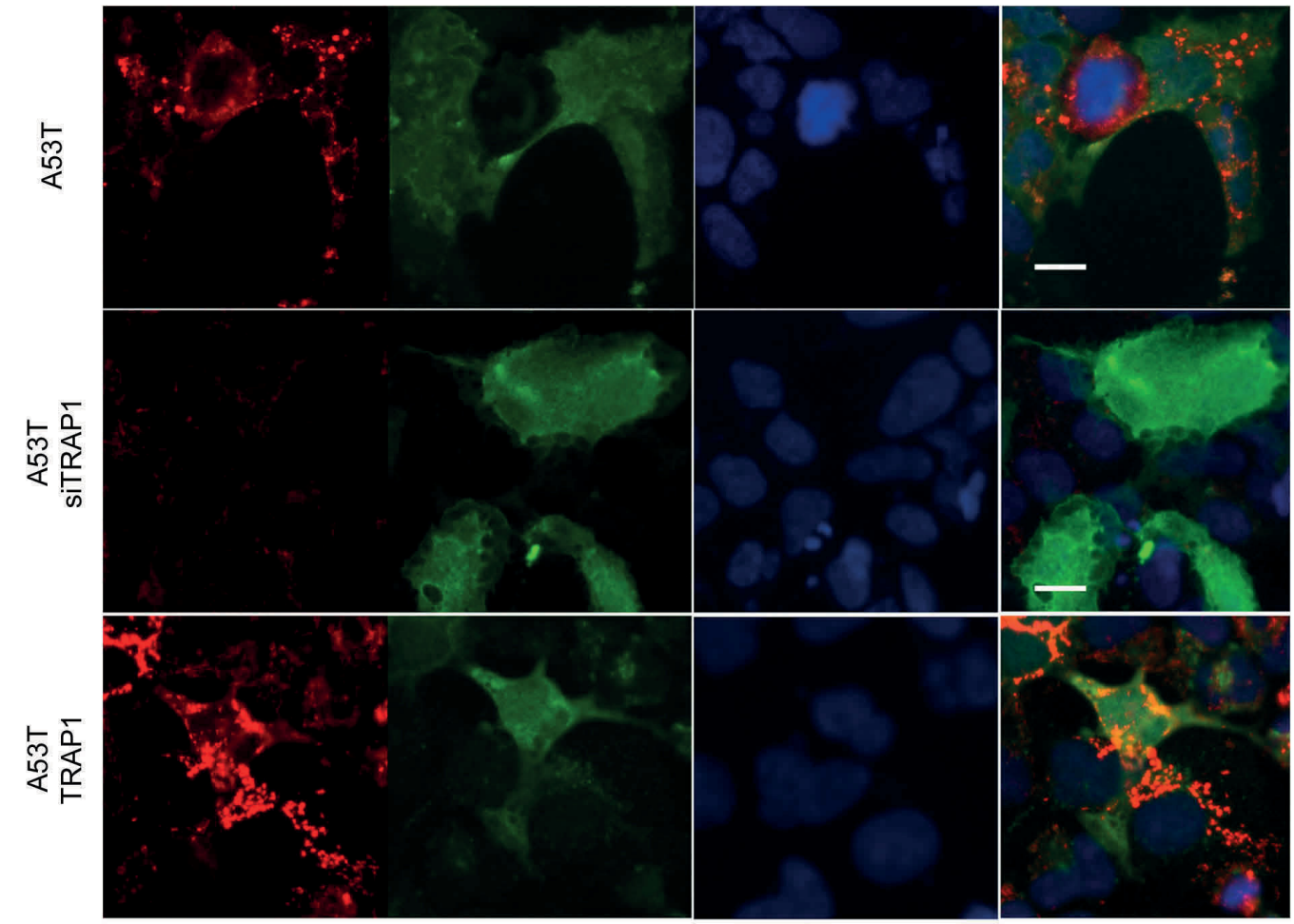

B

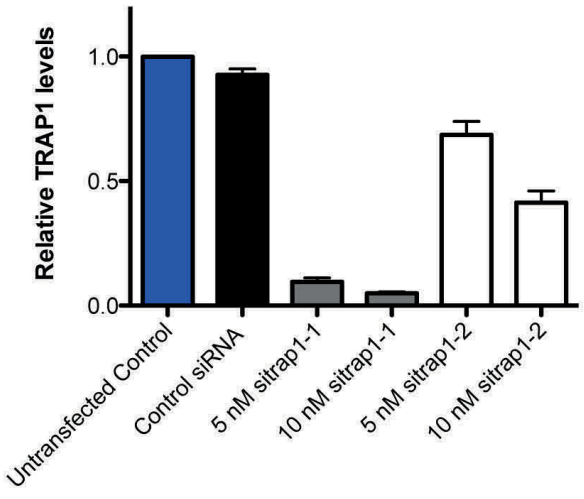

C

Compared condition	Sign.
10 nM sitrap1-1 vs Untransfected Control	***
10 nM sitrap1-1 vs Control siRNA	***
10 nM sitrap1-1 vs 5 nM sitrap1-2	***
10 nM sitrap1-1 vs 10 nM sitrap1-2	***
10 nM sitrap1-1 vs 5 nM sitrap1-1	ns
5 nM sitrap1-1 vs Untransfected Control	***
5 nM sitrap1-1 vs Control siRNA	***
5 nM sitrap1-1 vs 5 nM sitrap1-2	***
5 nM sitrap1-1 vs 10 nM sitrap1-2	***
10 nM sitrap1-2 vs Untransfected Control	***
10 nM sitrap1-2 vs Control siRNA	***
10 nM sitrap1-2 vs 5 nM sitrap1-2	***
5 nM sitrap1-2 vs Untransfected Control	***
5 nM sitrap1-2 vs Control siRNA	***
Control siRNA vs Untransfected Control	ns

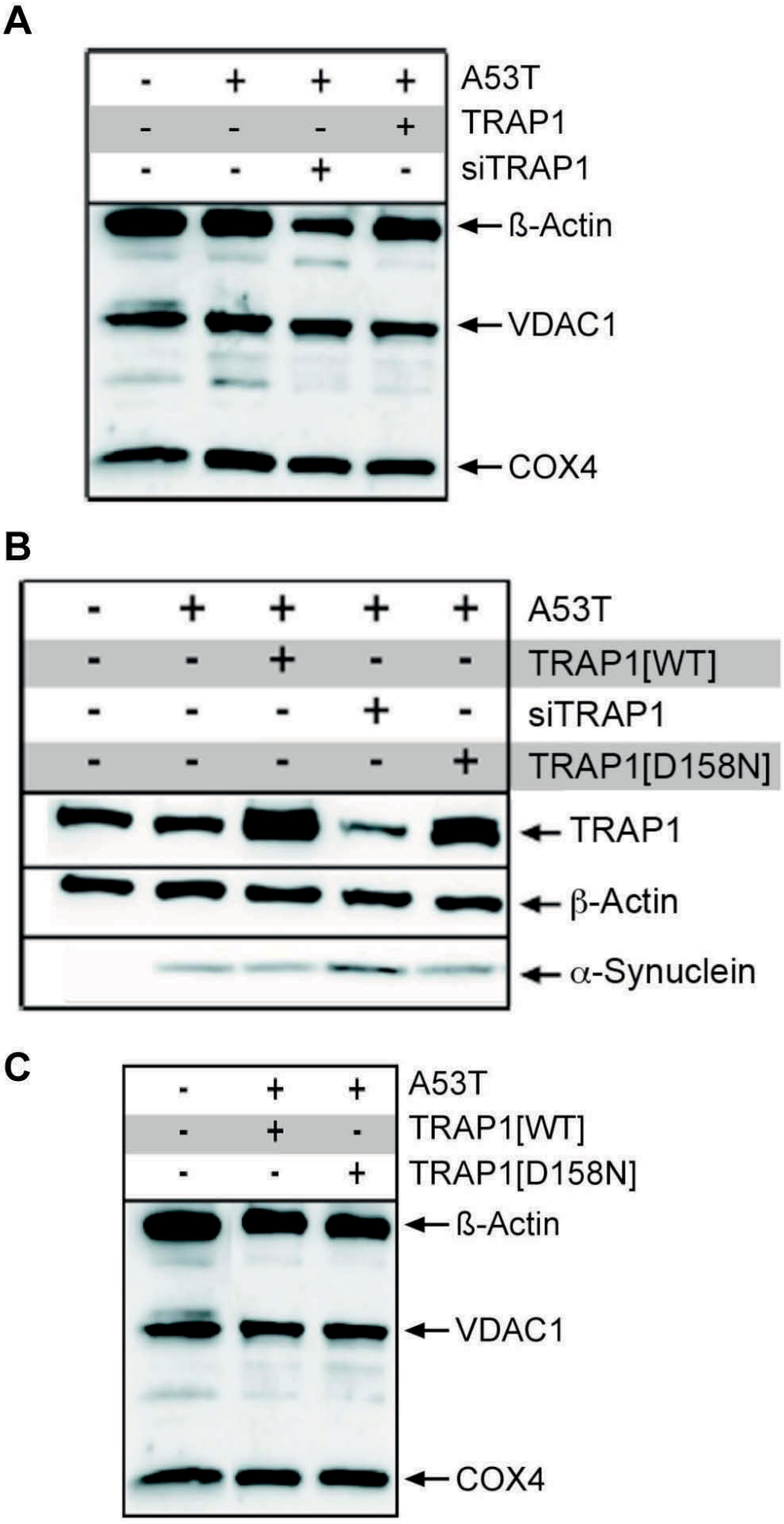
A
- + + + A53T
- - - + TRAP1
- - + - siTRAP1
ß-Actin
VDAC1
COX4
B
- + + + + A53T
- - + - - TRAP1[WT]
- - - + - siTRAP1
- - - - + TRAP1[D158N]
TRAP1
β-Actin
α-Synuclein
C
- + + A53T
- + - TRAP1[WT]
- - + TRAP1[D158N]
ß-Actin
VDAC1
COX4

A

HSP90 ATPase from different species vs human TRAP1 ATPase domain:

```
Human HSP90A IRYESLTDPSKLDSGKELHINLIPNKQDRTLTIVDTGIGMTKADLINNLGTIAKSGTKAF 240
Human HSP90B IRYESLTDPSKLDSGKELKIDIIPNPQERTLTLVDTGIGMTKADLINNLGTIAKSGTKAF 113
Fish  HSP90  IRYESLTDPTKLDSGKDLKIDIIPNVQERTLTLIDTGIGMTKADLINNLGTIAKSGTKAF 112
Yeast HSP82  IRYKSLSDPKQLETEPDLFIRITPKPEQKVLEIRDSGIGMTKAELINNLGTIAKSGTKAF 104
hTRAP1       LRHKLVSDGQALP---EMEIHLQTNAEKGTITIQDTGIGMTQEELVSNLGTIARSGSKAF 183
```

B

TRAP1 from different species:

```
Human   LRHKLVSDG-QALP----EMEIHLQTNAEKGTITIQDTGIGMTQEELVSNLGTIARSGSKAF 183
Mouse   LRHKLVCEG-QVLP----EMEIHLQTDAKKGTITIQDTGIGMTQEELVSNLGTIARSGSKAF 185
Fly     FRYTSLSAGGENLAGKDRPLEIRITTDKPLMQLIIQDTGIGMTKEELVSNLGTIARSGSKKF 166
Worm    RRYAELKGDVAEGP-----SEIRITTNKDKRTITFEDTGIGMNREDLVKFLGTIAKSGSKDF 140
```

THE JOURNAL OF BIOLOGICAL CHEMISTRY VOL. 283, NO. 20, pp. 13771–13779, May 16, 2008

Aberrant Folding of Pathogenic Parkin Mutants

*AGGREGATION VERSUS DEGRADATION**

Received for publication, September 6, 2007, and in revised form, March 14, 2008 Published, JBC Papers in Press, March 24, 2008, DOI 10.1074/jbc.M707494200

Julia S. Schlehe, A. Kathrin Lutz, Anna Pilsl, Kerstin Lämmermann, Katja Grgur, Iris H. Henn, Jörg Tatzelt, and Konstanze F. Winklhofer[1]

From the Department of Biochemistry, Neurobiochemistry, Adolf-Butenandt-Institute, Ludwig-Maximilians-University, Schillerstrasse 44, Munich D-80336, Germany

Loss-of-function mutations in the Parkin gene (*PARK2*) are responsible for the majority of autosomal recessive Parkinson disease. A growing body of evidence indicates that misfolding and aggregation of Parkin is a major mechanism of Parkin inactivation, accounting for the loss-of-function phenotype of various pathogenic Parkin mutants. Remarkably, wild-type Parkin is also prone to misfolding under certain cellular conditions, suggesting a more general role of Parkin in the pathogenesis of Parkinson disease. We now show that misfolding of Parkin can lead to two phenotypes: the formation of detergent-insoluble, aggregated Parkin, or destabilization of Parkin resulting in an accelerated proteasomal degradation. By combining two pathogenic Parkin mutations, we could demonstrate that destabilization of Parkin is dominant over the formation of detergent-insoluble Parkin aggregates. Furthermore, a comparative analysis with HHARI, an E3 ubiquitin ligase with an RBR domain highly homologous to that of Parkin, revealed that folding of Parkin is specifically dependent on the integrity of the C-terminal domain, but not on the presence of a putative PDZ-binding motif at the extreme C terminus.

Parkinson disease (PD)[2] is the second most common neurodegenerative disease after Alzheimer disease. Although most PD cases occur sporadically, familial variants share important features with sporadic PD, most notably the demise of dopaminergic neurons in the substantia nigra pars compacta. Consequently, insight into the function of PD-associated genes might promote our understanding of pathogenic mechanisms not only in familial, but also in sporadic PD. Five genes have unambiguously been linked to PD over the past decade, the genes encoding α-synuclein and LRRK2 for autosomal dominant PD, and those encoding Parkin, PINK1, and DJ-1 for autosomal recessive PD (reviewed in Refs. 1–3). So far, over a hundred different pathogenic mutations in the parkin gene have been identified, which account for the majority of autosomal recessive PD cases. Parkin is a member of the RBR (ring between ring fingers) protein family, characterized by the presence of two RING domains (really interesting new gene), which flank a cysteine-rich in-between RINGs (IBR) domain. Similarly to other RBR proteins, Parkin has an E3 ubiquitin ligase activity, mediating the attachment of ubiquitin to substrate proteins (4–6). Parkin can obviously mediate different modes of ubiquitylation, including monoubiquitylation, multiple monoubiquitylation, and polyubiquitylation both via lysine 48 and lysine 63, depending on the experimental conditions and the putative Parkin substrate analyzed (reviewed in Refs. 7 and 8). Importantly, the neuroprotective activity of Parkin seems to be associated with its ability to promote degradation-independent ubiquitylation (9, 10).

Different lines of evidence indicate that pathogenic parkin mutations result in a loss of Parkin function. Our initial studies revealed that misfolding and aggregation is characteristic for C-terminal deletion mutants of Parkin based on the following biochemical features specific for mutant Parkin: 1) insolubility in non-ionic and ionic detergents; 2) sedimentation in a sucrose step gradient; 3) resistance to a limited proteolytic digestion; 4) loss of membrane association; and 5) formation of scattered aggregates in cells determined by immunocytochemistry (11, 12). Alterations in the detergent solubility of Parkin and formation of Parkin aggregates/inclusion bodies have also been reported for various Parkin missense mutants (13–18). We also observed that even wild-type Parkin is prone to misfolding under severe oxidative stress (12). Remarkably, insoluble, catechol-modified Parkin could be detected in the substantia nigra of patients suffering from sporadic PD, suggesting a more general role of Parkin in the pathogenesis of PD (19). In support of this concept, the E3 ligase activity of Parkin has been shown to be impaired by nitrosative stress, and there is indeed evidence for the presence of *S*-nitrosylated Parkin in the brains of PD patients (20, 21).

Based on our finding that the deletion of C-terminal amino acids results in misfolding and aggregation of Parkin, we performed a comparative analysis of Parkin and HHARI, an E3 ubiquitin ligase with an highly homologous RBR domain. Although Parkin and HHARI share their propensity to misfold under severe oxidative stress, HHARI tolerates C-terminal deletions. However, the C-terminal domain of HHARI cannot rescue folding of C-terminally truncated Parkin. Instead, Parkin-HHARI fusion proteins are characterized by destabilization and rapid proteasomal degradation. This observation prompted us to analyze the two different phenotypes of

* This work was supported by the Deutsche Forschungsgemeinschaft (Sonderforschungsbereich 596) and the Max Planck Society. The costs of publication of this article were defrayed in part by the payment of page charges. This article must therefore be hereby marked "*advertisement*" in accordance with 18 U.S.C. Section 1734 solely to indicate this fact.

[1] To whom correspondence should be addressed: Tel.: 49-89-2180-75483; Fax: 49-89-2180-75415; E-mail: Konstanze.Winklhofer@med.uni-muenchen.de.

[2] The abbreviations used are: PD, Parkinson disease; E3, ubiquitin-protein isopeptide ligase; wt, wild type; HA, hemagglutinin; CMV, cytomegalovirus; pAb, polyclonal antibody; mAb, monoclonal antibody; HRP, horseradish peroxidase; PBS, phosphate-buffered saline; HHARI, human homologue of *Drosophila* ariadne.

Parkin misfolding, *i.e.* aggregation or destabilization, in more detail with a special focus on the specific role of the C terminus in Parkin folding.

EXPERIMENTAL PROCEDURES

Expression Constructs, Cell Culture, and Transfections—The following constructs were described previously: wild-type (wt) human Parkin, the W453X (Δ453–465), and R42P Parkin mutant, HA-ubiquitin, and IKKγ-FLAG (11, 12). Amino acid deletions and substitutions of Parkin were introduced by PCR cloning techniques: ΔFDV (Δ463–465), Parkin-*D.m.*CT (chimeric construct of human Parkin 1–450 and *Drosophila* Parkin 468–482), V465E, V465A, D464A, F463A, and R42P-W453X. All constructs were inserted into the pcDNA3.1 plasmid. The cDNA of HHARI was amplified by PCR from the RZPD clone IRATp970D0877D with the following primer pair: forward 5′-GCGGCTGAATTCGGATGGACTCGGACGAGGGCTAC-3′, reverse 5′-GGAGGCGGCCGCTCAGTCCTCAATGTAC-TCCCACAG-3′. The amplified fragment was digested with the restriction enzymes EcoRI and NotI and cloned into the pCMV-HA vector to obtain an N-terminally HA-tagged cDNA of HHARI. A C-terminal HHARI deletion mutant (Δ377–557) was generated using PCR cloning techniques, as well as fusion proteins of Parkin and HHARI: Parkin 1–449/HHARI 376–557 (449/376), Parkin 1–453/HHARI 379–557 (453/379), and Parkin 1–453/HHARI 395–557 (453/395). The plasmids encoding enhanced yellow fluorescent protein and cyan fluorescent protein (control protein) were purchased from Clontech. SH-SY5Y (German Resource Centre for Biological Material number ACC 209) and HEK293T (ATCC number CRL-1573) cells were cultivated and transfected with Lipofectamine/Plus (Invitrogen) as described earlier.

Antibodies and Reagents—The following antibodies were used: anti-Parkin rabbit polyclonal antibody (pAb) hP1 (12), anti-Parkin pAb #4230 (Cell Signaling), anti-Parkin mouse monoclonal antibody PRK8 (mAb, Millipore) anti-HA (mAb, Roche Applied Science), anti-active caspase-3 pAb (Promega, Madison, WI), Alexa 555-conjugated goat anti-rabbit pAb, anti-FLAG M2-HRP mAb, anti-HA-HRP mAb, anti-β-actin mAb (Sigma), anti-transferrin-receptor mAb (Zymed Laboratories Inc.), anti-glyceraldehyde-3-phosphate dehydrogenase mAb (Ambion), anti-LDH pAb (Santa Cruz Biotechnology, Santa Cruz, CA), anti-GFP mAb (BD Biosciences), horseradish peroxidase (HRP)-conjugated anti-mouse, and anti-rabbit IgG antibody (Promega). Kainate was purchased from Calbiochem, and complete protease inhibitor mixture from Roche Applied Science.

Western Blot Analysis—Proteins were analyzed by SDS-PAGE and Western blotting using polyvinylidene difluoride membranes (Millipore). The polyvinylidene difluoride membranes were blocked with blocking solution containing 5% nonfat dry milk in TBS containing 0.1% Tween 20 (TBS-T) for 1 h at room temperature and then incubated with the primary antibody in blocking solution for 16 h at 4 °C. After extensive washing with TBS-T, the membranes were incubated with HRP-conjugated secondary antibody for 40 min at room temperature. Following washing with TBS-T, the antigen was detected with the enhanced chemiluminescence (ECL) detection system (Amersham Biosciences).

Detergent Solubility Assay—As described earlier (22), transfected cells were harvested and lysed in detergent buffer (0.1% Triton X-100 or 0.5% Triton X-100/0.5% sodium deoxycholate in PBS). After centrifugation at 16,000 × *g* for 20 min at 4 °C, supernatant and pellet fractions were separated. The pellet fraction was washed with lysis buffer and resuspended in Laemmli sample buffer in a volume equal to the supernatant. To compare the relative distribution of the protein of interest, equal percentages of detergent-soluble and -insoluble fractions were analyzed by Western blotting.

Metabolic Labeling of Cellular Proteins—Cells were starved for 30 min in methionine-free Dulbecco's modified Eagle's medium (Invitrogen) and then labeled with 300 μCi/ml Pro-mix L-[^{35}S] *in vitro* cell label mix (Amersham Biosciences) in methionine-free Dulbecco's modified Eagle's medium for 1 h (pulse). When indicated, the proteasomal inhibitor MG132 (Calbiochem) was present during the pulse and chase periods. For the chase, labeling medium was removed, and cells were washed twice and then incubated in complete Dulbecco's modified Eagle's medium for 1 h. Radiolabeled cells were lysed in detergent buffer and fractionated into detergent-soluble and -insoluble fractions as described above. The supernatants were precleared with protein A-Sepharose (Pierce) for 30 min, the primary antibody hP1 was added, and the samples were incubated at 4 °C for 16 h. The antigen-antibody complexes were captured by the addition of immobilized protein A and then washed three times with detergent buffer. Proteins present in the immunoprecipitates were released from the protein A-Sepharose by the addition of Laemmli sample buffer containing 1% SDS and heating at 95 °C for 5 min. Immunoprecipitates were analyzed by SDS-PAGE. Gels were impregnated with Amplify (Amersham Biosciences), dried, and exposed to film.

Ubiquitylation Assay—Parkin or Parkin mutants, HA-ubiquitin, and when indicated IKKγ-FLAG were co-transfected in HEK293T cells. One day after transfection, protein lysates were prepared in denaturing lysis buffer (50 mM Tris/HCl, pH 7.4, 5 mM EDTA, 1% SDS, 15 units/ml DNase I, and protease inhibitor mixture) and incubated at 95 °C for 5 min. Protein extracts were diluted 1:10 with non-denaturing lysis buffer (50 mM Tris/HCl, pH 7.4, 300 mM NaCl, 5 mM EDTA, 1% Triton X-100, and protease inhibitor mixture). Immunoprecipitation of Parkin was performed with hP1 pAb followed by an incubation with protein A beads (Pierce); immunoprecipitation of IKKγ-FLAG was performed with M2 FLAG-agarose (Sigma). Immunoprecipitated proteins and input samples were analyzed by Western blotting using the antibodies indicated.

Immunocytochemistry and Fluorescence Microscopy—SH-SY5Y or HEK293T cells were grown on glass coverslips, transfected, fixed 1 day after transfection in 3% paraformaldehyde/sucrose in PBS for 10 min at room temperature, and permeabilized with 0.2% Triton X-100. Fixed cells were incubated with primary antibody (diluted in 1% bovine serum albumin and 10% goat serum) for 1 h at room temperature. After

washes with PBS, the coverslips were incubated with fluorescently labeled secondary antibodies for 1 h at room temperature. Finally, cells were embedded in Mowiol mounting medium (Calbiochem). Images were obtained on a Zeiss LSM 510 confocal microscope.

Membrane Fractionation—Transfected cells were harvested, incubated in hypo-osmotic buffer, and Dounce homogenized. After a low speed spin the homogenate was mixed with 60% iodixanol (Optiprep, Axis Shield) to obtain a final iodixanol concentration of 40%. The mixture was overlaid in a SW55 tube with 2.5 ml of 28% iodixanol diluted with TNE (50 mM Tris, 150 mM NaCl, pH 7.4) and 1 ml TNE on top. After ultracentrifugation in an MLS 50 swing-out rotor (Beckman) at 165,000 × *g* for 3 h, fractions were collected from top to bottom. Aliquots of these fractions were analyzed by Western blotting.

Fractionation of Mouse Brain Tissue—Mouse brains were isolated from 2-month-old mice, homogenized with 10 strokes in a glass potter in hypotonic buffer (20 mM citrate, 1 mM EDTA, and protease inhibitor mix). The tissue was further processed by a step of freeze-thaw using liquid nitrogen. After addition of 1% Brij-53 (Pierce), homogenates were low spin centrifuged to yield a post-nuclear supernatant. Glycerol was added to the post-nuclear supernatant to a final concentration of 5%. An ultracentrifugation step of 130,000 × *g* for 60 min at 4 °C resulted in a cytosolic fraction and a membrane fraction. The membrane fraction was resuspended in hypotonic buffer containing 1% Triton X-100 and ultracentrifuged for another 30 min. The supernatant and cytosolic fractions were analyzed by Western blotting.

Apoptosis Assay—Activation of caspase-3 was determined as described previously (23). Briefly, SH-SY5Y cells were grown on glass coverslips. 24 h after transfection, cells were incubated with kainate (500 μM) for 3 h. The cells were then fixed with 3% paraformaldehyde for 20 min, permeabilized with 0.2% Triton X-100 for 10 min at room temperature, and blocked with 1% bovine serum albumin in PBS for 1 h at room temperature. Fixed cells were incubated with anti-active caspase-3 antibody overnight at 4 °C, washed, and incubated with Alexa 555-conjugated secondary antibody for 1 h at room temperature. After extensive washing, cells were mounted onto glass slides and examined by fluorescence microscopy using a Zeiss Axioscope 2 plus microscope. To detect cells undergoing apoptosis, the number of activated caspase-3-positive cells out of at least 300 transfected cells was determined. Quantifications were based on at least three independent experiments.

Stress Treatment and Proteasomal Inhibition—To induce oxidative stress, transfected cells were incubated with 10 or 20 mM H_2O_2 in PBS for 30 min, harvested, and lysed in detergent buffer containing 0.5% Triton X-100/sodium deoxycholate in PBS. For inhibition of the proteasome, cells were treated with 5 μM MG132 (Calbiochem) for 16 h or 30 μM for 1 h during metabolic labeling.

Statistical Analysis—Data were expressed as means ± S.E. All transfections were performed in triplicates and repeated at least three times. Quantification of Western blots was performed with the FluoChem 8900 detection system and the Alpha Ease FC software. Statistical analysis among groups was performed using one-way analysis of variance. *p* values were <0.05.

RESULTS

HHARI Is Sensitive to Stress-induced Misfolding but Tolerates C-terminal Deletions—Another E3 ubiquitin ligase harboring an RBR domain is encoded by the human homologue of *Drosophila* ariadne (HHARI) gene. In comparison to Parkin, HHARI contains a glycine-rich region but lacks the N-terminal UBL domain (Fig. 1*A*). Recently, the solution structure of HHARI RING2 was determined by NMR studies, revealing a distinct topology of RING2 from classic RINGs (24). Based on the high sequence homology of RING2 between HHARI and Parkin, Capili and coworkers proposed a similar fold for Parkin RING2. To test whether the propensity of Parkin to misfold is a common feature of RBR proteins or a unique feature of Parkin, we generated a deletion mutant of HHARI (HHARI P378X), which was truncated behind the RBR domain, similarly to the pathogenic Parkin W453X mutant. A detergent solubility assay after expression of the mutants in HEK293T cells revealed that in comparison to wild-type (wt) HHARI there was no significant increase in the detergent-insoluble fraction when P378X was analyzed (Fig. 1*B*, *right panel*). In contrast, the Parkin W453X mutant almost quantitatively adopted an insoluble conformation under the same conditions (Fig. 1*B*, *left panel*), indicating that HHARI is significantly less sensitive to C-terminal truncations. Next we analyzed the propensity of Parkin and HHARI to misfold under severe oxidative stress. HEK293T cells transiently expressing wt Parkin or wt HHARI were subjected to hydrogen peroxide treatment and analyzed by the detergent solubility assay. As shown in Fig. 1*C*, high level oxidative stress induced the misfolding of both Parkin and HHARI, whereas yellow fluorescent protein was not affected under the same conditions. In conclusion, Parkin and HHARI share the sensitivity to stress-induced misfolding, which seems to be attributable to the cysteine-rich RBR domain. The arrangement of cysteines within RING domains is crucial to stabilize the native conformation, thus oxidation of critical cysteine residues will result in a collapse of the tertiary structure. However, the sensitivity to C-terminal deletions seems to be specific to Parkin.

The C-terminal Portion Adjacent to RING2 of HHARI Cannot Replace That of Parkin—To better understand the role of the C terminus in Parkin folding, we addressed the question of whether the C-terminal domain distal to RING2 of HHARI can compensate for the folding defect of C-terminally truncated Parkin. The rationale of this approach was the observation that folding of non-classic RING domains extends into the adjacent C-terminal region to stabilize RING2 (24). Because RING2 of Parkin and HHARI are supposed to share the tertiary structure, it is conceivable that the C-terminal domain of HHARI allows stabilization of Parkin RING2. To address this possibility experimentally, we generated three Parkin-HHARI chimeric constructs, differing in the length of either the Parkin or HHARI fragment (449/376, 453/379, and 453/395, Fig. 1*D*). HEK293T cells were transiently transfected with the chimeric constructs and analyzed by a detergent solubility assay 1 day after transfection. Surprisingly, we could not detect either of the chimeric proteins in a Western blot analysis. To test the

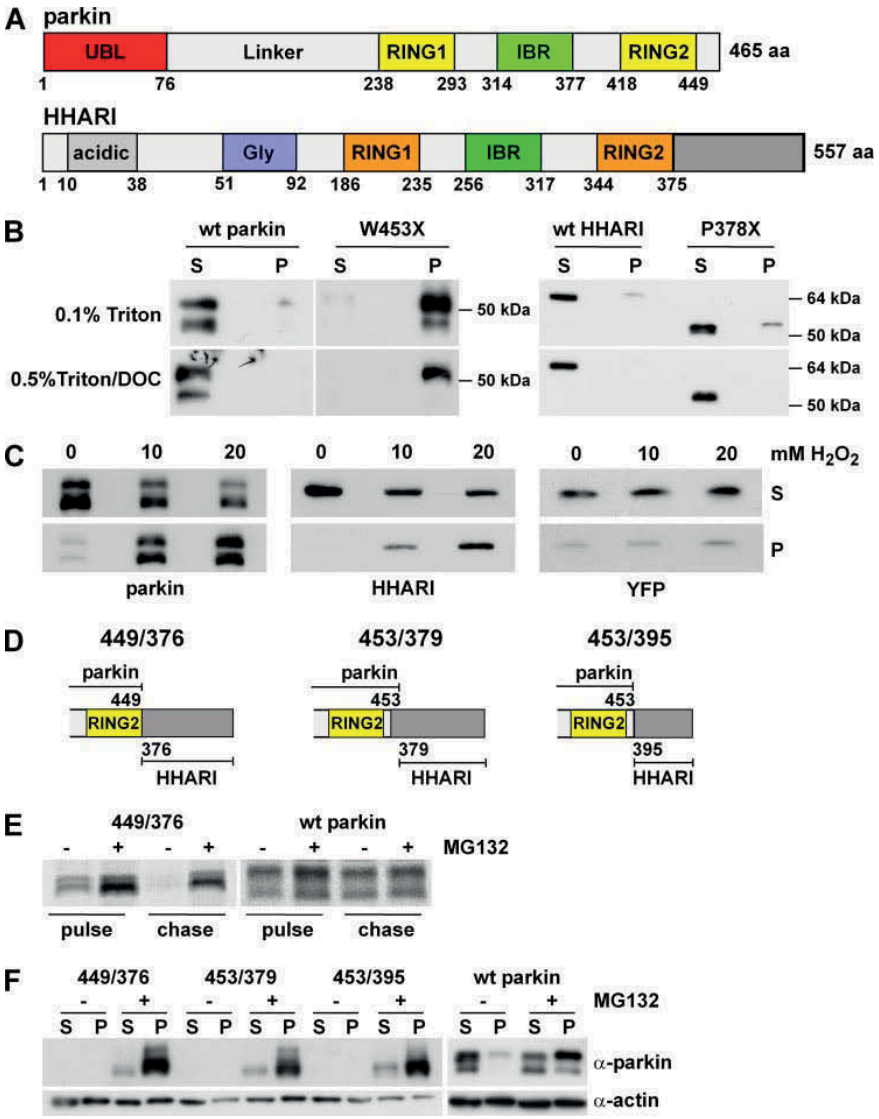

FIGURE 1. **Folding characteristics of Parkin and HHARI.** *A*, modular structure of Parkin and HHARI. *B*, Parkin is particularly vulnerable to C-terminal truncations. HEK293T cells were transiently transfected with wild-type (*wt*) and truncated mutants of Parkin or HA-tagged HHARI, harvested, lysed in 0.1% Triton X-100 or 0.5% Triton X-100/0.5% deoxycholate (*DOC*). Detergent-soluble (*S*) and insoluble (*P*) fractions were obtained by centrifugation and analyzed by Western blotting. Parkin was detected by the hP1 antiserum, and HHARI by an anti-HA monoclonal antibody. *C*, Parkin and HHARI are similarly vulnerable to misfolding induced by oxidative stress. HEK293T cells transiently expressing Parkin, HHARI, or yellow fluorescent protein (as a non-RBR protein) were treated with H_2O_2 at the concentrations indicated. After 30 min, cells were harvested, lysed in 0.5% Triton X-100/0.5% deoxycholate (*DOC*), and analyzed by the detergent solubility assay and Western blotting. *D–F*, chimeric Parkin proteins containing the C-terminal portion of HHARI adjacent to RING2 are detergent-insoluble and rapidly degraded by the proteasome. *D*, schematic presentation of the chimeric Parkin/HHARI proteins. *E*, HEK 293T cells transiently expressing the Parkin-HHARI construct 449/376 or wt Parkin were metabolically labeled with medium containing [^{35}S]methionine for 1 h (pulse) and chased for 1 h in the presence or absence of the proteasomal inhibitor MG132. The proteins were immunoprecipitated using the anti-Parkin antiserum hP1. *F*, the three chimeric Parkin/HHARI proteins and wt Parkin were transiently expressed in HEK293T cells in the presence or absence of the proteasomal inhibitor MG132 (5 μM, 16 h) and analyzed by the detergent solubility assay as described under *B*.

possibility of an increased proteasomal degradation of the chimeric proteins, we performed pulse/chase experiments in 449/376-expressing cells metabolically labeled with [^{35}S]methionine and analyzed the chimeric protein by immunoprecipitation. Indeed, >50% of the chimeric protein was degraded during the pulse (60 min), and after a chase of 60 min the protein could only be detected in the presence of MG132 (Fig. 1*E*). We then repeated the Western blot analysis and incubated the transfected cells in the presence of the proteasomal inhibitor MG132 for 16 h. It turned out that the chimeric proteins could be stabilized by MG132, but all of them were present in a predominantly detergent-insoluble conformation (Fig. 1*F*). Thus, the C-terminal domain of HHARI could not compensate for the folding defect observed for C-terminal deletion mutants of Parkin. Moreover, replacement of the C-terminal domain of Parkin next to RING2 by that of HHARI not only induced the formation of detergent-insoluble Parkin, but also led to a destabilization of the chimeric protein. These observations indicate that the C-terminal domain of Parkin exerts an essential and specific function in folding and stabilization of Parkin.

Misfolding of Pathogenic Parkin Mutants Can Lead to Aggregation or Destabilization of Parkin—The destabilization of Parkin-HHARI fusion proteins reminded us of some pathogenic Parkin mutants, which are also characterized by an accelerated proteasomal degradation. We reported previously that missense mutations within the N-terminal UBL domain induce a destabilization of Parkin (11). We now wondered whether this destabilization might be another manifestation of Parkin misfolding. To test this possibility, we expressed the R42P Parkin mutant in the absence and in the presence of the proteasomal inhibitor MG132. Indeed, the larger Parkin species (52 kDa), which comprises the UBL and thus the pathogenic mutation, was only detectable in the presence of the proteasomal inhibitor and predominantly occurred in the detergent-insoluble fraction (Fig. 2*A*). Please note that the smaller Parkin species (42 kDa) is generated due to the presence of an internal translation initiation site at codon 80, consequently, the smaller Parkin species lacks the UBL domain (11). This experiment indicated that the R42P mutant is degraded by the proteasome, because it obviously

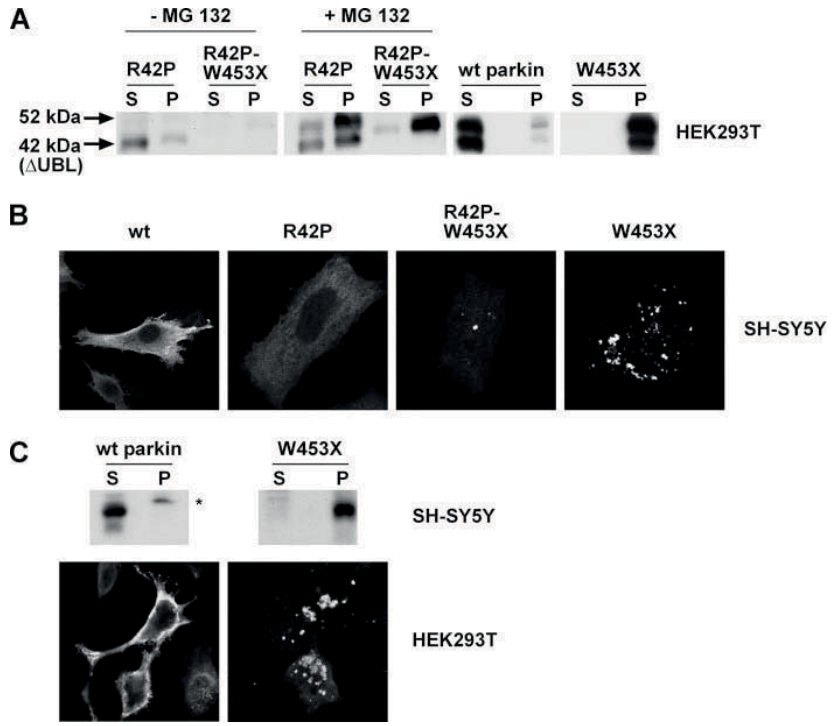

FIGURE 2. **Two phenotypes of Parkin misfolding.** *A*, HEK293T cells were transiently transfected with wt or mutant Parkin and treated the proteasomal inhibitor MG132 (5 μM, 16 h). Parkin present in the soluble and insoluble fraction was analyzed by the Western blotting as described under Fig. 1*B*. *B*, SH-SY5Y cells transiently expressing wt Parkin or the mutants indicated were analyzed by indirect immunofluorescence using the anti-parkin antiserum hP1. *C*, the misfolding phenotype of mutant Parkin is not cell type-specific. *Upper panel*: SH-SY5Y were transiently transfected with either wt or W453X Parkin. A detergent solubility assay was performed as described under Fig. 1*B*. The *asterisk* (*left panel*) indicates a non-specific band. *Lower panel*: HEK293T cells transiently expressing wt or W453X Parkin were analyzed by indirect immunofluorescence using the anti-Parkin antiserum hP1.

does not adopt a native conformation, similarly to the chimeric Parkin-HHARI constructs. Given that the formation of relatively stable detergent-insoluble aggregates is also a consequence of Parkin misfolding, exemplified by C-terminal deletion mutants and various point mutants, we asked which phenotype of Parkin misfolding might be dominant over the other. To this end, we generated the R42P-W453X double Parkin mutant. To facilitate the interpretation of the results, the internal translation initiation site, *i.e.* methionine at position 80 was replaced by threonine, which occurs at position 80 in murine Parkin. Remarkably, the R42P-W453X double Parkin mutant could be detected only in the presence of the proteasomal inhibitor MG132 in an almost exclusively detergent-insoluble conformation, indicating that destabilization of Parkin is dominant over the formation of stable aggregates (Fig. 2*A*). In line with the detergent solubility assay, immunofluorescence experiments performed with SH-SY5Y cells showed typical scattered aggregates of the W453X Parkin mutant, but almost no expression of the R42P-W453X double Parkin mutant under steady state conditions (Fig. 2*B*). The weak staining of R42P-expressing cells can be explained by the presence of the smaller Parkin species, which lacks the R42P mutation and therefore is not misfolded. We used SH-SY5Y cells for immunocytochemistry, because HEK293T cells display a disadvantageous nucleus-to-cytoplasm ratio for the analysis of cytosolic proteins. To provide evidence that the misfolding phenotype of Parkin mutants is not a cell type-specific phenomenon, we performed immunofluorescence experiments also in HEK293T cells and detergent solubility assays in SH-SY5Y cells (Fig. 2*C*).

The Putative PDZ-binding Motif at the C Terminus Is Dispensable for Parkin Folding—In previous studies we showed that pathogenic C-terminal truncations lead to misfolding and aggregation of Parkin (11, 12). Remarkably, the deletion of three C-terminal amino acids was sufficient to drastically interfere with the native folding of Parkin, leading to the formation of detergent-insoluble, aggregated Parkin (Fig. 3*A*). It has been suggested that the three amino acids (FDV) at the extreme C terminus of Parkin function as a PDZ-binding motif, which can mediate an interaction with the PDZ domain-containing proteins CASK and PICK1 (25, 26). We therefore addressed the question of whether this motif is necessary for Parkin to obtain or stabilize its native conformation. Interestingly, whereas other functional domains of Parkin, such as the UBL, RING1, RING2, and the IBR, are highly conserved between species, the FDV motif is present only in mammalian species, but not in non-mammalian vertebrates (*Gallus gallus*, *Fugu rubripes*, and *Danio rerio*) or non-vertebrates (*Drosophila melanogaster*, *Anopheles gambiae*, and *Caenorhabditis elegans*, Fig. 3*B*). The FDV sequence of Parkin falls into the class II PDZ-binding motif Φ-*X*-Φ, where Φ is a hydrophobic amino acid and *X* is any amino acid. To destroy the putative PDZ-binding motif, we replaced valine at position 465 by glutamic acid (V465E), a mutation that has been reported previously to disrupt PDZ-dependent interactions (27). In addition, we replaced the C-terminal domain of human Parkin (amino acids 451–465) by that of *Drosophila melanogaster* Parkin (amino acids 468–482), which lacks the C-terminal valine residue and thus a functional PDZ-binding motif (Parkin-*D.m.*CT). The detergent solubility assay revealed that both PDZ mutants, V465E and Parkin-*D.m.*CT, were almost entirely found in the detergent-soluble fraction, similarly to wt Parkin (Fig. 3*C*, *upper panel*). In line with this observation, the indirect immunofluorescence analysis did not show differences in the cellular distribution of wt Parkin and the C-terminal Parkin mutants (Fig. 3*C*, *lower panel*). To determine which amino acid of the FDV motif is crucial for Parkin folding, we replaced either phenylalanine, aspartate, or valine with alanine (V465A, D464A, and F463A). We observed that only the F463A mutant adopts a detergent-

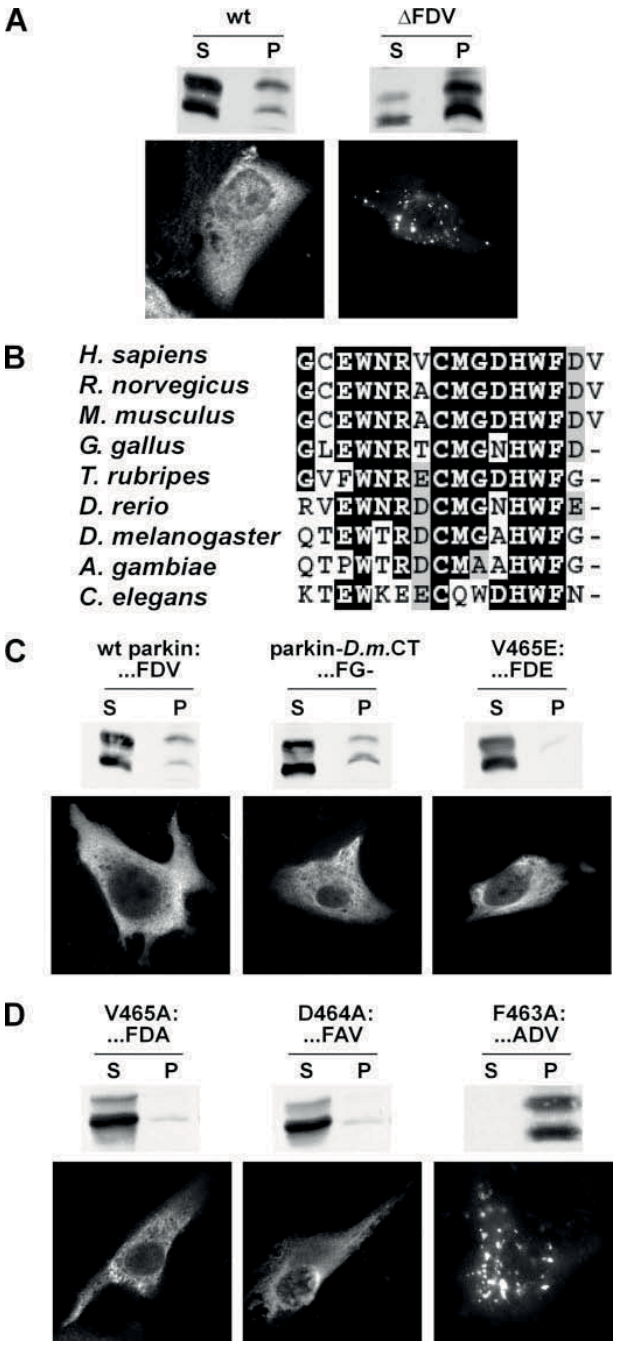

FIGURE 3. **Role of the putative PDZ-binding motif in Parkin folding.** *A*, deletion of the last three amino acids (FDV), comprising a putative PDZ-binding motif, leads to misfolding of Parkin. HEK293T (detergent solubility assay) or SH-SY5Y cells (indirect immunofluorescence) were transfected with wt Parkin or C-terminally truncated Parkin (ΔFDV) and analyzed as described in Fig. 2 (*A* and *B*). *B*, alignment of Parkin C termini of different species. The FDV motif is conserved only in mammalian species. *C*, the integrity of the FDV motif is dispensable for Parkin folding. HEK293T and SH-SY5Y cells were transiently transfected with wt Parkin or the Parkin mutants Parkin-*D.m.*CT (the last 15 amino acids of human wt Parkin replaced by the respective C-terminal amino acids of *Drosophila* parkin) or V465E (putative PDZ-binding motif disrupted) and analyzed by the detergent solubility assay and indirect immunofluorescence. *D*, the presence of phenylalanine at position 463 is crucial for Parkin folding. HEK293T and SH-SY5Y cells were analyzed as described above.

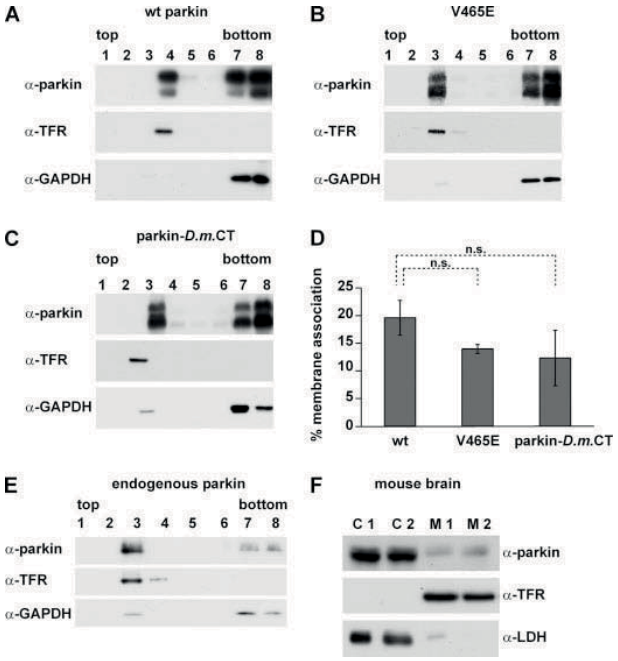

FIGURE 4. **The putative PDZ-binding motif is not necessary for the binding of Parkin to cellular membranes.** *A–C*, HEK293T cells were transiently transfected with wt Parkin or the Parkin mutants indicated. Total cell homogenates were subjected to density gradient centrifugation, and eight fractions were analyzed by Western blotting using antibodies against Parkin, the cytosolic protein glyceraldehyde-3-phosphate dehydrogenase (*GAPDH*), or the transmembrane protein transferrin receptor (*TFR*). *D*, quantification of membrane-associated Parkin or Parkin mutants (three independent experiments). *Error bars* indicate ± S.E.; *n.s.*, not significant. *E* and *F*, membrane association of endogenous Parkin. *E*, homogenates of SH-SY5Y cells were subjected to density gradient centrifugation and analyzed as described above. *F*, homogenates of mouse brain tissue were differentially centrifuged to enrich a microsomal fraction. To identify cytosolic (*C*)- and membrane (*M*)-enriched fractions, transferrin receptor (*TFR*) and lactate dehydrogenase (*LDH*) antibodies were used.

insoluble conformation and forms aggregates in cells, indicating that the phenylalanine at position 463 is essential (Fig. 3*D*). Of note, in contrast to the putative PDZ-binding motif, this phenylalanine is conserved between all species (Fig. 3*B*).

Membrane Association of Parkin Is Independent on the Integrity of the Putative PDZ-binding Motif—PDZ domains act as modules and scaffolds for protein-protein interactions and play a prominent role in organizing protein complexes at the plasma membrane. We and others have observed that Parkin can associate with membranes (11, 25, 28–30), which is recapitulated here for endogenous Parkin in SH-SY5Y cells (Fig. 4*E*) and mouse Parkin in brain lysates (Fig. 4*F*). Therefore, we analyzed a possible role of the putative PDZ-binding motif in targeting Parkin to membranes. HEK293T cells were transiently transfected with wt Parkin or the C-terminal PDZ Parkin mutants (V465E, Parkin-*D.m.*CT), and cell homogenates were fractionated by a density gradient centrifugation. The majority of wt Parkin was found in the bottom fractions, representing the cytosolic fractions. However, a fraction of wt Parkin colocalized with the transferrin receptor, indicating membrane association of Parkin (Fig. 4*A*). The Parkin constructs with a mutated PDZ-binding motif, Parkin-*D.m.*CT and V465E, were not significantly impaired in their ability to associate with membranes,

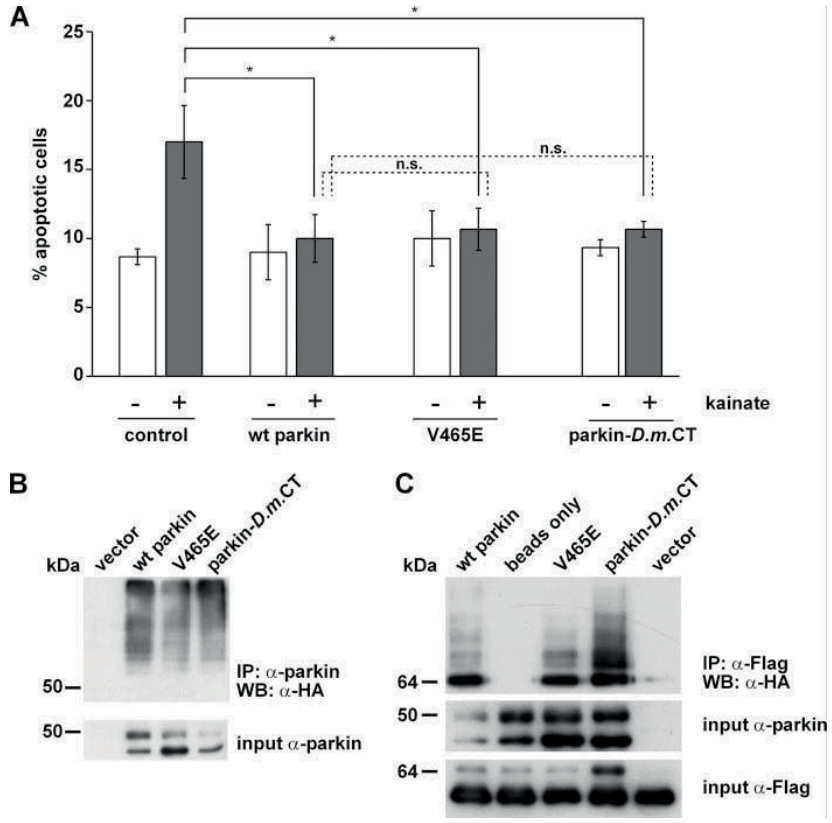

FIGURE 5. *A*, the neuroprotective activity of Parkin is not dependent on the putative PDZ-binding motif. SH-SY5Y cells were co-transfected with the indicated Parkin construct and yellow fluorescent protein to visualize transfected cells. 24 h after transfection, cells were incubated with 500 μM kainate for 3 h at 37 °C, fixed, permeabilized, and analyzed by indirect immunofluorescence using an antibody against active caspase 3. Shown is the percentage of apoptotic cells among the transfected cells. *, $p < 0.05$; *n.s.*, not significant. *B*, ubiquitylation of Parkin and PDZ Parkin mutants. HEK293T cells were transfected with the indicated Parkin constructs and HA-tagged ubiquitin. Parkin was immunoprecipitated under denaturing conditions and analyzed by Western blotting using an anti-HA antibody. *C*, ubiquitylation of IKKγ by Parkin and PDZ Parkin mutants. HEK293T cells co-expressing wt or mutant Parkin, IKKγ-FLAG, and HA-ubiquitin and were lysed, and IKKγ was immunoprecipitated with an anti-FLAG antibody under denaturing conditions. The immunocomplexes were analyzed by Western blotting using an anti-HA antibody.

suggesting that the integrity of the putative PDZ binding motif is not essential for membrane targeting, at least under steady-state conditions (Fig. 4, *B–D*). Of note, the fraction of membrane-associated endogenous parkin might even be higher, due to saturation of Parkin-binding sites at the membrane.

Parkin Lacking a Functional PDZ-binding Motif at the C Terminus Is Not Impaired in Its Neuroprotective Capacity—Parkin has been shown to protect neurons from stress-induced cell death in various model systems (reviewed in Refs. 7 and 31). We recently showed that activation of the NF-κB signaling pathway is an essential prerequisite for the neuroprotective capacity of Parkin (10). Given that PDZ domains have the capacity to assemble components of signaling pathways to specific subcellular sites, we reasoned that the putative PDZ-binding domain might play a role in orchestrating signaling pathways that mediate the neuroprotective activity of Parkin. To test this hypothesis, we analyzed the cytoprotective activity of Parkin mutants with a non-functional PDZ-binding motif. For this assay we used SH-SY5Y cells, which are characterized by a neuron-like phenotype and a dopaminergic capacity. SH-SY5Y cells transiently expressing wt or mutant Parkin were incubated in the presence or absence of kainate, an excitotoxin that activates ionotrophic glutamate receptors. Apoptotic cells were identified by indirect immunofluorescence using an antibody specific for activated caspase-3. As shown in Fig. 5*A*, the protective activity of V465E and Parkin-*D.m.*CT in response to kainate treatment was comparable to that of wt Parkin. Thus, the putative PDZ-binding motif at the C terminus of Parkin seems not to contribute to the neuroprotective activity of Parkin. To extend the functional analysis, we performed ubiquitylation experiments. Wt or mutant Parkin was co-expressed with HA-tagged ubiquitin in HEK293T cells, immunoprecipitated with an anti-Parkin antibody, and subjected to Western blotting using an anti-HA antibody. No significant differences in the amount of ubiquitylated Parkin could be detected (Fig. 5*B*). Next we tested the activity of wt and mutant Parkin to enhance ubiquitylation of IKKγ/NEMO (10). HEK293T cells were co-transfected with wt or mutant Parkin and FLAG-tagged IKKγ/NEMO and HA-tagged ubiquitin. Immunoprecipitation under denaturing conditions was performed with an anti-FLAG antibody, and precipitated proteins were subjected to a Western blot analysis using an anti-HA antibody. This experiment revealed that destroying the putative PDZ-binding motif at the C terminus does not interfere with the capacity of Parkin to promote ubiquitylation of IKKγ/NEMO (Fig. 5*C*). Ubiquitylation of IKKγ/NEMO was even higher in the presence of the C-terminal Parkin mutants; however, this observation can be explained by differences in the Parkin expression level. Nevertheless, the ubiquitylation activity of Parkin seems not to be dependent on the presence of the C-terminal PDZ-binding motif.

DISCUSSION

The formation of misfolded protein conformers is a common pathological denominator in various neurodegenerative diseases. PD is a paradigm for the possible consequences of protein misfolding. Misfolding can induce a gain of toxic function, exemplified by α-synuclein, a loss of physiological function, as shown for Parkin, or even a combination of both, which seems to apply to α-synuclein (reviewed in Ref. 32). Misfolding of Parkin induced by pathogenic mutations or cellular stress has been established as a major mechanism of Parkin inactivation,

accentuating a possible pathological role of Parkin even in sporadic PD (11–21, 33–35). It is obvious that the high cysteine content found in the RBR domain predisposes Parkin to oxidative stress-induced inactivation and misfolding, a phenomenon that has recently been shown experimentally (36). Interestingly, in comparison to other RBR proteins Parkin seems to be uniquely sensitive to dopamine-induced inactivation (33, 36).

Unfortunately, the three-dimensional structure of full-length Parkin has not been determined so far, which might be due to the high propensity of Parkin to misfold and the consequent difficulties in generating sufficient amounts of natively folded recombinant Parkin. In this study we describe two different manifestations of Parkin misfolding, leading to a loss of Parkin function. Pathogenic mutations leading to conformational alterations can induce either the formation of detergent-insoluble, aggregated Parkin, or the destabilization of Parkin, resulting in its rapid proteasomal degradation. In addition, we addressed intrinsic determinants of Parkin folding with a special focus on the role of the C-terminal domain.

Role of the Putative PDZ-binding Motif in Parkin Folding—Based on our previous observation that the deletion of more than two C-terminal amino acids drastically interfered with the folding of Parkin, we concentrated on a possible functional role of the last three C-terminal amino acids of Parkin, which have been proposed to constitute a PDZ-binding motif (25). Whereas all the other domains are highly conserved between species, the putative PDZ-binding motif can only be found in mammalian species, compatible with an additional function evolved in mammals. Replacing the C-terminal domain of human Parkin by that of *Drosophila* Parkin (Parkin-*D.m.*CT), which lacks a PDZ-binding motif as well as converting the predicted PDZ-binding motif into a non-functional one (V465E), did not alter the folding properties of Parkin. Because interactions between PDZ proteins and PDZ-binding motifs mediate the assembly of protein complexes specifically at membranes, we expected that the putative PDZ-binding domain of Parkin is involved in the targeting of Parkin to membranes. However, we could not detect significant differences between wild-type Parkin and mutant Parkin (Parkin-*D.m.*CT, V465E) in binding to cellular membranes determined by density gradient centrifugation under steady-state conditions. This observation does not exclude the possibility that, under certain conditions, for example in response to a specific stimulus, a transient PDZ-dependent interaction occurs. To determine the functional relevance of the putative PDZ-binding domain, we tested the neuroprotective capacity of the PDZ Parkin mutants in comparison to wild-type Parkin. Both mutants lacking a functional PDZ-binding domain (Parkin-*D.m.*CT and V465E) protected neuronal cells from stress-induced cell death similarly to wild-type Parkin. In line with this observation, the ubiquitylation activity of the PDZ Parkin mutants was not impaired in comparison to wild-type Parkin. Our results allow two interpretations. Either the C-terminal FDV motif is not an authentic PDZ-binding domain (no conservation between species, only low stringency consensus sequence), or an interaction of Parkin with PDZ proteins, such as CASK or PICK1 (25, 26), is associated with other properties or activities of Parkin than those we addressed in our study (folding, membrane association, neuroprotective activity).

The Two Facets of Parkin Misfolding: Aggregation and Degradation—To further address the role of the C-terminal domain in Parkin folding, we performed a comparative analysis between Parkin and HHARI, which also contains an RBR domain close to the C terminus. We found that HHARI is sensitive to oxidative stress-induced misfolding similarly to Parkin, which is in line with recent observations (33, 36). However, the propensity to misfold upon C-terminal truncations was specific for Parkin. We then replaced the C-terminal portion of Parkin by that of HHARI, to test whether the tolerance to C-terminal truncations can be transferred to Parkin. This strategy was based on the commonly held view that RING2 of the RBR domain extends into the adjacent C-terminal region to stabilize its fold (24). Surprisingly, different strategies to generate such a chimeric Parkin-HHARI protein resulted in the formation of unstable, misfolded conformers. Thus, although the RBR domain of Parkin and HHARI show a high degree of homology and possibly the same fold, the role of the C terminus in Parkin folding is unique.

Destabilization of Parkin is also induced by some pathogenic missense mutations within the UBL domain (11). The behavior of the chimeric Parkin-HHARI proteins led us to uncover the reason for the instability of the R42P mutant, which we described previously as the most unstable UBL mutant. Our results indicate that this mutant is rapidly degraded by the proteasome due to the formation of a non-native conformer. Our findings are in line with a recent study on the folding and structure of the UBL domain of Parkin. Safadi and Shaw showed by NMR spectroscopy that the R42P mutation causes the complete unfolding of the UBL (37).

In conclusion, our study demonstrates that conformational alterations of Parkin induced by pathogenic mutations can lead to either a decrease in detergent solubility and aggregation or destabilization of Parkin. Although our observations are based on overexpression of pathogenic Parkin mutants and aggregate formation not necessarily occurs in patients (38), there are consistent biochemical differences between wild-type Parkin and mutant Parkin, which are not dependent on expression levels: alterations in detergent solubility, sedimentation in a sucrose gradient, and resistance to a limited proteolytic digestion (C-terminal deletion mutants) as well as rapid proteasomal degradation (R42P). The fact that misfolding of Parkin can occur in two facets, aggregation or destabilization, is an interesting feature, which needs further mechanistic analysis. Conceptually, pathogenic mutations might induce the formation of different Parkin conformers or might affect Parkin folding at distinct stages of the folding pathway.

Acknowledgments—We are grateful to Christian Haass for continuous support and helpful discussions. We thank Anita Schlierf, Nicole Exner, Michael Willem, Siegfried Ussar and Angelika S. Rambold for advice and experimental help.

REFERENCES

1. Farrer, M. J. (2006) *Nature Rev.* **7**, 306–318
2. Moore, D. J., West, A. B., Dawson, V. L., and Dawson, T. M. (2005) *Annu.*

Rev. Neurosci. **28,** 57–87
3. Wood-Kaczmar, A., Gandhi, S., and Wood, N. W. (2006) *Trends Mol. Med.* **12,** 521–528
4. Imai, Y., Soda, M., and Takahashi, R. (2000) *J. Biol. Chem.* **275,** 35661–35664
5. Shimura, H., Hattori, N., Kubo, S., Mizuno, Y., Asakawa, S., Minoshima, S., Shimizu, N., Iwai, K., Chiba, T., Tanaka, K., and Suzuki, T. (2000) *Nat. Genet.* **25,** 302–305
6. Zhang, Y., Gao, J., Chung, K. K., Huang, H., Dawson, V. L., and Dawson, T. M. (2000) *Proc. Natl. Acad. Sci. U. S. A.* **97,** 13354–13359
7. Moore, D. J. (2006) *Biochem. Soc. Trans.* **34,** 749–753
8. Winklhofer, K. F. (2007) *Expert Opin. Ther. Targets* **11,** 1543–1552
9. Fallon, L., Belanger, C. M., Corera, A. T., Kontogiannea, M., Regan-Klapisz, E., Moreau, F., Voortman, J., Haber, M., Rouleau, G., Thorarinsdottir, T., Brice, A., van Bergen En Henegouwen, P. M., and Fon, E. A. (2006) *Nat. Cell Biol.* **8,** 834–842
10. Henn, I. H., Bouman, L., Schlehe, J. S., Schlierf, A., Schramm, J. E., Wegener, E., Nakaso, K., Culmsee, C., Berninger, B., Krappmann, D., Tatzelt, J., and Winklhofer, K. F. (2007) *J. Neurosci.* **27,** 1868–1878
11. Henn, I. H., Gostner, J. M., Tatzelt, J., and Winklhofer, K. F. (2005) *J. Neurochem.* **92,** 114–122
12. Winklhofer, K. F., Henn, I. H., Kay-Jackson, P., Heller, U., and Tatzelt, J. (2003) *J. Biol. Chem.* **278,** 47199–47208
13. Cookson, M. R., Lockhart, P. J., McLendon, C., O'Farrell, C., Schlossmacher, M., and Farrer, M. J. (2003) *Hum. Mol. Genet.* **12,** 2957–2965
14. Gu, W. J., Corti, O., Araujo, F., Hampe, C., Jacquier, S., Lucking, C. B., Abbas, N., Duyckaerts, C., Rooney, T., Pradier, L., Ruberg, M., and Brice, A. (2003) *Neurobiol. Dis.* **14,** 357–364
15. Hampe, C., Ardila-Osorio, H., Fournier, M., Brice, A., and Corti, O. (2006) *Hum. Mol. Genet.* **15,** 2059–2075
16. Kyratzi, E., Pavlaki, M., Kontostavlaki, D., Rideout, H. J., and Stefanis, L. (2007) *J. Neurochem.* **102,** 1292–1303
17. Sriram, S. R., Li, X., Ko, H. S., Chung, K. K., Wong, E., Lim, K. L., Dawson, V. L., and Dawson, T. M. (2005) *Hum. Mol. Genet.* **14,** 2571–2586
18. Wang, C., Tan, J. M., Ho, M. W., Zaiden, N., Wong, S. H., Chew, C. L., Eng, P. W., Lim, T. M., Dawson, T. M., and Lim, K. L. (2005) *J. Neurochem.* **93,** 422–431
19. LaVoie, M. J., Ostaszewski, B. L., Weihofen, A., Schlossmacher, M. G., and Selkoe, D. J. (2005) *Nat. Med.* **11,** 1214–1221
20. Chung, K. K., Thomas, B., Li, X., Pletnikova, O., Troncoso, J. C., Marsh, L., Dawson, V. L., and Dawson, T. M. (2004) *Science* **304,** 1328–1331
21. Yao, D., Gu, Z., Nakamura, T., Shi, Z. Q., Ma, Y., Gaston, B., Palmer, L. A., Rockenstein, E. M., Zhang, Z., Masliah, E., Uehara, T., and Lipton, S. A. (2004) *Proc. Natl. Acad. Sci. U. S. A.* **101,** 10810–10814
22. Tatzelt, J., Prusiner, S. B., and Welch, W. J. (1996) *EMBO J.* **15,** 6363–6373
23. Rambold, A. S., Miesbauer, M., Rapaport, D., Bartke, T., Baier, M., Winklhofer, K. F., and Tatzelt, J. (2006) *Mol. Biol. Cell* **17,** 3356–3368
24. Capili, A. D., Edghill, E. L., Wu, K., and Borden, K. L. (2004) *J. Mol. Biol.* **340,** 1117–1129
25. Fallon, L., Moreau, F., Croft, B. G., Labib, N., Gu, W. J., and Fon, E. A. (2002) *J. Biol. Chem.* **277,** 486–491
26. Joch, M., Ase, A. R., Chen, C. X., MacDonald, P. A., Kontogiannea, M., Corera, A. T., Brice, A., Seguela, P., and Fon, E. A. (2007) *Mol. Biol. Cell* **18,** 3105–3118
27. Penzes, P., Johnson, R. C., Sattler, R., Zhang, X., Huganir, R. L., Kambampati, V., Mains, R. E., and Eipper, B. A. (2001) *Neuron* **29,** 229–242
28. Kubo, S. I., Kitami, T., Noda, S., Shimura, H., Uchiyama, Y., Asakawa, S., Minoshima, S., Shimizu, N., Mizuno, Y., and Hattori, N. (2001) *J. Neurochem.* **78,** 42–54
29. Shimura, H., Hattori, N., Kubo, S., Yoshikawa, M., Kitada, T., Matsumine, H., Asakawa, S., Minoshima, S., Yamamura, Y., Shimizu, N., and Mizuno, Y. (1999) *Ann. Neurol.* **45,** 668–672
30. Stichel, C. C., Augustin, M., Kuhn, K., Zhu, X. R., Engels, P., Ullmer, C., and Lubbert, H. (2000) *Eur. J. Neurosci.* **12,** 4181–4194
31. Exner, N., Treske, B., Paquet, D., Holmström, K., Schiesling, C., Gispert, S., Carballo-Carbajal, I., Berg, D., Hoepken, H.-H., Gasser, T., Krüger, R., Winklhofer, K. F., Vogel, F., Reichert, A., Auburger, G., Kahle, P. J., Schmid, B., and Haass, C. (2007) *J. Neurosci.* **27,** 12413–12418
32. Winklhofer, K. F., Tatzelt, J., and Haass, C. (2008) *EMBO J.* **27,** 336–349
33. Lavoie, M. J., Cortese, G. P., Ostaszewski, B. L., and Schlossmacher, M. G. (2007) *J. Neurochem.* **103,** 2354–2368
34. Muqit, M. M., Davidson, S. M., Payne Smith, M. D., MacCormac, L. P., Kahns, S., Jensen, P. H., Wood, N. W., and Latchman, D. S. (2004) *Hum. Mol. Genet.* **13,** 117–135
35. Wang, C., Ko, H. S., Thomas, B., Tsang, F., Chew, K. C., Tay, S. P., Ho, M. W., Lim, T. M., Soong, T. W., Pletnikova, O., Troncoso, J., Dawson, V. L., Dawson, T. M., and Lim, K. L. (2005) *Hum. Mol. Genet.* **14,** 3885–3897
36. Wong, E. S., Tan, J. M., Wang, C., Zhang, Z., Tay, S. P., Zaiden, N., Ko, H. S., Dawson, V. L., Dawson, T. M., and Lim, K. L. (2007) *J. Biol. Chem.* **282,** 12310–12318
37. Safadi, S. S., and Shaw, G. S. (2007) *Biochemistry* **46,** 14162–14169
38. Jensen, L. D., Vinther-Jensen, T., Kahns, S., Sundbye, S., and Jensen, P. H. (2006) *Neuroreport* **17,** 1205–1208

Cell Death and Differentiation (2010), 1–14

www.nature.com/cdd

Parkin is transcriptionally regulated by ATF4: evidence for an interconnection between mitochondrial stress and ER stress

L Bouman[1], A Schlierf[1], AK Lutz[1], J Shan[2], A Deinlein[1], J Kast[1], Z Galehdar[3], V Palmisano[1], N Patenge[4], D Berg[4], T Gasser[4], R Augustin[5], D Trümbach[5], I Irrcher[3], DS Park[3,6], W Wurst[5,7], MS Kilberg[2], J Tatzelt[1] and KF Winklhofer*[,1]

Loss of parkin function is responsible for the majority of autosomal recessive parkinsonism. Here, we show that parkin is not only a stress-protective, but also a stress-inducible protein. Both mitochondrial and endoplasmic reticulum (ER) stress induce an increase in parkin-specific mRNA and protein levels. The stress-induced upregulation of parkin is mediated by ATF4, a transcription factor of the unfolded protein response (UPR) that binds to a specific CREB/ATF site within the parkin promoter. Interestingly, c-Jun can bind to the same site, but acts as a transcriptional repressor of parkin gene expression. We also present evidence that mitochondrial damage can induce ER stress, leading to the activation of the UPR, and thereby to an upregulation of parkin expression. *Vice versa*, ER stress results in mitochondrial damage, which can be prevented by parkin. Notably, the activity of parkin to protect cells from stress-induced cell death is independent of the proteasome, indicating that proteasomal degradation of parkin substrates cannot explain the cytoprotective activity of parkin. Our study supports the notion that parkin has a role in the interorganellar crosstalk between the ER and mitochondria to promote cell survival under stress, suggesting that both ER and mitochondrial stress can contribute to the pathogenesis of Parkinson's disease.
Cell Death and Differentiation advance online publication, 26 November 2010; doi:10.1038/cdd.2010.142

Mitochondrial dysfunction has long been implicated in the pathogenesis of Parkinson's disease (PD). Mitochondrial toxins targeting complex I of the electron transport chain can induce acute parkinsonism in humans and are being used to model PD in animals. More recently, several PD-associated genes have been shown to influence mitochondrial function, morphology, dynamics and turnover (reviewed in Winklhofer and Haass[1] and Schapira[2]). In addition to mitochondrial dysfunction, several lines of evidence indicate that endoplasmic reticulum (ER) stress may contribute to the pathogenesis of PD (reviewed in Wang and Takahashi[3] and Lindholm *et al.*[4]). First, toxins such as MPTP, 6-OHDA or rotenone, used to induce parkinsonism in animal models, have been shown to cause ER stress.[5–7] Second, ER stress accounts for at least some aspects of α-synuclein toxicity. α-Synuclein has been shown to block ER to Golgi vesicular trafficking in different model systems,[8] and overexpression of α-synuclein can induce ER stress.[8,9] Finally, ER stress has been documented in dopaminergic neurons of the parkinsonian brain, exemplified by increased levels of phospho-PERK, phospho-eIF2α and caspase-4.[10,11] The link between PD and ER dysfunction was recently reinforced by the observation that the E3 ubiquitin ligase parkin can protect cells from ER stress-induced cell death induced by the overexpression of Pael-R, a putative parkin substrate prone to misfolding within the secretory pathway.[12,13] Mutations in the parkin gene were identified as a cause of early onset PD in Japanese families.[14] Since then, more than 100 mutations have been described in patients of diverse ethnic backgrounds, accounting for the majority of autosomal recessive parkinsonism.

ER stress originates from the accumulation of unfolded secretory proteins, perturbations in calcium homeostasis or redox status, alterations in glycosylation or energy deprivation. The ER has evolved sophisticated stress response signaling pathways collectively called the unfolded protein response (UPR), destined to increase the ER folding capacity, to reduce the folding load and to restore ER homeostasis (reviewed in Ron and Walter[15]). Conversely, when ER stress conditions are severe or persistent, apoptotic cell death is induced (reviewed in Kim *et al.*[16]).

Recent research revealed that the ER physically and functionally interacts with mitochondria to influence key

[1]Adolf Butenandt Institute, Neurobiochemistry, Ludwig Maximilians University, Munich, Germany; [2]Department of Biochemistry and Molecular Biology, Genetics Institute, Shands Cancer Center and Center for Nutritional Sciences, University of Florida College of Medicine, Gainesville, FL, USA; [3]Cellular and Molecular Medicine, University of Ottawa, Ottawa, Ontario, Canada; [4]Department of Neurodegeneration, Hertie Institute for Clinical Brain Research, University of Tübingen, and German Center for Neurodegenerative Diseases, Tübingen, Germany; [5]Helmholtz Center Munich, German Research Center for Environmental Health, Technical University Munich, Institute of Developmental Genetics and German Center for Neurodegenerative Diseases, Munich/Neuherberg, Germany; [6]Department of Cogno-Mechatronics Engineering, Pusan National University, Pusan, South Korea and [7]Max Planck Institute of Psychiatry, Munich, Germany
*Corresponding author: KF Winklhofer, Adolf Butenandt Institute, Neurobiochemistry, Ludwig Maximilians University, Schillerstrasse 44, Munich, D-80336, Germany. Tel: +49 89 2180 75483; Fax: +49 89 2180 75415; E-mail: Konstanze.Winklhofer@med.uni-muenchen.de
Keywords: ATF4; c-Jun; ER stress; parkin; Parkinson's disease; UPR
Abbreviations: CCCP, carbonyl cyanide m-chlorophenyl hydrazone; ChIP, chromatin immunoprecipitation; EMSA, electrophoretic mobility shift assays; ERAD, ER-associated degradation; IGFBP1, insulin growth factor binding protein 1; JNK, c-Jun N-terminal kinase; MAPK, mitogen-activated protein kinase; MEFs, mouse embryonic fibroblasts; RNAi, RNA interference; TG, thapsigargin; TM, tunicamycin; TTS, transcriptional start site; UPR, unfolded protein response; wt, wildtype
Received 09.4.10; revised 10.8.10; accepted 09.9.10; Edited by M Piacentini

aspects of cellular physiology and viability (reviewed in Pizzo and Pozzan[17]). Interactions between these organelles allow the exchange of metabolites and are implicated in the regulation of calcium signaling and cell death pathways. Our study shows that parkin expression is increased on ER stress and mitochondrial stress through the PERK/ATF4 branch of the UPR. Increased expression of parkin prevents ER stress-induced mitochondrial damage and cell death, providing evidence for a functional link between parkin, ER stress and mitochondrial integrity.

Results

Mitochondrial membrane dissipation causes ER stress and leads to transcriptional upregulation of parkin. The protonophore CCCP is being used to induce mitochondrial damage in various model systems. CCCP renders the mitochondrial inner membrane permeable for protons and causes dissipation of the proton gradient. We previously observed that the complex I inhibitor rotenone induces an upregulation of parkin mRNA and protein levels.[18] CCCP has recently been shown to cause the translocation of parkin to damaged mitochondria, which are then removed by autophagy.[19] We, therefore addressed the question whether CCCP might also have an impact on the transcriptional regulation of parkin. Parkin transcripts were significantly increased both in CCCP-treated SH-SY5Y cells and primary mouse cortical neurons (Figures 1a and b). To get insight into the underlying mechanism, we screened the parkin promoter for possible binding sites (BSs) of stress-regulated transcription factors by using TFSEARCH (http://www.cbrc.jp/research/db/TFSEARCH.html).[20] We discovered a putative CREB/ATF site in the parkin promoter located from −169 to −161 bp relative to the transcriptional start site (TSS). A further in-depth analysis identified this site as a possible binding sequence for ATF4 (Figures 1c and 3a). The CREB/ATF site within the parkin promoter is conserved among species (Figure 1c), supporting the notion that this site might be functionally relevant. An additional ATF4-binding site is located downstream of the TSS within the first intron of human, bovine and rodent parkin (Figure 1c).

ATF4 is a transcription factor, which is activated under ER stress. Some toxins used to model PD have been associated with ER stress, therefore we analyzed whether mitochondrial membrane dissipation induced by CCCP can cause ER stress. Regulation of gene expression in response to ER stress is mediated by the UPR, a stress-response program that re-establishes cellular homeostasis by the combinatorial action of specific transcription factors, binding to ER stress-responsive elements in the regulatory regions of UPR target genes (reviewed in Ron and Walter[15]). To test whether CCCP induces ER stress, we cloned a luciferase reporter construct containing the ER stress-responsive element ERSE-II (ERSE-II-luc, Supplementary Figure 5). Treatment of cells transiently expressing the luciferase reporter construct with tunicamycin (TM) induced an increase in luciferase expression, demonstrating the functionality of this ER stress reporter construct (Figure 1d). Moreover, CCCP was also able to significantly increase luciferase expression from ERSE-II-luc (Figure 1d). In addition, we quantified mRNA levels of the ER chaperone BiP, which is a major target of the UPR. CCCP treatment caused an upregulation of BiP mRNA, indicating that the mitochondrial toxin CCCP can induce ER stress (Figure 1e).

Parkin gene expression is upregulated in response to ER stress. In a next step, we tested whether expression of parkin is influenced by ER stress. SH-SY5Y cells were incubated with either the ER Ca^{2+}-ATPase inhibitor thapsigargin (TG) or the N-glycosylation inhibitor TM. Both ER stressors significantly increased the levels of parkin mRNA with a maximum at 12 h after treatment (Figures 2a and b). Another classical inducer of ER stress is amino acid starvation. We therefore made use of L-histidinol, a histidine analog, which inhibits activation of histidine by histidyl-tRNA synthetase. Also in this ER stress paradigm, parkin mRNA levels increased (Figure 2c). Notably, the upregulation of parkin under ER stress, induced by TG, TM or L-histidinol, was also observed on the protein level (Figures 2d–f), and was not restricted to SH-SY5Y cells, as a significant upregulation of parkin in response to TG or TM treatment was also observed in HEK293T cells, mouse embryonic fibroblasts (MEF) and primary mouse cortical neurons (Figures 2g–i). Interestingly, the upregulation of parkin upon ER stress in not dependent on PINK1 expression (data not shown).

Parkin is a target of the UPR through the PERK/ATF4 pathway. To test whether the putative ATF4-binding site within the parkin promoter mediates upregulation of parkin in response to ER stress, we created a luciferase reporter construct using the pGL3-luc promoter vector containing the putative ATF4-binding site (in triplicate) in front of a sequence coding for luciferase (park-luc, Figure 3a). As a positive control, we cloned the confirmed ATF4-binding site of the IGFBP1 promoter[21] analogously to the park-luc construct. This control construct was termed ATF4-responsive element (ATF4RE)-luc (Figure 3a). As a negative control, we cloned a mutant park-luc construct, harboring two point mutations in the putative ATF4-binding motif (mut. park-luc, Figure 3a). We tested park-luc in comparison with ATF4RE-luc under ER stress conditions and observed that luciferase expression from both reporter constructs was increased to a similar extent, whereas mutant park-luc behaved like the pGL3-luc vector control, both in HEK293T and SH-SY5Y cells (Figure 3b). Of note, CCCP treatment also induced increased transcription from both ATF4RE-luc and park-luc (Supplementary Figures 1A and B). Moreover, forced expression of ATF4 or upstream PERK also activated transcription from park-luc (Figure 3C). In line with this observation, dominant-negative ATF4ΔN, which lacks the N-terminal transcriptional activation domain,[22] significantly interfered with the ER stress-induced activation of park-luc (Figure 3d).

To increase experimental evidence for a role of endogenous ATF4 in mediating the transcriptional upregulation of parkin under ER stress, we knocked down ATF4 expression by RNAi. SH-SY5Y cells were transfected with ATF4 small-interfering RNA (siRNA) or control siRNA, and the efficiency of the ATF4 knockdown was verified at the mRNA and protein level (Figure 4a, right panel). Of note, ATF4 is specifically

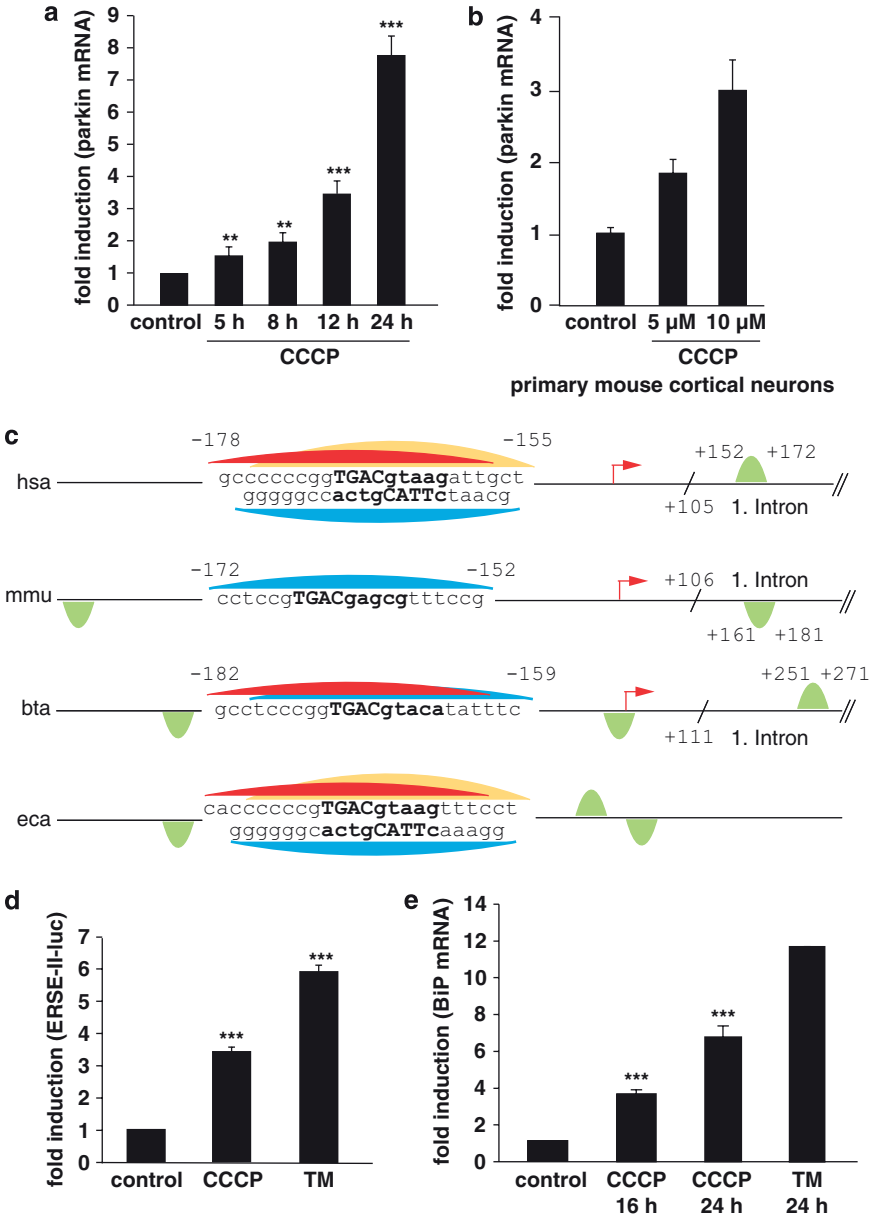

Figure 1 Mitochondrial stress induced by CCCP activates the UPR and leads to an upregulation of parkin. (**a**) Parkin mRNA levels are increased in response to mitochondrial membrane dissipation, induced by CCCP. SH-SY5Y cells were incubated with 10 μM CCCP for the indicated time. Cells were collected and total cellular RNA was isolated and subjected to quantitative RT-PCR using parkin-specific primers. The amount of RNA of each sample was normalized with respect to the endogenous housekeeping gene β-actin. Shown is the fold increase of parkin-specific mRNA compared with untreated control cells. (**b**) Parkin mRNA is upregulated upon CCCP treatment in primary mouse cortical neurons. Primary cortical neurons derived from embryonic mouse brain were incubated with CCCP (10 μM) for 12 h and analyzed as described in (**a**). (**c**) Human, mouse, bovine and equine promoter sequences of parkin, which are elongated downstream of the transcription start site (TSS) by 150 bp. Red arrow indicates the TSS and positions are denoted with relative to the TSS. The CREB/ATF-binding sites are indicated by semicircles. Red, yellow and blue semicircles are predicted by three different binding motifs, which correspond to a Genomatix-defined family of 14 matrices describing the CREB/ATF-binding site. The red and yellow colored binding sites are conserved between *Homo sapiens*, *Bos taurus* and *Equus caballus*, and *H. sapiens* and *E. caballus*, respectively, whereas the blue binding site is conserved across all four species. The green semicircles (not conserved) are additional binding sites. Downstream of the TSS, in the first intron of the parkin gene, an additional CREB/ATF-binding site is located in *H. sapiens*, *Mus musculus* and *B. taurus*. The consensus ATF4-binding site is written in bold letters. hsa, *Homo sapiens*; mmu, *Mus musculus*; bta, *Bos taurus*; eca, *Equus caballus*. (**d** and **e**) CCCP activates the UPR and causes ER stress. (**d**) The ER stress luciferase reporter construct ER stress-response element II (ERSE-II-luc) is activated by CCCP. HEK293T cells were transfected with the ERSE-II-luc reporter. At 24 h after transfection, the cells were treated with 10 μM CCCP for 24 h. As a positive control, the cells were treated with the ER stressor tunicamycin (2 μg/ml, 24 h). Shown is the fold induction of luciferase activity in CCCP-treated cells in comparison with non-treated control cells. Quantification is based on triplicates of at least three independent experiments. (**e**) BiP expression is increased in response to CCCP treatment. As an indicator of ER stress, BiP mRNA levels were analyzed in SH-SY5Y cells treated with CCCP (10 μM) for the indicated time by quantitative RT-PCR as described in Figure 1a. Tunicamycin (2 μg/ml) was used as a positive control to induce ER stress. ***$P<0.001$, **$P<0.01$

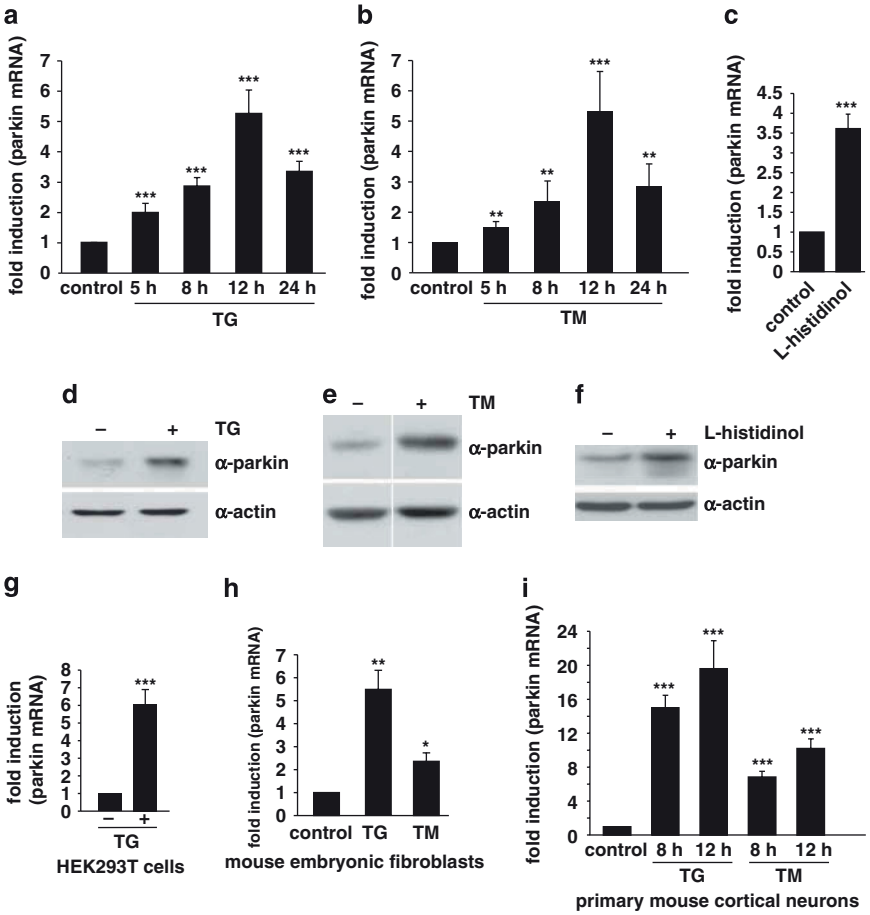

Figure 2 Parkin gene expression is upregulated in response to ER stress. (**a** and **b**) Parkin mRNA levels are increased under ER stress induced by thapsigargin or tunicamycin. SH-SY5Y cells were incubated with 1 μM thapsigargin (TG) (**a**) or 2 μg/ml tunicamycin (TM) (**b**) for the indicated time. Cells were collected and total cellular RNA was isolated and subjected to quantitative RT-PCR using parkin-specific primers. The amount of RNA of each sample was normalized with respect to the endogenous housekeeping gene β-actin. The same results were obtained when 18sRNA was used as a control gene (data not shown). Shown is the fold increase of parkin-specific mRNA compared with untreated control cells. (**c**) Amino acid starvation leads to an upregulation of parkin mRNA. SH-SY5Y cells were treated with 2 mM L-histidinol in cell culture medium, containing 10% dialysed FCS, for 14 h. The cells were then collected and total cellular RNA was isolated and subjected to quantitative RT-PCR using parkin-specific primers as described under Figure 1a. (**d–f**) Parkin protein expression is increased after ER stress induced by TG, TM, or amino acid starvation. Expression of endogenous parkin after treatment of SH-SY5Y cells with TG (**d**), TM (**e**) or L-histidinol (**f**) for 14 h was analyzed by western blotting using the anti-parkin mAb PRK8. Loading was controlled by re-probing the blots for β-actin. The western blot image (**e**) was re-arranged by excluding one line, as indicated by a white line; all samples originate from one gel. (**g–i**) Parkin mRNA is upregulated on ER stress in HEK293T cells, mouse embryonic fibroblasts and primary mouse cortical neurons. HEK293 T cells (**g**), mouse embryonic fibroblasts (**h**), or primary cortical neurons derived from embryonic mouse brain (**i**) were incubated with TG (1 μM) or TM (2 μg/ml; primary cortical neurons: 3 μg/ml) for 12 or 8 h and 12 h (primary cortical neurons) and analyzed as described in (**a**). $^{***}P<0.001$, $^{**}P<0.01$, $^{*}P<0.05$

induced after ER stress, whereas under non-stress conditions expression levels are low. Remarkably, in ATF4-deficient cells, the upregulation of parkin induced by ER stress (TG) or mitochondrial stress (CCCP) was significantly reduced (Figure 4a, left panel). The same results were obtained employing two different ATF4-specific siRNA duplexes (data not shown). Moreover, we analyzed the transcriptional regulation of parkin in primary cortical neurons derived from ATF4-knockout mice.[23] The upregulation of parkin on ER stress was significantly reduced in ATF4-deficient neurons (Figure 4b), indicating that ATF4 indeed has an important role in the stress-induced regulation of parkin expression. Interestingly, in our experimental approach, a transient downregulation of ATF4 had a more severe effect on the stress-induced regulation of parkin than a stable knockout of ATF4. It is conceivable that compensatory effects in ATF4-knockout mice account for this observation.

Finally, binding of ATF4 to the parkin promoter could be demonstrated by chromatin immunoprecipitation (ChIP) assays using a polyclonal anti-ATF4 antibody. A rabbit polyclonal antibody (pAb) against chicken IgG was used as a nonspecific control. After isolation of crosslinked chromatin from cells incubated with or without TG, immunoprecipitated DNA was analyzed by real-time PCR. The ChIP analysis revealed specific binding of ATF4 to the parkin promoter after 2 and 8 h of TG treatment in both HEK293T and SH-SY5Y cells (Figure 4c).

c-Jun acts as a transcriptional repressor of parkin and has a dominant effect on ATF4. When we performed electrophoretic mobility shift assays using the putative ATF4-binding site of the parkin promoter as a radiolabeled probe (park oligo), we observed a second complex in addition to the ATF4–DNA complex. This complex showed a reduced

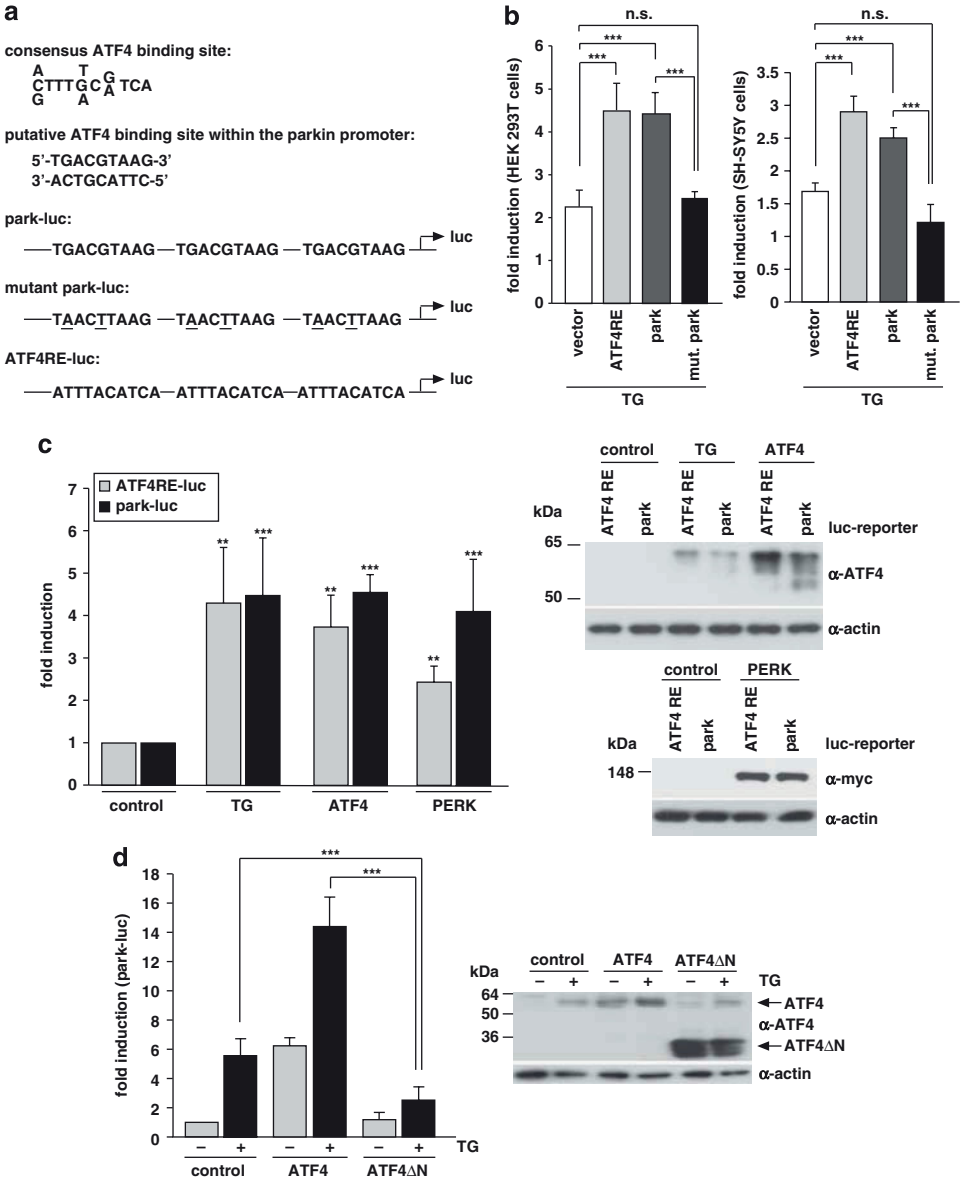

Figure 3 Transcriptional upregulation of parkin under ER stress is mediated by ATF4. (**a**) Schematic representation of the consensus ATF4-binding site, the putative ATF4-binding site within the parkin promoter and the luciferase reporter constructs cloned for the analysis described in the following: park-luc contains the putative ATF4-binding site of the parkin promoter in triplicate, mutant park-luc habors two point mutations within the putative ATF4-binding site, and ATF4RE-luc contains the confirmed ATF4-binding site of the insulin growth factor binding protein 1 (IGFBP1) promoter in triplicate. Of note, the putative binding site for ATF4 within the parkin promoter is located on the complementary strand in 5′ → 3′ direction. (**b**) The park-luc reporter construct is induced after ER stress. HEK293 T cells or SH-SY5Y cells were transfected with either the control luciferase reporter construct pGL3-luc (vector), the ATF4RE-luc construct containing the confirmed ATF4-binding site, the park-luc construct or the park-luc construct with a mutated ATF4 binding site (mut. park). At 8 h after transfection, cells were incubated with 1 μM thapsigargin (TG) and collected after 14 h of treatment. Shown is the fold induction of luciferase activity in stressed cells compared with the non-stressed control based on triplicates of at least three independent experiments. (**c**) Increased expression of ATF4 or upstream PERK induces transcription from the park-luc reporter construct. HEK293T cells were co-transfected with the ATF4RE-luc reporter plasmid or the park-luc reporter plasmid and ATF4, PERK or GFP (as a control). As a positive control, one set of cells was treated with TG as described under (**b**) Shown is the fold induction of luciferase activity compared with GFP-expressing control cells based on triplicates of at least three independent experiments (left panel). Expression levels of ATF4 and PERK were analyzed by immunoblotting using the anti-ATF4 pAb C-20 or the anti-myc mAb 9E10 (right panels). Notably, TG treatment (1 μM, 14 h) induced the increased expression of endogenous ATF4. Loading was controlled by re-probing the blots for β-actin. (**d**) A dominant-negative mutant of ATF4 (ATF4ΔN) interferes with the activation of the park-luc reporter construct in response to ER stress. HEK293T cells were co-transfected with the park-luc reporter plasmid and ATF4, ATF4ΔN, or GFP (as a control). At 8 h after transfection, cells were incubated with 1 μM TG for 14 h. Shown is the fold induction of luciferase activity in comparison with GFP-expressing control cells based on triplicates of at least three independent experiments (left panel). Expression levels of ATF4 and ATF4ΔN were analyzed by immunoblotting using the anti-ATF4 pAb C-20 (right panel). Loading was controlled by re-probing the blots for β-actin. ***$P<0.001$, **$P<0.01$, n.s. = not significant

mobility in comparison with the ATF4–park oligo complex, and its relative intensity was increased after ER stress (Figure 5a, lanes 1, 2). By testing various antibodies against transcription factors that could bind to the CREB/ATF site for their potential to supershift the upper band, we found that c-Jun is also able to bind to the park oligo. The respective

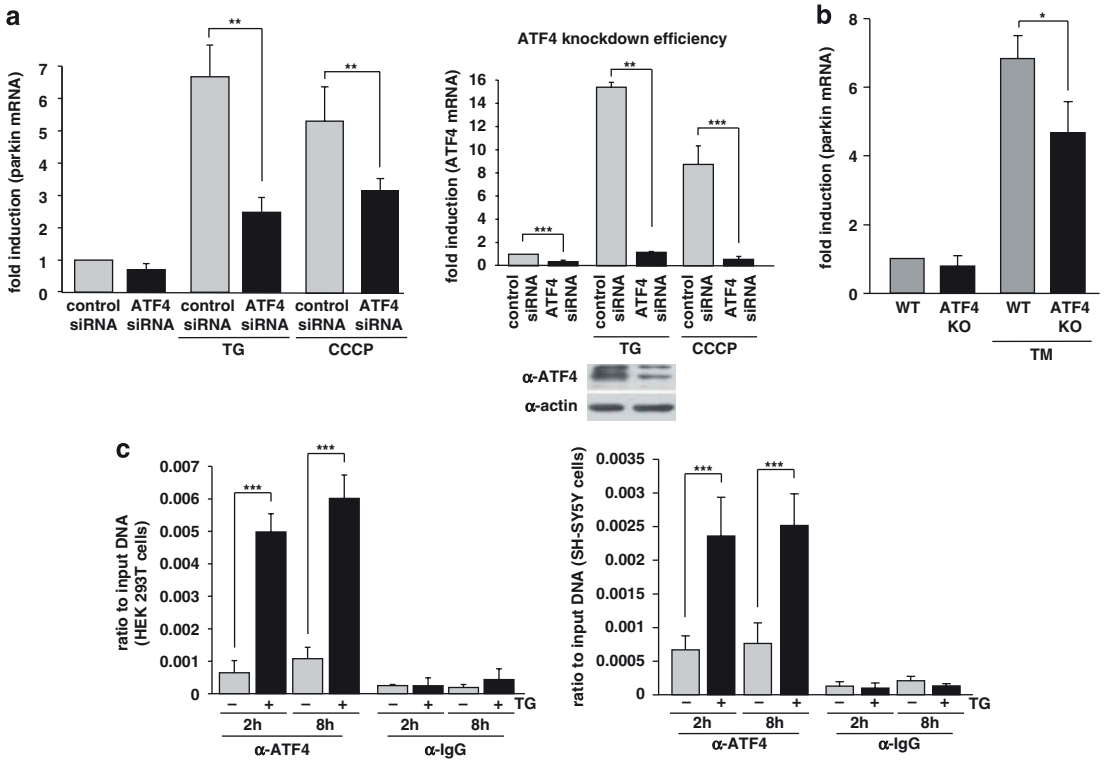

Figure 4 ATF4 binds to the parkin promoter and mediates parkin upregulation in response to ER and mitochondrial stress. (**a**) ER and mitochondrial stress-induced upregulation of parkin is impaired in ATF4-deficient cells. SH-SY5Y cells were transfected with ATF4-specific or control siRNA duplexes. Two days later, cells were re-transfected with siRNA duplexes and then incubated with 1 μM TG or 10 μM CCCP for 14 h. The cells were collected and analyzed as described in Figure 1a by quantitative RT-PCR using parkin-specific or ATF4-specific primers. The amount of RNA of each sample was normalized with respect to β-actin. Shown is the fold increase of parkin mRNA in response to TG or CCCP treatment (left panel). The efficiency of ATF4 downregulation was determined by quantitative RT-PCR (right panel) and western blotting (lower right panel) using the anti-ATF4 pAb C-20. (**b**) ER stress-induced upregulation of parkin is impaired in primary cortical neurons from ATF4-knockout mice. Primary cortical neurons from ATF4-deficient or wild-type mice were treated with tunicamycin (3 μg/ml) for 8 h. Total RNA was isolated and analyzed using parkin-specific primers as described in Figure 1a. (**c**) ATF4 binds to the parkin promoter *in vivo*. HEK293T cells or SH-SY5Y cells incubated with or without 300 nM TG for 2 and 8 h were used to perform a ChIP analysis using a pAb specific for ATF4 in comparison with a nonspecific rabbit IgG. For the final real-time PCR step, primers specific for the parkin promoter region were used. $^{***}P<0.001$, $^{**}P<0.01$, $^{*}P<0.05$

Figure 5 c-Jun suppresses the upregulation of parkin after ER stress. (**a**) c-Jun binds to the parkin oligonucleotide harboring the CREB/ATF-binding site. HEK293 T cells were incubated with 2 μM thapsigargin (TG) and collected after 3 h. Nuclear extracts were prepared and tested for binding to the ^{32}P-labeled oligonucleotide comprising the putative ATF4-binding site within the parkin promoter (park oligo; lanes 1–5) by an electrophoretic mobility shift assay (EMSA). The labeled oligonucleotides were incubated with nuclear extracts in the absence or presence of a 100-fold excess of unlabeled park oligo (lane 5) to compete with the binding reaction. To test for supershift activity, the anti-c-Jun pAb (N) sc-45X (lane 3) or the anti-ATF4 pAb C-20 (lane 4) was added to the binding reaction. (**b**) c-Jun decreases transcription from the park-luc reporter after ER stress. HEK293 T cells were co-transfected with the park-luc reporter construct and c-Jun or GFP (as a control). Eight hours after transfection, the cells were treated with 1 μM TG for 14 h. Shown is the fold induction of luciferase activity in c-Jun-expressing cells in comparison with GFP-expressing control cells based on triplicates of at least three independent experiments. Expression levels of c-Jun were analyzed by immunoblotting using the anti-c-Jun pAb (N) sc-45 (lower panel). Protein (3 μg) of total cell lysates was loaded. Loading was controlled by re-probing the blots for β-actin. (**c**) c-Jun suppresses the ATF4-mediated activation of the park-luc construct. HEK293 T cells were co-transfected with the park-luc reporter plasmid and either GFP (as a control), ATF4 plus GFP or ATF4 plus c-Jun. Eight hours after transfection, the cells were treated with 1 μM TG for 14 h. Shown is the fold induction of luciferase activity in ATF4-expressing cells in comparison with ATF4- and c-Jun-expressing cells based on triplicates of at least three independent experiments. Expression levels of ATF4 and c-Jun were analyzed by immunoblotting using the anti-ATF4 pAb C-20 or the anti-c-Jun pAb (N) sc-45. Protein (3 μg) of total cell lysates was loaded. Loading was controlled by re-probing the blots for β-actin (lower panel). (**d**) ER stress-induced upregulation of parkin is increased in c-Jun-deficient cells. SH-SY5Y cells were transfected with c-Jun-specific or control siRNA duplexes. One day later, cells were re-transfected with siRNA duplexes and incubated with 1 μM TG for 14 h. The cells were collected and analyzed as described in Figure 1a by quantitative RT-PCR using parkin-specific primers. The amount of RNA of each sample was normalized with respect to β-actin. Shown is the fold increase of parkin mRNA in response to TG treatment (upper panel). The efficiency of c-Jun downregulation was determined by western blotting using the anti-c-Jun anti-c-Jun pAb (N) sc-45 (lower panel). Protein (30 μg) of total cell lysates was loaded. (**e**) JNK3 decreases transcription from the park-luc reporter. HEK293 T cells were co-transfected with the park-luc reporter plasmid and JNK3 or GFP (as a control). Twenty four hours after transfection, the cells were treated with 1 μM TG for 8 h. Shown is the fold induction of luciferase activity in JNK3-expressing cells in comparison with GFP-expressing control cells based on triplicates of at least three independent experiments. Expression levels of JNK3 were analyzed by immunoblotting using an anti-JNK pAB (lower panel). Loading was controlled by re-probing the blots for β-actin. (**f**) The JNK inhibitor SP600125 increases parkin upregulation in response to ER stress. SH-SY5Y cells were treated with or without the JNK inhibitor SP600125 (10 μM) for 24 h. Thapsigargin was added after 10 h for additional 14 h. To quantify parkin-specific mRNA, cells were collected and analyzed as described in Figure 1a for quantitative RT-PCR using parkin-specific primers. The amount of RNA of each sample was normalized with respect to β-actin. Shown is the fold increase of parkin mRNA. Parkin protein levels were analyzed by immunoblotting using an anti-parkin PRK8 mAb (lower panel). The efficiency of SP600125 was controlled by blotting against phosphorylated c-Jun using the phospho-specific anti-c-Jun antibody X (Ser63) II pAb. Protein (15 μg) of total cell lysates was loaded. Loading was controlled by re-probing the blots for c-Jun and β-actin. $^{***}P<0.001$, $^{**}P<0.01$, $^{*}P<0.05$

band was supershifted by an anti-c-Jun antibody (Figure 5a, lane 3) and was competed by an excess of unlabeled park oligo (Figure 5a, lane 5). To test whether c-Jun might have an impact on the transcriptional regulation of parkin, we first analyzed the effect of c-Jun on the park-luc reporter construct. Interestingly, increased levels of c-Jun significantly reduced transcription from park-luc under ER stress (Figure 5b). Moreover, c-Jun suppressed the ATF4-induced activation of park-luc, both under basal and ER stress conditions, indicating a dominant-negative effect (Figure 5c). Next we performed a c-Jun knockdown approach by RNAi. c-Jun-specific siRNA duplexes were transfected into SH–SY5Y cells, resulting in a reduction of c-Jun mRNA by ~87% under normal conditions and by ~69% under ER stress conditions (Supplementary Figure 2). The knockdown efficiency was also verified at the protein level (Figure 5d, lower panel). Notably, in c-Jun-deficient cells, parkin upregulation in response to ER stress was significantly increased and also in non-stressed cells more parkin was expressed when c-Jun was silenced (Figure 5d, upper panel). These results indicate that c-Jun can bind to the ATF4-binding site within the parkin promoter to mediate repression of parkin expression. c-Jun is a major target of JNKs, a subfamily of the MAPK superfamily. JNK1 and JNK2 are ubiquitously expressed, whereas JNK3 is primarily found in brain, heart and testes. As JNK3 has been linked to cell death in several models of neurodegeneration (reviewed in Waetzig and Herdegen[24]), we tested whether it has an impact on parkin expression. Increased expression of JNK3 indeed significantly suppressed transcription from the park-luc construct (Figure 5e). Moreover, treatment of cells with the JNK inhibitor SP600125 increased

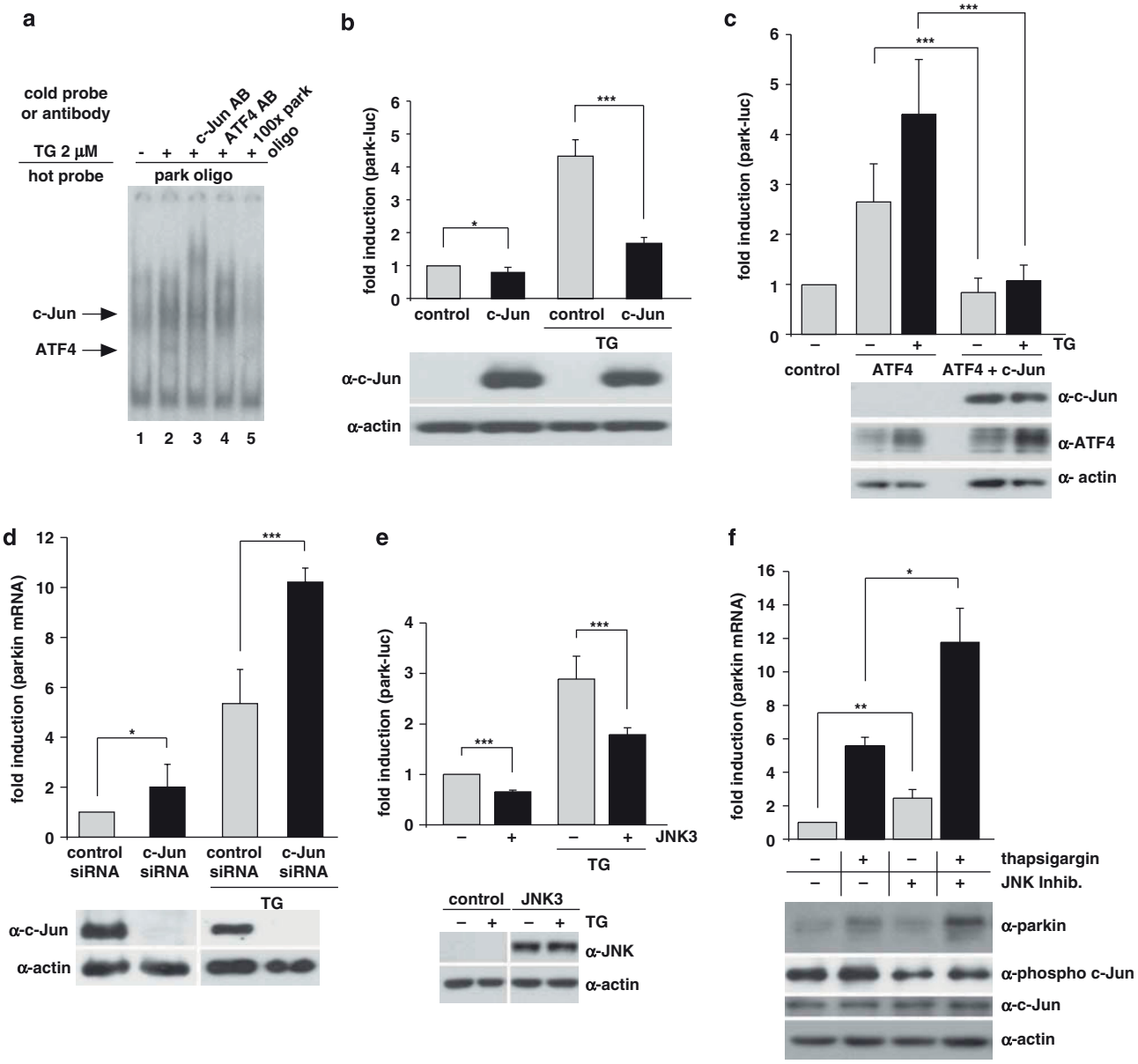

parkin mRNA and protein levels both under stress and non-stress conditions (Figure 5f).

Parkin protects cells from ER stress-induced cell death. Conceptually, upregulation of parkin in response to ER stress might help to preserve cellular function and survival within the adaptive phase of the UPR. To test the capacity of parkin to protect cells from ER stress-induced toxicity, we treated SH-SY5Y cells transiently expressing wildtype (wt) or mutant parkin with TG or TM. Cells undergoing apoptosis were analyzed by indirect fluorescence using an antibody specific for activated caspase-3. In contrast to control cells and cells expressing pathogenic parkin mutants, cells overexpressing wt parkin were protected against apoptosis induced by ER stress (Figure 6a). To increase evidence for a role of endogenous parkin in coping with ER stress, we analyzed the consequences of a parkin knockdown induced by RNAi. Parkin knockdown cells showed a significant increase in apoptotic cells after ER stress in comparison with control siRNA-transfected cells (Figure 6b). A decrease in the viability of parkin-deficient SH-SY5Y and HEK293T cells after ER stress was also observed by employing the MTT assay (Supplementary Figures 3A and B). Notably, the increased vulnerability of parkin-deficient cells to ER stress-induced cell death could be rescued by the expression of

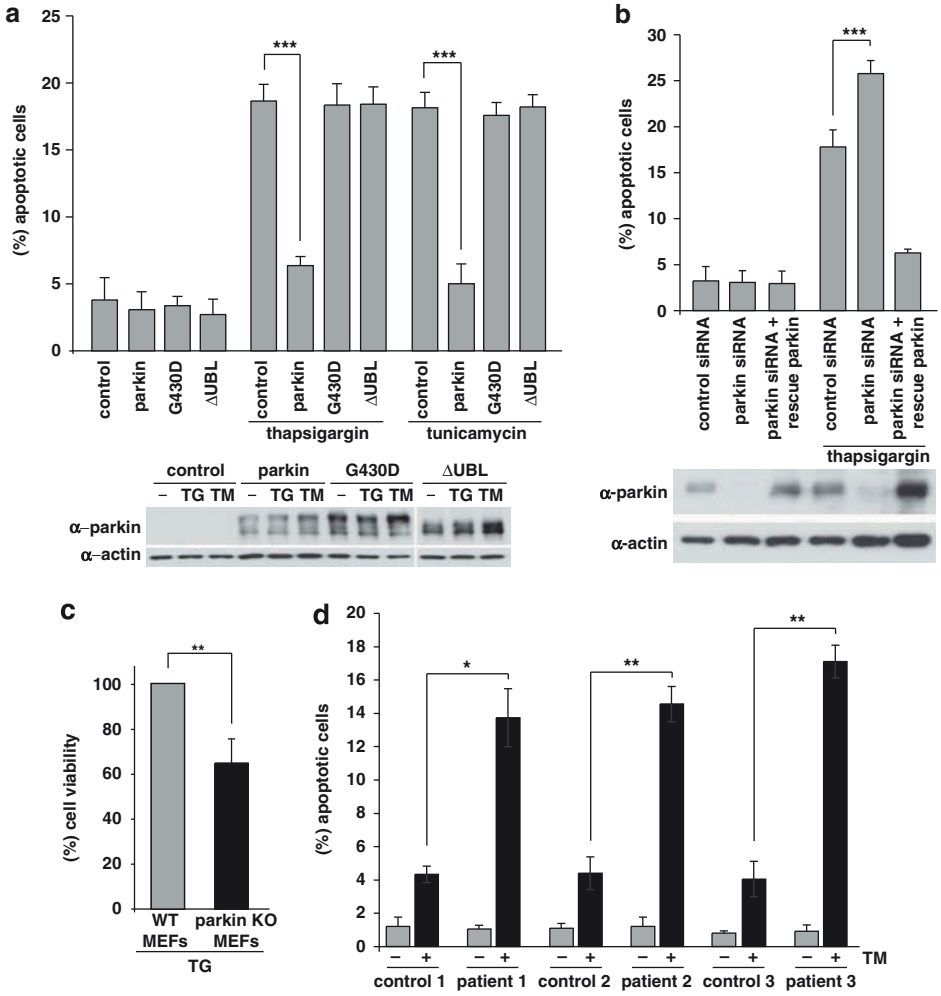

Figure 6 Parkin protects cells from ER stress-induced cell death. (**a**) Increased expression of wild-type (wt) parkin protects cells from ER stress-induced cell death. SH-SY5Y cells were co-transfected with EYFP (as a control) and wt parkin or the pathogenic parkin mutants G430D or ΔUBL. Twenty four hours after transfection, cells were incubated with 10 μM thapsigargin (TG) or 5 μg/ml tunicamycin (TM) at 37 °C for 8 h, fixed, permeabilized, and then the activation of caspase-3 was analyzed by indirect immunofluorescence using an anti-active caspase-3 pAb. Shown is the percentage of apoptotic cells among transfected cells. Parkin expression levels were determined by immunoblotting using the anti-parkin PRK8 mAb. Loading was controlled by re-probing the blots for β-actin (lower panel). (**b**) Parkin-deficient cells are more vulnerable to ER stress-induced cell death. SH-SY5Y cells were transfected with parkin-specific or control siRNA duplexes and co-transfected with EYFP (as a control) or siRNA-resistant wt parkin (rescue parkin). Three days later, the cells were stressed with TG (10 μM) for 8 h fixed, permeabilized, and then the activation of caspase-3 was analyzed by indirect immunofluorescence as described in A. Parkin expression levels were determined by immunoblotting using the anti-parkin PRK8 mAb. Loading was controlled by re-probing the blots for β-actin (lower panel). (**c**) Mouse embryonic fibroblasts (MEFs) derived from parkin-knockout mice are more vulnerable to ER stress than wt MEFs. MEFs from wt or parkin-knockout (ko) mice were stressed with TG (10 μM) for 16 h and then cellular viability was determined by the MTT assay. Shown is the relative viability of ko MEFs in comparison with wt MEFs after TG treatment. Quantification is based on five independent experiments. (**d**) Skin fibroblasts of patients carrying pathogenic mutations in the parkin gene are more vulnerable to ER stress. Skin fibroblasts from patients and control indivduals were stressed with tunicamycin (TM, 10 μM) for 24 h, fixed, permeabilized, and then the activation of caspase-3 was analyzed by indirect immunofluorescence as described in (**a**). ***$P<$ 0.001, **$P<0.01$, *$P<0.05$

siRNA-resistant parkin, confirming a parkin-specific effect (Figure 6b). In addition, we analyzed the viability of MEFs derived from parkin-knockout mice[25] under ER stress conditions. In comparison with MEFs derived from wt mice, the parkin-knockout MEFs showed a decreased viability under ER stress induced by TG (Figure 6c). Moreover, primary skin fibroblasts from three patients with mutations in the parkin gene displayed a significant increase in cell death in response to TM treatment compared with age- and gender-matched control fibroblasts from healthy individuals (Figure 6d). Of note, levels of CHOP, phospho-c-Jun and phospho-JNK, which have been associated with the proapoptotic branch of ER stress pathways, were increased in patient fibroblasts under ER stress (Supplementary Figure 4).

Parkin does not decrease the level of ER stress and functions independently from the proteasome. The experiments described above established a protective role of parkin in response to ER stress. To address the question whether parkin may have an effect on the severity of ER stress, we quantified the mRNA levels of the ER chaperone BiP in parkin-knockdown cells in response to ER stress. After ER stress induced by TG, BiP, mRNA was highly upregulated (~15-fold compared with untreated cells). Interestingly, downregulation of parkin had no significant impact on BiP mRNA levels, both under basal conditions and ER stress (Figure 7a). In addition, parkin-knockout MEFs did not show increased levels of BiP mRNA after TG or TM treatment when compared with control MEFs (Figure 7b). These results indicated that the transient or stable loss of parkin does not cause ER stress. In line with these results, increased expression of parkin did not significantly influence the level of ER stress as monitored by luciferase reporter assays using four different ER stress-responsive elements (ESRE, ERSE-II, UPR and ATF4RE), which cover all branches of the UPR (Figure 7c and Supplementary Figure 5). In a next step, we tested whether the protective activity of parkin under ER stress is dependent on the proteasome. SH-SY5Y cells were exposed to TG in the

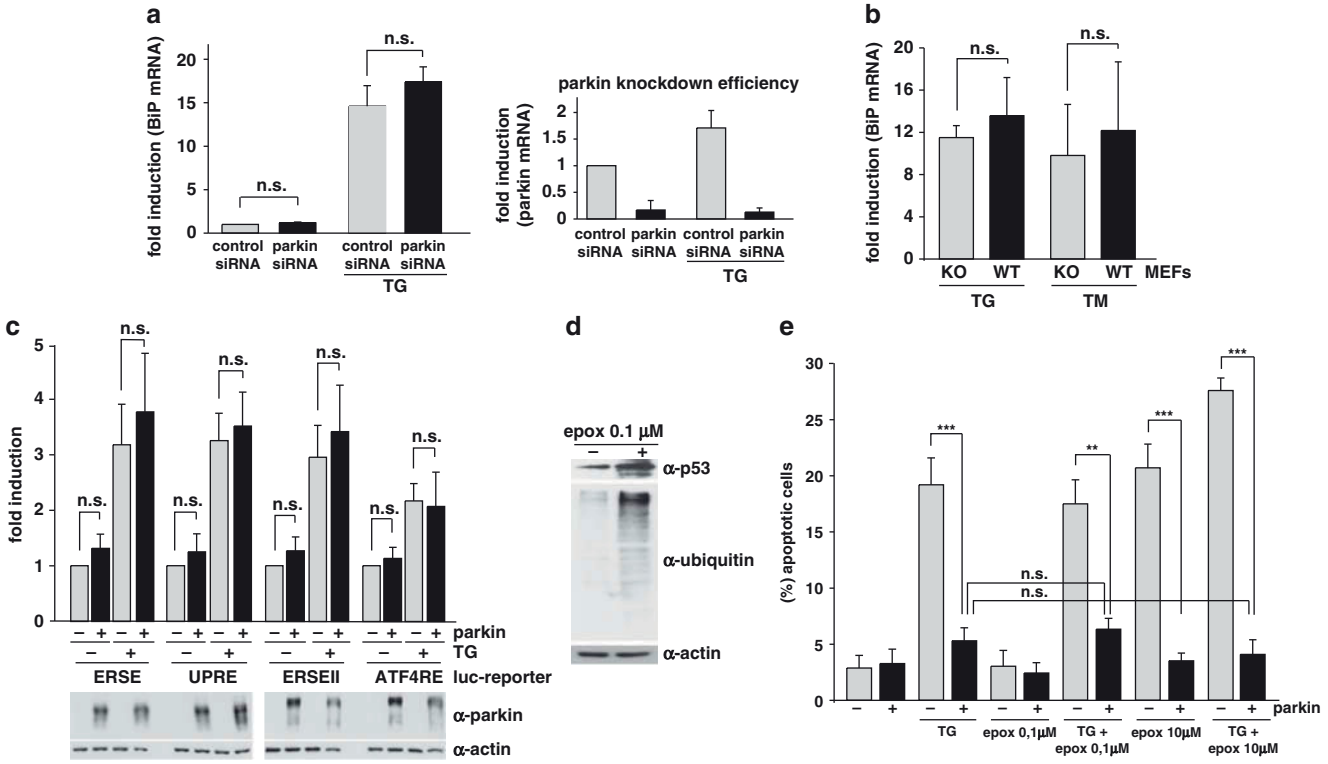

Figure 7 Parkin has no direct effect on ER stress. (**a**) Parkin deficiency does not increase the level of ER stress. SH-SY5Y cells were transfected with parkin-specific or control siRNA duplexes. Three days later, the cells were stressed with 1 μM thapsigargin (TG) for 5 h. As an indicator of ER stress BiP mRNA levels were analyzed by quantitative RT-PCR as described in Figure 1a (left panel). To test for the efficiency of parkin knockdown, parkin mRNA levels were quantified in parallel (right panel). (**b**) The level of ER stress is not increased in mouse embryonic fibroblasts (MEFs) derived from parkin-knockout mice. MEFs from wildtype (wt) or parkin-knockout (ko) mice were stressed with 1 μM TG or 2 μg/ml tunicamycin (TM) for 5 h. The levels of BiP mRNA were analyzed by RT-PCR as described in Figure 1a. (**c**) Overexpression of parkin has no influence on the ER stress level determined by ER stress reporter constructs. HEK293 T cells were co-transfected with the ER stress reporter plasmids indicated (Supplementary Figure 5) and either parkin or GFP (as a control). Twenty four hours after transfection, the cells were treated with 1 μM TG for 8 h. Shown is the fold induction of luciferase activity in parkin-expressing cells in comparison with GFP-expressing control cells. Quantification is based on triplicates of at least three independent experiments. Expression levels of parkin were analyzed by immunoblotting using the anti-parkin pAb 2132 (lower panel). Loading was controlled by re-probing the blots for β-actin. (**d** and **e**) The protective activity of parkin after ER stress is independent of the proteasome. (**d**) The efficiency of proteasomal inhibition by epoxomycin was demonstrated by an accumulation of endogenous p53 and ubiquitylated proteins. For immunoblotting, an anti-p53 and anti-ubiquitin mAb was used. Loading was controlled by re-probing the blots for β-actin. (**e**) Proteasomal inhibition does not impair the protective activity of parkin. SH-SY5Y cells were cotransfected with EYFP (as a control) or wild-type parkin. Twenty four hours after transfection, cells were incubated with 10 μM thapsigargin (TG) and/or epoxomycin (epox, 0.1 or 10 μM) for 8 h, fixed, permeabilized, and then activation of caspase-3 was analyzed as described in Figure 6a. ***$P<0.001$, **$P<0.01$, n.s. = not significant

presence of the proteasomal inhibitor epoxomycin. First, we used a non-toxic concentration of epoxomycin (0.1 μM), which efficiently inhibited the proteasome, as shown by an increase in endogenous p53 levels and an accumulation of ubiquitylated proteins (Figure 7d). Notably, the efficiency of parkin to protect against ER stress-induced cell death was not impaired when the proteasome was inhibited. Furthermore, increasing parkin expression also prevented cell death induced by a toxic concentration of epoxomycin (10 μM), indicating that protein degradation through the proteasome is not required for the acute prosurvival effect of parkin (Figure 7e).

Parkin interferes with ER stress-induced mitochondrial damage. Obviously, parkin does not reduce ER stress *per se*, but it can protect cells from ER stress-induced cell death. Based on the fact that parkin has an impact on mitochondrial integrity,[26] we analyzed the effect of ER stress on mitochondrial morphology and determined whether parkin might have a role in this pathway. SH-SY5Y cells were incubated with the fluorescent dye DiOC6(3) to visualize mitochondria in living cells by fluorescence microscopy. Under normal conditions, when mitochondrial fusion and fission activities are balanced, cells show a tubular mitochondrial network. When fission is increased with relative to fusion, small rod-like or spherical mitochondria can be observed, which are classified as fragmented. Typically, about 70% of SH-SY5Y cells show a tubular mitochondrial network under normal conditions, the remaining 30% are characterized by fragmented mitochondria.[26,27] ER stress, induced by either TM or TG increased the percentage of cells with fragmented mitochondria up to 70% (Figure 8a). Remarkably, enhanced expression of parkin significantly reduced ER stress-induced mitochondrial fragmentation (Figures 8a and b). Moreover, we observed that parkin loss of function increases the vulnerability of cells to ER stress-induced mitochondrial dysfunction, as cellular ATP production in response to ER stress was significantly reduced in parkin-deficient SH-SY5Y cells (Figure 8c). Thus, parkin maintains mitochondrial integrity under ER stress, and prevents alterations in mitochondrial morphology and bioenergetics.

Discussion

In this study, we show that parkin is transcriptionally upregulated by mitochondrial and ER stress via the UPR to promote viability under cellular stress. We identified the transcription factor ATF4 as a key factor in the stress-induced regulation of parkin expression, which binds to a CREB/ATF site within the parkin promoter. An essential role for ATF4 in the regulation of parkin expression was substantiated by the following observations: First, a dominant-negative ATF4 mutant prevented ER stress-induced upregulation of parkin. Second, in ATF4-knockdown cells and primary neurons from ATF4-knockout mice, parkin upregulation in response to ER stress was significantly impaired. Finally, we could demonstrate by a ChIP assay that ATF4 indeed binds to the parkin promoter. Our analysis also revealed that c-Jun acts as a transcriptional repressor of parkin. Intriguingly, c-Jun can bind to the same site within the parkin promoter as ATF4 to induce downregulation of parkin expression. What might be the physiological relevance of this observation? Conceptually, c-Jun may terminate the ATF4-mediated upregulation of parkin expression by competing with ATF4 on the parkin promoter. In line with this scenario, we observed that c-Jun has a dominant effect on ATF4; it can suppress ATF4-mediated upregulation of parkin expression. It is also conceivable that severe or prolonged ER stress leads to a preferential binding of c-Jun to the parkin promoter to suppress cytoprotective pathways and to favor the elimination of irreversibly damaged cells by proapoptotic pathways. In support of this view, CHOP, a proapoptotic transcription factor activated upon severe or prolonged ER stress, suppressed parkin expression (Supplementary Figure 6). Parkin transcription was also repressed by JNK3, a kinase upstream of c-Jun, which has been implicated in neuronal cell death pathways in dopaminergic neurons.[28,29] Indeed, our data show that the use of a JNK inhibitor is able to increase parkin expression, particularly under stress conditions. Interestingly, parkin has been reported to suppress JNK activity in cellular models and *Drosophila melanogaster*.[30,31] In line with these studies, we observed that phospho-JNK and phospho-c-Jun levels are increased in parkin-deficient patient fibroblasts under ER stress (Supplementary Figure 4). Our finding that the JNK pathway can negatively regulate parkin gene expression suggests a reciprocal interaction between parkin and JNK3, which might be instrumental in the dichotomy of cell survival and death. Depending on the cellular context and the severity of stress conditions, parkin can shift the balance towards cell survival by attenuating JNK3 signaling, whereas JNK3 gaining the upper hand, suppresses prosurvival pathways, either directly or indirectly, for example by inhibiting the expression of parkin.

The increased expression of parkin in response to ER stress clearly serves as a cytoprotective function. Cells overexpressing wt but not mutant parkin are protected against ER stress-induced cell death, whereas parkin-deficient cells show an increased vulnerability to ER stress. It will now be interesting to determine which cell types are affected in their response to stress by the loss of parkin function. On the basis of the emerging concept of non-cell autonomous cell death in neurodegeneration, it is conceivable that an impaired stress response in glial cells in the neighborhood of dopaminergic cells can contribute to nigrostriatal degeneration.

Neither an acute nor a permanent loss of parkin function *per se* causes ER stress. Furthermore, increased parkin expression does not decrease the severity of ER stress, arguing against a direct role of parkin in the ERAD pathway. In support of this notion, the antiapoptotic activity of parkin is independent of the proteasome. We observed that proteasomal inhibition does not impair the ability of parkin to prevent ER stress-induced cell death. Which activity of parkin might then be responsible for its protective effect under ER stress? In this context, it is important to note that organellar stress within cells cannot be regarded in an isolated manner. In fact, our study adds evidence for an interaction between the ER and mitochondria in response to stress.[32] ER stress can induce mitochondrial stress, resulting in a bioenergetic deficit and mitochondrial fragmentation. Our working model would

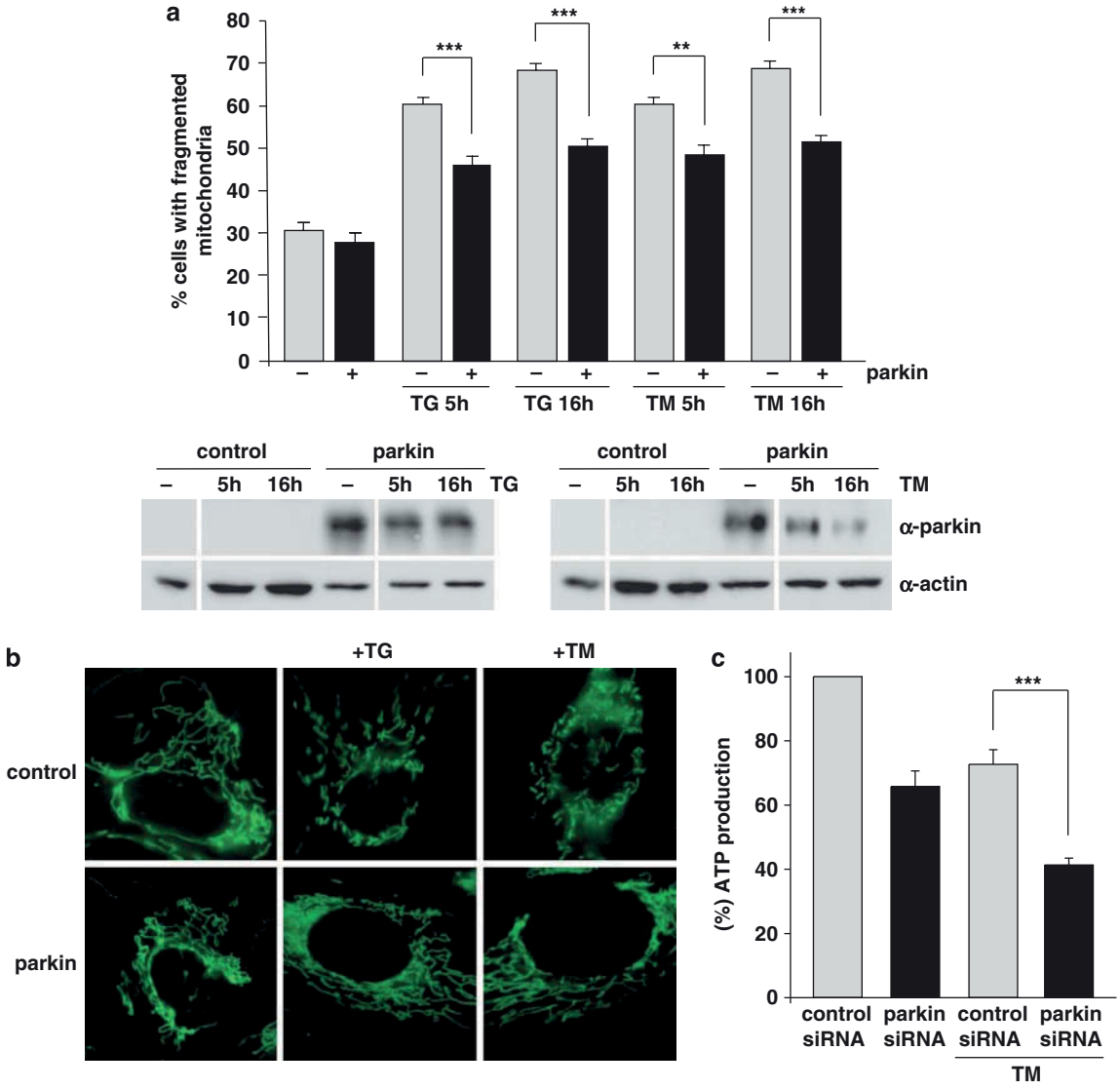

Figure 8 Parkin prevents mitochondrial damage and dysfunction induced by ER stress. (**a** and **b**) Increased parkin expression suppresses ER stress-induced mitochondrial fragmentation. SH-SY5Y cells were transfected with parkin or mCherry (as a control). One day after transfection, the cells were treated with thapsigargin (TG, 1 μM for 5 or 16 h) or tunicamycin (TM, 2 μg/ml for 5 or 16 h). Mitochondria were visualized by life cell microscopy after incubating cells with the fluorescent dye DiOC6(3). (**a**) The mitochondrial morphology was classified as tubular or fragmented (small rod-like or spherical mitochondria). Shown is the percentage of cells with fragmented mitochondria. Quantifications were based on triplicates of three independent experiments. For each experiment $\geqslant$300 cells per coverslip of triplicate samples were assessed. Expression levels of parkin were analyzed by immunoblotting using the anti-parkin pAb 2132 (lower panel). Loading was controlled by re-probing the blots for β-actin. (**b**) Examples of mitochondrial morphologies of the experiment described in (**a**). Treatment of cells with TG or TM cause a disruption of the tubular mitochondrial network, which can be suppressed by increased parkin expression. (**c**) Parkin deficiency increases ATP depletion in response to ER stress. SH-SY5Y cells were transfected with parkin or control siRNA duplexes. On day 2 after transfection, the cells were shifted to low-glucose medium containing 3 mM glucose instead of 25 mM. On day 3, the cells were treated with 2 μg/ml tunicamycin (TM) for 5 h and the steady-state cellular ATP levels were measured by a bioluminescence assay. Cultured cells derived from tumors derive almost all of their energy from aerobic glycolysis rather than mitochondrial oxidative phosphorylation; in addition, stimulation of glycolysis in the presence of glucose inhibits mitochondrial respiration. Therefore, low glucose concentrations in the medium forces the cells to relay on oxidative phosphorylation to generate sufficient ATP. ***$P<0.001$, **$P<0.01$

suggest that, at this interplay, parkin seems to enter the stage, preventing the pathophysiological consequences of ER stress on mitochondrial integrity (Figure 9). The next important step will be to figure out what the precise role of parkin might be in the communication between the ER and mitochondria.

Materials and Methods

DNA constructs. The following constructs were described previously: wt human parkin, G430D, ΔUBL mutant parkin,[18] ATF4,[33] ATF4ΔN,[22] PERK,[34] c-Jun,[35] JNK3,[36] Bcl-2-FLAG[37] and mCherry.[26] To generate siRNA-resistant parkin, four silent mutations were introduced into human wt parkin, to prevent binding of parkin-specific siRNA1 (Invitrogen, Karlsruhe, Germany). The following mutations were introduced by standard PCR cloning techniques: C 1038 to T, G 1044 to A, C 1053 to A and A 1059 to G. The luciferase reporter constructs were cloned by subcloning the UPR element (UPRE), the ER stress response element (ERSE), ERSE-II, the ATF4 binding site of the IGFBP-1 promoter (ATF4RE) or the ATF4 binding element of the parkin promoter (PARK) in triplicate flanked by *Nhe*I and *Bgl*II restriction sites into the pGL3 promoter vector (Promega, Mannheim, Germany). To generate the *renilla* luciferase construct, the SV40 promoter from the pGL3 vector

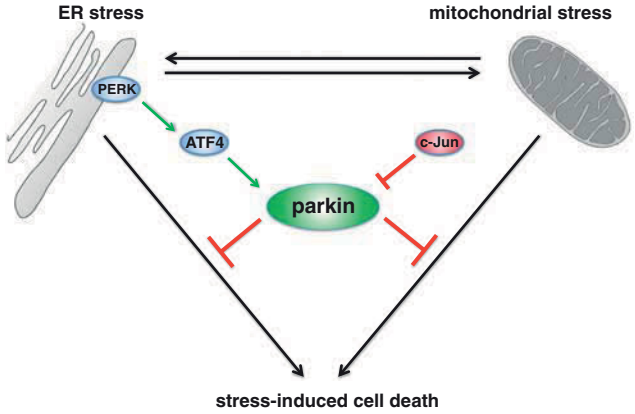

Figure 9 Interplay between ER stress, mitochondrial stress and parkin. ER stress can induce mitochondrial damage, such as alterations in mitochondrial morphology and bioenergetics. Conversely, mitochondrial stress can induce ER stress, reflected by the induction of the unfolded protein response (UPR). Parkin is transcriptionally upregulated in response to both mitochondrial and ER stress by ATF4, a transcription factor of the UPR. The stress-induced transcriptional upregulation of parkin is antagonized by c-Jun, which is activated by the JNK pathway. Increased expression of parkin under stress conditions protects cells from stress-induced cell death, explaining the high vulnerability of parkin-deficient cells to cellular stress

was subcloned into the phRL-TK vector (Promega), thereby replacing the HSV-TK promoter. The plasmids encoding enhanced yellow fluorescent protein (EYFP) and enhanced green fluorescent protein (EGFP) were purchased from Clontech (Mountain View, CA, USA).

Cell culture and transfections. SH-SY5Y (DSMZ number ACC 209) and HEK293T (ATCCC number CRL-1573) cells were transfected with Lipofectamine Plus (Invitrogen) according to the manufacturer's instructions. For RNA interference, SH-SY5Y or HEK293T cells were reversely transfected with Stealth siRNA (Invitrogen) using Lipofectamine RNAiMAX (Invitrogen) for SH-SY5Y cells and Lipofectamine 2000 (Invitrogen) for the HEK293T cells.

Antibodies and reagents. The following antibodies were used: anti-parkin mouse monoclonal antibody (mAb) PRK8 (Millipore, Schwalbach, Germany); anti-parkin pAb 2132, anti-ubiquitin P4D1 pAb (Cell Signaling Technology, Danvers, MA, USA); anti-SAPK/JNK pAb, anti-phospho-SAPK/JNK (Thr183/Tyr185) pAb and anti-phospho-c-Jun (Ser63) II rabbit pAb (Cell Signaling Technology); anti-CHOP mAb (Santa Cruz Biotechnology, Santa Cruz, CA, USA); anti-β-actin mAb, anti-Flag M2 mAb and anti-myc 9E10 mAb (Sigma, Taufkirchen, Germany); anti-c-Jun (N) sc45 rabbit pAb, anti-c-Jun (N) sc45X rabbit pAb, anti-CREB-2 C-20 rabbit pAb and anti-TRAF6 (H-274) rabbit pAb (Santa Cruz Biotechnology); anti-ATF4 pAB (Cocalico Biologicals, Reamstown, PA, USA); anti-p53 mAb (Calbiochem/Merck, Darmstadt, Germany); anti-active caspase-3 rabbit pAb (Promega); Alexa 555-conjugated goat anti-rabbit pAb (Sigma); horseradish peroxidase (HRP)-conjugated anti-mouse and anti-rabbit IgG antibody (Promega). Thapsigargin was purchased from Sigma, TM from Fluka/Sigma (Taufkirchen, Germany), epoxomycin from Calbiochem, L-histidinol from Sigma, the JNK inhibitor SP600125 from Enzo Life Sciences (Loerrach, Germany), and dialysed FCS and 3,3′-dihexyloxacarbocyanine iodide (DiOC6(3)) from Invitrogen. The mounting medium Mowiol (Calbiochem) was supplemented with 4′ 6-diamidino-2-phenylindole (Sigma).

Western blot analysis. SDS-PAGE and western blotting was described earlier.[18] Antigens were detected with the enhanced chemiluminescence detection system (Amersham Biosciences, Freiburg, Germany) or the Immobilon Western chemoluminiscent HRP substrate (Millipore).

Mouse embryonic fibroblast cultures. Primary mouse fibroblasts were isolated from parkin-knockout and wt mice with the same genetic background.[25] E12.5 mouse embryos were extracted, and the head and inner organs were removed. The remaining tissue was dissociated by trypsination and trituration.

Primary cortical neuronal culture. Cortical neurons were cultured from wt or ATF4 transgenic mouse embryos at E14.5–E15.5 days of gestation and individually dissected. Briefly, neurons from each embryo were plated individually, into six-well dishes ($\sim$3 million cells/well) coated with poly-D-lysine (100 μg/ml) in serum-free medium (MEM/F12 (1:1) supplemented with 6 mg/ml D-glucose, 100 μg/ml transferrin, 25 μg/ml insulin, 20 nM progesterone, 60 μM putrescine and 30 nM selenium) as described previously.[38] At 2 days *in vitro*, cortical neurons were treated with TM (3 μg/ml) for 8 h. Stock solutions of TM were prepared in DMSO (Sigma Aldrich, Oakville, ON, Canada) and diluted in culture media immediately before addition. Total RNA was isolated from cells at indicated time points using TRIzol reagent as per manufacturer's instructions (Invitrogen). Concentrations of RNA were measured on a spectrophotometer at λ260 nm.

Human primary fibroblast cultures. Punch-skin biopsy samples were taken from PD patients with compound heterozygous mutations (c101delAG, het. del ex3/4; patients 1 and 2) or a heterozygous mutation (het. dupl. ex7; patient 3) in the parkin gene. Genotyping was performed using direct DNA sequencing and the Multiplex ligation-dependent probe amplification parkin gene dosage kits (P051; MRC-Holland, Amsterdam, Holland), covering all exons of the parkin gene, as well as other known Mendelian PD genes. Sex and age-matched control fibroblasts from healthy individuals were provided by the Department of Orthopedics (Universitätsklinik für Orthopädie, Eberhard Karls University, Tübingen, Germany). Chopped tissue pieces were placed into a tissue culture flask and carefully covered with maintenance medium (RPMI medium supplemented with 10% fetal bovine serum and 1% penicillin/streptomycin, 1 mM sodium pyruvate). Cultures were kept at 37 °C in a humidified atmosphere containing 5% CO_2. Collected fibroblasts were aliquoted and frozen for storage between passages 2 and 10.

Real-time RT-PCR. Real-time RT-PCR was performed, as described before.[18] Briefly, SH-SY5Y cells were incubated with 1 μM TG, 2 μg/ml TM, 10 μM CCCP or 10 μM SP600125 for the indicated time. Total cellular RNA was isolated according to manufacturer's instructions (RNaesy mini kit, QIAGEN, Hilden, Germany). cDNA was synthesized using iScript cDNA Synthesis Kit (Bio-Rad, München, Germany). For the quantification of human parkin mRNA, the TaqMan Gene Expression Assay (parkin: Hs01038827-m1; beta actin: P/N 4326315E; 18sRNA: P/N 4319413E) (Applied Biosystems, Foster City, CA, USA) was used. For all other mRNA quantifications, PCR reactions were performed with 2 $\times$ Power SYBR Green PCR Master Mix (Applied Biosystems) and 1 μM of each primer pair; mouse (m) parkin forward primer (F): 5′-AAACCGGATGAGTGGTGAGT-3′; m-parkin reverse primer (R): 5′-AGCTACCGACGTGTCCTTGT-3′; m-actin-β F: 5′-AGCCTTCCTTCTTGGG TATG-3′; m-actin-β R: 5′-GGTCTTTACGGATGTCAACG-3′; m-BiP F: 5′-GCCTCA TCGGACGCACTT-3′; m-BiP R: 5′-GGGGCAAATGTCTTGGTT-3′; human (h) ATF4: F: 5′-CCCTTCACCTTCTTACAACCTC-3′; h-ATF4 R: 5′-GTCTGGCTTCCTATCTC CTTCA-3′; h-c-Jun F 5′-CGCCTGATAATCCAGTCCA-3′; h-c-Jun R: 5′-CCTGCTC ATCTGTCACGTTC-3′ ; h-BIP F: 5′-GCTCGACTCGAATTCCAAAG-3′; h-BIP R: 5′-GATCACCAGAGAGCACACCA-3′; h-actin-β F: 5′-TGGACTTCGAGCAAGAGA TG-3′; h-actin-β R: 5′-AGGAAGGAAGGCTGGAAGAG-3′. Quantification was performed with 7500 Fast Real Time System (Applied Biosystems) based on triplicates per primer set. Gene expression was normalized with respect to endogenous housekeeping control genes, β-actin and 18sRNA, which were not influenced by ER stress. Relative expression was calculated for each gene using the $\Delta\Delta C_T$ method. Statistical analysis of RT-PCR data is based on at least three independent experiments with tripicates samples.

Luciferase assays. HEK293T or SH-SY5Y cells transiently expressing *renilla* luciferase and *firefly* luciferase reporter plasmids were subjected to the stress treatment indicated. Luciferase activity of cell lysates was determined luminometrically using an LB96V luminometer (Berthold Technologies, Bad Wildbad, Germany) by the dual luciferase assay system (Promega) as specified by the manufacturer. The measured values were analyzed with WinGlow Software (Berthold Technologies). Quantification was based on at least three independent experiments. For each experiment, each transfection was performed at least in triplicate.

Apoptosis and cell viability assays. Activation of caspase-3 was determined as described previously.[37] Briefly, SH-SY5Y cells or skin fibroblasts were grown on glass coverslips. Twenty four hours after transfection (for parkin knockdown 3 days later), cells were incubated with TG, TM and/or epoxomycin as

indicated. The cells were then fixed, and activated caspase-3 detected by indirect immunofluorescence using an anti-active caspase-3 antibody. To detect cells undergoing apoptosis, the number of activated caspase-3-positive cells out of at least 300 transfected cells was determined using a Zeiss Axioscope 2 plus microscope (Carl Zeiss, Göttingen, Germany). Quantifications were based on triplicates of at least three (SH-SY5Y cells) or two (human skin fibroblasts) independent experiments. For each experiment $\geqslant$300 cells per coverslip of triplicate samples were assessed. For the cell viability assays, SH-SY5Y cells, HEK293T cells or MEFs were plated into 12-well plates. SH-SY5Y cells and HEK293T cells were reversely transfected with parkin or control siRNA. Two days later, the cells were stressed with TM or TG as indicated and the Vybrant MTT Cell Proliferation Assay was performed according to manufacturer's instructions (Invitrogen).

Electrophoretic mobility shift assay. Nuclear extracts were prepared as described earlier.[18] For the binding reaction, 10 μg of extracts were incubated with 10 mM HEPES (pH 7.9), 50 mM NaCl, 5 mM $MgCl_2$, 2 mM DTT, 0.1 mM EDTA, 5% glycerol, 10 μg BSA, 2 μg poly(dI-dC) and 0.2 ng (20 000 cpm) of ^{32}P-labeled, double-stranded park oligonucleotide (5′-CCCCGGTGACGTAAGATTGC-3′) in a final volume of 20 μl. For supershift assays, 0.2 μg of the ATF4 antibody or 2 μg of the c-Jun (N) sc45X antibody, for competition experiments 50 ng (100 $\times$) of cold-park oligonucleotide was added to the binding reaction. After binding on ice for 30 min, mixtures were loaded onto non-denaturating 4% polyacrylamide gels in 0.5 $\times$ TBE (45 mM Tris borate and 1 mM EDTA). Gels were electrophoresed at 4°C for 4 h at 160 V, dried, and exposed for autoradiography at $-$80°C.

Chromatin immunoprecipitation. HEK293T or SH-SY5Y cells were replenished with fresh medium 12 h before initiating all treatments to ensure that the cells were in the basal state. To trigger the UPR, fresh medium containing 300 nM TG was added. To monitor ATF4 binding to the parkin gene, a ChIP assay was performed as previously described.[39] The ATF4 antibody was a rabbit polycolonal antibody. Enrichment of DNA at the parkin promoter region that contains the potential ATF4 binding site was analyzed with quantitative real-time PCR. A 5 μl aliquot of DNA was mixed with 62.5 pmol of each PCR primer and 12.5 μl of SYBR Green PCR master mix (Applied Biosystems) in a 25 μl total volume. The real-time PCR was performed with a DNA Engine Opticon 3 system (Bio-Rad). The reaction mixtures were incubated at 95°C for 15 min, followed by amplification at 95°C for 15 s and 60°C for 60 s for 35 cycles. All experiments were performed in triplicate and each sample was subjected to PCR in duplicate. The primers used were: forward: 5′-GTTGCTAAGCGACTGGTCAA-3′ and reverse: 5′-CAGCCCCCCACC GCCGCC-3′.

Fluorescent staining of mitochondria. SH-SY5Y cells were grown on 15 mm glass coverslips, and were fluorescently labeled with 0.1 μM DiOC6(3) in cell culture medium for 15 min. After washing the coverslips with medium, living cells were analyzed for mitochondrial morphology by fluorescence microscopy as described previously[26] using a Leica DMRB microscope (Leica, Wetzlar, Germany). Cells were categorized in two classes according to their mitochondrial morphology: tubular or fragmented. Quantifications were based on three independent experiments. For each experiment, the mitochondrial morphology of $\geqslant$300 transfected cells per coverslip of triplicate samples was assessed.

Measurement of cellular ATP levels. A quantitative determination of ATP in SH-SY5Y cells was performed using the ATP Bioluminescence Assay Kit HS II (Roche, Mannheim, Germany) according to the manufacturer's instructions. Briefly, SH-SY5Y cells were reversely transfected with the indicated siRNA duplexes. Twenty four hours before collecting, the culture medium was replaced by low-glucose medium containing 3 mM instead of 25 mM glucose. Five hours, before the measurement, cells were treated with 2 μg/ml TM. Cells were washed twice with PBS, scraped off the plate and then lysed according to the provided protocol. The ATP content of the samples was determined using an LB96 V luminometer (Berthold Technologies), analyzed with WinGlow Software (Berthold Technologies) and normalized to total protein levels. Quantification was based on at least three independent experiments. For each experiment, each transfection was performed at least in triplicate.

Bioinformatics. Transcription factor (TF) BSs were identified by the TFSEARCH[20] and the MatInspector[40] program. All sequences were derived from the promoter sequence retrieval database ElDorado 02-2010 (Genomatix, Munich, Germany). Promoter sequences of parkin from four different mammalian species were aligned with the DiAlign TF program[40] in the Genomatix software suite GEMS Launcher to evaluate the overall promoter similarity and to identify conserved CREB/ATF BSs. The promoter sequences were defined as in ElDorado and elongated at the 3′ end of the promoter (downstream) by 150 bp. Position weight and matrices were used according to Matrix Family Library Version 8.2 (Genomatix) (January 2010) for promoter analyses. The BSs were considered as 'conserved BSs' if the promoter sequences of human and the orthologs can be aligned in the region of CREB/ATF BSs with the help of the DiAlign TF program (using default settings).

Statistical analysis. Data were expressed as means $\pm$ S.E. Statistical analysis was carried out using ANOVA. *$P<0.05$, **$P<0.01$, ***$P<0.001$.

Conflict of interest

The authors declare no conflict of interest.

Acknowledgements. This work was supported by the Deutsche Forschungsgemeinschaft (SFB 596 'Molecular Mechanisms of Neurodegeneration' to KFW, JT and WW), the German Ministry for Education and Research (NGFN plus 'Functional Genomics of Parkinson's Disease' to KFW, TG and WW), the Helmholtz Alliance 'Mental Health in an Ageing Society' (to KFW, TG and WW), the Hans and Ilse Breuer Foundation (to LB), the Heart and Stroke Foundation of Canada, Heart and Stroke Foundation of Ontario and the Canadian Institutes of Health Research (to DSP). Funding for MSK was from the National Institutes of Health (DK-52064). Il was supported by a postdoctoral fellowship from Canadian Institutes of Health Research (CIHR). We are grateful to Christian Haass for continuous support and stimulating discussions. We thank Dr Tim Townes for providing the ATF4-knockout mice, Alexis Brice and Olga Corti for the parkin-knockout mice, Torsten Kluba for human skin fibroblasts from control individuals, Carsten Culmsee for primary mouse cortical neurons, Daniel Krappmann for the c-Jun plasmid, Kimitoshi Kohno and Hiroto Izumi for the ATF4 plasmid, Gerald Thiel for the ATF4ΔN and CHOP plasmids, David Ron for the PERK plasmid and Vicky Wätzig and Thomas Herdegen for the JNK3 plasmid. We thank Kerstin Lämmermann and Christian Naumann for technical assistance and Jonathan Lin for advice on ATF4 western blotting.

1. Winklhofer KF, Haass C. Mitochondrial dysfunction in Parkinson′s disease. *Biochimica Et Biophysica Acta* 2010; **1802**: 29–44.
2. Schapira AH. Mitochondria in the aetiology and pathogenesis of Parkinson's disease. *Lancet Neurol* 2008; **7**: 97–109.
3. Wang HQ, Takahashi R. Expanding insights on the involvement of endoplasmic reticulum stress in Parkinson's disease. *Antioxid Redox Signal* 2007; **9**: 553–561.
4. Lindholm D, Wootz H, Korhonen L. ER stress and neurodegenerative diseases. *Cell Death Differ* 2006; **13**: 385–392.
5. Ghribi O, Herman MM, Pramoonjago P, Savory J. MPP+ induces the endoplasmic reticulum stress response in rabbit brain involving activation of the ATF-6 and NF-kappaB signaling pathways. *J Neuropathol Exp Neurol* 2003; **62**: 1144–1153.
6. Ryu EJ, Harding HP, Angelastro JM, Vitolo OV, Ron D, Greene LA. Endoplasmic reticulum stress and the unfolded protein response in cellular models of Parkinson's disease. *J Neurosci* 2002; **22**: 10690–10698.
7. Holtz WA, O'Malley KL. Parkinsonian mimetics induce aspects of unfolded protein response in death of dopaminergic neurons. *J Biol Chem* 2003; **278**: 19367–19377.
8. Cooper AA, Gitler AD, Cashikar A, Haynes CM, Hill KJ, Bhullar B *et al.* Alpha-synuclein blocks ER-golgi traffic and Rab1 rescues neuron loss in Parkinson's models. *Science* 2006; **313**: 324–328.
9. Smith WW, Jiang H, Pei Z, Tanaka Y, Morita H, Sawa A *et al.* Endoplasmic reticulum stress and mitochondrial cell death pathways mediate A53T mutant alpha-synuclein-induced toxicity. *Hum Mol Genet* 2005; **14**: 3801–3811.
10. Hoozemans JJ, van Haastert ES, Eikelenboom P, de Vos RA, Rozemuller JM, Scheper W. Activation of the unfolded protein response in Parkinson's disease. *Biochem Biophys Res Commun* 2007; **354**: 707–711.
11. Moran LB, Croisier E, Duke DC, Kalaitzakis ME, Roncaroli F, Deprez M *et al.* Analysis of alpha-synuclein, dopamine and parkin pathways in neuropathologically confirmed parkinsonian nigra. *Acta Neuropathol (Berl)* 2007; **113**: 253–263.
12. Imai Y, Soda M, Inoue H, Hattori N, Mizuno Y, Takahashi R. An unfolded putative transmembrane polypeptide, which can lead to endoplasmic reticulum stress, is a substrate of parkin. *Cell* 2001; **105**: 891–902.
13. Imai Y, Soda M, Takahashi R. Parkin suppresses unfolded protein stress-induced cell death through its E3 ubiquitin-protein ligase activity. *J Biol Chem* 2000; **275**: 35661–35664.

14. Kitada T, Asakawa S, Hattori N, Matsumine H, Yamamura Y, Minoshima S *et al.* Mutations in the parkin gene cause autosomal parkinsonism. *Nature* 1998; **392**: 605–608.
15. Ron D, Walter P. Signal integration in the endoplasmic reticulum unfolded protein response. *Nat Rev Mol Cell Biol* 2007; **8**: 519–529.
16. Kim I, Xu W, Reed JC. Cell death and endoplasmic reticulum stress: disease relevance and therapeutic opportunities. *Nat Rev Drug Discov* 2008; **7**: 1013–1030.
17. Pizzo P, Pozzan T. Mitochondria-endoplasmic reticulum choreography: structure and signaling dynamics. *Trends Cell Biol* 2007; **17**: 511–517.
18. Henn IH, Bouman L, Schlehe JS, Schlierf A, Schramm JE, Wegener E *et al.* Parkin mediates neuroprotection through activation of IkappaB kinase/nuclear factor-kappaB signaling. *J Neurosci* 2007; **27**: 1868–1878.
19. Narendra D, Tanaka A, Suen DF, Youle RJ. Parkin is recruited selectively to impaired mitochondria and promotes their autophagy. *J Cell Biol* 2008; **183**: 795–803.
20. Heinemeyer T, Wingender E, Reuter I, Hermjakob H, Kel AE, Kel OV *et al.* Databases on transcriptional regulation: TRANSFAC, TRRD and COMPEL. *Nucleic Acids Res* 1998; **26**: 362–367.
21. Marchand A, Tomkiewicz C, Magne L, Barouki R, Garlatti M. Endoplasmic reticulum stress induction of insulin-like growth factor-binding protein-1 involves ATF4. *J Biol Chem* 2006; **281**: 19124–19133.
22. Steinmuller L, Thiel G. Regulation of gene transcription by a constitutively active mutant of activating transcription factor 2 (ATF2). *Biol Chem* 2003; **384**: 667–672.
23. Masuoka HC, Townes TM. Targeted disruption of the activating transcription factor 4 gene results in severe fetal anemia in mice. *Blood* 2002; **99**: 736–745.
24. Waetzig V, Herdegen T. Context-specific inhibition of JNKs: overcoming the dilemma of protection and damage. *Trends Pharmacol Sci* 2005; **26**: 455–461.
25. Itier JM, Ibanez P, Mena MA, Abbas N, Cohen-Salmon C, Bohme GA *et al.* Parkin gene inactivation alters behaviour and dopamine neurotransmission in the mouse. *Hum Mol Genet* 2003; **12**: 2277–2291.
26. Lutz AK, Exner N, Fett ME, Schlehe JS, Kloos K, Lammermann K *et al.* Loss of parkin or PINK1 function increases Drp1-dependent mitochondrial fragmentation. *J Biol Chem* 2009; **284**: 22938–22951.
27. Sandebring A, Thomas KJ, Beilina A, van der Brug M, Cleland MM, Ahmad R *et al.* Mitochondrial alterations in PINK1 deficient cells are influenced by calcineurin-dependent dephosphorylation of dynamin-related protein 1. *PLoS one* 2009; **4**: e5701.
28. Hunot S, Vila M, Teismann P, Davis RJ, Hirsch EC, Przedborski S *et al.* JNK-mediated induction of cyclooxygenase 2 is required for neurodegeneration in a mouse model of Parkinson's disease. *Proc Natl Acad Sci USA* 2004; **101**: 665–670.
29. Brecht S, Kirchhof R, Chromik A, Willesen M, Nicolaus T, Raivich G *et al.* Specific pathophysiological functions of JNK isoforms in the brain. *Eur J Neurosci* 2005; **21**: 363–377.
30. Hasegawa T, Treis A, Patenge N, Fiesel FC, Springer W, Kahle PJ. Parkin protects against tyrosinase-mediated dopamine neurotoxicity by suppressing stress-activated protein kinase pathways. *J Neurochem* 2008; **105**: 1700–1715.
31. Cha GH, Kim S, Park J, Lee E, Kim M, Lee SB *et al.* Parkin negatively regulates JNK pathway in the dopaminergic neurons of Drosophila. *Proc Natl Acad Sci USA* 2005; **102**: 10345–10350.
32. Hom JR, Gewandter JS, Michael L, Sheu SS, Yoon Y. Thapsigargin induces biphasic fragmentation of mitochondria through calcium-mediated mitochondrial fission and apoptosis. *J Cell Physiol* 2007; **212**: 498–508.
33. Tanabe M, Izumi H, Ise T, Higuchi S, Yamori T, Yasumoto K *et al.* Activating transcription factor 4 increases the cisplatin resistance of human cancer cell lines. *Cancer Res* 2003; **63**: 8592–8595.
34. Harding HP, Zhang Y, Ron D. Protein translation and folding are coupled by an endoplasmic-reticulum-resident kinase. *Nature* 1999; **397**: 271–274.
35. Krappmann D, Wulczyn FG, Scheidereit C. Different mechanisms control signal-induced degradation and basal turnover of the NF-kappaB inhibitor IkappaB alpha *in vivo*. *EMBO J* 1996; **15**: 6716–6726.
36. Waetzig V, Herdegen T. A single c-Jun N-terminal kinase isoform (JNK3-p54) is an effector in both neuronal differentiation and cell death. *J Biol Chem* 2003; **278**: 567–572.
37. Rambold AS, Miesbauer M, Rapaport D, Bartke T, Baier M, Winklhofer KF *et al.* Association of Bcl-2 with misfolded prion protein is linked to the toxic potential of cytosolic PrP. *Mol Biol Cell* 2006; **17**: 3356–3368.
38. Aleyasin H, Cregan SP, Iyirhiaro G, O'Hare MJ, Callaghan SM, Slack RS *et al.* Nuclear factor-(kappa)B modulates the p53 response in neurons exposed to DNA damage. *J Neurosci* 2004; **24**: 2963–2973.
39. Chen H, Pan YX, Dudenhausen EE, Kilberg MS. Amino acid deprivation induces the transcription rate of the human asparagine synthetase gene through a timed program of expression and promoter binding of nutrient-responsive basic region/leucine zipper transcription factors as well as localized histone acetylation. *J Biol Chem* 2004; **279**: 50829–50839.
40. Cartharius K, Frech K, Grote K, Klocke B, Haltmeier M, Klingenhoff A *et al.* MatInspector and beyond: promoter analysis based on transcription factor binding sites. *Bioinformatics* 2005; **21**: 2933–2942.

Supplementary Information accompanies the paper on Cell Death and Differentiation website (http://www.nature.com/cdd)